

Compaction and spheroid formation modulates stemness and differentiation of human pancreas organoids

Dissertation

to obtain the doctoral degree of the natural sciences
submitted to Department 15 - Life Sciences
Johann Wolfgang Goethe-Universität Frankfurt am Main

Sanam Saeifar

Tehran, Iran

Frankfurt am Main, 2023

(D 30)

I hereby declare that my doctoral thesis titled “Compaction and spheroid formation modulates stemness and differentiation of human pancreas organoids”.

Accepted as dissertation from the Department 15 of - Life Sciences at Johann Wolfgang Goethe-Universität Frankfurt am Main, Frankfurt am Main, Germany

Dekanin: Prof. Dr. Sven Klimpel

1. Referee: Prof. Dr. Ernst H.K. Stelzer

2. Referee: Prof. Dr. Stefan Eimer

3. Referee: Prof. Dr. Franziska Matthäus

Supervisor: Dr. Francesco Pampaloni

Date of the disputation:



Buchmann Institute
for Molecular Life Sciences



Compaction and spheroid formation modulates stemness and differentiation of human pancreas organoids

Sanam Saeifar

Physical Biology / Physikalische Biologie

Buchmann Institute for Molecular Life Sciences

Cluster of Excellence – Macromolecular Complexes

Johann Wolfgang-Goethe-Universität– Frankfurt am Main

2018-2022

تقدیم به پدر و مادر عزیزم

علی ساعی فر
فریبا خلیلی پراپری

**DEDICATED
TO
MY LOVELY PARENTS**

**Ali Saeifar
Fariba Khalili Parapari**

Never give up, never surrender!

You can make it, be patient!

Acknowledgment

I would like to propose a vote of thanks to Prof. Dr. Ernst Hans Karl Stelzer for giving me the opportunity to work in the Buchmann Institute for Molecular Life Sciences (BMLS).

Furthermore, I would like to express my deep appreciation for Dr. Francesco Pampaloni, who kindly agreed to be my project supervisor for this thesis. I owe a debt of gratitude to my great supervisor, Dr. Francesco Pampaloni, who strongly supported for his continuous support for my study and research, with his patience, motivation, and enthusiasm.

Without his help, I could not carry out my research and the write up of my thesis in a competent manner.

In addition, my sincere thanks goes to Bettina Spöth, for helping me with official paper works, Michaela Koller, Berit Reinhardt, Sigrun Becker, Heinz Schewe, for introducing me the microscopes, Sven Plath, for designing virtual 3D mould, Franziska Krämer and Marc Pereyer for implantation of cell tracking program, Katharina Hötte, Isabell Smyrek, Alexander Schmitz, Biena Mathew, Frederic Strobl, Victor Perez Meza, Lotta Hof, Till Moreth, Michael Koch, Kaja Nicole Wächtershäuser, Julia Ratke, Louise Breideband, Levin Hafa, Ryan Sarkar and Kristina Mirkes and my master students: Deniz Ucan, Fabian Swoboda, Vania Cesar and all the other members of the Department of the Physical Biology of Goethe University Frankfurt am Main, whom I am grateful for their help during this project.

I owe many thanks to my great friends, Dr. Frederic Strobl and Franziska Krämer for scientific discussions and mental support and proofreading my thesis and pointing out my possible errors, another thanks belongs to the Kopie-Corner and its highly qualified staff for their top services.

Finally, my special gratitude goes towards my lovely parents, my father and mother, for their unceasing encouragement and invaluable support throughout my life.

I am especially thankful for their dear care and support during the difficult times preceding my master studies.

Contents

ACKNOWLEDGMENT	I
LIST OF FIGURES	V
LIST OF TABLES	XII
ABBREVIATIONS	XIII
GENERAL ABBREVIATION	XIII
GREEK LETTERS	XVII
SI-PREFIXES	XVII
UNITS	XVII
ABSTRACT	XVIII
1. INTRODUCTION	1
1.1. PANCREAS	1
1.1.1. Pancreas anatomy	1
1.1.2. Islets of Langerhans	2
1.1.3. Pancreas development and differentiation	5
1.1.4. Pancreatic disorders	7
1.1.5. Future therapeutic strategies for diabetes	9
1.1.6. Cell replacement therapy for diabetes	10
1.2.2. Applications of 3D cell culture	18
1.2.3. Current challenges in 3D cell culture	19
1.2.4. Common forms of 3D cell culture	21
1.3. MICROSCOPY	24
1.3.1. The importance of microscopy in biology	24
1.3.2. 3D cell cultures require specific microscopes for imaging	25
1.3.3. Advantages and disadvantages of imaging 3D specimens	25
1.4. AIM OF THIS THESIS	27
2. MATERIALS AND METHODS	28
2.1. MATERIALS	28
2.1.1. Chemicals	28
2.1.2. Buffers and Solutions	30
2.1.3 Cell line	31
2.1.4 Culture Medium	31
2.1.5 List of primers for RT-qPCR used in this study	32
2.1.6 Antibodies	34
2.1.7 Microscopes	35
2.1.8 Equipment	36
2.2 METHODS	38
I. CELL CULTURE	38
2.2.1 Cell line and cell culture	38
2.2.2 Thawing and cryopreservation	41
2.2.3 Formation of monotypic spheroids from human pancreatic progenitor cells	42
2.2.4 Triple co-culture spheroid formation	43
II. MICROSCOPY	44
2.2.5 Wide-field fluorescence microscopy	44

2.2.6	<i>Confocal laser scanning microscopy</i>	45
2.2.7	<i>Light sheet-based fluorescence microscopy</i>	45
III:	MOLECULAR AND CELLULAR SPHEROID CHARACTERIZATION	50
2.2.6	<i>Live-dead assay (LDA)</i>	50
2.2.7	<i>Short-term cell tracking with CellTracker dyes in spheroids</i>	51
2.2.8	<i>EdU incorporation assay for organoids</i>	51
2.2.10	<i>cDNA synthesis in organoids and spheroids</i>	53
2.2.11	<i>Reverse Transcription-quantitative Polymerase Chain Reaction (RT-qPCR)</i>	54
2.2.12	<i>Immunofluorescence staining</i>	54
IV:	DATA ANALYSIS	56
2.2.13	<i>Processing of RT-qPCR data</i>	56
2.2.14	<i>Nuclei segmentation in organoids and spheroids</i>	57
2.2.15	<i>Spheroid volume measurement in 3D confocal image stacks with ImageJ</i>	57
2.2.16	<i>Segmentation and tracking the cells during aggregation</i>	58
2.2.17	<i>Statistical analysis</i>	59
3:	RESULTS	60
3.1:	ORGANOIDS EXPANSION	61
3.1.1	<i>hPO efficiently grow in both expansion and differentiation medium</i>	61
3.1.2	<i>Optimization steps leading to the formation of well-defined homotypic hPO spheroids</i>	67
3.1.3	<i>Aggregation of hPO cells with the liquid-overlay technique (LOT) produces single and compact spheroid in both expansion and differentiation medium</i>	73
3.1.4	<i>The presence of all three cell types (hPO, hMSC, HUVEC) are essential for spheroid formation in differentiation medium</i>	77
3.2:	PHENOTYPICAL CHARACTERIZATION	81
3.2.1	<i>The morphology of both pancreas organoids and spheroids variates in expansion and differentiation media</i>	81
3.2.2	<i>The differentiation medium induces cell polarization in hPO and hPO spheroids</i>	86
3.2.3	<i>hPO spheroids show multiple internal acinar structures</i>	89
3.2.4	<i>Monitoring the aggregation process of pancreas progenitor cell spheroids with time-lapse light sheet microscopy</i>	92
3.2.5	<i>HDMEC segregate in external layers in the co-culture pancreas spheroids</i>	99
3.3:	GENOTYPICAL CHARACTERIZATION	101
3.3.1	<i>Significant reduction in the expression of progenitor genes detected in HPO spheroids cultured in differentiation medium</i>	101
3.3.2	<i>Differentiation medium prevents the proliferation of pancreas progenitor cells in both organoids and spheroids</i>	105
3.3.3	<i>Spheroid formation in differentiation medium drives the gene expression of hPO cells towards endocrine differentiation</i>	108
3.3.4	<i>Significant decrease in expression of epithelial and progenitor markers in pancreas progenitor cells following the formation of spheroids</i>	112
3.3.5	<i>Detection of hallmarks of epithelial-to-mesenchymal transition (EMT) by IF staining after spheroid formation</i>	115
4:	DISCUSSION	118
4.1	DIFFERENTIATION MEDIUM SUSTAINS HPO ORGANOIDS AND SPHEROIDS GROWTH AND INDUCES PHENOTYPICAL CHANGES	119
4.2	FURTHER OPTIMIZATION OF THE LIQUID-OVERLAY TECHNIQUE (LOT) IMPROVES PANCREAS PROGENITOR CELL SPHEROID FORMATION	123
4.3	DIFFERENTIATION MEDIUM CAUSES REMARKABLE NUCLEAR REARRANGEMENT WITHIN HPO SPHEROIDS AND ORGANOIDS	125

4.4 THE COMBINATION OF SPHEROID CULTURE AND DIFFERENTIATION MEDIUM DETERMINES THE ENDOCRINE FATE OF THE PANCREAS PROGENITOR CELLS	128
4.5 LONG TERM IMAGING OF DYNAMIC CELL BEHAVIOR AND CELL TYPE SEGREGATION DURING SPHEROID FORMATION WITH LIGHT SHEET MICROSCOPY	132
5. CONCLUSION AND OUTLOOK	138
5.1 CONCLUSION	138
5.2 OUTLOOK.....	140
6. SUMMARY – ENGLISH	142
7. ZUSAMMENFASSUNG – DEUTSCH	146
8. SUPPLEMENTS.....	150
8.1 SUPPLEMENTAL FIGURES.....	150
8.2 SUPPLEMENTAL TABLES	152
8.3 SUPPLEMENTAL MACRO CODE:.....	172
9. REFERENCES	173
10. POSTERS AND PUBLICATIONS.....	204
10.1 POSTERS	204
10.2 PUBLICATIONS	204
STATUTORY DECLARATION	205

List of figures

- Figure 1: Overview of adult pancreas. The pancreas is a sigmoid shape organ located right behind the stomach beside the liver and spleen. The pancreas is divided into an exocrine part (acinar and duct tissue) and an endocrine part (islets of Langerhans). (Modified from Shih HP et al., 2013) 1**
- Figure 2: Schematic illustration of islets of Langerhans. The pancreas is a mixed (exocrine and endocrine) glandular organ. The exocrine part of the pancreas is involved in digestion, and these associated structures are known as the pancreatic acinus and duct. The endocrine cells form cluster like structures so-called islets of Langerhans and scattered through the pancreas. Islets of Langerhans release different hormones such as glucagon (α cell), insulin (β cell), somatostatin (δ cell), and pancreatic polypeptide (γ or PP cell) and play important role in homeostasis (Created with BioRender). 3**
- Figure 3: Generating β -like cells from adult somatic cells by inducing trans-differentiation. In particular, β -like cells can be generated from different adult somatic cells such as hepatocytes, enterocytes, α cells, ductal cells, acinar cells, or by self-regeneration of pre-existing β cells. Up or down regulation of adult somatic cells causes trans-differentiation and leads to the formation of insulin positive cells with a β -like phenotype (Modified from G. Basile et al., 2019) (Created with BioRender). 11**
- Figure 4: Drawing of cell replacement in human islets. Several mechanisms could be applied on different cell types within human body in order to increase the amount of β cells in T1D patients. (created with BioRender). (Modified form Dr. Cord Dohrmann) 13**
- Figure 5: Schematic illustration of 2D and 3D cell culture. A: Traditional 2D monolayer cell culture and 3D cell culture systems; B: The structure of 3D spheroid with different zones of cells with the models of oxygenation, nutrition, and CO₂ removal. 3D spheroid from inside to outside. The regions are necrotic zone (innermost), quiescent viable cell zone (middle), and proliferating zone (outermost). (according to Nipha Chaicharoenaudomrung et al., 2019) (created with BioRender). 17**
- Figure 6: Human pancreatic organoids (hPOs) in expansion medium. hPOs are 3D cell structures consist of progenitor cells that form bubble-like structures in different sizes within the BME2. The bright field images were processed using Zeiss SteREO Discovery.V8 with 2x and 8x magnification; scale bar: 500 μ m. 21**
- Figure 7: A presentation of 3D spheroid microregions and nutrient and waste gradients. The spherical geometry of the cells within the MCTS are characterized by an external proliferating region and an internal quiescent zone (caused by the gradient of nutrient and oxygen diffusion), which surrounds a necrotic core, mimicking the cellular heterogeneity observed in solid tumors (created with BioRender). 23**
- Figure 8: Schematic illustration of expansion and differentiation protocol. Based on Meritxell Huch's protocols samples need to be cultured 7 days in expansion and differentiation mediums. Expansion protocol has several signaling pathway's inhibitors, and differentiation protocol contains 3 types of mediums (EM, EM2, and DM), which decrease in inhibitors' concentration stepwise. In both protocols mediums are replaced on the 2nd and 4th day. Samples are ready to be collected on day 7 (created with BioRender). 39**
- Figure 9: Schematic drawing of hPO cultivation process. For cultivation, hPOs are fragmented with vigorous pipetting up and down in cold basal medium which dissociates hPOs into small homogeneous aggregates, that are then embedded in fresh BME2. The mixture of BME2 and hPOs is placed on the bottom of each well respectively. After polymerization of BME2 drops in the incubator, medium is added to each well and plate is cultured in standard incubator conditions. The aggregates later develop into new circular organoids (adopted from Hiroyuki Miyoshi et al., 2013) (created with BioRender). 40**
- Figure 10: General workflow of proposed method. In mono-culture, after trypsinizing hPOs, 3,000 cells are seeded in agarose-coated 96-well plates and hPOs are cultured based on 2 different protocols. For making triple co-culture samples, at first all three cell types are trypsinized to single cells, followed by determining the number of cells in each group. Afterwards, the mixture of cell suspension in the ratio of 1:1:1 is performed. Triple spheroids with 3000 cells are formed in each well and cultured under 2 different protocols respectively (created with BioRender). 44**

- Figure 11:** The process of Z1 holder formation. After placing the pre-cut FEP foil into the vacuum-forming machine, the machine should be pre-heated to 480°C to 500°C. Next, the FEP foil is lifted and approached to the heater. The heating process is improved by keeping an industrial dryer close to it manually. The FEP foil is kept in this position to become flexible and start to stretch downwards. This part takes for ca. 30 sec. (the images are modified from Louise Breideband protocol). 47
- Figure 12:** Final steps in preparing Z1 holders. (A) By applying the vacuum with the machine and releasing the pre-warmed FEP foil simultaneously towards the mould, the FEP foil is stuck to the capillaries and forms the Z1 holders based on the shape of mould. (B) The mould should be detached afterwards, and the shrinking tube is used to seal the connection points. After sterilization the holders are ready to use for acquisition. 48
- Figure 13:** CAD drawings of mould for Z1 holder. To improve the process of aggregation during spheroid formation, the holders tip is changed. The newly designed tips (A) are sharper and more elongated compared to the previous versions (B). The CAD drawings are done by Sven Plath and later the mould is printed with LCD-based SLA 3D printer Photon S; scale bar (B): 200 µm. 49
- Figure 14:** Experimental flow for EdU incorporation assay. hPOs are cultured based on expansion and differentiation protocols, afterwards on day 7 EdU labeling marker is added to the mediums (10 µM) and they are incubated for 4h. Next, organoids are collected and fixed on the same day, being stained with secondary antibody (Alexa Fluor® 488 (1:200)) and Hoechst 33342 (1:500) respectively. sec., secondary; AB, Antibody; EM, Expansion medium; EM2, Expansion medium 2; DM, Differentiation medium (created by BioRender). 52
- Figure 15:** hPO organoids grow in both expansion and differentiation medium documented during taking time-lapse in the Cell Observer microscope (A) and cultivating in the incubator (B). hPOs are diced in small fragment and mixed with fresh BME2 respectively. 10 µl mixture of BME2 and hPOs were placed on the bottom of 96 well-plate. After polymerization in the incubator, 100 µl expansion or differentiation medium was added to each well. hPOs have been cultivated for 7 days based on expansion and differentiation protocol. Medium was refreshed on days 2nd and 4th. After 24 h, hPOs start to grow and form a spherical and luminal structure in both mediums. The bright field images have been processed using Zeiss Cell Observer microscope with Plan Aplanachromat 5x/0.16 objective lens (A) and Zeiss SteREO Discovery.V8 with 2x magnification (B). The time-lapse image sequences are acquired at 30 min intervals for 7 days. Exp.: Expansion; Diff.: Differentiation; h: hours; EM: Expansion medium; EM2: Expansion medium 2; DM: Differentiation medium; scale bar (A): 20 µm; scale bar (B): 500 µm. 64
- Figure 16:** (A) Two hPOs are fusing together after turning to mature spherical structure. After culturing fragments of hPOs in fresh BME2, fragments start to grow and turn to spherical structures. When reaching to the mature size, hPOs fuse together and share their lumen. (B) hPOs change their size by pumping in and out periodically during cultivation within BME2. hPOs pump in and out continuously, which leads to the expanding and shrinking regularly during cultivation in BME2. The images have been processed using Zeiss Cell Observer microscope with Plan Aplanachromat 5x/0.16 objective lens. The time-lapse image sequences are acquired at 30 min intervals for 7 days. h: hours; scale bar: 20 µm. 65
- Figure 17:** Expansion and differentiation medium has no effect on the mortality of hPOs. After 7 days, hPOs are stained with FDA (green, alive cells) and PI (red, dead cells) to discriminate between living and dead cells. As a positive control, cells were treated with DMSO for 5 min before staining. No dead cell is detected within organoids. Representative images for each condition are shown. The images have been processed using Zeiss Cell Observer microscope with Plan Aplanachromat 5x/0.16 objective lens; Excitation-Emission: 561 nm - 670/70 nm (PI), 488 nm - 525/45 nm (FDA). Exp.: Expansion; Diff.: Differentiation; PC: positive control; scale bar: 20 µm. 66
- Figure 18:** (A) Adding matrigel to the medium negatively affects spheroid size and IF staining. (B) Brightfield image reveals hPO spheroids covered with a cloudy-like structure due to the presence of matrigel in the medium. Spheroids are stained with Phalloidin 488 and presents the cellular cytoskeleton. Representative images are shown. Spheroids are optically cleared, and the images have been processed using Zeiss

- confocal LSM 780 microscopes with a Plan-Apochromat 20x/0.8 M27 objective lens. Excitation-Emission: 488 nm - 615 nm (Phalloidin 488); Exp.: Expansion; scale bar: 100 μ m. 70
- Figure 19:** Quantitative analysis of hPOs nuclei number per spheroid after 7 days of cultivation in Expansion and Differentiation medium. For each condition three independent experiments with at least three technical replicates were performed. Data are quantified with ImageJ plugin 3D object counter. The line inside the box denotes the standard error. Excel 365 software is used to illustrate the graphic and perform T-test for statistics analysis. The cultivation in expansion medium significantly increases the nuclei number per spheroid. Exp.: Expansion; Diff.: Differentiation. 71
- Figure 20:** hPOs form a single and compact spheroid by using a cell strainer. By passing the cell suspension through the cell strainer, single and compact spheroid is formed based on the liquid overlay technique (LOT). The images have been processed using Zeiss Axiovert 40 CFL microscope with 5x/0.12 ph0, 10x/0.25 ph1, and 20x/0.35 ph1 objective; D: Day; EM.: Expansion medium; scale bar: 100 μ m, close-up: 50 μ m. 72
- Figure 21:** hPOs form single and compact spheroid in both expansion and differentiation medium within 7 days based on the liquid overlay technique (LOT). 3000 single cells were seeded in agarose-coated 96-well plates. After 7 days hPOs aggregate and spheroids form in each well. The medium was replaced every two days. The images have been processed using W Plan-Apochromat microscope with 5x/0.12 ph0, 10x/0.25 ph1, and 20x/0.35 ph1 objective lenses; Exp.: Expansion; Diff.: Differentiation; D: Day; EM: Expansion medium; EM2: Expansion medium 2; DM: Differentiation medium; scale bar: 200 μ m, close-up: 100 μ m. 74
- Figure 22:** hPO spheroids have spherical morphology and regular borders. Cell nuclei are stained with DAPI (blue) and Phalloidin (green and white) presented in the cell cytoskeleton. Representative Z-project images are shown. Spheroids are optically cleared, and the images have been processed using Zeiss confocal LSM 780 microscopes with a Plan-Apochromat 20x/0.8 M27 objective lens. Excitation-Emission: 405 nm - 450/50 nm (DAPI), 488 nm - 615 nm (Phalloidin 488). DAPI= cell nucleus; scale bar: 100 μ m. . 75
- Figure 23:** The mortality of hPOs have been analysed after aggregation by live/dead assay. After aggregation, spheroids were stained with FDA (green, alive cells) and PI (red, dead cells) to discriminate between living and dead cells. As a positive control, cells were treated with DMSO for 5 min. No dead cell was detected within spheroids. Representative images for each condition are shown. The images have been processed using Zeiss Axiovert 40 CFL microscope with 10x/0.25 ph1; Excitation-Emission: 561 nm - 670/70 nm (PI), 488 nm - 525/45 nm (FDA); PC: positive control; scale bar: 200 μ m. 76
- Figure 24:** hPOs form single and compact spheroid in both expansion and differentiation medium within 7 days based on the liquid overlay technique (LOT). 3000 single cells were seeded in agarose-coated 96-well plates. After 7 days hPOs aggregate and spheroids are formed in each well. The medium was replaced every two days. Representative images for each condition are shown. The images have been processed using W Plan-Apochromat microscope with 5x/0.12 ph0, 10x/0.25 ph1, and 20x/0.35 ph1 objective lenses; Exp.: Expansion; Diff.: Differentiation; D: Day; scale bar: 200 μ m. 79
- Figure 25:** Mixture of hPO, hMSC, and HDMEC (ratio 1:1:1) formed just single and compact spheroid in differentiation medium within 7 days based on the liquid overlay technique (LOT). 3000 single cells for the mixture of cells (ratio of 1:1:1) were seeded in agarose-coated 96-well plates. After 4 days hPOs were aggregate and spheroids were formed in both conditions, however in the last 3 days the spheroids in differentiation medium start to diverge. The medium was replaced every two days. Representative images for each condition are shown. The images have been processed using W Plan-Apochromat microscope with 5x/0.12 ph0, 10x/0.25 ph1, and 20x/0.35 ph1 objective lenses; Exp.: Expansion; Diff.: Differentiation; D: Day; EM: Expansion medium; EM2: Expansion medium 2; DM: Differentiation medium; scale bar: 200 μ m, close-up: 100 μ m. 80
- Figure 26:** IF staining presents the overall (A, B) and cross section (A1, B1) of hPO spheroid and organoid. Nuclei staining with DAPI reveals the single-layer and bubble-like structure of the organoids as well as spherical and multilayer formation of spheroids. Representative images for each condition are shown. Spheroids are optically cleared, and the images have been processed using Zeiss confocal LSM780 microscope with

- W Plan-Apochromat 20x/084 M27; Excitation-Emission: 405 nm - 450/50 nm (DAPI); scale bar: 50 μ m, close-up: 25 μ m..... 83*
- Figure 27: Quantitative analysis of hPO nuclei number per spheroid and organoid after 7 days cultivation in Exp. and Diff. medium. For each condition three independent experiments with at least three technical replicates were performed. Data have been quantified with ImageJ plugin 3D object counter. The lines inside the boxes denote the standard error. Excel 365 software is used to illustrate the graphic and perform T-test for statistics analysis. ns: not significant; Exp.: Expansion; Diff.: Differentiation. 84**
- Figure 28: Quantitative analysis of spheroid volume and cells per spheroid after aggregation in Exp. and Diff. medium. For each condition three independent experiments with at least three technical replicates were performed. Data have been quantified with ImageJ plugin 3D object counter. The lines inside the boxes denote the standard error. Excel 365 software is used to illustrate the graphic and perform T-test for statistics analysis. Exp.: Expansion; Diff.: Differentiation. 85**
- Figure 29: Differentiation medium leads to the basal localization of nucleus in some organoids. IF staining with phalloidin 488 reveals that cell nucleus in some organoids, cultured in differentiation medium, are strongly basal-polarized. Representative images for each condition are shown. The images have been processed using Zeiss confocal LSM780 microscope with W Plan-Apochromat 20x/084 M27; Excitation-Emission: 405 nm - 450/50 nm (Hoechst 33342), 561 nm - 670/70 nm (Phalloidin); scale bar: 50 μ m, close-up: 10 μ m..... 87**
- Figure 30: Strong basal polarization in the external layer of the spheroid, cultured in differentiation medium. IF staining with phalloidin 488 reveals that cell nucleus in the outer layer of the spheroids, cultured in differentiation medium, are strongly basal-polarized. Representative images for each condition are shown. Spheroids are optically cleared, and the images have been processed using Zeiss confocal LSM780 microscope with W Plan-Apochromat 20x/084 M27; Excitation-Emission: 405 nm - 450/50 nm (DAPI), 561 nm - 670/70 nm (Phalloidin); scale bar: 50 μ m, close-up: 10 μ m. 88**
- Figure 31: Spheroids consist of small cavity-like structures in all cases. After IF staining the cytoskeleton, circular and bubble-like structures are detected within spheroids in all cases. Representative images for each condition are shown. Spheroids are optically cleared, and the images have been processed using Zeiss confocal LSM780 microscope with W Plan-Apochromat 20x/084 M27; Excitation-Emission: 405 nm - 450/50 nm (DAPI), 561 nm - 670/70 nm (Phalloidin 568); scale bar: 50 μ m..... 90**
- Figure 32: hPOs maintain their original growth pattern and pump in and out constantly during aggregation. hPOs were trypsinized to single cells followed by staining with 5 μ M CellTracker™ Orange CMTMR. The process of aggregation was monitored in a time-lapse by Z1 microscope. The formation of bubble-like structures that were pumping in and out continuously, inside of the spheroids during aggregation has been monitored, respectively. The time-lapse image sequences have acquired at 30 min intervals for 4 days. Arrows are pointing at acinus-like structure within spheroids. Representative images for each condition are shown. The images have been processed using Z1 microscope with Det.: W Plan-Apochromat 20x/1.0 UV-VIS; Illum.: Zeiss LSFM 10x/0.2; Laser: 561 nm-571 nm; scale bar: 50 μ m. 91**
- Figure 33: (A) hPOs stained with 5 μ M CellTracker™ Orange and accumulated at the bottom of Z1 holder. After trypsinizing the hPOs, single cells were counted and placed in Z1 holder. By stepwise centrifuging, cells were collected at the end of the Z1 holder. (B) A compact spheroid detected within Z1 holder after 4 days. Arrows are pointing at bubble-like structures formation which represents pumping function during hPOs growth, respectively. Representative images for each condition are shown. The images were processed using Z1 microscope with Det.: W Plan-Apochromat 20x/1.0 UV-VIS; Illum.: Zeiss LSFM 10x/0.2; Laser: 561 nm - 571 nm. scale bar: 100 μ m..... 94**
- Figure 34: Formation of multiple spheroids in different sizes within FEP foil during/after (?) 4 days incubation. hPOs could be stained harmlessly with 5 μ M CellTracker™ Orange CMTMR and staining did not impair spheroid formation. The progress of aggregation inside of the Z1 holder was checked after 4 days. Rounded and compact spheroids in different sizes were detected inside the Z1 holder. Spheroids form a clear barrier from the neighbor cells. Representative images for each condition are shown. The images were processed using Zeiss Cell Observer microscope with W Plan Apochromat 10x/0.25 ph1, 20x/0.35**

- ph1, 32x/0.40 ph1 objective lens; Excitation-Emission: 561 nm - 670/70 nm; scale bar: 100 μ m; close-up: 25 μ m..... 95
- Figure 35: Spheroid formation progress in FEP foil in 2 days inside Z1 microscope. hPOs were trypsinized to single cells followed by staining with 5 μ M CellTracker™ Orange CMTMR, after which they were placed inside Z1 holder. Process of aggregation was monitored with time-lapse method using Z1 microscope. Time-lapse image sequences were acquired at 30 min intervals for 2 days. Initially, the cells were attached to the surface of the FEP foil but remained dynamic. Then the cells started to aggregate and form small aggregates. Finally, the clusters compacted to form spherical aggregates that detached from other neighbor cells. Representative images for each condition are shown. The images were processed using Z1 microscope with Det.: W Plan-Apochromat 20x/1.0 UV-VIS; Illum.: Zeiss LSM 10x/0.2; Laser: 561 nm - 571 nm; scale bar: 100 μ m. 96**
- Figure 36: Cell localization assessment during spheroid formation within FEP foil using Z1 microscope. Two populations of hPOs and hMSC were incubated with 5 μ M CellTracker™ Orange CMTMR and HUVEC cells were stained with 1 μ M CellTracker Green CMFDA, mixed together, they were placed at the bottom of the Z1 holder afterwards for spheroid formation. The aggregation progress was monitored with time-lapse method using Z1 microscope. Time-lapse image sequences were acquired at 30 min intervals for 2 days. Initially the cells were mixed uniformly, over the time hPOs and hMSC were concentrated in the center and begin to round up and compact. Simultaneously, HUVEC cells moved to the external part of the spheroid. Representative images for each condition are shown. Images were processed using Z1 microscope with Det.: W Plan-Apochromat 20x/1.0 UV-VIS; Illum.: Zeiss LSM 10x/0.2; Laser: 488 nm - 615 nm, 561 nm - 571 nm; scale bar: 100 μ m 97**
- Figure 37: Prevascularized network in the external layer of a triple spheroid. HUVC cells migrate to the external layer of the spheroid during (spheroid?) formation. Arrows indicate cells approaching to one another, forming a micro prevascular network around the spheroid. Representative images for each condition are shown. The images were processed using Z1 microscope with Det.: W Plan-Apochromat 20x/1.0 UV-VIS; Illum.: Zeiss LSM 10x/0.2; Laser: 488 nm - 615 nm, 561 nm - 571 nm; scale bar: 50 μ m 98**
- Figure 38: Strong external localization of HDMEC within the spheroid. Co-culturing hPO with hMSC and HDMEC in Differentiation medium show significant accumulation of HDMEC in the outer layer of the spheroid. Representative images for each condition are shown. Spheroids are optically cleared, and the images have been processed using Zeiss confocal LSM 780 microscopes with a Plan-Apochromat 20x/0.8 M27 objective lens. Excitation-Emission: 405 nm - 450/50 nm (DAPI), 488 nm - 615 nm (Alexa Fluor 488). CD31 = HDMEC marker, DAPI= cell nucleus; scale bar: 100 μ m, close-up: 50 μ m 100**
- Figure 39: Immunofluorescent staining visualizes the effect of cell aggregation and differentiation medium on progenitor gene expression. hPOs have labeled with progenitor marker (Sox9). Progenitor markers are detected inside and in the periphery of the spheroid. Cell nuclei are stained with DAPI and Hoechst 33342. Representative images for each condition are shown. Spheroids have optically cleared, and the images have been processed using Zeiss confocal LSM780 microscope with W Plan-Apochromat 10x/03 M27 (organoid) and W Plan-Apochromat 20x/084 M27 (spheroid); Excitation-Emission: 405 nm - 450/50 nm (DAPI and Hoechst 33342), 645 nm - 765 nm (SOX9); Exp.: Expansion; Diff.: Differentiation; scale bar: 50 μ m. 103**
- Figure 40: Progenitor gene expression changes are validated by RT-qPCR. A remarkable difference in hLGR5 and hSOX9 expression is detected due to the differentiation medium and aggregation. For each condition three independent experiments with at least three technical replicates have performed. Relative expression of hLGR5 and hSOX9 is normalized to the geometric means of hRPL13 and hTBP (housekeeping genes) and later to the expression in hPO organoids cultivated in expansion medium. The lines inside the boxes denote the standard error. Excel 365 software was used to illustrate the graphic and perform T-test for statistics analysis, and the statistical significance was defined as $p < 0.05$. ns: not significant; Exp.: Expansion; Diff.: Differentiation..... 104**
- Figure 41: Cell proliferation is inhibited in the differentiation medium. The proliferation signal is only detected in the hPO spheroids cultured in an Expansion medium. hPOs are labeled with proliferation marker (Ki67)**

- and Anti-EdU. Cell nuclei are stained with Hoechst 33342. Representative images for each condition are shown. Spheroids were optically cleared, and the images have been processed using Zeiss confocal LSM780 microscope with W Plan-Apochromat 10x/03 M27 and W Plan-Apochromat 20x/084 M27; Excitation-Emission: 405 nm - 450/50 nm (Hoechst 33342), 488 nm - 525/45 nm (Ki67 and Anti-EdU); Scale bar: 100 μ m. 106
- Figure 42: Quantification of proliferation rate within hPO organoids and spheroids after 7 days of cultivation in expansion and differentiation medium. Differentiation medium significantly decreases the ratio of proliferated cells in all conditions compared to the expansion medium. Spheroid formation has inducer effect on proliferation per se. For each condition 3 independent experiments with at least 5 technical replicates were performed. Data are normalized with total nuclei per sample then quantified with ImageJ plugin 3D object counter. Excel 365 software was used to illustrate the graphic and perform T-test for statistics analysis. The lines inside the boxes denote the standard error. Exp.: Expansion; Diff.: Differentiation. 107**
- Figure 43: Cultivation under differentiation medium affects the localization of insulin within hPO organoids. Organoids have been cultured under expansion and differentiation mediums for 7 days followed by fixation and immunofluorescent staining against insulin. Insulin expression is detected in the basal membrane under differentiation medium and IF staining visualizes the cytoplasmic and point-like structure for insulin expression in hPO that has been cultured in expansion medium. Z-project represents the expression of insulin in all of the hPOs in both conditions. Cell nuclei are stained with Hoechst 33342. Representative images for each condition are shown. The images have been processed using Zeiss confocal LSM780 microscope with W Plan-Apochromat 10x/03 M27; Excitation-Emission: 405 nm - 450/50 nm (Hoechst 33342), 645 nm - 765 nm (insulin); Exp.: Expansion; Diff.: Differentiation; scale bar: 50 μ m; close-up:25 μ m 109**
- Figure 44: Nuclei-expression of Pdx1 within hPO organoids under expansion and differentiation medium. Organoids have been cultured under expansion and differentiation mediums for 7 days followed by fixation and immunofluorescent staining against Pdx1. IF staining visualizes the expression of Pdx1 in the nucleus of hPO organoids under expansion and differentiation medium. Z-project represented the expression of Pdx1 in the entire of the hPOs in both conditions. Cell nuclei are stained with Hoechst 33342. Representative images for each condition are shown. The images have been processed using Zeiss confocal LSM780 microscope with W Plan-Apochromat 10x/03 M27; Excitation-Emission: 405 nm - 450/50 nm (Hoechst 33342), 561 nm - 607 nm (Pdx1); Exp.: Expansion; Diff.: Differentiation; scale bar: 50 μ m. 110**
- Figure 45: Aggregation coupled with the cultivation in differentiation medium causes the highest expression of β cell and differentiation markers within hPOs. The RT-qPCR results validate the strong difference in β cell and differentiation markers between hPO spheroids cultured in differentiation medium and other groups. For each condition three independent experiments with at least three technical replicates were performed. Relative expression of each gene was normalized to the geometric means of hRPL13 and hTBP (housekeeping genes) and later to the expression in hPO organoids cultivated in expansion medium. The lines inside the boxes denote the standard error. Excel 365 software was used to illustrate the graphic; Exp.: Expansion; Diff.: Differentiation. 111**
- Figure 46: Immunofluorescent staining visualizes the expression of ductal marker after cultivation under expansion and differentiation medium within hPO organoids. Organoids have been cultured under expansion and differentiation mediums for 7 days followed by fixation and immunofluorescent staining against Krt19. Krt19 is detected in all of the hPOs in both conditions. Cell nuclei are stained with Hoechst 33342. Representative images for each condition are shown. The images have been processed using Zeiss confocal LSM780 microscope with W Plan-Apochromat 10x/03 M27; Excitation-Emission: 405 nm - 450/50 nm (Hoechst 33342), 561 nm - 670/70 nm (Krt19); Exp.: Expansion; Diff.: Differentiation; scale bar: 50 μ m. 113**
- Figure 47: A similar reduction in ductal and progenitor markers are detected due to the spheroid formation. The RT-qPCR results validate strong and similar decreasing in the expression of Krt19, ductal marker, and**

- SOX9, progenitor marker after spheroid formation. For each condition three independent experiments with at least three technical replicates have been performed. Relative expression of each gene is normalized to the geometric means of hRPL13 and hTBP (housekeeping genes) and later to the expression in hPO organoids cultivated in expansion medium. The lines inside the boxes denote the standard error. Excel 365 software was used to illustrate the graphic; Exp.: Expansion; Diff.: Differentiation..... 114*
- Figure 48: Mesenchymal markers (Vim) detected in the entire of the spheroids in both conditions. IF staining strongly visualized the expression of mesenchymal marker after cultivation under expansion and differentiation medium within hPO spheroids. Spheroids have been cultured under expansion and differentiation mediums for 7 days followed by fixation and IF staining against Vim. Cell nuclei are stained with Hoechst 33342. Representative images for each condition are shown. The images have been processed using Zeiss confocal LSM780 microscope with W Plan-Apochromat 10x/03 M27; Excitation-Emission: 405 nm - 450/50 nm (Hoechst 33342), 561 nm - 670/70 nm (Vim); Exp.: Expansion; Diff.: Differentiation 116**
- Figure 49: Quantitative analysis of epithelial-to-mesenchymal transition (EMT) markers by RT-qPCR results. A) Ductal markers (hEPCAM and Krt19) significantly decrease after aggregation and cultivation in differentiation medium. B) Spheroid formation has positive effect on the expression of mesenchymal genes (hCDH2 and hVIM). For each condition three independent experiments with at least three technical replicates were performed. Relative expression of each gene was normalized to the geometric means of hRPL13 and hTBP (housekeeping genes) and later to the expression in hPO organoids cultivated in expansion medium. The lines inside the boxes denote the standard error. Excel 365 software was used to illustrate the graphic; Exp.: Expansion; Diff.: Differentiation. 117**
- Figure 50: Nucleofection on hPOs under expansion medium after 7 days. Organoids were turned to single cells and after electroporation were cultured under expansion medium for 7 days followed by imaging with brightfield microscope. Transfection was applied with pmaxGFPTM vector by P3 Primary Cell 4D-NucleofectorTM X Kit S (LONZA) on hPO in expansion medium after seven days. Representative images for each condition are shown. The images were processed using Zeiss confocal LSM780 microscope with Zeiss Axiovert 40 CFL microscope with 40x/0.40 ph1 objective lens; Excitation-Emission: 470/40 nm – 525/50 nm (GFP); scale bar:50 µm. 150**
- Figure 51: Formation of a three-dimensional mini-sized vascularized mouse islet in co-cultures of islets with HUVECs and human MSCs. The arrowheads indicate the blood vessel-like structures. Scale bars: 250 µm (Takahashi, Y. et al. (2018))..... 151**

List of tables

Table 1: Table of different cell types in islets.....	4
Table 2: List of somatic cell types as candidates for regenerating new β cells within human and mouse. (Modified from G. Basile <i>et al.</i> , 2019)	12
Table 3: Primary differences between 2D and 3D cell culture:	15
Table 4: List of chemicals used in this study, including supplier.....	28
Table 5: The composition of buffers and solutions used in this study.....	30
Table 6: Information about cell lines used in this study.....	31
Table 7: The composition of medium for 2D and 3D cultivation used in this study.....	31
Table 8: List of primers for RT-qPCR	32
Table 9: Primary antibodies used in this study	34
Table 10: Secondary antibodies used in this study	34
Table 11: Fluorescent dyes used in this study.....	35
Table 12: Microscopes and corresponding objectives used in this study	35
Table 13: Fluorescent filters used in this study.....	36
Table 14: Equipment for spheroid formation and cell cultivation used in this study	36
Table 15: Proportion of counted cells per organoids and spheroids done with 3D object counter plugin for ImageJ.	152
Table 16: Proportion of spheroid volume in microns ³	158
Table 17: Proportion of proliferated cells per organoids and spheroids.	162
Table 18: RT-qPCR results of the genes. The Ct values were normalized to the geometric mean of the housekeeping genes (RPL13 and TBP) and hPO organoids in expansion medium based on the $\Delta\Delta Ct$ method.	168

Abbreviations

General abbreviation

Abbreviation	Meaning
2D	Two-dimensional
3D	Three-dimensional
BM	Basement membrane
BME2	Basement membrane extract type 2
BMLS	Buchmann Institute For Molecular Life Sciences
BSA	Bovine Serum Albumin
CD31	Cluster of differentiation 31
CDH2	Cadherin 2
CLSM	Confocal laser scanning microscopy
CO₂	Carbon dioxide
CRS	Cell Recovery solution
d.p.c.	Days post coitum
DAPI	4',6-diamidino-2-phenylindole
ddH₂O	Double-distilled water
DKA	Diabetic ketoacidosis
DM	Human differentiation medium
DMEM	Dulbecco's Modified Eagle Medium
DMSO	Dimethyl-Sulfoxide
DNA	Deoxyribonucleic acid
e.g.	For example (exempli gratia)
et al.,	And others (et alium)
ECM	Extracellular matrix proteins
EDTA	Ethylenediaminetetraacetic acid
EdU	5-ethynyl-2'-deoxyuridine
EHS	Engelbreth-Holm-Swarm
EM	Electron microscopy
EM	Expansion medium with recombinant R-spondin

EM2	Expansion medium with recombinant R-spondin 2
EMT	Epithelial-to-mesenchymal transition
EPCAM	Epithelial cell adhesion molecule
ESCs	Embryonic stem cells
FBS	Fetal Bovine Serum
FDA	Fluorescein Diacetate
FGF-10	Fibroblast growth factor 10
FOXA2	Forkhead box A2
GDM	Gestational diabetes mellitus
GOI	Gene of interest
Ins; INS	Insulin
HDMECs	Human microvascular endothelial cells
hEGF	Recombinant human epithelial growth factor
Hh	Hedgehog
hMSC	Human mesenchymal stem cells
hPOs	Human pancreas organoids
hPSCs	Human pluripotent stem cells
IF	Immunofluorescence
iPSCs	Induced pluripotent stem cells
JBS	Johanson Blizzard syndrome
Krt19; KRT19	Cytokeratin 19
IgG	Immunoglobulin G
LOT	Liquid-overlay technique
LSFM	Light sheet-based fluorescence microscopy
Lgr5	Leucine-rich repeat-containing G-protein coupled receptor 5
Mafa; MaFA	V-maf musculoaponeurotic fibrosarcoma oncogene homolog A
Mafb; MaFB	V-maf musculoaponeurotic fibrosarcoma oncogene homolog B
MCTS	Multicellular tumor spheroids
LDA	live-dead assay
LN₂	Liquid nitrogen
LSM	Laser scanning microscope

m	Mouse
Ncad; CDH2	N-cadherin
Neurod1; NEUROD1	Neurogenic differentiation 1
Ngn3; NGN3	Neurogenin 3
Pax6; PAX6	Paired box gene 6
PBS	Phosphate buffered saline
Pdx1; PDX1	Pancreas/duodenum homeobox protein 1
PERT	Pancreatic enzyme replacement therapy
PFA	Paraformaldehyde
PI	Propidium iodide
PNLIP	Pancreatic lipase deficiency
PP	Pancreatic polypeptide
P/S	Penicillin/Streptomycin
Ptch	Patched
REM	Reflection electron microscope
rhR-spondin	Recombinant human R-spondin
ROCK	Rho-associated protein kinase
RPL13	Ribosomal Protein L13
RT	Room temperature
RT-qPCR	Reverse transcription – quantitative Polymerase Chain Reaction
rcf	Relative centrifugal force
RIs	Refractive indices
SDS	Shwachman Diamond syndrome
SEM	Scanning electron microscope
SIM	Structured illumination microscopy
STORM	Stochastic optical reconstruction microscopy
Sox9; SOX9	SRY related HMG box 9
Sox17; SOX17	Sex determining region Y-box 17
T1D	Diabetes type 1
T2D	Diabetes type 2
TBP	TATA-binding protein

TEM	Transmission electron microscope
TGF-β	Transforming growth factor β
TNF-α	Tumor necrosis factor α
TRIzol™ Reagent	Total RNA Isolation Reagent
TOC	Tissue optical clearing
VEGF-A	vascular endothelial growth factor-A
Vim; VIM	Vimentin
Wnt; WNT	Wingless Int-1
[v/v]	Volume per volume
[w/v]	Weight per volume

Greek letters

Greek letter	Meaning
α	Alpha
β	Beta
δ	Delta
ϵ	Epsilon
γ	Gamma

SI-Prefixes

SI-Prefix	Meaning
k	Kilo (10^3)
c	Centi (10^{-2})
m	Milli (10^{-3})
μ	Micro (10^{-6})
n	Nano (10^{-9})

Units

Unit	Meaning
$^{\circ}\text{C}$	Centigrade
d.p.c.	Days post coitum
g	Gram
h	Hour
Da	Dalton
L	Liter
m	Meter
M	Molarity (mol/l)
min	Minute
V	Voltage

Abstract

The incidence of diabetes type 1 (T1D) in children and young adults is increasing worldwide. T1D is well treated by insulin administration. However, there is currently no long-lasting cure for this ailment. The success rate of pancreatic islet transplantation to treat T1D is limited by the availability of patient-matched islets and the necessity of using life-long immunosuppressive medication. The difficulties caused by transplantation can be overcome by generating bio-engineered pancreatic islets from patient-derived progenitor cells. Aim of this thesis is to establish new strategies for the generation and analysis of pancreatic lineages derived from human progenitor cells. It reports on the optimization of a technique to form human pancreatic spheroids from hollow monolayered human pancreas organoids (hPOs) to investigate how cell-cell and cell-matrix interaction can be leveraged to induce endocrine differentiation of the pancreas progenitor cell organoids. We introduce cell aggregation protocols to generate endocrine pancreas cell lineages from ductal pancreatic cells. Next, we study the effect of co-culture with stromal and endothelial cells to promote cell differentiation toward a pancreatic fate enhancing β cells productivity.

This thesis has focused on identifying the differences in gene expression along with phenotypical transformation during differentiation of human pancreatic organoids (hPOs) towards human β cells to be used in the future of cellular therapeutics in treating T1D patients.

Keywords: human pancreatic organoids (hPOs), differentiation, spheroid, diabetes type 1.

1. Introduction

1.1. Pancreas

1.1.1. Pancreas anatomy

Pancreas is an elongated exocrine and endocrine organ, placed in the left part of the body under the heart and close to the spleen (Figure 1).^{1,2} Nearly 95% of pancreatic mass belongs to exocrine compartment and is composed of two major cell types: acinar and ductal cells. Several acinar cells line with epithelial cells, which produce zymogen granules, and form acini structures within pancreas. The exocrine part consists of several lobules containing numerous acini. Acini is involved in the food digestion. The zymogen granules are secretory vesicles that release trypsinogen, procarboxypeptidase, amylase, and lipase that hydrolyze food.² Ductal cells form approximately 10% of the pancreas mass and make networks called small pancreas ductule. Pancreas ductule is connected to the larger ducts which forms major pancreatic duct. Fat digestive enzymes are released through the pancreatic duct and merge with the common bile ducts into the first 10 cm of digestive system, called duodenum (Figure 1).

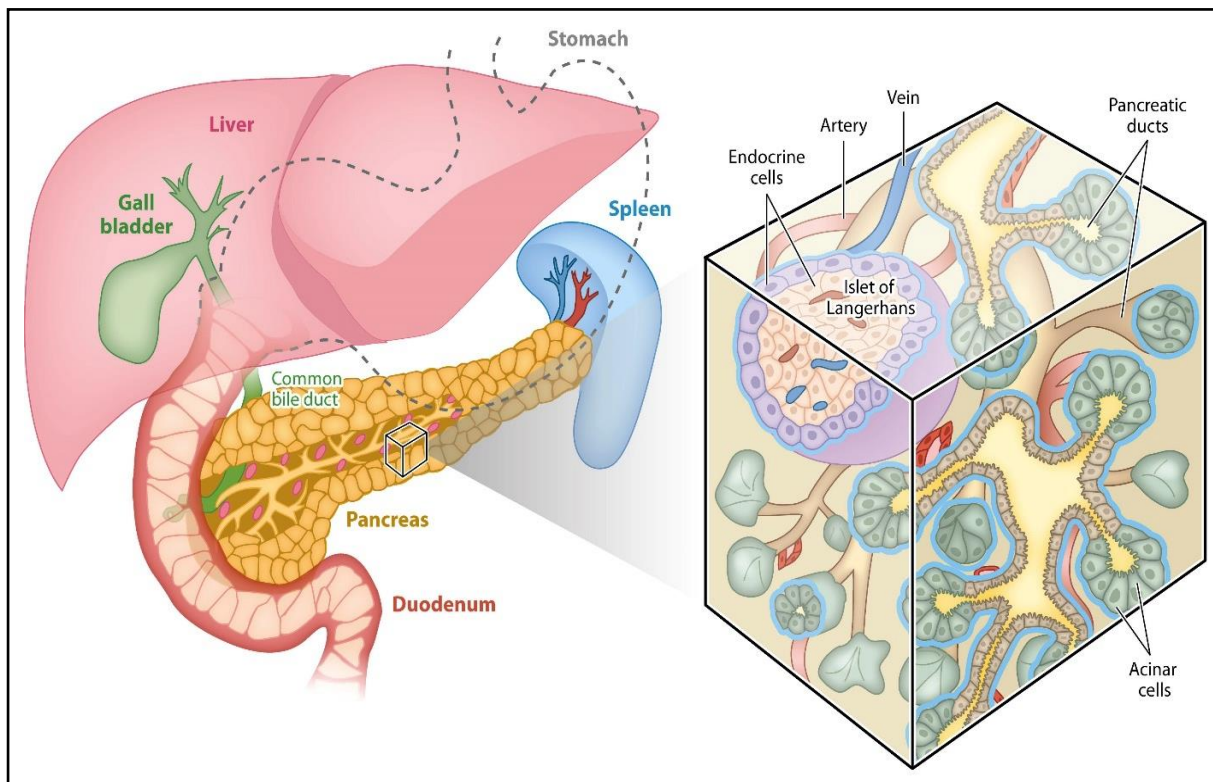


Figure 1: Overview of adult pancreas. The pancreas is a sigmoid shape organ located right behind the stomach beside the liver and spleen. The pancreas is divided into an exocrine part (acinar and duct tissue) and an endocrine part (islets of Langerhans). (Modified from Shih HP et al., 2013)

To provide the optimal milieu for enzymatic activity and protect the pancreas ducts from acinar secreted enzymes, ductal cells secrete bicarbonate which neutralizes stomach acidity respectively.³⁻⁶ In contrast, the endocrine part of pancreas releases its hormones directly in the blood. The endocrine cells form small and rounded cluster-like structures, so-called *islets of Langerhans*, which take around 1–2% of the entire pancreatic mass.⁷⁻⁹ Islets of Langerhans consist of compact cell aggregates comprising five different main cell types: α (alpha), β (beta), δ (delta), ϵ (epsilon), and γ (gamma) or PP (pancreatic polypeptide) cells that secrete glucagon, insulin, somatostatin, ghrelin and pancreatic polypeptide, respectively.^{8,10,11}

Homeostasis is defined as a self-regulating process by which biological systems maintain to relatively stabilize internal state and used to describe organ's activities. Highly sophisticated network of various hormones from different parts of the body such as brain, pancreas, liver, intestine as well as adipose and muscle tissue are involved in maintaining homeostasis. Within this network, the pancreas plays a significant key role by producing and secreting insulin and its opponent glucagon to control normal blood glucose levels. Pancreatic internal hormones, insulin and glucagon together, affect cell's functionality directly. Insulin is released from the β cells and considered as the main internal pancreatic hormone. Insulin is the most important hormone since it facilitates each single cell within body to be nourished, similarly, it controls the function of cell gates on the surface of cell membranes and ensures entering glucose in the cells which leads to monitoring the glucose levels in the blood.^{7,12,13}

1.1.2. Islets of Langerhans

The Islets of Langerhans were characterized for the first time by the pathologist Paul Langerhans in 1869.¹⁴ An adult human pancreas comprises between 3.2 and 14.8 million islets, with a total volume between 0.5 and 2.0 cm³. The proportion of cellular composition and architecture of pancreatic islets varies between and within species.¹⁵ In general, each islet consists of a central core of β cells, surrounded by α , δ , ϵ , and γ or PP (pancreatic polypeptide) cells.^{7,15,16} β cells are the predominant cell types within islets by comprising up to 60% of the islets' mass, followed by α cells with 30% of islets' mass.¹⁷ The 10% remainder made up of δ , ϵ , γ or PP cells, that are randomly distributed throughout the islets (Figure 2).¹⁸

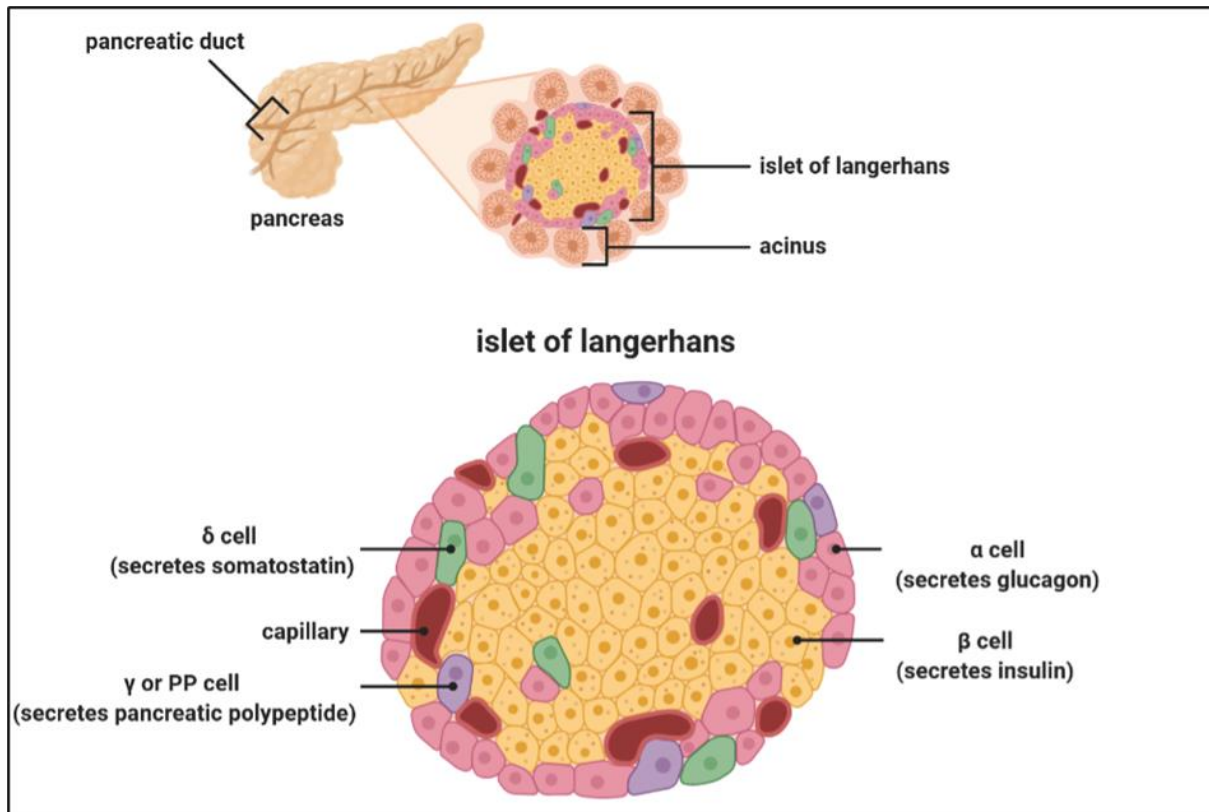


Figure 2: Schematic illustration of islets of Langerhans. The pancreas is a mixed (exocrine and endocrine) glandular organ. The exocrine part of the pancreas is involved in digestion, and these associated structures are known as the pancreatic acinus and duct. The endocrine cells form cluster like structures so-called islets of Langerhans and scattered through the pancreas. Islets of Langerhans release different hormones such as glucagon (α cell), insulin (β cell), somatostatin (δ cell), and pancreatic polypeptide (γ or PP cell) and play important role in homeostasis (Created with BioRender).

Islets of Langerhans are compact structures of different cells with different functions and hormones.^{8,15} Each cell type is stimulated by individualized signals and releases specific hormone, therefore islets are directly responsible for maintaining homeostasis.^{7,19}

The two most prominent cell types in islets, β and α cells, are essential for the maintenance of blood glucose homeostasis. α cells produce and release glucagon, a peptide hormone that increases the concentration of glucose and fatty acids in the blood and categorises as a catabolic hormone in the body. In contrast, β cells make and release an opposing hormone called insulin.^{7,20} The secretion of insulin by pancreatic β cells plays a critical role in the regulation of glucose. Insulin opposes glucagon and decreases glucose concentration in the blood by increasing glucose uptake by the liver, skeletal muscle, and adipose tissue via specialized receptors.^{7,19} δ cells release somatostatin the inhibitor for both insulin and glucagon. ϵ cells make ghrelin, which play different roles in triggering of appetite, increasing fat storage and stimulation of growth hormones release by the pituitary gland.²¹ γ or PP cells

are responsible for producing pancreatic polypeptides, which are involved in the digestive system. Pancreatic polypeptides decrease gastric acid secretion, gastric emptying, and upper intestinal motility.^{17,20,22} The islet cell's communication through extracellular spaces and gap junctions are required for normal homeostasis. Besides the endocrine cells, the islets contain numerous other cell types such as: vascular cells, other stromal cells, immune cells, and neural elements (Table 1).^{23,24}

Table 1: Table of different cell types in islets.

Different Cell Types in Islets				
Endocrine cells	Stromal cells	Vascular cells	Immune cells	Neural cells
α cells	Fibroblasts	Endothelial cells	Granulocytes	Neurons
β cells	Myofibroblasts	Vascular smooth muscle cells	Lymphocytes	Schwann cells
δ cells	Stellate cells	Pericytes	Macrophages	
ϵ cells	Kajal cells	Adventitial stromal cells	Dendritic cells	
γ or PP cells	Occasional duct cells		Mast cells	

The islets of Langerhans consist of highly specialized networks of arterioles, capillaries, and venules forming the microvasculature system.²³ The localization and proportion of islets within lobules play a significant role in the architecture of the pancreatic microvasculature.²⁵ Pancreatic islets are extensively vascularized and contain fenestrated capillaries that form a glomerular-like network within islets.²⁶ Due to the high local production of vascular endothelial growth factor-A (VEGF-A) by the β cells, endocrine capillaries are approximately 10 times more abundant than exocrine pancreatic capillaries and receive up to 20% of the pancreatic blood flow.^{9,26,27} The neurovascular system, secretion of insulin from β cells, endothelium-derived mediators, and other hormones regulate islet blood flow respectively. The islet blood flow is usually disturbed in glucose metabolism disorders.^{7,21} Most β cells face at least parts of their cytoplasm towards fenestrated islet capillaries.²³ The close and compact capillaries network in the islets facilitates monitoring glucose levels and the release of the necessary amount of insulin in the bloodstream. It is worth noting that this glomerulus-like structure ensures that insulin is efficiently delivered into bloodstream and in general to insulin-sensitive organs, such as liver, adipose, muscle and hypothalamus, which plays an important role in the stabilization of homeostasis within the body.^{23,27}

The islet microvascular system are quite variable in size but architecturally are like the other veins in the body and contributes to the blood perfusion of pancreatic islets respectively.^{26,28,29} An extended neurovascular system, which consists of several neurons and vascular cells, penetrates through the central core of the islet participating in hormone production and homeostasis.^{21,30}

1.1.3. Pancreas development and differentiation

In the past two decades, knowledge of how does the pancreas develop during embryogenesis has considerably advanced.^{31,32} Particularly, the molecular basis of pancreatic development and cell differentiation has been intensively studied.

Both exocrine and endocrine parts of pancreas develop from the dorsal and ventral bud during embryogenesis and arises from the foregut endodermal lining of the duodenum in the first month of human embryonic life.³² Single immature epithelial duct cells from endocrine cells develop in the first ten weeks of gestation, followed by vascularization of islets in week 16 of gestation.¹¹ The process is proceeded by encapsulation with connective tissues at the same time.³² Final development takes place by differentiation of pre-islet cells into specific islet cell types during the second half of gestation.³³ Neogenesis or the formation of new islet cells from pancreatic progenitor/stem cells is widely accepted as being responsible for the initial embryonic formation of the endocrine pancreas.³⁴

Pancreas organogenesis comprises of coordinated and highly complex interaction of signaling and expression of different transcriptional networks that has a stepwise process. A critical step in this process is the decision made by pancreatic progenitor cells for adopting an endocrine fate. Transcription factors play critical roles in gene expression, through binding to specific enhancer sequences which leads to differentiation.^{11,20} Pancreas/duodenum homeobox protein 1 (PDX1), forkhead box A2 (FOXA2), and sex determining region Y-box 17 (SOX17) are involved in early pancreatic progenitor formation.^{35,36} Several other transcription factors such as Neurogenin 3 (Ngn3, also known as Neurog3) and neurogenic differentiation 1 (NEUROD1) are cooperating during endocrine lineage specification and differentiation.³⁶ Late maturation of beta cells is tightly regulated by transcription factors including V-maf musculoaponeurotic fibrosarcoma oncogene homolog A (MaFA), V-maf musculoaponeurotic fibrosarcoma oncogene homolog B (MaFB), paired box gene 6 (PAX6), and estrogen related receptor gamma respectively.^{8,31,37-39}

Among all transcription factors, PDX1, NEUROG3, and MafA are the most important ones during islet development.³⁷ The *Ngn3* controls the endocrine fate decision. Its expression is scattered cells within the cords of pancreatic progenitor cells that form the fetal pancreatic ducts and is necessary for differentiation towards endocrine cells.³⁷

Pdx1 is expressed broadly in the pancreas cells during the first several days of pancreas development. Studies show that progenitor form all the mature pancreatic cell types expressing *Pdx1* respectively. Pre-islet cells are histologically recognized in day 9 (E9.0-E9.5) of development by expressing *Pdx1*. Both *Pdx1* and *Ptf1a*, pancreas transcription factor 1 subunit alpha, are transcription factors being expressed in the early stage of pancreas development, therefore used as a marker for.³⁵

MafA, also known as RIPE3b1, binds to the promoter region of the insulin gene and leads to insulin expression in response to glucose. *MafA* is detected in week 21 and its expression gradually increases after birth. It is also repeatedly reported that *MafA* is important in regenerating functional and mature β cells from pluripotent stem cells.^{37,40} In addition to this, Regulated Hedgehog (*Hh*) signaling pathway is required for proper pancreas development and organogenesis. Activation of this pathway depends on the binding of a *Hh* ligand to its transmembrane receptor Patched (*Ptch*).⁴¹

Several developmental disorders can also lead to anatomic abnormalities of the pancreas and its ducts or can be part of complex disorders that affect multiorgan systems. Other genetic mutations can lead to metabolic abnormalities that affect the pancreas exclusively or increase the lifetime risk for developing pancreatitis or pancreatic diabetes.

1.1.3.1 Function and development of β cells

β cells are the most studied cells of the pancreas. In humans, β cells are located in the center of the islets of Langerhans.² They make up to 60% of the cells in the islets.¹⁷ Total number of mature β cells varies significantly among individuals. It is noteworthy that small islets contain almost only β cells, on the contrary other endocrine cell types are mainly presented in the larger islets.⁴²

β cells differentiate from non- β cell precursors through a process termed neogenesis.³⁴ β cell replication continues and significant neogenesis occurs during the neonatal period within the human body.⁴³ β cells are found in week 9 of gestation.⁴⁴ They are capable of replicating from the beginning of week 9 d.p.c. (days post conception) respectively. β cells are mostly maintained by self-replication rather than differentiation. The high rate of β cell replication

during pancreas development is responsible of the high expression of β cell mass within islets.⁴⁵ The first endocrine cells are closely associated with the ductal epithelium, which may be caused by the differentiation from precursor cells.^{46,47} The expression of insulin and glucagon has been reported from β cells during fetal period. β cells develop their insulin secretion ability and become more mature after birth.⁴⁸

1.1.3.2. Role of other cell types on β cells functionality and development

Cell crosstalk in tissues is complex and has a significant effect on cell function and cell fate.⁴⁹ β cells are highly interconnected via blood vessel network, which allows the β cells to sense glucose level in the blood and release a tightly regulated amount of insulin in the blood. In addition, blood vessels play a unique role during all stages of prenatal pancreas development, which demonstrated a close relationship between the development of endocrine islets and blood vessels.⁴⁹ Furthermore, human microvascular endothelial cells (HDMECs) cooperate in the pancreatic niche and their absence can cause pancreatic agenesis.²⁸ Efficient interaction between HDMECs and human pluripotent stem cells (hPSCs) leads to the generation of functional pancreatic β cells.

1.1.4. Pancreatic disorders

An increasing incidence of pancreatic disorders, either acute *pancreatitis* or chronic *pancreatitis*, has been recorded in patients, possibly due to higher awareness among physicians.^{7,50} Acute pancreatitis is common and is the leading cause of hospitalization among gastrointestinal disorders in the world since problems with the *pancreas* can interrupt both digestive part and glucose levels in blood and affect the whole body.¹ There are some anatomic abnormalities in childhood, which would cause symptomatic pancreatic disease that are usually treated surgically.⁵¹ Biochemical abnormalities that are caused by enzyme deficiencies are mostly treated with medical therapies.⁵² Aside from different types of pancreatic cancers such as pancreatic adenocarcinoma and nonfunctional islet cell tumor, there are other disorders and diseases of pancreas, like cystic fibrosis, Jeune syndrome, Pearson Syndrome, Johanson Blizzard syndrome (JBS), Shwachman Diamond syndrome (SDS) and isolated pancreatic enzyme deficiencies (pancreatic lipase deficiency or PNLIP), that can have various degrees of seriousness and complications.^{50,53–56}

1.1.4.1. Diabetes mellitus

Diabetes mellitus, commonly known as diabetes, is a chronic and metabolic disease that causes high concentration of sugar (glucose) in the bloodstream.⁵⁷ Diabetes happens when the pancreas is no longer capable of synthesize insulin, or when the body cannot use the

insulin it produces.⁷ Diabetes mellitus is also a common disease among patients with pancreatic cancer, chronic pancreatitis, and disorders of the exocrine pancreas.⁵⁰ Diabetes includes direct and indirect symptoms in the patient, which can affect their health and life for short or long time.⁵⁸ In many cases patients die due to the side effects of diabetes such as, blindness and kidney dysfunctional diseases. The three main types of diabetes are: type 1 diabetes (T1D), type 2 diabetes (T2D), and gestational diabetes mellitus (GDM).⁵⁹

Type 1 diabetes (T1D), also called as juvenile *diabetes* or insulin-dependent *diabetes*, is a chronic disease in which the pancreas produces little or no insulin.^{60,61} T1D is an organ-specific autoimmune disease, which means that the immune system mistakenly attacks the pancreas and destroys the β cells, therefore the body cannot produce insulin.^{34,62,63} The incidence of T1D is increasing significantly between children and teenagers.^{60,64}

Type 2 diabetes (T2D), formerly known as adult-onset *diabetes* or insulin resistance *diabetes*, is the most common form of diabetes.^{13,65,66} High calory intake and lack of exercise are the most contributing causes of T2D.⁶⁶ In this type of diabetes, the body cannot effectively use the insulin, which leads the body to rely on alternative energy sources.⁶⁷ Over the time most people with T2D would require oral drugs and/or insulin shots to control their blood glucose levels.

Gestational diabetes mellitus (GDM) is a temporary type of diabetes consisting high blood sugar levels during pregnancy which usually disappears after giving birth.^{57,68} Like other types of diabetes, GDM extremely affects mother's homeostasis. It can affect mother's and the baby's health. These babies are at increased risk of developing type 2 diabetes later in life.^{69,70}

1.1.4.2. Treatment of diabetes mellitus type 1 and 2

The main goal of diabetes treatment is to control blood sugar (glucose) levels in the bloodstream so as to prevent complications of the disease.⁷ Diabetes, particularly T1D, results from the lack of pancreatic β cells.³⁴ For patients with T1D and T2D, the main treatment is based on the injection of exogenous insulin or insulin analogues, without this regular daily injection patients would develop life-threatening diabetic ketoacidosis (DKA) .^{62,71} Currently, there is no cure for T1D, therefore patients with T1D require lifelong multiple insulin injections over the day to maintain normal glucose levels.⁴⁵ Furthermore, dietary changes and individualized physical exercises play a critical role in managing T1D.⁶⁷ T2D patients have a wider range of treatment options in comparison with T1D patients. Lifestyle modification

coupled with the application of oral antidiabetic drugs such as metformin are suggested for T2D treatment.⁶⁶ Diet and exercise can help patients to control their blood pressure together with blood lipid and glucose levels.^{66,67}

1.1.5. Future therapeutic strategies for diabetes

As noted above, a characteristic feature that is common in T1D is the progressive loss of functional β cells' mass which leads to poor glucose levels control.^{57,72} Hopes for diabetes treatment are grouped in drug therapy, gene therapy and transplantation, while these strategies require significant improvements in wide scale clinical applications.

1.1.5.1. Drug therapy

Insulin therapy as daily regular injection (two to three times per day) is the basis in treatment of T1D, albeit, it does not solve all the problems in the T1D patients.^{61,73} Parallel to this treatment, researchers have been focusing on the production of different kinds of drugs, meaning to stimulate insulin secretion, increase insulin sensitivity, or inhibit the antagonists of this hormone as the potential treatment for T2D.⁷² Furthermore, Metformin is the first medication prescribed for T2D and everyone diagnosed with T2D needs to take it regularly.^{66,73} Metformin is effective, safe, and inexpensive and it may reduce the risk of cardiovascular events.⁶⁶ Diet and exercise can also help patients to manage T2D.^{66,74} The diabetic patients need to deal with the absent of insulin in their body, besides that in some cases, they suffer from pancreatic enzyme deficiency continuously, which is treated with pancreatic enzyme replacement therapy (PERT) coupled with vitamin supplementation.⁷⁵

1.1.5.2. Gene therapy

Gene therapy by viral vector and non-viral transduction is highly promising for the treatment of T1D.⁶² Researchers approach from many different angles to find a specific treatment for T1D such as prevention of β cell autoimmunity by the suppression of autoreactive T cells or the replacement of the insulin gene.⁷⁶⁻⁷⁸ Even though gene therapy is one of the basic treatments in autoimmune diabetes, this method requires more research to be considered as an efficient and safe treatment for T1D.⁶²

1.1.5.3. Transplantation

Allogeneic islet transplantation serves as a source of insulin-secreting beta-cells for the maintenance of normal glucose levels and treatment of T1D. Transplantation has emerged as

a promising treatment, nonetheless, researchers are still facing two critical challenges: first, the protection of β -cells from autoimmunity, and second, the supply of reliably functional β -cells.^{79–82} At the same token, insufficient donor resources, high rates of islet graft failure, and the necessity for lifelong immune suppression therapies are major obstacles to the widespread application of this therapeutic approach. To overcome these problems, transplanting pancreatic islet obtained by differentiating adult stem cells has recently emerged as a suitable treatment. Transplanting autologous differentiated cells can increase the chances of success by avoiding the immune response of the patient following a xenotransplantation.. Furthermore, this way the scarcity of donated islets would be overcome and the patients would avoid the assumption of immune suppressor medication, which long-term increases the probability of developing cancer and further autoimmune diseases.^{45,61,83}

1.1.6. Cell replacement therapy for diabetes

One of the promising methods to overcome today's treatments (daily injection or subcuticular pumps) for diabetic patients is the cellular therapy by which the lost β cells in disease processes could be restored/replaced by surrogate insulin-secreting cells including those derived from multipotent pancreas progenitors. This was demonstrated by Noor *et al.*, 2017 in an animal model in details. She has shown that rats rendered diabetic by the β cell toxin streptozotocin could be cured by implantation of isogeneic islets.⁸⁵ however, clinical diabetes researchers are facing two critical challenges. First, protection of the new β cells from autoimmunity and immune rejection, and second, development of β cells that are readily available and reliably functional.^{34,86,87}

To increase the number of functional β cells in patients, insulin-producing cells can be generated from non-pancreatic somatic cells (hepatocytes or intestinal cells), pancreatic exocrine cells (acinar and ductal cells), or pancreatic islet cells (α cells) by inducing trans-differentiation. Differentiated β cells can be expanded by reversible immortalization and the generation of insulin-producing cells from embryonic or adult stem cells. It is possible that new insights into endocrine pancreas development would ultimately lead to manipulation of progenitor-cell fate towards the beta-cell phenotype of insulin production, storage, and regulated secretion. Both allogeneic and autologous surrogate beta cells are likely to require protection from recurring autoimmunity 34,87–89. This protection might take the form of tolerization, cell encapsulation, or cell engineering with immune protective genes 62,92. If

successful, these approaches could lead to widespread cell replacement therapy for type 1 diabetes (Table 2, Figure 3).

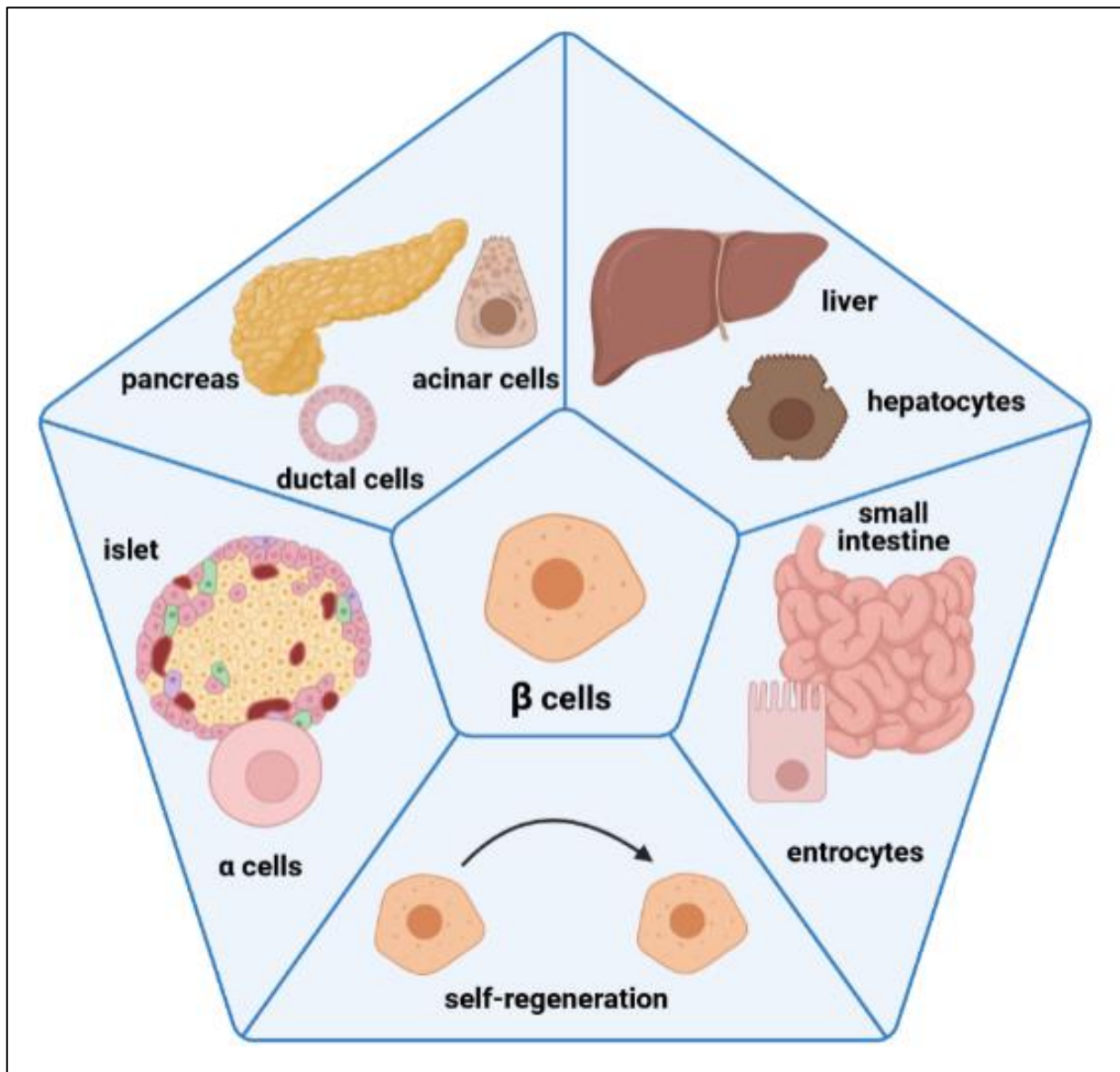


Figure 3: Generating β -like cells from adult somatic cells by inducing trans-differentiation. In particular, β -like cells can be generated from different adult somatic cells such as hepatocytes, enterocytes, α cells, ductal cells, acinar cells, or by self-regeneration of pre-existing β cells. Up or down regulation of adult somatic cells causes trans-differentiation and leads to the formation of insulin positive cells with a β -like phenotype (Modified from G. Basile et al., 2019) (Created with BioRender).

Table 2: List of somatic cell types as candidates for regenerating new β cells within human and mouse. (Modified from G. Basile *et al.*, 2019)

Cell type	Treatment/modification	Species	Reference
Hepatocytes	Overexpression of Pdx1, NeuroD1, Ngn3, MafA/B	Mouse	90
Adult and fetal hepatocytes	Overexpression of Pdx-1	Human	91
Enterocytes	Overexpression of Pdx1, Ngn3, MafA - GLP1 treatment	Mouse	92
Enteroendocrine progenitors	Downregulation of FoxO1	Mouse	93
Enterocytes	Downregulation of FoxO1 - GLP1 treatment	Human	94
Acinar cells	Overexpression of Pdx1, Ngn3, MafA - treatment with cytokines, EGF or CNTF	Mouse	95
Acinar cells	Treatment with BMP-7	Human	96
Ductal cells	Transduction of Pdx1	Rat	97
Ductal cells	Treatment with cytokines	Mouse/human	98,99
α cells	Overexpression of Pax4 - downregulation of Arx and Dnmt1 - treatment with alloxan, PDL, or acinar damage	Mouse	100,101
α cells	Treatment with GABA, artemisinin	Mouse/human	102,103
α cells	Overexpression of Pdx-1 and MafA	Human	104–106

The pancreas in T1D usually has very few surviving β cells, so just enhancing sufficient replication of these remaining β -cells to reach a critical mass is a difficult and perhaps unreachable goal, even if the autoimmune destruction could be controlled.

Nevertheless, enhancing differentiation or regeneration of other cell within pancreas may have more potential to provide an increase in new β cells that could then replicate further to provide enough insulin to reverse diabetes. The cell types that can be used as a source for generating new β cells, including the mechanisms are presented in Figure 4.

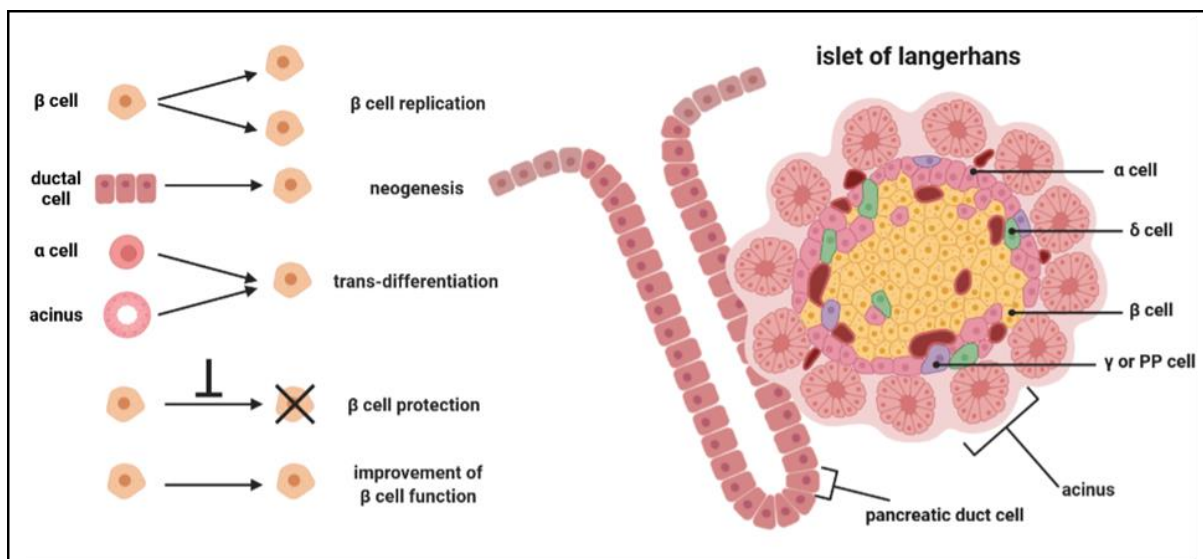


Figure 4: Drawing of cell replacement in human islets. Several mechanisms could be applied on different cell types within human body in order to increase the amount of β cells in T1D patients. (created with BioRender). (Modified from Dr. Cord Dohrmann)

1.2. 3D cell culture

Three-dimensional (3D) cell culture is a method that allows cells to grow and interact with surrounding extracellular network and other cells in three dimensions.^{107–109} 3D cell culture provides an effective platform for further identification of the biological characteristics of cells (especially tumor cells), particularly in the drug discovery area.^{108,110} At the same time, 3D cell culture improves our knowledge about cell dynamics in *in vivo*-mimicking conditions and plays an important role in understanding cell biology, organ function, neuroscience, regenerative medicine, and disease model.^{109,111,112} 3D cell culture leads to the creation of more predictive biomimetic tissue models, which are physiologically more relevant and predictive than 2D cultures, in which cells are grown in a flat monolayer on a plate.¹¹³ In traditional 2D cell culture, cells are cultivated on the hard plastic or glass dishes or flasks for growing.¹¹⁴ In contrast, cells have constant interactions with extracellular matrix proteins (ECM) and naturally grow and differentiate in 3D environments inside the body.¹¹⁵ In fact, most of these interactions are lost, or significantly reduced, in 2D cell culture.¹¹⁶ In the last two decades, due to the realization of the limitations of 2D cell culture, the use of different 3D cell cultures such as spheroids, organoids, and tissue engineering via 3D bioprinting have been implemented.¹¹² Advanced 3D cell culture allows researchers to bridge the gap between classical 2D cell culture and *in vivo* animal models.¹⁰⁹

Improving 3D cell culture to accurately replicate the physiological environment, plays a significant role in providing more meaningful scientific conclusions.^{117,118} 3D cell culture is a suitable method to study cell biology, since 3D environment allows cells to interact with surrounding matrix at all three dimensions, which provides more contact space and stimulation input.¹¹⁹ This feature plays a fundamental role in achieving an *in vivo*-like cellular function.¹²⁰ In this method, cells are capable of closely resemble *in vivo* cellular communication. As a result, cell behaviors are totally different from those cultured in 2D cell culture environment.^{108,121,122} Moreover, it has been revealed that, in contrast to monolayer culture, the lifespan of cells is substantially extended in 3D compare to 2D cell culture, suggesting the potential for conducting long-term investigation of cell growth and effects of drugs.¹²³ Significantly modification of signaling transduction and gene expression apart from morphological changes have reported in cells cultured in 3D.^{119,124} Currently, a variety of 3D cell culture methods have created excellent experimental tool for researchers and are counted as a perfect alternative to the animal models.¹¹⁶ 3D cell culture can significantly *reduce* or replace the use of laboratory animals.¹⁰⁹

However, cells in 3D culture, especially spheroids, also experience a limited diffusion of nutrients, oxygen, hormones, effector proteins such as growth factor and enzymes, as well as removal of cellular wastes and carbon dioxide (CO₂) into the culture medium, which is critical for the establishment of tissue scale.^{112,120,125–127} As a result, large spheroids (>500 μm in diameter) are characterized by an external proliferating zone, an internal quiescent zone and central necrotic zone, caused by physiochemical gradients, which resembles the cellular heterogeneity of *in vivo* solid tumors.^{112,128} To comparison more efficiently, differences between 2D and 3D cell culture are listed in Table 3.

Table 3: Primary differences between 2D and 3D cell culture:

2D cell culture	3D cell culture	Reference
Supraphysiological mechanical signals caused by high stiff surfaces / stiffness of surfaces	Tunable, relatively low stiffness of environment closer to that of tissues	109,111,112
Continuous, flat surface available for unencumbered adhesion, spreading, and migration	Nano- and micro-scale 3D surfaces provided by ECM fibers and guided and hindered cell motility by matrix porosity	107,115
delivering the same amount of nutrients and growth factors to all cells	Unequal share of nutrients and growth factors amongst cells	107,114,119
Less resistance to drug treatments by cells	More resistance to drug treatments by cells	115
Soluble gradients absent without microfluidics	Gradients of soluble factors, nutrients, and oxygen based on diffusion through gel or cell aggregations	112,128
morphogenesis constraints and dominated cell-substrate interactions by 2D geometry	Free self-organization and dominated cell-cell interactions in multicellular 3D structures	129
Poor cell differentiation	Well differentiated cells	130,131
Highly replicable and easily interpretable	Possible difficulty in replication and data interpretation	107,108,132
Automatic apical-basal Polarization	Self-generated apical-basal polarization by embedded cells	133

1.2.1. Techniques for generating 3D cell culture

Even with all these advances, 3D cell culture still is unable to fully recapitulate the natural environment of cells, because the cells are in close contact with ECM in the body.¹²⁰ On account of this, researchers have begun to investigate how embedding cells within 3D hydrogels impacted cell behavior and phenotype and have been improving 3D cell culture generation.⁸⁶

In general, 3D cell culture can be broadly divided into two main categories: scaffold-based or scaffold-free methods.^{117,118,134}

- Scaffold-based methods use animal derived or synthetic materials like hydrogels or structural 3D scaffolds as a support for seeding cells to aggregate, proliferate, and migrate, for generating a 3D structure.¹²⁹
- Scaffold-free methods rely on encouraging the self-aggregation of cells via specialized culture plates or physical parameters to prevent cell attachment.¹²⁰

Two of the most prominent 3D cellular structures used are organoids (most frequently grown in scaffold-based systems), and spheroids (grown in scaffold-free systems).^{107,121} Understanding the key differences between the two methods allows to select the most suitable method. Scaffold-free methods are often preferred, since they contain no exogenous components, which could interfere with the experiment by blocking drug or growth factor delivery.¹¹⁸ On the other hand, inconsistency in size of the samples has frequently reported in scaffold-free methods, and some cell types do not aggregate at all without a scaffold present.^{135,136} Scaffold-based methods offer greater control over design and architecture of the forming microstructure.¹³³ It's important to note that, the scaffold itself can absorb the test compound, which needs to be taken into account in pharmacology studies.¹³⁷

The most common hydrogels used in scaffold-based methods that have reported to be compatible with human cells are alginate, matrigel and Cultrex™ basement membrane extract (BME2). Alginate has been well studied for encapsulation of various cell types such as neural stem cells and is one of the best candidates for 3D cell culture.¹³⁶ Matrigel is a basement membrane protein solution, obtained from mouse sarcoma cells. It contains approximately 1,000 different proteins, but is mainly composed of laminin, collagen IV, and entactin.¹³⁸ Matrigel forms a viscous liquid at cold temperatures (<8 °C), solidifies rapidly after a short

incubation at room temperature (RT) and forms a hydrogel.¹¹⁵ Matrigel is suitable for the culture of embryonic stem cells (ESCs).¹³⁹ The cultrex[®] basement membrane extract-2 (BME-2) is a soluble form of basement membrane purified from Engelbreth-Holm-Swarm (EHS) tumor.¹⁴⁰ BME-2 undergoes gelation at 37 °C and forms a reconstituted basement membrane.¹⁰⁸ The major components of BME-2 include laminin, collagen IV, entactin, and heparan sulfate proteoglycan.¹⁴¹

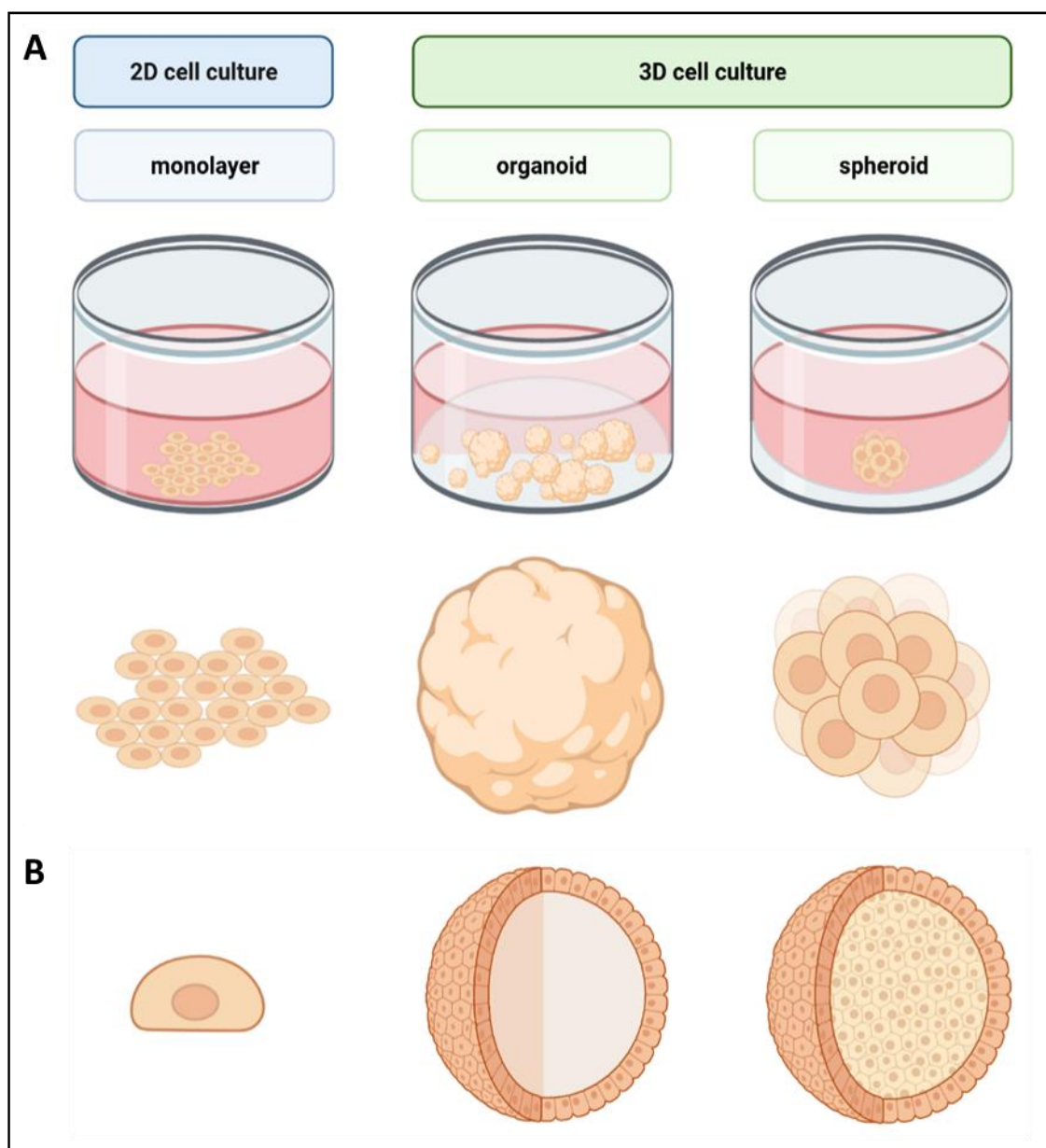


Figure 5: Schematic illustration of 2D and 3D cell culture. A: Traditional 2D monolayer cell culture and 3D cell culture systems; B: The structure of 3D spheroid with different zones of cells with the models of oxygenation, nutrition, and CO₂ removal. 3D spheroid from inside to outside. The regions are necrotic zone (innermost), quiescent viable cell zone (middle), and proliferating zone (outermost). (according to Nipha Chaicharoenaudomrung et al., 2019) (created with BioRender).

Difficulties in development of new anticancer drugs and *in vitro* tissue modeling have raised a necessity to generate a new cell culture method.^{108,142} High-throughput systems based on monolayer cell cultures are widely used to test new anticancer drugs, however the similarity to *in vivo* model and the prediction value of the monolayer are limited significantly and negatively affects the efficacy of drugs and development of tumor resistance mechanisms.^{108,115} Tumor spheroids can recapitulate most of the properties of solid tumors like the establishment of penetration barriers, the accumulation of non-proliferating or necrotic cell populations in center.¹⁴³ Therefore, tumor spheroids are the best choice for the development of drug resistance and to improve the *in vivo* predictability of new cancer drugs.¹²⁵

Various culture techniques are used to generate spheroid.¹³⁰ One of the most common methods is called liquid-overlay technique (LOT).¹⁴⁴ In this technique, trypsinized cells are placed on dishes covered with a thin layer of agarose. The coating prevents cell attachment to the dish, therefore cells could aggregate, grow in a 3D structure and form spheroid.^{112,117,145} Cultivation in spinner and gyratory bioreactors are used frequently to produce high-throughput samples. Trypsinized cells are placed in a culture vessel with a magnetic stirrer inhibiting cell attachment to the substrate and improve cell-cell adhesion.^{141,146} Alternatively, spheroids are grown in a hanging drop deposited on a microplate lid. The cells start to aggregate due to the gravity.^{110,142} Despite all these advantages, these techniques are limited by long-time cultivation, formation of unequal-size spheroids, or difficult mechanical accessibility.^{147,148} However, the standardization of a protocol working for large variety of tumor cell lines to rapidly generate high-throughput spheroid with homogenous size in a plate format accessible to subsequent analysis is still a challenge.^{86,149}

Several further tools are needed to achieve drug screening in 3D cell culture, including advanced light microscopes for measurement of drugs or antibody permeation into spheroids and to monitor respiratory activity, cell viability and further physiological alterations of spheroid detected with suitable biosensors.^{108,150,151}

1.2.2. Applications of 3D cell culture

Beyond fundamental cell biology, 3D cell cultures represent effective platforms for accomplishing wide range of applications in the field of biomedical engineering, tissue engineering and drug discovery.^{122,152} Drug discovery and tissue engineering benefit from the

capacity of 3D cell culture in providing more physiological relevant information and more predictive data for *in vivo* tests.¹⁰⁸ Additionally, 3D cell culture contains biological ECM. ECM is strongly contributive to the cell dynamics, because of this, it provides reliable results of cell metabolism, which would be advantageous for various applications such as investigation of tumor models.^{117,120}

1.2.2.1. Construction for tissue model system

3D hydrogel matrix gives cells the opportunity to grow into clusters then forming spheroids, which are self-assembling cell colonies.¹¹⁶ Spheroids resemble *in vivo* tissue since they effectively realize cellular communication and develop their own ECM. Moreover, they enable cell migration, differentiation, survival, growth, as well as cell polarization.¹¹⁹ Tissue-like gradients of oxygen, carbon dioxide, nutrients, and waste make spheroid an excellent model for mimicking solid tissues, not vascularized tumors, and early embryos which are applicable to tumor therapy and stem cell research.^{110,153}

It should be noted that, the possibility of co-culturing multi-type of cells in a spheroid form, has made it popular for investigation of tissue function, formation, cell-cell communication, and tumor growth.^{123,154,155}

1.2.2.2. Construction for drug testing

3D cell culture has presented researchers a tool to culture cells in *in vitro* environments much similar to their natural cellular environments, making it so attractive for drug testing and screening.^{110,115,116} 3D cell culture plays a critical role in investigation of cell-drug interaction and screening potential drug candidates, which implies significant challenges for pharmacological applications.¹⁵⁶

1.2.3. Current challenges in 3D cell culture

As discussed in the previous section, despite developments and improvements in 3D cell culture, several critical issues remains challenging.¹⁵⁷ Among the different cues experienced by cells moving from 2D to 3D cultures, the mechanical environment is surely one of the factors with the largest influence on the cell's phenotype.^{123,158} One challenge of 3D cell cultures is to find the most appropriate hydrogel system compatible for the desired cell model and application.¹⁵⁹ The hydrogels influence cell differentiation, cell-matrix interaction, and promotion of cell spreading and migration.^{136,160} However, most of the 3D matrix

compositions do not fully satisfy the *in vivo* structural or functional requirements. Blood vessel-like vascular system formation in 3D biological matrix for nutrient delivery which is critically important for 3D cell culture and tissue engineering represents another challenge in 3D cell culture.^{161–163} The formation of hierarchical microvascular networks similar to capillary density and connection of microvascular networks with other vessels has not yet been achieved.^{107,164,165} Beside this, other challenges such as cultivation of multiple cell types mimicking the tissue-specific architecture of cell-cell interaction, inducing stem cell differentiation into different cell types, and *in vivo* like cell arrangement within spheroids are poorly solved.^{112,113,132,166} Solving these key challenges is fundamental to fully understand cell dynamics, tissue modeling, and drug screening as well as stepping toward recapitulating 3D cell culture instead of laboratory animals and construction of artificial transplantable organs.

1.2.4. Common forms of 3D cell culture

Organoids and spheroids are the most widespread three-dimensional cultures.^{108,130} Spheroids are mostly generated from cancer cell lines or tumor biopsies through scaffold-free methods (liquid over-layer or hanging drop) based on cell aggregation in ultra-low attachment plates.^{107,167,168} On the other hand, organoids are derived from stem cells embedded in animal-derived or synthetic hydrogels such as matrigel or BME-2.^{86,169}

1.2.4.1. Organoids

Organoids consist of organ-specific cells, such as pancreas, stomach, brain, lungs, prostate, liver, bladder.^{170,171} Organoids are composed by primary or progenitor cells, embryonic stem cells (ESCs), and induced pluripotent stem cells (iPSCs) that mimic the behavior of human tissue.^{172,173} They often rely on artificial ECM, like Matrigel or BME-2, to promote their self-organization.^{139,141} Organoids have the capacity to grow under an *in vivo* condition owing to their self-renewal/self-assemble capacity. When given a scaffolding extracellular

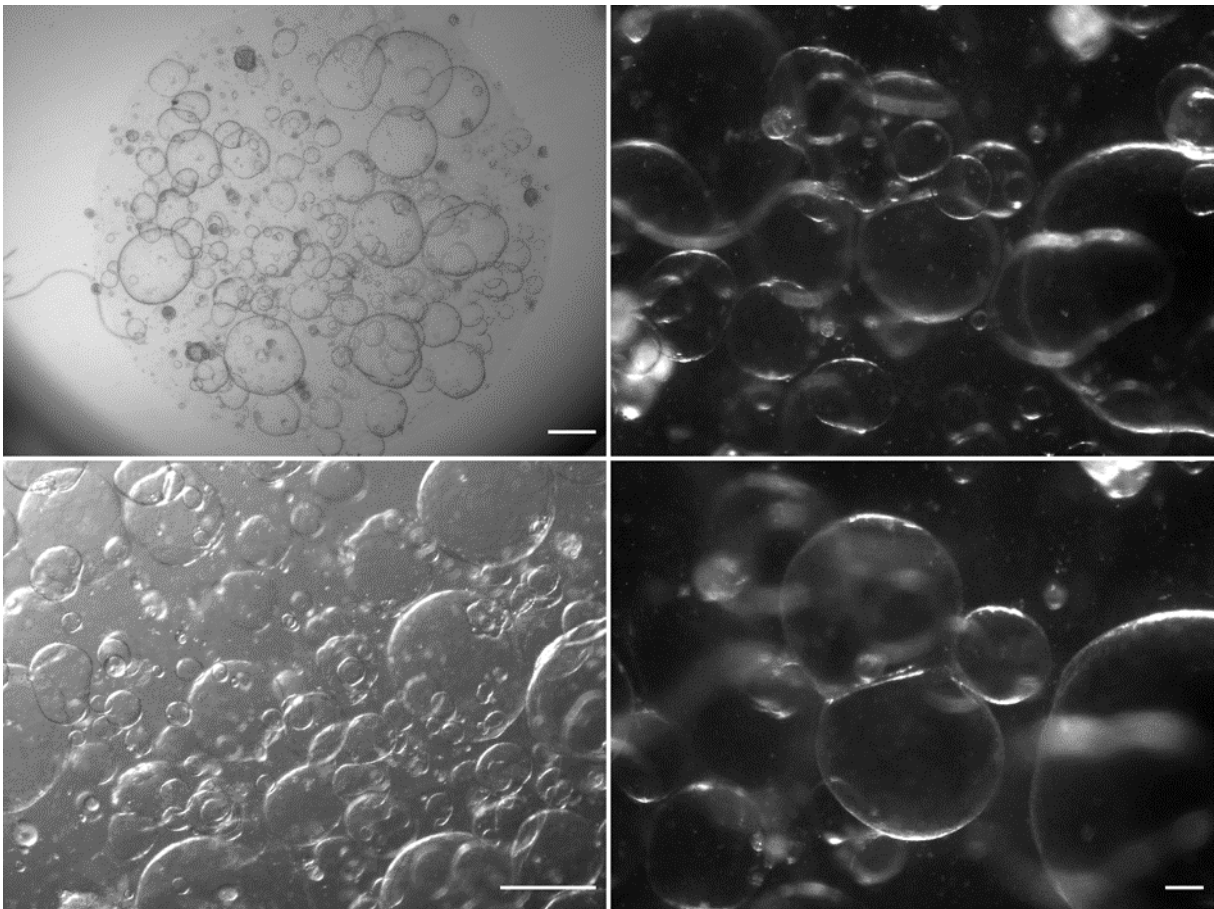


Figure 6: Human pancreatic organoids (hPOs) in expansion medium. hPOs are 3D cell structures consist of progenitor cells that form bubble-like structures in different sizes within the BME2. The bright field images were processed using Zeiss SteREO Discovery.V8 with 2x and 8x magnification; scale bar: 500 μ m.

environment, they form a 3D structure that presents a similar organization and functionality as an organ.⁶ Organoids are a long-term culture system, which means both normal and diseased cells need a long culture time to develop in 3D conditions (in the range of 10 days). Not only do organoids maintain cell population but also cell type composition and tissue structure are preserved.¹⁷⁴ Additionally, organoids can be generated from diseased tissues other than cancer cells including cystic fibrosis and liver disorders such as α 1-antitrypsin deficiency and Alagille syndrome.^{175–177} Moreover, deriving organoids from a variety of stem cell types which provide a heterogeneous culture of stem cells and differentiated progeny, turns them into living biobanks of tissues.¹⁷⁸ Organoids are widely used to mimic disease pathology and eventually effective identification for personalized treatments.^{128,158,179} Moreover, organoids are useful for studying signal pathways, cancer drugs responses, and tissue functions.^{180,181} It is noteworthy to mention, organoids present physiologically relevant original organ, therefore they are applied in development, disease modelling regenerative medicine, and drug discovery (Figure 6).^{170,182}

1.2.4.2. Cellular spheroids

Spheroids are 3D cell structures generated by the self-aggregation of single cell type or multicellular co-culture of the cells under low-adhesion culture conditions such as agarose substrates.^{107,128,143} Immortalized tumor cell lines as well as primary cells, embryonic stem cells, hepatocytes, nervous cells, or mammary epithelial cells can form spheroids.¹¹⁷ Cell crosstalk in tissues is complex and have significant effect on cells' fate.⁴⁹ Spheroids mimic several physiological characteristics such as morphological features, cell growth and allows us to investigate the effect of cell-cell as well as cell-matrix interactions.^{136,144,183} Gene expression is significantly altered in cells grown as spheroids compared to monolayer cultures. One reason for this is that in 2D cell culture cells are uniformly exposed to equal medium concentrations, in contrast, this phenomenon is not presented in spheroid due to the multicellular structure and strong penetration gradient.^{88,184}

Multicellular tumor spheroids (MCTS) are powerful biological *in vitro* model that can mimic the microenvironment of tissues as a result are considered better models than 2D cell culture and used frequently for investigating tumor cell physiology and responding to therapeutic agents.^{145,150,167,185}

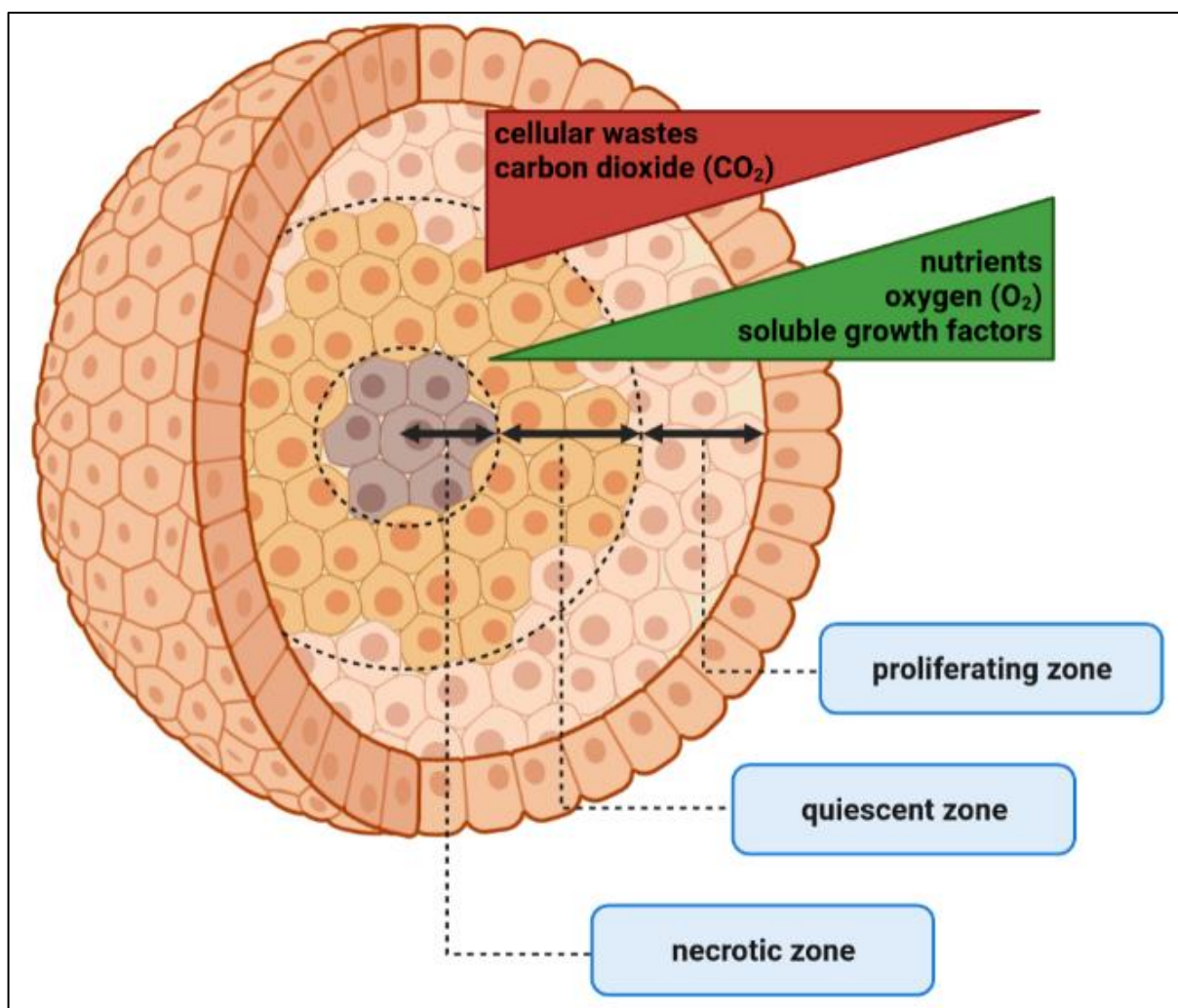


Figure 7: A presentation of 3D spheroid microregions and nutrient and waste gradients. The spherical geometry of the cells within the MCTS are characterized by an external proliferating region and an internal quiescent zone (caused by the gradient of nutrient and oxygen diffusion), which surrounds a necrotic core, mimicking the cellular heterogeneity observed in solid tumors (created with BioRender).

Multicellular tumor spheroids (MCTS) are routinely employed as 3D cell culture models since they capture some aspects of the 3D structure of primary not vascularized solid tumors. Large MCTS (>500 μm in diameter) contain multicellular layers in which the gradient of nutrients, oxygen and metabolic waste mimic important features of real tumors.^{128,150} (Figure 7). Additionally, MCTS can be generated in double or triple co-culture that presents tumor complexity respectively.¹⁶⁸

Spheroids have emerged as a powerful tool to narrow down the gap between the *in vitro* and *in vivo* model.¹⁰⁹ Even so, the widespread use of spheroids in research is limited by technical hurdles for their generation and handling.¹⁸⁷

1.2.4.3. What are the differences between organoids and spheroids?

3D cell culture has advanced in several directions and overcome many limitations of 2D cell culture, therefore have gained an increasing interest in recent decades.¹⁶⁰ Spheroids and organoids are both most frequently used in 3D cell cultures. Despite some remarkable similarities, there are fundamental differences between spheroids and organoids.¹⁸⁸ Unlike spheroids formed out of cancer cell lines or tumor biopsies, organoids contain tissue-specific stem cells, or progenitor cells from various organs.¹⁵⁶ In general, organoids have a remarkable proliferation and differentiation potential and can be expanded long-term *in vitro*. In contrast, long-term cultivation of spheroids is challenging, possibly due to the gradient of nutrients and metabolic waste and development of central necrotic core within spheroid through time.¹⁷⁸ Spheroids and organoids both contain multiple cell types, however their research fields are relatively different. Organoids have wide utility in organ development studies, personalized cell therapy, and disease modeling.¹³¹ Cellular spheroids are widely used in the cancer biology research, drug discovery research and toxicity testing. A clear recent trend is organoids replacing cellular spheroids also in the latter research fields^{178,189}

1.3. Microscopy

1.3.1. The importance of microscopy in biology

Many of the most important discoveries in modern biology would be impossible without the recent developments in microscopy.¹⁹⁰

Widefield microscopy: It is one of the most basic microscopy techniques and it refers to a basic illumination of the whole sample with intense light sources such as halogen, metal halide lamps or LED.¹⁹³ **Confocal laser scanning microscopy (CLSM):** During imaging, light is focused on a defined spot at a specific depth within the sample. The out-of-focus light is excluded by inserting a pinhole aperture. Confocal microscopy offers several advantages such as improving the resolution and elimination or reduction of background information by removing^{194–196}. **Light sheet fluorescence microscopy (LSFM):** It is an intermediate-to-high optical resolution microscope that uses a laser light sheet to optically section the sample. In this type of microscope, the illumination and detection are placed separately and orthogonally with each other, meaning that the detection objective lens is set up perpendicularly to the optical path of the laser light sheet.¹⁹⁷ This microscope provides high-speed imaging and it is

optimally suited for the time-lapse imaging with minimized bleaching and phototoxicity within samples.^{198–200}

1.3.2. 3D cell cultures require specific microscopes for imaging

3D cell cultures are relatively opaque, thick and strongly scatter light. For these reasons, 3D cell cultures are challenging specimens for light microscopy. In many cases, detailed information about the inner region of the samples would be missed.²⁰⁸ Nevertheless, modern confocal laser scanning microscopes and light sheet fluorescence microscopes allows to deeper penetrate in large samples and provide a detailed visualization of the morphology and spatial distribution of cellular structures within 3D specimens.¹⁹⁷ Applying new microscopes answer the needs to study the complexities of cell–matrix interactions within 3D cell culture systems. They have improved the illumination to increase resolution, capture in-depth and high quality images, reveal new information about cell behavior and function in advanced biomaterials that previously has been difficult or impossible to measure.^{209–212}

1.3.3. Advantages and disadvantages of imaging 3D specimens

Reconstruction of *in vivo* environment and determining the cross-effect between the cell organization and cell function are the fundamental goals of the researchers. To achieve these goals, a better understanding of organelle composition is needed. 3D cell culture represents a dramatic step forward as their innate ability is to replicate *in vivo* environment of a cell in *in vitro*. Therefore, researchers have been trying hard to apply the most optimized imaging methods to assess physiological and phenotypical details.

Imaging 3D specimens can be interactive, allowing the viewer to gather information from cellular interactions within the 3D microenvironment and the large-scale manufacture of cells. 3D imaging is highly effective at revealing internal and external cellular structures in organisms representing the known phylogenetic diversity. Although it has taken quite a long time to gain representable 3D imaging and several professional image processing are needed, it is an accepted and trustworthy approach for cellular visualization. As mentioned previously, one of the well-known limitations of 3D cell culture remains with the challenges in image processing. 3D image processing is time-consuming and requires powerful processing units and software. In addition, 3D cell culture is commonly very thick and opaque, at least a few hundred micrometers, therefore, extra preprocessing techniques such as tissue optical clearing (TOC) are required.

1.3.3.1. Tissue optical clearing (TOC)

The 3D cell culture (organoids and spheroids) has been receiving great attention from the researchers in recent decades since they are capable of resembling human tissues in *in vivo* and minimizing the utilization of laboratory animals. Despite all these privileges new challenges in 3D imaging has appeared. Because of the opaqueness of 3D cell cultures, it is harder to obtain sharp images with high clarity by standard imaging reagents and techniques. To overcome this challenge, tissue optical clearing (TOC) is required. TOC vary greatly in complexity in terms of applicability, duration, and cost, but all target the same. A fluorescently labeled thick specimen must be “cleared/become transparent” to increase light depth penetration, reduce light scattering and facilitate 3D imaging. Light scattering is caused by the various refractive indices (RIs) between surrounding medium and specimen layers. The refractive indices within specimen changes according to the biomolecular composition of each layer. The simplest way to obtain equivalent transparency is to compensate the refractive index of the surrounding medium to the highest refractive index (i.e., lipids). This is obtained by replacing extracellular water with solutions of high refractive indices (RIs). Either water-based agents such as denaturants and detergents or organic solvents are used to perform TOC. What is notable here is, some TOC carry out hazardous chemicals that can harm the morphology of specimen due to the dehydration and affect the propagation of light during imaging, therefore makes them less attractive.

TOC is very proficient, since it gives the researchers the possibility to study objects in very large and complicated samples such as thick slabs of tissue or 3D cell cultures (organoids or spheroids). Performing very large samples are not the only benefits of TOC. There are many interesting biological problems that can be modeled in samples with sizes in order of a few hundred microns. Incorporating TOC with standard immunostaining protocols would open the door to observation of the cellular structures of transparent and light-permitting specimens. This could have a dramatic and immediate impact on many fields and does not require any specialized equipment.

1.4. Aim of this thesis

The goal of this thesis is investigating the influence of cell aggregation, cell compaction and spheroid formation on the endocrine differentiation of human pancreas progenitor cells. To this aim, first a technique to generate spheroids from human pancreatic progenitor cells organoids (hPO) using liquid overlay technique (LOT) was established. Next, co-cultures of hPOs cells with hMSC and HDMEC has been performed to determine the effect of mesenchymal and endothelial cells on the differentiation of the progenitor cells to functional insulin-releasing cells *in vitro*. The phenotypical changes of the pancreas progenitor spheroids at multiple size scales were investigated by immunofluorescence microscopy. To quantify phenotypical changes, nuclei segmentation and volume measurement were performed

Cultivation in both proliferation and differentiation media of the hPO spheroids was performed can inhibit and stimulate different signaling pathways and co-culture application in spheroid increase cell-cell interaction and develop diffusion barriers, which is leading to impact proliferation and cell survival. Furthermore, one of the concerns of this study was to investigate the changes in expression of pancreatic differentiation related genes, along with cell polarization in hPO-derived spheroids.

Understanding the effect of 3D structures will improve our knowledge about hPOs cell-cell interaction and suggest strategies to induce differentiation in pancreas progenitor cells leading to the generation of β cells. Our results could be evaluated as cellular therapeutics for T1D.

2. Materials and Methods

2.1. Materials

2.1.1. Chemicals

Table 4: List of chemicals used in this study, including supplier

Chemicals	Supplier	Article no.
2,2',2''-nitrilotriethanol (Triethanolamine)	Sigma-Aldrich, Steinheim, Germany	90279-500ml
A83-01	Tocris Bioscience, Minneapolis, Minnesota, United States	2939
Accutase™ Cell Dissociation Reagent	Gibco™, ThermoFisher Scientific, Waltham, MA, United States	A1110501
Agarose, low melt	VWR, Radnor, PA, United States	35-1020
Albumin Fraction V (BSA)	Carl Roth GmbH & Co. KG, Karlsruhe, Germany	8076.4
B-27 minus vitamin A	Gibco™, ThermoFisher Scientific, Waltham, MA, United States	12587-010
cDNA synthesis kit	ThermoFisher Scientific, Waltham, MA, United States	K1671
Cell Recovery Solution	Corning®, Corning, New York, United States	734-0107P
CellTracker Green CMFDA	Gibco™, ThermoFisher Scientific, Waltham, MA, United States	C2925
CellTracker™ Orange CMTMR	Gibco™, ThermoFisher Scientific, Waltham, MA, United States	C2927
Chloroform, ACS	MP Biomedicals, Santa Ana, CA, United States	193814
Click-iT™ EdU Cell Proliferation Kit, Alexa Fluor™ 488 dye	ThermoFisher Scientific, Waltham, MA, United States	C10337
Cultrex RGF BME, type 2	R&D systems, Rocky Hill, New Jersey, United States	3533-005-02
DAPT	Tocris Bioscience, Minneapolis, Minnesota, United States	2634-10mg
Dimethyl sulfoxide (DMSO)	Carl Roth GmbH & Co. KG, Karlsruhe, Germany	A994.1
DMEM (1x)	Gibco™, ThermoFisher Scientific, Waltham, MA, United States	31053-028
Donkey serum (normal)	Millipore Sigma, St. Louis, MO, United States	S30-100m
Endothelial Cell Growth Medium 2	Promocell, Heidelberg, Germany	C-22020
Endothelial Cell Growth Supplement	Promocell, Heidelberg, Germany	C-39225

Ethanol	Carl Roth GmbH & Co. KG, Karlsruhe, Germany	P075.2
Ethanol, for molecular biology	Fisher Bioreagents, Pittsburgh, PA, United States	BP2818-500
Ethylenediaminetetraacetic acid (EDTA)	Carl Roth GmbH & Co. KG, Karlsruhe, Germany	8043.1
Fibroblast growth factor 10 (FGF-10)	PeproTech, Rocky Hill, New Jersey, United States	100-26-500ug
Forskolin	Tocris Bioscience, Minneapolis, Minnesota, United States	1099
GlutaMax	Gibco™, ThermoFisher Scientific, Waltham, MA, United States	35050038
Goat serum	Life Technologies, Darmstadt, Germany	G9023
Hellmanex® III	Hellma, Nürnberg, Germany	9-307-011-4-507
HEPES	Gibco™, ThermoFisher Scientific, Waltham, MA, United States	1 5630-056
Human [Leu15]-Gastrin I	Millipore Sigma, St. Louis, MO, United States	G9145
Mesenchymal Stem Cell Growth Medium 2	Promocell, Heidelberg, Germany	C-28009
Mesenchymal Stem Cell Growth Supplement	Promocell, Heidelberg, Germany	C-39809
Milk powder	Carl Roth GmbH & Co. KG, Karlsruhe, Germany	T145
Milli Q H ₂ O	-	-
MitoTracker® Deep Red FM	Gibco™, ThermoFisher Scientific, Waltham, MA, United States	M22426
N-2	Gibco™, ThermoFisher Scientific, Waltham, MA, United States	17502-048
N-acetylcysteine	Millipore Sigma, St. Louis, MO, United States	A9165-5g
Paraformaldehyde (PFA)	Millipore Sigma, St. Louis, MO, United States	P6148
Penicillin/ Streptomycin (P/S)	Gibco™, ThermoFisher Scientific, Waltham, MA, United States	15140-122
PGE-2	Tocris Bioscience, Minneapolis, Minnesota, United States	2296
Phosphate buffered saline (PBS), pH 7.4	Gibco™, ThermoFisher Scientific, Waltham, MA, United States	10010-015
Propan-2-ol	Honeywell, Muskegon, MI, United States	33539-1L
qPCR MasterMix	ThermoFisher Scientific, Waltham, MA, United States	A46109
Recombinant human epithelial growth factor (hEGF)	PeproTech, Rocky Hill, New Jersey, United States	AF-100-15-1mg
Recombinant human Noggin	PeproTech, Rocky Hill, New Jersey, United States	120-10C-20ug
Recombinant human R-spondin (rhR-spondin)	PeproTech, Rocky Hill, New Jersey, United States	120-38-500ug

Recovery™ - Cell culture freezing medium	Gibco™, ThermoFisher Scientific, Waltham, MA, United States	12648-010
Sucrose	Carl Roth GmbH & Co. KG, Karlsruhe, Germany	4621
Triton-X 100	Millipore Sigma, St. Louis, MO, United States	T8787
TripLE	ThermoFisher Scientific, Waltham, MA, United States	12605010
TRIzol	ThermoFisher Scientific, Waltham, MA, United States	15596026
Trypan blue	Sigma-Aldrich, Steinheim, Germany	T8154-20ML
Tween-20	Carl Roth GmbH & Co. KG, Karlsruhe, Germany	9127.1
Ultrapure™ Distilled DNase/RNase Water	Gibco™, ThermoFisher Scientific, Waltham, MA, United States	10977-035
Urea	Sigma-Aldrich, Steinheim, Germany	U1250
Y-27632	R&D systems, Rocky Hill, New Jersey, United States	1254.1

Furthermore, aliquot components, which are not listed above, were prepared by the members of Stelzer lab, Buchmann Institute For Molecular Life Sciences (BMLS), Goethe University Frankfurt, DE.

2.1.2. Buffers and Solutions

Table 5: The composition of buffers and solutions used in this study

Types	Composition
Blocking solution	0.1 % BSA, 0.3 % triton X-100, 10 % fresh goat/donkey serum in PBS
Coating solution	1 % BSA in PBS
Fixative solution	4 % [w/v] Paraformaldehyde
PBS + P/S	2 % Pen-Strep in PBS
Permeabilization solution	0.3 % triton X-100 in PBS
CUBIC2	50 wt % Sucrose, 25 wt % Urea, 10 wt % 2,2',2''-nitrilotriethanol (Triethanolamine) in H ₂ O

2.1.3 Cell line

Table 6: Information about cell lines used in this study

Name	Cell type	Organism	Tissue	Lot number	Age	Gender
Human Pancreatic Organoid (hPO) primary	Organoid	<i>Homo sapiens</i> , human	Pancreas duct	1805	63	Female
Human Dermal Microvascular Endothelial Cells (HDMEC)	Endothelial cells	<i>Homo sapiens</i> , human	Dermis of juvenile foreskin	C-12260	2	Male
Human Mesenchymal Stem Cells (hMSC)	Stem cells	<i>Homo sapiens</i> , human	Bone marrow	438Z012.1	61	Male

2.1.4 Culture Medium

Table 7: The composition of medium for 2D and 3D cultivation used in this study

Materials	Concentration	Final concentration
Basal medium	485 ml advanced DMEM/F12	
	5 ml 1 M HEPES	10 mM
	5 ml PenStrep	1 %
	5 ml 100x GlutaMax	1x
Human stock medium (2x)	9.4 ml basal medium	
	400 µl 50x B27	2x
	200 µl 100x N-2	2x
	50 µl N-acetylcystein	2.5 mM
Human expansion medium with recombinant R-spondin (EM)	5 ml basal medium	
	5 ml human stock medium	1x
	10 µl recombinant R-spondin	1 µg/ml
	100 µl nicotinamide	10 mM
	10 µl hEGF	50 ng/ml
	10 µl FGF-10	100 ng/ml
	10 µl Noggin	25 ng/ml
	10 µl Gastrin	10 nM
	10 µl A83-01	5 µM
	10 µl Forskolin	10 µM
3 µl PGE-2	3 µM	

Human expansion medium 2 (EM2)	5 ml basal medium	
	5 ml human stock medium	1x
	10 µl recombinant R-spondin	1 µg/ml
	10 µl hEGF	50 ng/ml
	10 µl A83-01	100 ng/ml
	3 µl PGE-2	25 ng/ml
Human differentiation medium (DM)	5 ml basal medium	
	5 ml human stock medium	1x
	2 µl DAPT	2 µM
Human endothelial cells growth medium	472.8 ml Endothelial Cell Growth Medium	
	27.2 ml Endothelial Cell Growth Supplement	5x
Human mesenchymal stem cells	450 ml Mesenchymal Stem Cell Growth Medium 2	
	50 ml Mesenchymal Stem Cell Growth Supplement	10x

2.1.5 List of primers for RT-qPCR used in this study

Table 8: List of primers for RT-qPCR

Primer	Sequence	Derived from	Supplier
hRPL13_FW	AAGATCCGCAGACGTAAGGC	NCBI	biomers.net GmbH, Ulm, Germany
hRPL13_RV	GGACTCCGTGGACTTGTTCC	NCBI	biomers.net GmbH, Ulm, Germany
hTBP_FW	TAAGAGAGCCACGAACCACG	NCBI	biomers.net GmbH, Ulm, Germany
hTBP_RV	TTGTTGGTGGGTGAGCACA	NCBI	biomers.net GmbH, Ulm, Germany
hINS_FW	AAGAGGCCATCAAGCAGATCA	Georgakopoulos et al., 2020	biomers.net GmbH, Ulm, Germany
hINS_RV	CAGGAGGCGCATCCACA	Georgakopoulos et al., 2020	biomers.net GmbH, Ulm, Germany
hKRT19_FW	CGCGGCGTATCCGTGTCCTC	Georgakopoulos et al., 2020	biomers.net GmbH, Ulm, Germany
hKRT19_RV	AGCCTGTTCCGTCTCAAACCTGGT	Georgakopoulos et al., 2020	biomers.net GmbH, Ulm, Germany
hLGR5_FW	ACCAGACTATGCCTTTGGAAAC	8810200832-000150	MilliporeSigma, St. Louis, MO, United States

hLGR5_RV	TTCCCAGGGAGTGGATTCTAT	8810200832-000160	MilliporeSigma, St. Louis, MO, United States
hNGN3_FW	CCGGTAGAAAGGATGACGCC	NCBI	biomers.net GmbH, Ulm, Germany
hNGN3_RW	GGTCACTTCGTCTTCCGAGG	NCBI	biomers.net GmbH, Ulm, Germany
hNKX6-_FW	CTCGTTTGGCCTATTCGTTG	8810200832-000190	MilliporeSigma, St. Louis, MO, nited States
hNKX6-_RW	TCTGTCTCCGAGTCCTGCTT	8810200832-000200	MilliporeSigma, St. Louis, MO, United States
hPDX1_FW	AGCTGCCTTTCCCATGGAT	8810200832-000170	MilliporeSigma, St. Louis, MO, United States
hPDX1_RW	GTTCAACATGACAGCCAGCT	8810200832-000180	MilliporeSigma, St. Louis, MO, United States
hSOX9_FW	TACCCGCACTTGCACAAC	8810200832-000110	MilliporeSigma, St. Louis, MO, United States
hSOX9_RW	TCTCGCTCTCGTTCAGAAGTC	8810200832-000120	MilliporeSigma, St. Louis, MO, United States
hCHGA_FW	ACACACTTTCCAAGCCCAGC	NCBI	biomers.net GmbH, Ulm, Germany
hCHGA_RW	GCCTCCTTGGAAATCCTCTCTT	NCBI	biomers.net GmbH, Ulm, Germany
hCHGB_FW	CTCCGACAGCCAAGTCTCTG	NCBI	biomers.net GmbH, Ulm, Germany
hCHGB_RW	GCATGTGTTTCCGATCTGGC	NCBI	biomers.net GmbH, Ulm, Germany
hVIM_FW	AAATGGCTCGTCACCTTCGT	NCBI	biomers.net GmbH, Ulm, Germany
hVIM_RW	TTGCGCTCCTGAAAACTGC	NCBI	biomers.net GmbH, Ulm, Germany
hCDH2_FW	GATGAAAGACCCATCCACGC	NCBI	biomers.net GmbH, Ulm, Germany
hCDH2_RW	TGCTCACCACCACTACTTGAG	NCBI	biomers.net GmbH, Ulm, Germany
hEPCAM_FW	GCTGGCCGTAAACTGCTTTG	Dossena et al., 2020	biomers.net GmbH, Ulm, Germany
hEPCAM_RW	ATCATTGTTCTGGAGGGCCC	Dossena et al., 2020	biomers.net GmbH, Ulm, Germany

2.1.6 Antibodies

Table 9: Primary antibodies used in this study

Primary antibody	Lot number	Host	Dilution	Supplier
α -CD31	ab24590	Mouse	1:100	Abcam, Cambridge, United Kingdom
α -E-cadherin	3195	Rabbit	1:100	Cell Signaling Technologies, Danvers, MA, United States
α -Insulin	I2018	Mouse	1:100	MilliporeSigma, St. Louis, MO, United States
α -Krt19	STJ24355	Rabbit	1:100	St John's Laboratory Ltd, London, United Kingdom
α -N-cadherin	13116	Rabbit	1:100	Cell Signaling Technologies, Danvers, MA, United States
α -Ngn3	ab38548	Rabbit	1:50	Abcam, Cambridge, United Kingdom
α -Pdx1	ab47383	Goat	1:50	Abcam, Cambridge, United Kingdom
α -Sox9	AB5535	Rabbit	1:50	MilliporeSigma, St. Louis, MO, United States
α -Vimentin	5741	Rabbit	1:100	Cell Signaling Technologies, Danvers, MA, United States

Table 10: Secondary antibodies used in this study

Secondary antibody	Species	Lot number	Dilution	Supplier
α -goat-AF488™	Donkey	A11055	1:400	Molecular Probes, ThermoFisher Scientific, Waltham, MA, United States
α -mouse-AF488™	Goat	A21131	1: 250	Molecular Probes, ThermoFisher Scientific, Waltham, MA, United States
α -mouse-AF568™	Donkey	A10037	1:400	Molecular Probes, ThermoFisher Scientific, Waltham, MA, United States
α -rabbit-AF488™	Goat	A11008	1:400	Molecular Probes, ThermoFisher Scientific, Waltham, MA, United States
α -rabbit-AF568™	Goat	A11011	1:400	Molecular Probes, ThermoFisher Scientific, Waltham, MA, United States

Table 11: Fluorescent dyes used in this study

Name	Article no.	Dilution	Supplier
DAPI (5 mg ml ⁻¹)	D1306	1: 200	Invitrogen™, ThermoFisher Scientific, Waltham, MA, United States
Fluorescein Diacetate (FDA)	F7378	1: 200	Millipore Sigma, St. Louis, MO, United States
Phalloidin-AF488™	A12379	1: 200	Molecular Probes, ThermoFisher Scientific, Waltham, MA, United States
Phalloidin-AF568™	A22283	1: 200	Molecular Probes, ThermoFisher Scientific, Waltham, MA, United States
Phalloidin-AF647™	A22287	1: 200	Molecular Probes, ThermoFisher Scientific, Waltham, MA, United States
Propidium iodide (PI)	P4170	1: 100	Millipore Sigma, St. Louis, MO, United States
Hoechst 33342	H1399	1: 500	Molecular Probes, ThermoFisher Scientific, Waltham, MA, United States

2.1.7 Microscopes

Table 12: Microscopes and corresponding objectives used in this study

Name	Types	Objectives	Camera
Zeiss SteREO	Discovery.V8	Plan Apo S, 0.63x FWD 81 mm	AxioCam ICc1 S/N 285872441
Zeiss CellObserver	Cell Observer	Plan-Apochromat 5x/0.16	AxioCam MR R3
Zeiss AxioObserver	LSM780	Plan-Apochromat 20x/0.8 M27	n/a
Zeiss AxioObserver	Z1	Detection: W Plan-Apochromat 20x/1.0 UV-VIS Illumination: Zeiss LSFM 10x/0.2	Zeiss 9713 400100-9010

Table 13: Fluorescent filters used in this study

Fluorescent filters set	microscopes	Excitation	Detection
PI	Cell Observer	538 – 562 nm	570 – 640 nm
AlexaFluor™ 488	Cell Observer	450 – 490 nm	500 – 550 nm
AlexaFluor™ 647	LSM780	633 nm	638 – 755 nm
AlexaFluor™ 568	LSM780	561 nm	568 – 644 nm
AlexaFluor™ 488	LSM780	488 nm	490 – 562 nm
Hoechst 33342	LSM780	405 nm	410 – 502 nm
DAPI	LSM780	405 nm	410 – 502 nm
AlexaFluor™ 568	Zeiss AxioObserver Z1	561 nm	571 nm
AlexaFluor™ 488	Zeiss AxioObserver Z1	488 nm	498 nm

2.1.8 Equipment

Table 14: Equipment for spheroid formation and cell cultivation used in this study

Equipment	Article no.	Supplier
20 µl glass capillary	BR708718	BRAND GmbH & Co. KG, Wertheim am Main, Germany
200 µl glass capillary	BR708757	BRAND GmbH & Co. KG, Wertheim am Main, Germany
24 well plate	662 102	Greiner AG, Kremsmünster, Austria
48 well plate	677 102	Greiner AG, Kremsmünster, Austria
96 well plate	655 185	Greiner AG, Kremsmünster, Austria
96 well imaging plate	S1605-0000-C	Sarstedt, Nümbrecht, Germany
96 well qPCR plate	MLL9061	BioRad, Hercules, CA, United States
96 well qPCR plate	AB-0700	ThermoFisher Scientific, Waltham, MA, United States
96CFX thermo cycler	C1000 Touch	BioRad, Hercules, CA, United States
Adhesive film	MSB1001	BioRad, Hercules, CA, United States
Cell culture flask (25 cm ²)	690160	BD Bioscience
Cell culture flask (75 cm ²)	658170	BD Bioscience
Cell Strainer	352235	Corning®, Corning, New York, United States
Centrifuge 5810R	n/a	Eppendorf AG, Hamburg, Germany
Cryo vials	377267	ThermoFisher Scientific, Waltham, MA, United States
Eppendorf tubes (0.5 ml)	S1605-0000-C	StarLab International GmbH, Hamburg, Germany
Eppendorf tubes (1.5 ml)	S1615-5510-C	StarLab International GmbH, Hamburg, Germany
Eppendorf tubes (1.5 ml)	0030 108.051	Eppendorf AG, Hamburg, Germany

Falcon tubes (15 ml)	188 271	Greiner AG, Kremsmünster, Austria
Falcon tubes (50 ml)	227 261	Greiner AG, Kremsmünster, Austria
FEP foil	FEP200A	DuPont de Nemours International SA, Geneva, Switzerland
Glass capillary	1201502	Hilgenberg GmbH, Malsfeld, Germany
hemocytometer (Neubauer)	40441001	Hecht-Assistant, Sondheim vor der Rhön, Germany
heracell™ 150i CO ₂ -Incubator	n/a	ThermoFisher Scientific, Waltham, MA, United States
laminar flow hood Clean Air	n/a	PMV
Infinite® F200	n/a	TECAN Trading AG, Männedorf Switzerland
laminar flow hood Clean Air	n/a	PMV
laminar flow hood maxisafe 2020 cabinet	n/a	Thermo Scientific
multipette X stream	11510205	Eppendorf AG, Hamburg, Germany
parafilm	P7793	MilliporeSigma, St. Louis, MO, United States
Pasteur pipettes	M4230NO250 SP4	Kimble, VWR, Radnor, PA, United States
PCR strips	A1402-3700	StarLab International GmbH, Hamburg, Germany
Pipette tips (1000 µl)	S1111-6001	StarLab International GmbH, Hamburg, Germany
Pipette tips (200 µl)	S1113-1000	StarLab International GmbH, Hamburg, Germany
Pipette tips (20 µl)	S1110-3000	StarLab International GmbH, Hamburg, Germany
Pipette tips with filter (1000 µl)	0030 078.578	Eppendorf AG, Hamburg, Germany
Pipette tips with filter (100 µl)	0030 078.543	Eppendorf AG, Hamburg, Germany
Pipette tips with filter (20 µl)	0030 078.500	Eppendorf AG, Hamburg, Germany
qPCR bench		Peqlab, VWR, Radnor, PA, United States
Shrinking tube	E255532	G-APEX, Yuanlin City, Taiwan
Vortex	Vortex Genie 2	Scientific Industries, Bohemia, NY, United States

2.2 Methods

I. Cell culture

2.2.1 Cell line and cell culture

In this work, human pancreatic organoid (hPO) as 3D cell culture and primary Human Dermal Microvascular Endothelial Cells (HDMEC) and human mesenchymal stem cells (hMSC) as 2D cell culture have been expanded.

The hPOs isolated by Lorenza Lazzari's group (Policlinico di Milano, Milan, Italy) were cultured by using two different protocols of expansion and differentiation. The expansion and differentiation media were originally developed by Meritxell Huch's group (MPI-CBG, Dresden, Germany) in the framework of the LSFM4LIFE project. Both media were tested on the novel hPO spheroids developed in this work. The hMSC and HDMEC were purchased from PromoCell (PromoCell, Heidelberg, Germany) and cultured according to manufacturer's protocol.

Based on the original expansion protocol, the human pancreas organoids organoids and hPO spheroids were cultured for 7 days in expansion medium (EM) (Table 7). The medium was exchanged in day 2 and 4. Samples were ready to be collected on day 7. However, differentiation protocol consists of 3 different mediums (Table 7). Samples were cultured in expansion medium (EM) (Table 7) for two days, then the medium was removed completely and replaced by expansion medium 2 (EM2) (Table 7). On day 4, the medium was changed to human differentiation medium (DM) (Table 7). After 3 days, the samples were ready to be harvested for further experiments (Figure 8).

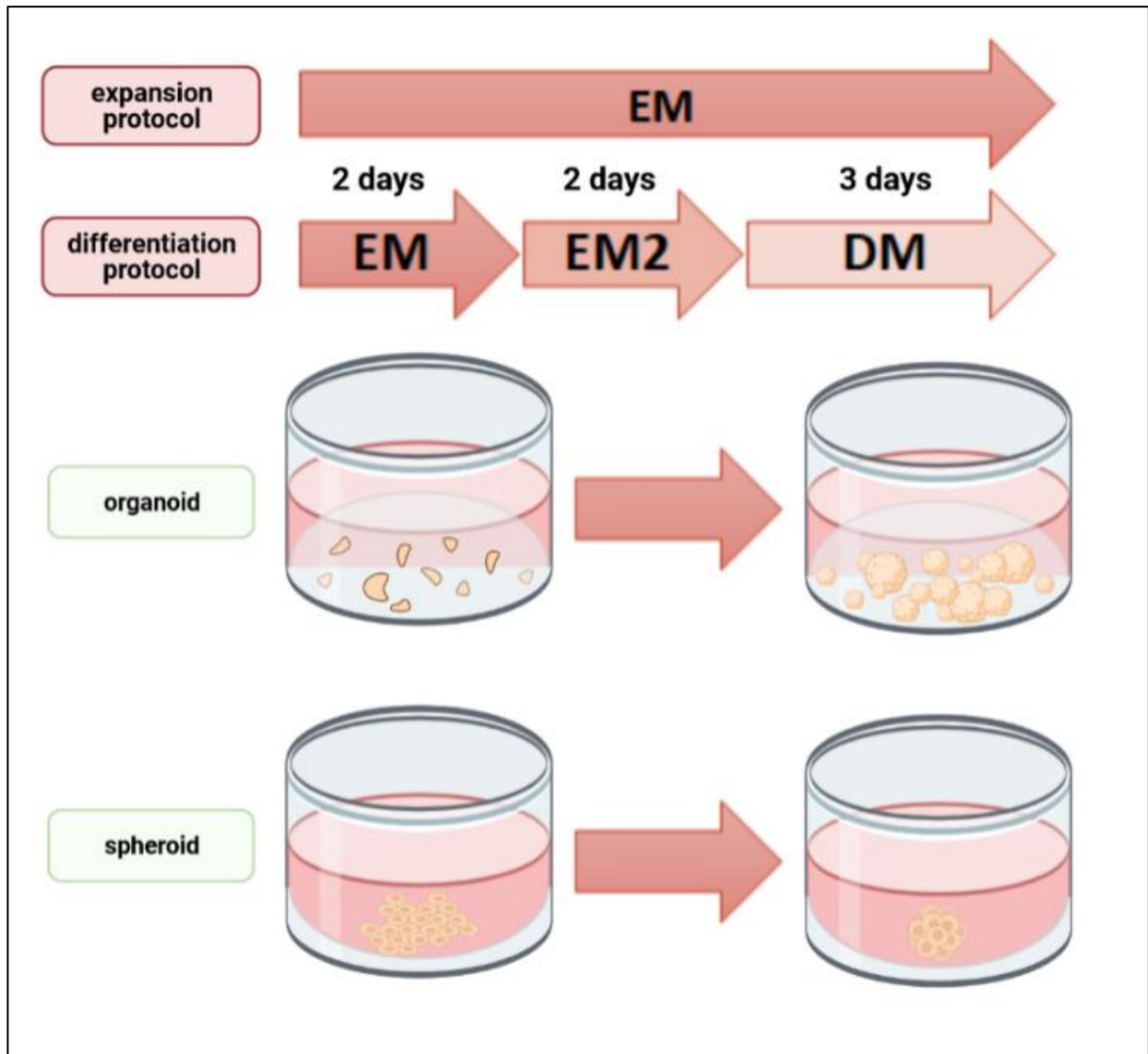


Figure 8: Schematic illustration of expansion and differentiation protocol. Based on Meritxell Huch's protocols samples need to be cultured 7 days in expansion and differentiation mediums. Expansion protocol has several signaling pathway's inhibitors, and differentiation protocol contains 3 types of mediums (EM, EM2, and DM), which decrease in inhibitors' concentration stepwise. In both protocols mediums are replaced on the 2nd and 4th day. Samples are ready to be collected on day 7 (created with BioRender).

2.2.1.1 Human pancreatic organoids (hPOs)

The hPOs were generated from healthy subjects and has been cultured in 25 μ l BME-2 droplets covered with 250 μ l expansion medium (Table 7) under standard cell culture conditions (5% CO₂, 21% O₂, 95% humidity incubated in 37 °C). hPOs should be passaged every 10 to 14 days based on the growth rate and the organoid size.

For hPO expansion, BME2 drops containing fully formed hPOs were dissolved in 5 ml of cold basal medium (Table 7). After centrifuging at 250 rpm for 5 min at +8 °C and discarding the supernatant carefully, 5 ml basal medium were added then hPOs were pipetted up and down with a pre-coated Pasteur pipette an additional ~20 times. Pipetting up and down disrupted the spherical organoids into small cell fragments that after centrifuging once more under the same conditions were then embedded in fresh BME2. The fresh BME2 drops containing hPOs were formed in each well and have been incubated at 37 °C for 10-15 min to solidify. Additionally, expansion medium was added to each well.²¹³ The small cell fragments developed into new spherical organoids within 3-4 days. Medium was replaced every 2 days respectively. Medium contained 10 μ M Y-27632 (Table 4) for the first 2 days.

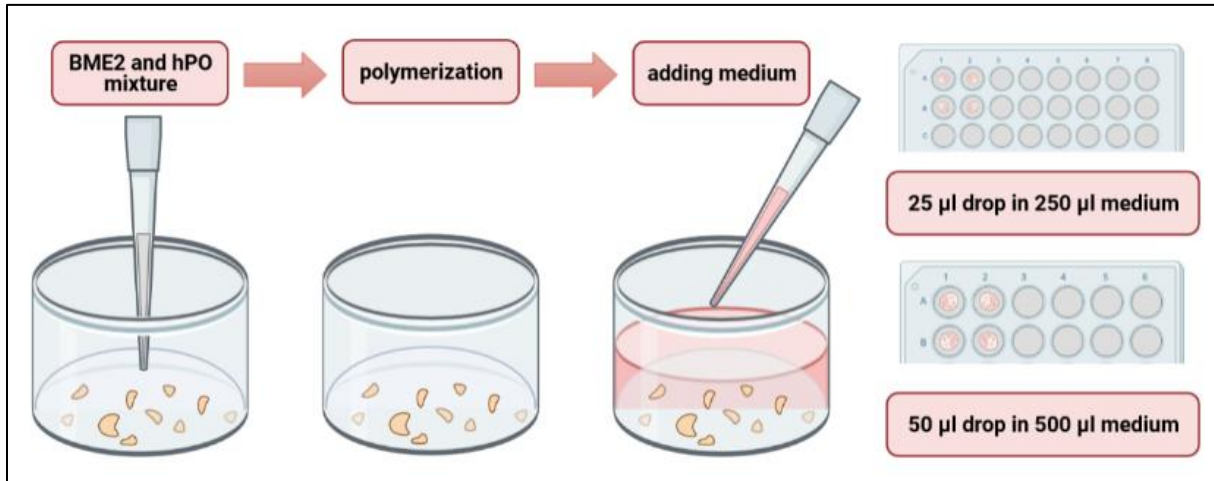


Figure 9: Schematic drawing of hPO cultivation process. For cultivation, hPOs are fragmented with vigorous pipetting up and down in cold basal medium which dissociates hPOs into small homogeneous aggregates, that are then embedded in fresh BME2. The mixture of BME2 and hPOs is placed on the bottom of each well respectively. After polymerization of BME2 drops in the incubator, medium is added to each well and plate is cultured in standard incubator conditions. The aggregates later develop into new circular organoids (adopted from Hiroyuki Miyoshi et al., 2013) (created with BioRender).

2.2.1.2 Primary Human Dermal Microvascular Endothelial Cells (HDMEC) and Human Mesenchymal Stem Cells (hMSC)

HDMEC and hMSC cells have been grown as a monolayer in cell culture flasks (25 cm²) (Table 14) in the 5 ml appropriated culture medium (Table 7). Both cell lines were incubated at 37°C in an atmosphere of 5 % CO₂, 21 % O₂, and 95 % humidity. Cells were propagated as soon as they reached 80 – 90 % confluence.

Both cell lines have been subcultured by removing the old medium and washing the cells once with 2 ml pre-warmed PBS (Table 4). Then, cells were detached from the surface by adding 3 ml TripLE (Table 4) and incubated for 5 min at 37°C. After incubation, 3 ml fresh culture medium were added to inactivate the enzymatic reaction. Subsequently, the cell suspensions was centrifuged at 300 rpm for 5 min at room temperature (RT) and the supernatant discarded. Pellets were re-suspended in 5 ml fresh pre-warmed medium. Ultimately, cells were plated at a density of approximately 5,000 - 6,000 single cells per cm² into the appropriate flasks. Media were regularly replaced every 2 days.

2.2.2 Thawing and cryopreservation

2.2.2.1 Thawing and cryopreservation of hPOs

Cryovials containing hPOs were thawed rapidly by submerging the lower half of the cryovials into a 37°C water bath. After melting approximately 95% of the cell suspension within the cryovial, the cell suspension was transferred to 5 ml pre-warmed basal medium (Table 7) that immediately centrifuged at 8 °C and 250 rpm. The supernatant was carefully removed, and the pellet has been gently mixed with BME2 and cultured according to the previous chapter (2.2.1.1 Human pancreatic organoids (hPOs)).

To maximize early growth of thawed organoids from small crypts or fragments, the expansion medium (Table 7) was supplemented with Y27632 (Table 4), an inhibitor of Rho-associated protein kinase (ROCK). After this initial treatment, this inhibitor was no longer required for subsequent culture.

After dissociating BME2 containing hPOs, in 5 ml basal medium (Table 7) and centrifuging once at 8 °C and 250 rpm, supernatant was discarded and 2 ml basal medium (Table 7) was added to the samples. hPOs were diced into small fragments by pipetting up and down several times. The cell suspension was centrifuged again at the same condition followed by discarding the

supernatant respectively. The pellet was resuspended in 500 µl freezing medium (Table 4) per cryovial and aliquoted. To reach to optimal growth rate after thawing hPOs of 3 to 4 wells cultured in 24 well plate was placed in one cryovial. After aliquoting, cryovials were placed in freezing containers, Mr. Frosty freezing devices (Table 14) and cooled at a rate of $-1^{\circ}\text{C}/\text{min}$ to reach -80°C , then after at least 24 h, transferred in liquid nitrogen (LN_2) tank for long-term vapor phase storage.

2.2.2.2 Thawing and cryopreservation of hMSC and HDMEC

Recommended protocols for thawing and cryopreservation 2D cells were utilized for hMSC and HDMEC.

The cryovials were removed from liquid nitrogen (LN_2) tank and placed into a 37°C water bath, ensuring the whole cell suspension was not melted completely. The entire cell suspension was then transferred from the cryovial to the 25T flask (Table 14) and 5 ml appropriated medium was added respectively. The flask was incubated, allowing cells to settle and adhere for at least 24 h. On the following day, the old medium has removed gently and was replaced with 5 ml of fresh medium.

After trypsinizing the cells and determining cell number, the required cells, 1 million per cryovial, have been centrifuged at 300 rpm for 5 min at room temperature (RT) and the supernatant was discarded gently. The cell pellet was resuspended in freezing medium (Table 7) and aliquoted among cryovials. Followed by keeping the cryovials for at least 24h in freezing containers, “Mr. Frosty” freezing device (Table 14) at a rate of 1°C per minute at -80°C . Once the cooling process was completed all cryovials were transferred directly to liquid nitrogen (LN_2) tank until required for further experimentations.

2.2.3 Formation of monotypic spheroids from human pancreatic progenitor cells

Liquid-overlay technique (LOT) during spheroid formation, has been performed.¹⁴³ For this procedure 96-well plates were used.

A low-melting agarose (Table 4) stock solution (1%) was prepared in PBS (Table 4). Prior to seeding cells, the agarose was melted in a microwave oven and the bottoms of 96-well plates with flat bottoms were coated with 50 µl liquid agarose, respectively. Plates were gently tapped at each side to form concave agarose wells. After cooling for at least 1.5 h at 4°C , the

plates were ready to use. The agarose is necessary to prevent the cells from attaching to the ground and improve the spheroid formation.

All steps have been performed on ice to promote depolymerization of the BME-2 and to slow down the metabolism of the hPOs in nutrient-reduced conditions. After reaching 70 % confluence (every 10 – 14 days), BME-2 drops, containing hPOs, were dissolved in 1 ml cold basal medium and transferred to a 15 ml falcon tube with 2 ml ice-cold basal medium per well (max. 8 wells per tube). The cell suspension has been centrifuged at 250 rpm for 5 min at 8 °C followed by removing the supernatant carefully. Pellet was trypsinized by adding 3 ml TripLE (Table 4) and placing in 37°C. After incubation for 15 min, 3 ml fresh basal medium were added to inactivate the enzymatic reaction. The cell suspension was passed through the cell strainer (Table 14), to remove all cell fragments and make a constant single cell suspension.

Subsequently, cell suspension was mixed with trypan blue (Table 4) (ratio 1:4) to determine the number of cells. In contrast to dead cells, trypan blue does not penetrate the membrane of intact cells and therefore living cells can be discriminated against dead cells. Having mixed the cell suspension and trypan blue properly, 10 µl was pipetted in the hemocytometer (Table 14). By using a wide field microscope, cells of all four squares were counted. Once the total cell number was determined, the cell concentration was calculated with following equation:

Equation 1:

$$total\ cells/ml = total\ cells\ counted \times \frac{dilution\ factor}{\#\ of\ squares} \times 10,000\ cells/ml$$

$$\# \ of \ squares = 4 \quad \text{Dilution factor} = 5$$

For spheroid formation, 100 µl of a cell suspension, containing 3,000 single cells have been pipetted per well.

To concentrate cells at the center of the well, plates have been centrifuged for 15 min at RT at 270 rpm. Afterwards plates have been incubated for 7 days based on 2 different protocols (expansion and differentiation) under standard cell culture conditions, to allow them to aggregate and form circular spheroids.

2.2.4 Triple co-culture spheroid formation

The spheroid formation based on liquid overlay technique was performed as described in previous part (2.2.3 Formation) up to the counting single cells step. When counting each cell type (hPOs, HDMEC, hMSC) is finished, 100 µl of a cell suspension, containing 3,000 single cells

with the ratio of 1:1:1 was pipetted per well. Having cells incubated for 7 days based on their differentiation protocol, under standard cell culture conditions, the successful formation of spheroids was checked by optical microscopy.

The general workflow adopted from the recent publications is shown in Figure 10^{117,143}.

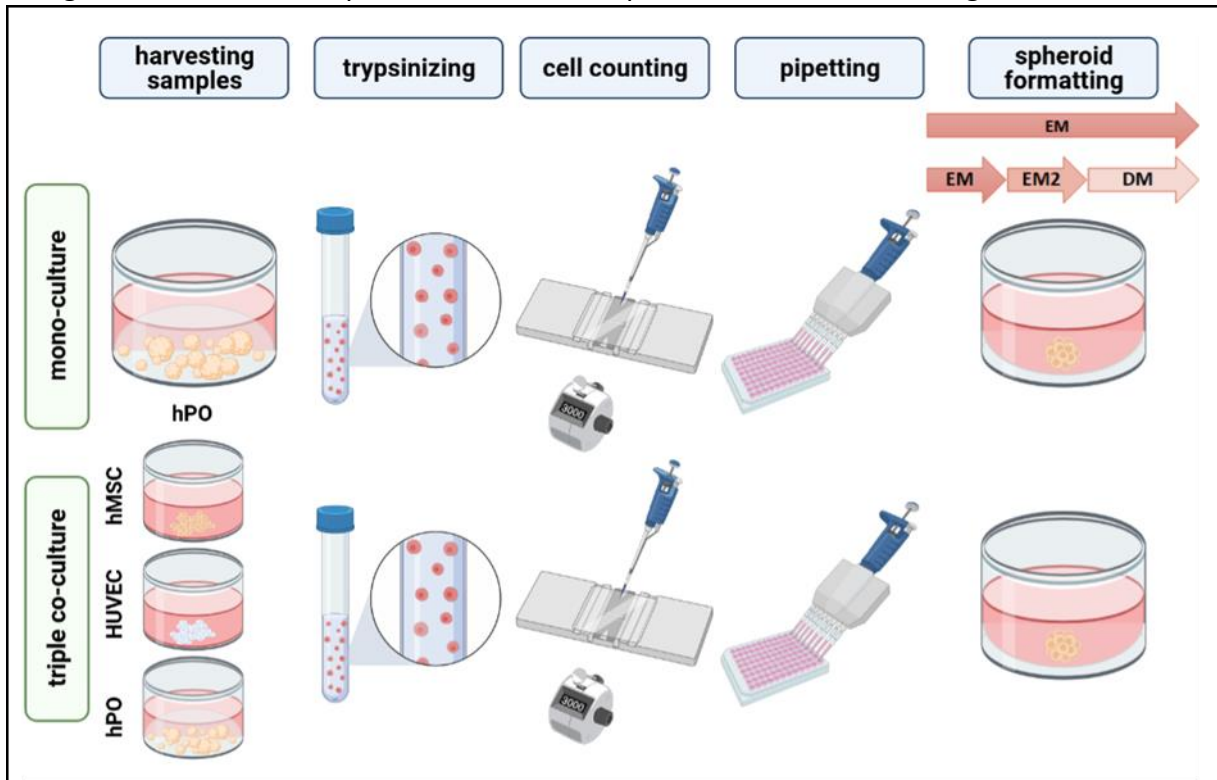


Figure 10: General workflow of proposed method. In mono-culture, after trypsinizing hPOs, 3,000 cells are seeded in agarose-coated 96-well plates and hPOs are cultured based on 2 different protocols. For making triple co-culture samples, at first all three cell types are trypsinized to single cells, followed by determining the number of cells in each group. Afterwards, the mixture of cell suspension in the ratio of 1:1:1 is performed. Triple spheroids with 3000 cells are formed in each well and cultured under 2 different protocols respectively (created with BioRender).

II. Microscopy

2.2.5 Wide-field fluorescence microscopy

The transmission images of hPO organoids, which represent their growth pattern, were obtained by the Zeiss SterEO Discovery.V8 with the 2x magnification and the image sets were processed using ZEN imaging software.

Time-lapse images have been recorded with the Axio Observer.Z1 (Carl Zeiss) with a Fluar 10x/0.50 M27 objective lens for a duration of 7 days with 30 minutes intervals. Incubation conditions of 37°C and 5% CO₂ were maintained during the whole acquisition period and the air was being humidified using humidified CO₂ coupled with a VE water filled beaker. The time-

lapse was ended with LDA (2.2.6.1 LDA in organoids). The LDA results were acquired with 488 nm and 568 nm laser.

2.2.6 Confocal laser scanning microscopy

Confocal laser scanning microscopy was performed with a Zeiss LSM780 (Carl Zeiss) microscope. After IF staining, the hPO organoids were placed in a Lumox[®] 96-well plate (Sarstedt) filled with PBS with a flat, foil bottom prior to imaging. The plate was then placed into the microscope. ZEN imaging software (Carl Zeiss) has been used for image processing. To frame hPO spheroids, the procedure was the same, albeit the samples needed to be optically cleared with CUBIC2 for 5 min before imaging (2.2.12.3 Optical clearing technique in spheroid vs. organoid). Secondary antibody controls are shown in supplementary figures.

2.2.7 Light sheet-based fluorescence microscopy

In order to record the aggregation process and frame (live image) the hPOs with more details, at first the cells were Fluorescently stained with CellTracker (2.2.7 Short-term cell tracking with CellTracker dyes in spheroids) then imaged with the Zeiss Light-Sheet Microscope Z1.

Before imaging, ultra-thin fluoroethylene propylene (FEP) foil cuvettes were formed. The basic mould was first designed by Sven Plath with Inventor[®] CAD software and was later printed with resin by the LCD-based SLA 3D printer Photon S (Anycubic) (Figure 13). The thin glass capillaries were cut in 7mm and curved (round) at its edges by keeping for some seconds in front of the fire to avoid ripping the FEP foil during formation. The pre-rounded capillaries were placed inside the resin mould.

The pre-cut square piece of FEP foil was placed into the frame of the vacuum-forming machine (JT-18, Jin Tai Machining Company) and was secured by closing the latch. The machine was pre-warmed, and the temperature was being checked frequently till it was reached 480°C to 500°C. Next, the FEP foil has brought up directly close to the heater and was heated for 1 minute. In the meantime, the mould was placed on the middle of the metal grid and under the FEP foil respectively. Improving by an industrial dryer, heating has been proceeded until the FEP foil became flexible and started to stretch towards mould. This part could have taken ca. 30 sec (Figure 11). The heating process was ended almost simultaneously, applying the machine vacuum by pressing MODEL and lowering the platform towards mould by raising the lever manually which ensue the FEP foil to fall onto the mould at high speed. To avoid further

heating and to cool down the FEP cuvettes at RT the machine was turned off. Then, the mould was carefully extracted, and cuvettes were attached to the glass capillaries. To attach the cuvettes to a longer capillary and assemble it inside the Z1 holder for imaging, a short shrinking tube (around 3 cm) was required. Parafilm was used to wrap around the connection point. While the shrinking tube was placed between the cuvette and longer capillary, the shrinking tube has been heated by an industrial dryer for ca. 30 sec until the tube shrank and the connection was sealed completely. Before starting the heating, a pipette tip was placed on top of the cuvette to protect it from the heat and deformation. When the process was finished, the longer capillary was discarded gently followed by incubating the cuvette overnight at RT for sterility in 2% Hellmanex® III (Table 4). On the next day, the cuvettes were placed in PBS and stored in PBS at 4°C for imaging (Figure 12).

The cell suspension for mono-culture and triple-culture was prepared as described previously (Formation and Triple co-culture spheroid formation). 10 µl of the cell suspension was added to the FEP foil cuvette. The process was performed by applying 10 µl tips to avoid air bubbles. Afterwards, FEP foil cuvettes were placed inside the 15 ml falcon and have been centrifuged for 15 min at RT at 270 rpm to increase the aggregation of the cells at the bottom of the cuvette. Next, the cuvette was filled with expansion medium (Table 7) and connected to the longer capillary, which had filled with expansion medium in advance. The connection and the tip of the micropipette had sealed with parafilm or silicon. The prepared cuvettes then could be placed in the cuvette holder of the Z1 microscope which then has immersed in the Z1 chamber filled with PBS + 20% Pen/Strep (Table 4). Before the acquisition, the light sheets had calibrated manually to produce high quality images. The setting would be saved and reused. Acquisitions were taken with Zeiss LSM 10x/0.2 as an illumination objective and W Plan-Apochromat 20x/1.0 UV-VIS as a detection objective. The time-lapse has been performed over 3 days with 30 min interval at 37°C and 5% CO₂. Later, images were analyzed using Fiji software (Version. 1.49k).



Figure 11: The process of Z1 holder formation. After placing the pre-cut FEP foil into the vacuum-forming machine, the machine should be pre-heated to 480°C to 500°C. Next, the FEP foil is lifted and approached to the heater. The heating process is improved by keeping an industrial dryer close to it manually. The FEP foil is kept in this position to become flexible and start to stretch downwards. This part takes for ca. 30 sec. (the images are modified from Louise Breideband protocol).

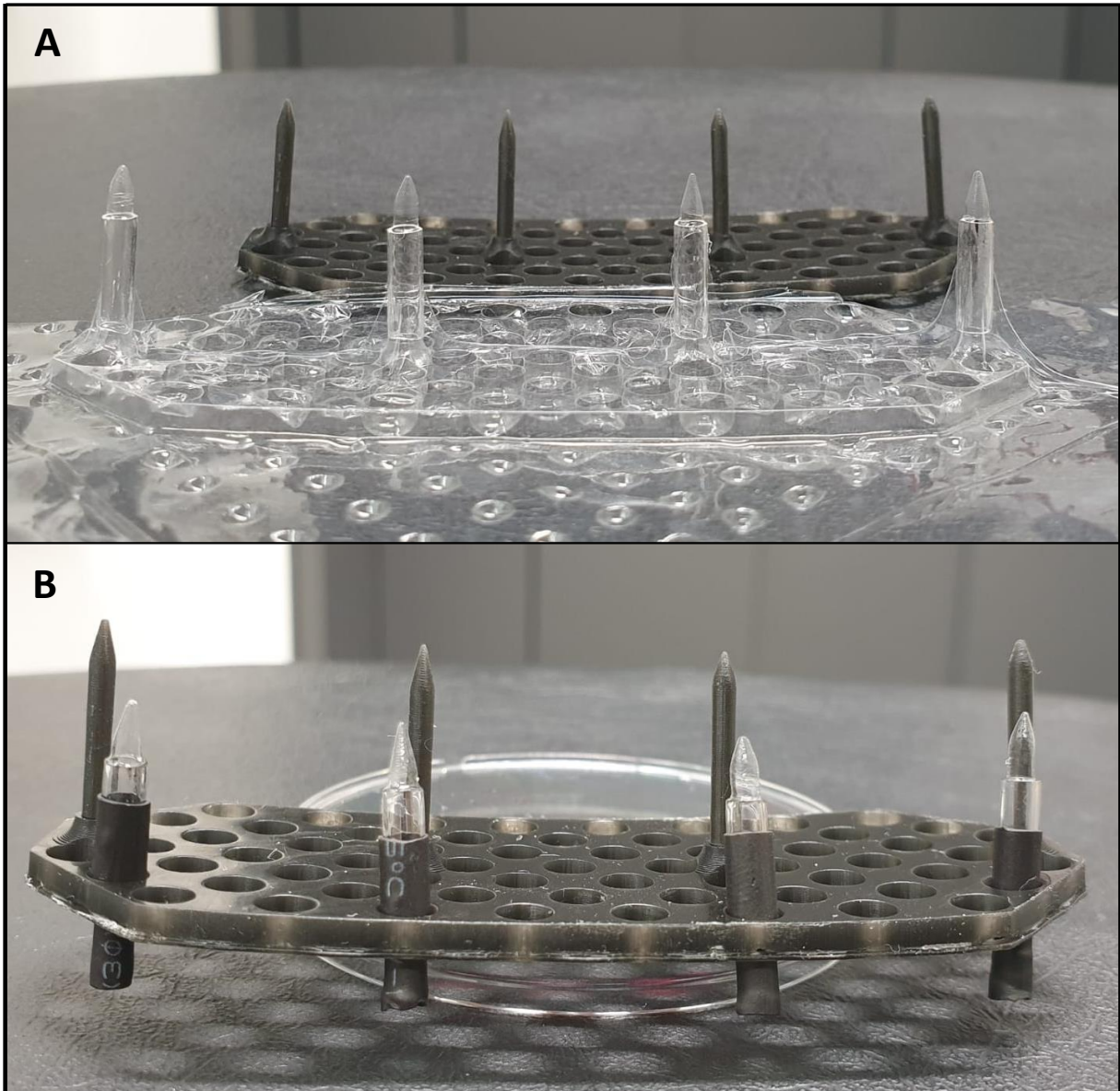


Figure 12: Final steps in preparing Z1 holders. (A) By applying the vacuum with the machine and releasing the pre-warmed FEP foil simultaneously towards the mould, the FEP foil is stuck to the capillaries and forms the Z1 holders based on the shape of mould. (B) The mould should be detached afterwards, and the shrinking tube is used to seal the connection points. After sterilization the holders are ready to use for acquisition.

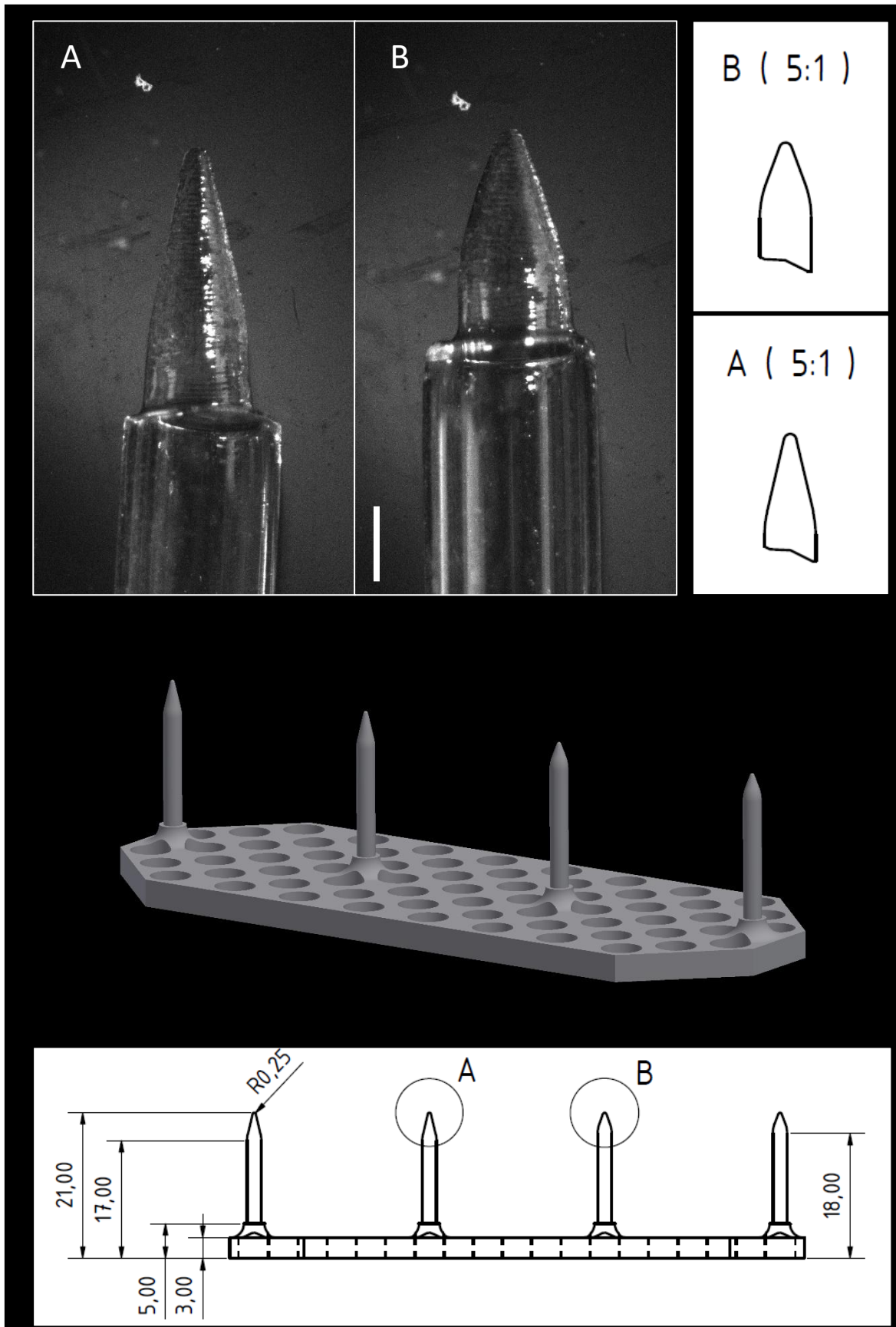


Figure 13: CAD drawings of mould for Z1 holder. To improve the process of aggregation during spheroid formation, the holders tip is changed. The newly designed tips (A) are sharper and more elongated compared to the previous versions (B). The CAD drawings are done by Sven Plath and later the mould is printed with LCD-based SLA 3D printer Photon S; scale bar (B): 200 μm .

III: Molecular and cellular spheroid characterization

2.2.6 Live-dead assay (LDA)

The aim of the live-dead assay (LDA) is to distinguish between living and dead cells within the spheroids and organoids and determine the ability of hPOs to maintain or recover viability after trypsinization, aggregation and cultivation in both protocols. With this aim, FDA-PI double staining was performed. Fluorescein diacetate (FDA) (Table 4) which is an acetylated derivative of the green fluorescent dye fluorescein that stain live cells and is usually coupled with propidium iodide (PI) (Table 4), which stains DNA and RNA inside of dead cells.²¹⁴ In FDA-PI double staining, living cells appear bright green and dead cells red. Positive controls were conducted by incubating samples in 500 μ l DMSO (Table 4) for 5 min (organoids) and 30 min (spheroids) respectively. Since FDA and PI are sensitive to light, all steps have been performed in the dark. Fluorescence images were obtained using Carl Zeiss Cell Observer Widefield microscope (organoids) and Zeiss Axiovert 40 CFL fluorescence microscope (spheroids), equipped with Objective Fluor 10x/0.50 M27 lens controlled by ZEN software. Further image processing has been done by ImageJ software (Version. 1.49k).

2.2.6.1 LDA in organoids

In day 7, medium was removed from each well and hPOs have been incubated with 5 μ g/ml FDA and 5 μ g/ml PI in basal medium (Table 7) for 15 min before being washed twice by PBS and imaged in PBS.

2.2.6.1 LDA in spheroids

After collecting the spheroids in 1.5 ml tube, the medium was discarded, and 1 ml fresh pre-warmed basal medium (Table 7) was added to each tube. Each condition has been incubated with 5 μ g/ml FDA (Table 4) and 5 μ g/ml PI (Table 4) for 1.5 h. During incubation phase, samples were being rotated every 30 min for 1.5 h. Later on, the medium was discarded then the spheroids have been washed for 10 min with 1.5 ml PBS 5 times. Afterwards, spheroids were fixed with 1 ml of 4% PFA (Table 4) for 20 min, followed by washing up for 10 min with 1.5 ml PBS 5 times to be stored in 4°C for further experiments.

2.2.7 Short-term cell tracking with CellTracker dyes in spheroids

Fluorescent cell tracker dyes are powerful tools that facilitate imaging and tracking cells within live organisms. CellTracker dyes enable direct visualization of biological processes like cell proliferation, cell migration, and cell-cell interactions.

Before starting the process of staining, propriated stock from each cell tracker was prepared. 5 μ M CellTracker™ Orange CMTMR (Table 4), 0.5 μ M MitoTracker® Deep Red FM (Table 4), and 1 μ M CellTracker Green CMFDA (Table 4) in DMSO were utilized based on manufacturer's instructors.

Having trypsinized the cells, described in previous chapter (2.2.2 Formation), 1 μ l from diluted stock was added to 999 μ l DMEM (serum free medium) and cells have been incubated for 15 min at 37 °C, followed by centrifuging and discarding the supernatant respectively. Afterwards samples were ready to be monitored during aggregation in Z1 microscope.

2.2.8 EdU incorporation assay for organoids

To confirm our observation that proliferation is affected during cultivation within both expansion and differentiation mediums, EdU staining has been performed using the Click-iT EdU Alexa Fluor 488 kit. The 5-ethynyl-2'-deoxyuridine (EdU) incorporation assay has been used to detect DNA synthesis and has determined the cell proliferation. EdU is a synthetic nucleoside which is used as an analogue of thymidine during DNA replication. It is incorporated into new synthesized DNA, therefore new proliferated cells can be distinguished in living tissues. The EdU detection method described below is in accordance with the ThermoFisher factory manuscript.

On day 7, after removing the old medium, hPOs have been incubated in 250 μ L basal medium (Table 7) containing 10 μ M EdU for 4 h under standard cell culture condition (37 °C, 5% CO₂ and 95% O₂). The control group has been only treated with basal medium. Afterwards, hPOs have been fixed with 200 μ L 4% PFA (Table 4) for 20 min on ice, followed by incubation in 500 μ L cell recovery solution (Table 4) for 2 h on ice and shaker (Table 14). Next, hPOs were collected in 1.5 ml tube (Table 14) and have been washed for 10 min with 1.5 ml PBS 3 times (Table 4). To allow the Alexa Fluor® 488 (1:200) and Hoechst 33342 (1:500) penetrate the hPOs, 300 μ L permeabilization solution (Table 5) per well were added and samples were being shaken slowly on ice for 30 min. Another washing step with 300 μ L cold PBS (Table 4) followed

by incubation in 400 μ L reaction cocktail (Table 5) for 40 min at room temperature (RT) on the shaker has been applied. To improve the signal intensity of Hoechst 33342 (1:500), the probes have been re-stained for 30 min at 37 $^{\circ}$ C on the thermomixer afterwards (Table 14). Lastly, the samples were washed once with 300 μ L cold PBS (Table 4) and stored in 4 $^{\circ}$ C for further experimentations (Figure 14). Fluorescence images were obtained using Zeiss Cell Observer fluorescence microscope equipped with W Plan-Apochromat 20x/0.84 M27 objective lens and controlled by ZEN software. Further image processing has been done by ImageJ software (Version. 1.49k).

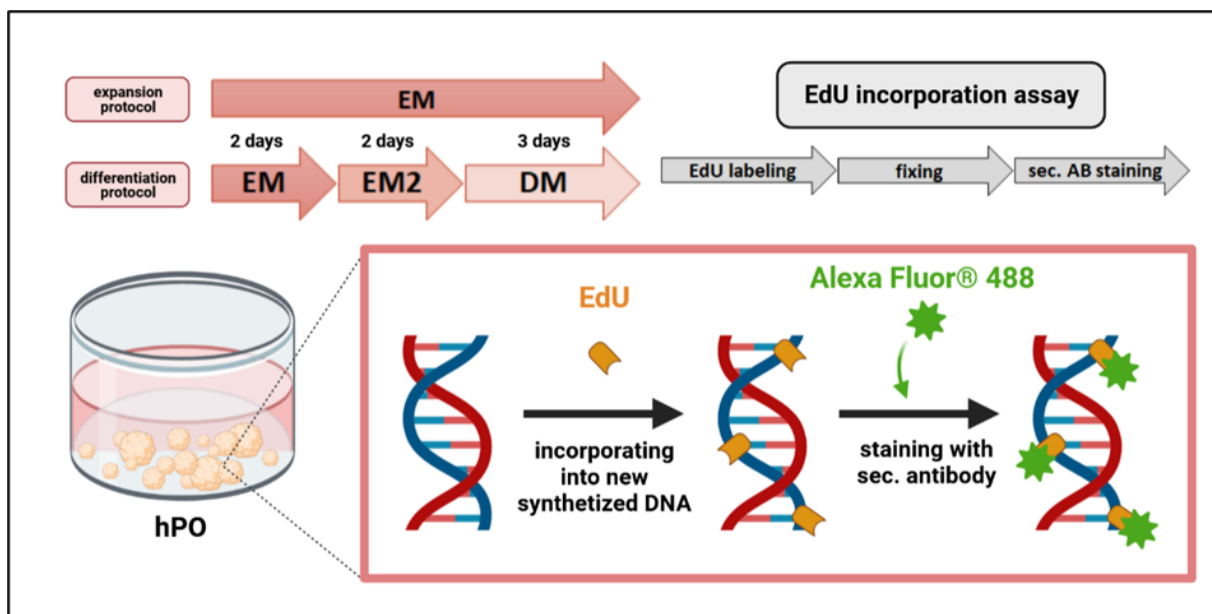


Figure 14: Experimental flow for EdU incorporation assay. hPOs are cultured based on expansion and differentiation protocols, afterwards on day 7 EdU labeling marker is added to the mediums (10 μ M) and they are incubated for 4h. Next, organoids are collected and fixed on the same day, being stained with secondary antibody (Alexa Fluor[®] 488 (1:200)) and Hoechst 33342 (1:500) respectively. sec., secondary; AB, Antibody; EM, Expansion medium; EM2, Expansion medium 2; DM, Differentiation medium (created by BioRender).

2.2.9 Total RNA isolation

Total RNA extraction from both organoids and spheroids samples was performed using TRIzol™ Reagent (Total RNA Isolation Reagent) (Table 4). TRIzol is an acid-guanidinium-phenol based reagent ideally designed for the simultaneous isolation of DNA, RNA, and protein from cells. TRIzol based isolation is a single-step procedure and suitable for PCR analysis. After solubilization and addition of chloroform (Table 4), sequential precipitation of RNA, DNA, and protein is formed. The upper colorless aqueous phase contains RNA followed by white

interphase that solves DNA and the protein is extracted in the red organic phase at the bottom of the tube.

2.2.9.1 Total RNA isolation in organoids

Having removed the old medium and each well washed once with 250 μ l PBS, four 25 μ l BME droplets have resuspended in 1.5 ml ice-cold TRIzol reagent per condition and transferred to 2 ml Eppendorf tube (Table 14). Each sample was homogenized respectively and after 5 min of incubation at RT, 300 μ l chloroform was added to each tube. To mix each sample properly, tubes were shaken vigorously for 15 sec. The Homogenate was separated into three phases by incubation for 2-3 min at RT and the phases were parted additionally by centrifugation at 15,000 x g for 15 min at 4 °C. Subsequently, the upper colorless aqueous phase was transferred into a fresh RNase/DNase free 1.5 ml Eppendorf tube (Table 14). Later, RNA was precipitated from the aqueous layer by adding 750 μ l reaction-grade isopropanol. The tubes were inverted four times and have been incubated for 10 min at RT followed by centrifugation at 15,000 x g for 10 min at 4 °C. As the supernatant had removed, the RNA pellet was washed by 750 μ l 75% ethanol to remove impurities and collected through centrifugation at 7,500 x g for 5 min at 4 °C. Most of the supernatant was discarded and the pellet was dried at RT. Subsequently, the pellet was solved in 10 μ l RNase/DNase-free water (Table 4) and has been incubated for 15 min at 55°C. The RNA concentration was determined by measuring 1 μ l of the RNA solution in the NanoPhotometer® NP80 (Table 14) based on the manufacturer's instructions. The synthesized RNA was stored at -80°C for long-term storage.

2.2.9.2 Total RNA isolation in spheroids

For RNA isolation in spheroids, after collecting the spheroids in 1.5 ml tube, the medium was removed, and samples was washed for 10 min with 1.5 ml PBS 5 times (Table 4). The RNA isolation was then performed as described in previous part (2.2.9.1 Total RNA isolation in organoids).

2.2.10 cDNA synthesis in organoids and spheroids

The cDNA was synthesized from total RNA using the Maxima First Strand cDNA synthesis kit (Table 4). Total RNA was reverse transcribed in a 20 μ l reaction volume, as the manufacturer's instructions. 1 μ l dsDNase buffer and 1 μ l DNase were mixed with 4 μ g total RNA then RNase/DNase-free water (Table 4) were added to this mixture up to 10 μ l followed by incubation for 2 min at 37 °C. Additionally, 4 μ l cDNA synthesis buffer, 2 μ l Maxima Enzyme

Mix together with 4 μ l RNase/DNase-free water was added to the tube then the reaction mix was vortexed and spun down respectively. Reverse transcription was being executed in a PCR cycler (Table 14) in three steps of incubation; starting with 10 minutes at 25°C, followed by 20 minutes at 50°C, and finally 5 minutes at 85°C. Samples were stored at -20°C for subsequent analysis.

2.2.11 Reverse Transcription-quantitative Polymerase Chain Reaction (RT-qPCR)

SYBR[®] Green qPCR MasterMix (Table 4) is designed for highly sensitive and accurate quantification of gene expression and is therefore suitable for RT-qPCR reactions. SYBR[®] Green is a dsDNA-binding dye which intercalates nonspecifically into dsDNA, allowing measurement of the amount of PCR product.

For RT-qPCR, the primers (Table 8) were reconstituted to a final concentration of 100 μ M with RNase/DNase-free water (Table 4) and the primer pairs were further diluted in RNase/DNase-free water with a final concentration of 4 μ M per primer. The primer pairs can be stored at -20 °C for long-term storage. The cDNA was diluted 1:10 in RNase/DNase-free water with 1:4 Yellow sample buffer. The SYBR Green MasterMix was diluted in RNase/DNase-free water in 1:1.6 ratio. As soon as diluted SYBR Green MasterMix and diluted cDNA were mixed together, 9 μ l of the reaction mix was added to each qPCR plate well (Table 14) followed by distributing 1 μ l primer pair solution to each well. The plate was sealed with adhesive film (Table 14) then centrifuged to concentrate the reaction mix in the bottom and remove bubbles. The qPCR reaction was performed in a 96CFX thermo cycler (Table 14) in triplicates. No template samples were included as negative control. The plate was stored at -20°C for further experiments.

2.2.12 Immunofluorescence staining

Immunofluorescence (IF) staining is a technique for fluorescently labeling a biological target within a sample. IF utilizes fluorescent-labeled antibodies to detect specific antigens and typically requires fixation, permeabilization of cells, blocking, and incubation with primary and secondary antibodies. No longer than antibody incubation, nuclei staining is performed with dyes such as DAPI or Hoechst 33342 (Table 11) which intercalate into DNA of the cells. Samples were placed with additional PBS in the Lumox[®] 96-well plate (Table 14) with a flat, foil bottom

(organoids) and microscope slide (Table 14) (spheroids) for acquisition. To capture, the fixed and fluorescently labelled samples (organoids and spheroids), a Carl Zeiss LSM780 confocal microscope was utilized. Secondary antibody controls are shown in supplementary figures.

2.2.12.1 Fixation and immunofluorescence staining in organoids

Having removed the old medium, 300 μ l 4 % PFA (Table 4) was added to each well. hPOs have been incubated for 30 min on ice while being shaken on a laboratory shaker (Table 14). A 1,000 μ l pipette tip was cut at the tip and covered with coating solution (Table 5). Fixed hPOs were transferred gently to the 1.5 ml Eppendorf tube (Table 14). Then hPOs have been washed 2 times for 10 min with 500 μ l PBS, incubated later with 500 μ l Cell Recovery solution (CRS) (Table 4) on ice for at least 2 h while shaking to have the residual of BME2 removed. After washing the organoids with 500 μ l PBS properly they have been incubated in 0.3% Triton X-100 diluted in PBS (Table 5) for 30 min at RT followed by incubation in blocking solution (Table 5) for 3 h at RT on the rotator. Next, organoids were incubated with primary antibody overnight at 37°C (Table 9). Having washed organoids 3 times for 10 min with 500 μ l PBS, incubation with DAPI (1:200) or Hoechst 33342 (1:500) (Table 11) coupled with secondary antibody (Table 10) (1:400) diluted in blocking solution for 24 h at 37°C on the thermoshaker (Table 14) was performed.

2.2.12.2 Fixation and immunofluorescence staining in spheroids

Spheroids were collected then fixed with 1 ml 4% PFA for 20 min on the rotator followed by washing for 5 min with 1.5 ml PBS 3 times. Spheroids have been permeabilized (Table 5) for 30 min at RT. The Triton X-solution was then discarded, and the spheroids have been incubated in blocking solution (Table 5) for 3 h at RT on the rotating mixer. This step is essential to prevent unspecific binding of the antibodies. Afterwards, spheroids have been incubated with primary antibody overnight at 37°C (Table 9), washed for 10 min with 500 μ l PBS 3 times again incubated but with DAPI (1:200) or Hoechst 33342 (1:500) (Table 11) coupled with secondary antibody (Table 10) (1:400) diluted in blocking solution for 24 h at 37°C on the thermoshaker (Table 14). Next, spheroids have been washed for 10 min with 500 μ l PBS 3 times respectively, soon after placing them on microscope slide incubated for 5 min in CUBIC2 (Table 5) they were ready to be imaged.

2.2.12.3 Optical clearing technique in spheroid vs. organoid

Optical clearing enables light to transport through the sample and reduces light scattering by matching refractive indices of cleared sample and the surrounding medium, therefore enhances the quality of the images. Respecting their cellular structure, being made of one single cell layer clearing is not essential for organoids, in contrast due to their compactness, spheroids needed to be cleared. Therefore, 5 min incubation in CUBIC2 (Table 5) have been performed for spheroids before acquisition.

IV. Data analysis

2.2.13 Processing of RT-qPCR data

RT-qPCR is one of the most sensitive, reliable, common, and quantitative methods to analyze the gene expression. This method allows to compare multiple genes simultaneously. One common method to analyze relative gene expression data is the Livak-Schmittgen method ($2^{-\Delta\Delta Ct}$), which compares two values in the exponent representing the normalized expression values in the gene of interest (GOI) relative to the housekeeping genes.

To determine the effect of each protocol (expansion vs. differentiation) and cellular structure (organoid vs. spheroid) coupled with the effects of different cell types within triple co-culture samples, RT-qPCR was performed and changes in the expression of differentiation and progenitor genes has been examined.

In this experiment, the calculation was done by using $\Delta\Delta Ct$ method between the relative expression of a GOI and the housekeeping genes (RPL13 and TBP), hPOs (organoids and spheroids) in expansion medium were determined as control group. For each gene triplicate independent experiments were performed, and the relative expression was calculated and presented in Box plots. The results were calculated and visualized by using Microsoft Excel 365.

To start the calculation, after determining the average between the triplicate of each GOI and the housekeeping genes, ΔCt for each GOI was calculated by subtracting the Ct as number of the GOI from that of the housekeeping genes (Equation 2).

Equation 2:
$$\Delta Ct_{(GOI)} = Ct_{(GOI)} - Ct_{(hauskeeping\ genes)}$$

The $\Delta\Delta Ct$ value was calculated to present the differences between the expression of the GOI in treated sample (in our case, cultivated in differentiation medium) and control (in this case, cultivated in expansion medium) based on equation 3.

$$\text{Equation 3: } \Delta\Delta Ct (GOI) = \Delta Ct (GOI)_{(treated\ sample)} - \Delta Ct (GOI)_{(control)}$$

The $\Delta\Delta Ct$ value is equal to the \log_2 (fold change), therefore, \log_2 is equal to the subtraction of the ΔCt (GOI) of treated sample from the ΔCt (GOI) of control as well (Equation 4).

$$\text{Equation 4: } \Delta\Delta Ct (GOI) = \log_2(\text{fold change})$$

In this circumstance, the fold change was then calculated by using equation 5:

$$\text{Equation 5: } \text{Fold change (GOI)} = 2^{(-\Delta\Delta Ct)}$$

2.2.14 Nuclei segmentation in organoids and spheroids

The “3D object counter” plugin for ImageJ is a straightforward 3D cell counter which is based on a user-specified intensity threshold to separate signal and background, resulting in a segmented image. This plugin was used to determine the number of cells in each organoid and spheroid. The “3D object counter” plugin for ImageJ also characterizes various nuclei features of the imaged samples, such as nuclei volume and cell density in the sample. In this plugin, specific IF staining coupled with efficient optical clearing technique is the necessary initial step for obtaining reliable data.

2.2.15 Spheroid volume measurement in 3D confocal image stacks with ImageJ

Volume is one of the most important features for the characterization of a spheroid under different conditions. It is often used to describe the effectiveness of the treatment (in our case, cultivation in differentiation medium vs. expansion medium). ImageJ has several tools for measuring object morphological features, albeit it is built to process a single image most of the times and is not so well developed for 3D image stacks. To repeat measurements across the entire stack, some macro programming is required. The macro programming written by Dr. Thomas Villani, at Visikol Inc was applied to measure the volume of spheroids. (<https://visikol.com/2018/11/blog-post-loading-and-measurement-of-volumes-in-3d-confocal-image-stacks-with-imagej/>).

After opening the image stack in ImageJ by going to *File > Open Samples > Image*, all channels should be split. This is accomplished by using the *Image > Color > Split Channels* menu option. Cytoskeleton channel (IF stained with phalloidin) was chosen for volume measurement. A suitable threshold selects the pixel of interest based on the intensity of the pixel value. This is done by selecting *Image > Adjust > Threshold* (or hit Ctrl+Shift+T). The *Otsu* method from the automatic threshold dropdown box was chosen. The next step was to configure the measurements to extract the required quantitative parameters from the thresholded object. For this we selected *Analyze > Set Measurements* menu option from ImageJ and marking *Area*, *Mean gray value*, *Stack position* and *Limit to Threshold* checkboxes. To measure the total volume, macro code was used (the code is reported in the Supplemental information). The macro measures each image in the stack individually and sums the area measurement multiplying this sum by the depth of each slice looping through each image in the stack. As a result, the total volume is displayed.

2.2.16 Segmentation and tracking the cells during aggregation

To acquire three-dimensional information about spheroid formation, it was necessary to identify individual cells and track their movement over time in three dimensions during aggregation process. Three-dimensional nuclei segmentation followed by tracking was performed to determine the number of cells in each spheroid. The nuclei segmentation characterizes various nuclei features of the imaged spheroids, including the number, volume, and cell density of the nuclei within the spheroids.

The organoid's cells were labeled using CellTracker dyes (2.2.7 Short-term cell tracking with CellTracker dyes in spheroids) for the live imaging with Zeiss Light-Sheet Microscope Z1. CellTracker dyes penetrate in the cells with no detectable deleterious effect and provide a bright fluorescence signal even after more than 4 days of repeated scanning without impairing cell viability. The green CellTracker emits fluorescence (excited at 488 nm) at 498 nm, and the Deep Red CellTracker is excited at 561 nm and emits at 571 nm, respectively.

It should be mentioned that the technique of cell tracking and imaging with Zeiss Light-Sheet Microscope Z1 used herein relies heavily upon the ability to prepare and form a tight Z1 holder (Light sheet-based fluorescence microscopy) and to reconstruct data into meaningful three-dimensional representations. Several preliminary steps such as combining more than 100 individual image stacks, brightfield and contrast setting, cropping and deconvolution was

necessary to remove out-of-focus information from individual stacks to facilitate more accurate reconstructions.

The disadvantage of working with such large amounts of data was overcome by parallel computing, which greatly reduces the processing time necessary to deconvolve the data. With a more user-friendly interface and powerful computation resources, this technique promises to ease the deconvolution process further.

2.2.17 Statistical analysis

The results were calculated, analyzed, and visualized using Microsoft Excel 365. For normal distribution data, the Student's t-test was done, and the statistical significance was defined as $p < 0.05$. For each condition 3 independent experiments with at least 3 technical replicates have been performed, the relative expression was calculated and presented in column charts.

3. Results

The main aim of this work was inducing differentiation of pancreatic progenitor cells towards the endocrine lineage during pancreas development using 3D cell culture technique and optimized media. The combination of liquid overlay technique (LOT) with the appropriate culture media in led to the successful formation of compact spheroids. A thorough characterization by immunofluorescent (IF) staining, optical clearing, and imaging with confocal laser scanning microscopy and light-sheet fluorescence microscopy has been performed. The process of hPO cells aggregation to spheroids has been evaluated via time-lapse imaging with bright field and light sheet microscopy.

Furthermore, triple co-culture spheroid has been performed to determine the crosstalk between different cell types and their effect on human pancreatic progenitors, cell differentiation, and spheroid formation. The morphological and molecular properties have been examined with advanced microscopy and molecular biology analyses.

The Results chapter is divided into three sections. First, we show that the optimized LOT represents an effective protocol to generate compact and multilayer spheroid starting from a conventional culture of monolayered acinar organoid. Next, we show that the culture of both hPO and hPO spheroids in different media formulations determines remarkable phenotypical differences. Finally, we analyze the mRNA expression for all investigated culture conditions.

The ultimate goal of this thesis is to be able to control human pancreatic progenitors and induce endocrine differentiation to boost the production of β cells *in vitro* as a means of β cells replacement therapy for type 1 diabetes (T1D).

3.1 Organoids expansion

3.1.1 hPO efficiently grow in both expansion and differentiation medium

To test the general applicability of the expansion and differentiation protocols on hPOs, organoids derived from a human pancreas have been cultured in corresponding medium formulations (Table 7). Before starting the test, the derived cultures were expanded a minimum of 4 passages and frozen for long-term storage in liquid nitrogen (LN₂) tank (2.2.2.1 Thawing and cryopreservation of hPOs).

Here time-lapse imaging of sub-cultured hPOs in both expansion and differentiation medium for 7 days as explained in previous section (2.2.1.1 Human pancreatic organoids (hPOs)) is performed and have been directly observed with Zeiss Cell Observer microscope. The time-lapse image sequences are acquired at 30 min intervals for 7 days. Furthermore, to increase the reliability of the results, hPOs are monitored in parallel with time-lapse experiment in incubator under standard cell culture conditions with a Zeiss Axiovert 40 CFL microscope. Images have been processed afterwards using ImageJ software (Version. 1.49k). Triplicate batches of each organoid have been separately cultured (Figure 15).

No remarkable differences were observed by evaluating bright field images of hPOs cultivation process from day 0 to 7 in both mediums. Within the first 2 days after cultivation, the organoids start to grow and acquire a typical and hollow acinar phenotype, which is a single cell layer surrounding liquid-filled lumen (Figure 15). hPOs were pulsing during cultivation and consequently their size oscillates (Figure 16). Moreover, hPOs were motile in BME2. In some wells, migration is leading to fusion of hPOs with one another (Figure 16). Importantly, organoid outgrowth varies considerably in both media; some organoids show high growth rates in BME2 while others grow poorly or even shrink over time (Figure 15).

To extend this observation, LDA (2.2.6.1 LDA in organoids) was applied to determine cell death in individual organoids embedded in BME2 in each medium. As cell viability plays a fundamental role in all forms of cell culture, organoids have been treated with FDA and PI after 7 days of cultivation in BME2, simultaneously to assess organoid viability. No dead cells are observed in both conditions which confirms that neither protocol affect the viability of hPOs (Figure 17).

Taken all together, we verified that organoids are capable of growth and viability in both media despite a neglecting difference in the number of nuclei per organoids between differentiation and expansion medium.

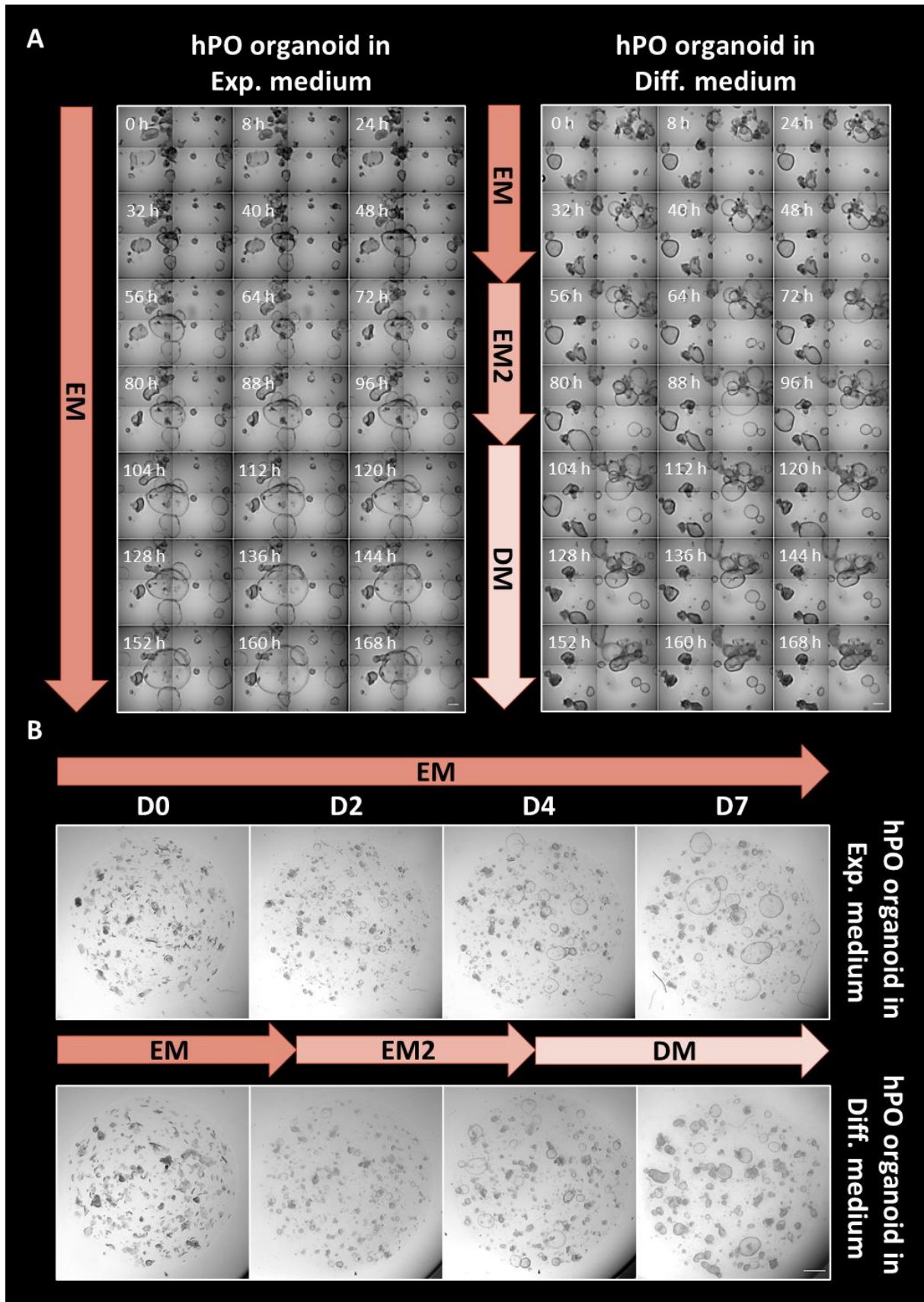


Figure 15: hPO organoids grow in both expansion and differentiation medium documented during taking time-lapse in the Cell Observer microscope (A) and cultivating in the incubator (B). hPOs are diced in small fragment and mixed with fresh BME2 respectively. 10 μ l mixture of BME2 and hPOs were placed on the bottom of 96 well-plate. After polymerization in the incubator, 100 μ l expansion or differentiation medium was added to each well. hPOs have been cultivated for 7 days based on expansion and differentiation protocol. Medium was refreshed on days 2nd and 4th. After 24 h, hPOs start to grow and form a spherical and luminal structure in both mediums. The bright field images have been processed using Zeiss Cell Observer microscope with Plan Achromat 5x/0.16 objective lens (A) and Zeiss SterEO Discovery.V8 with 2x magnification (B). The time-lapse image sequences are acquired at 30 min intervals for 7 days. Exp.: Expansion; Diff.: Differentiation; h: hours; EM: Expansion medium; EM2: Expansion medium 2; DM: Differentiation medium; scale bar (A): 20 μ m; scale bar (B): 500 μ m.

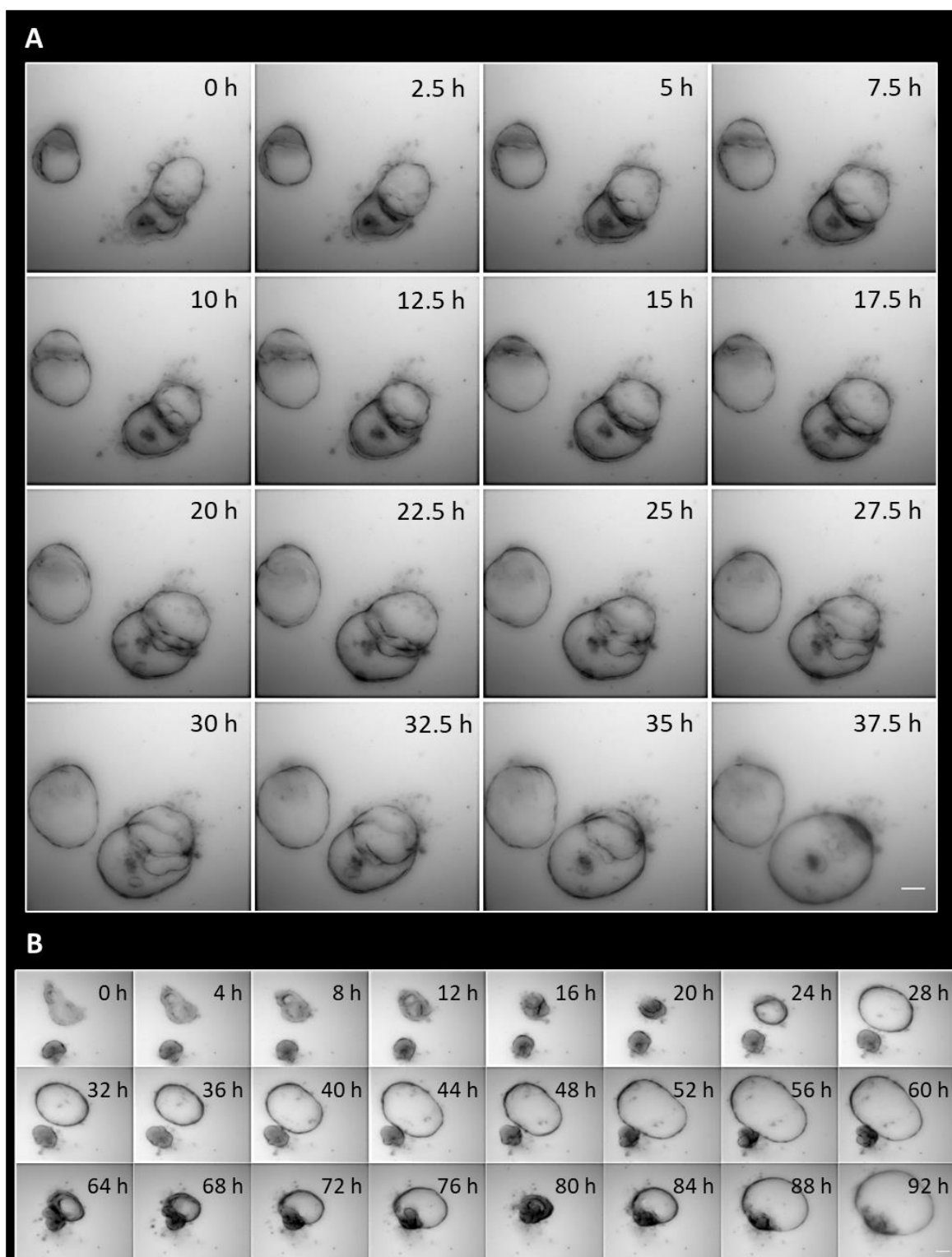


Figure 16: (A) Two hPOs are fusing together after turning to mature spherical structure. After culturing fragments of hPOs in fresh BME2, fragments start to grow and turn to spherical structures. When reaching to the mature size, hPOs fuse together and share their lumen. **(B) hPOs change their size by pumping in and out periodically during cultivation within BME2.** hPOs pump in and out continuously, which leads to the expanding and shrinking regularly during cultivation in BME2. The images have been processed using Zeiss Cell Observer microscope with Plan Apochromat 5x/0.16 objective lens. The time-lapse image sequences are acquired at 30 min intervals for 7 days. h: hours; scale bar: 20 μ m.

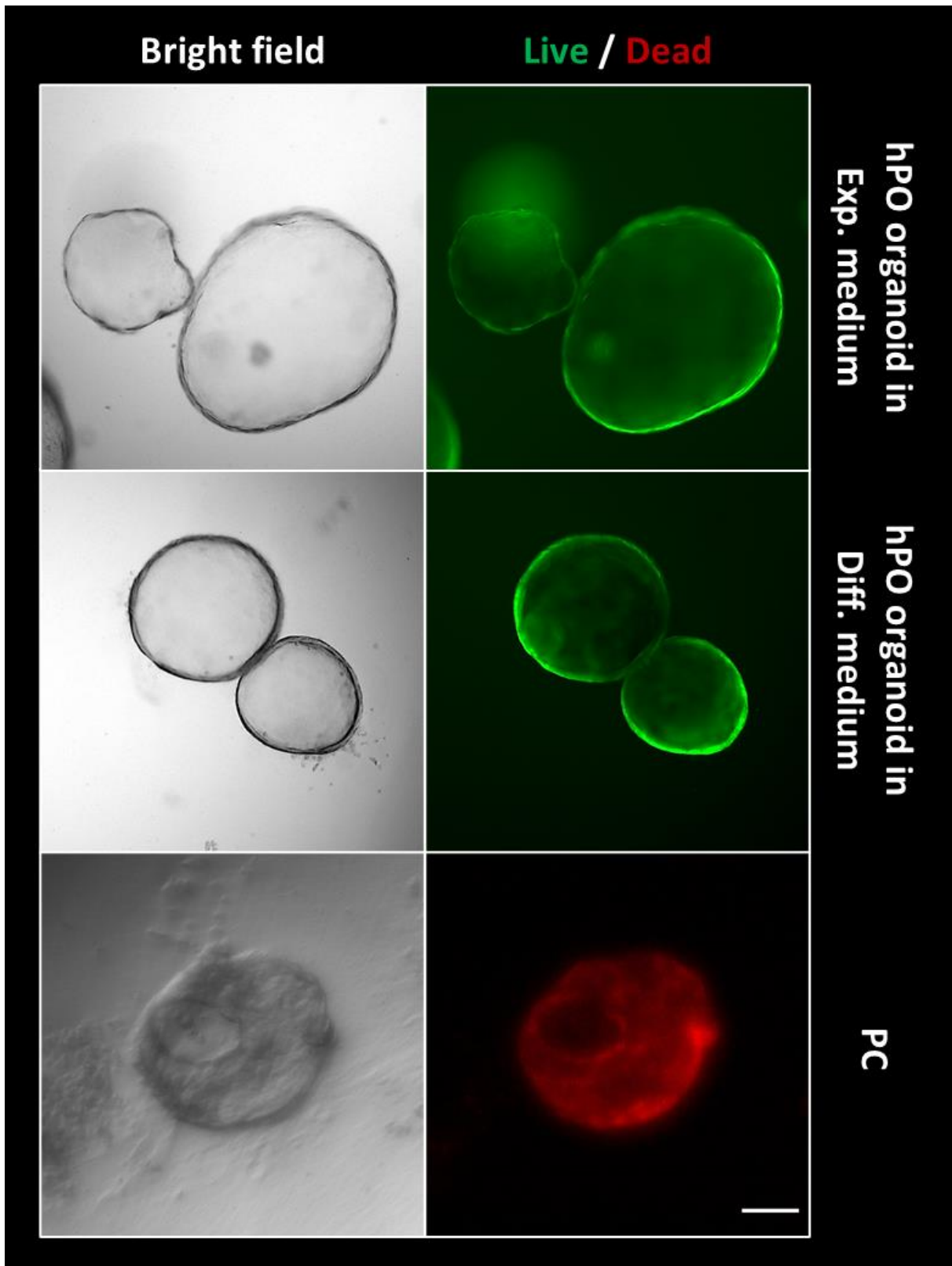


Figure 17: Expansion and differentiation medium has no effect on the mortality of hPOs. After 7 days, hPOs are stained with FDA (green, alive cells) and PI (red, dead cells) to discriminate between living and dead cells. As a positive control, cells were treated with DMSO for 5 min before staining. No dead cell is detected within organoids. Representative images for each condition are shown. The images have been processed using Zeiss Cell Observer microscope with Plan Apochromat 5x/0.16 objective lens; Excitation-Emission: 561 nm - 670/70 nm (PI), 488 nm - 525/45 nm (FDA). Exp.: Expansion; Diff.: Differentiation; PC: positive control; scale bar: 20 μ m.

3.1.2 Optimization steps leading to the formation of well-defined homotypic hPO spheroids

Initially, two different approaches for creating spheroids were tested: hanging drops and liquid overlay techniques (LOT). Due to the limitation in medium volume and starting cell number, long-time cultivation, and the need of multiple media exchange, hanging drop was considered not to be efficient for the scope of this work. Therefore, liquid-overlay technique (LOT) was selected for the experiments.

Next, how different starting cell number (in mono-culture and triple co-culture) and ratio of different cell types (in triple co-culture) may affect spheroid formation was assessed. Size and shape of spheroids have been observed overtime by brightfield microscope. Spheroids are formed from a starting cell number of 1000, 2000, and 3000 hPOs and cultured for 7 days in expansion medium. All starting cell numbers result in the aggregation to form spheroid in the first 48 hours, however only 3000 single cells is capable to form a compact and circular spheroid while other groups form unstable aggregations, which are not compact during collection, fixation, and IF staining for further experiments. Therefore 3000 single cells as a starting cell number was used during the whole thesis. Since there has been no previous studies to indicate the ratio of hMSC, HDMEC and pancreas progenitors within the body during pancreas development, as to avoid complexity, the ratio of 1:1:1 in triple co-culture is utilized.

To improve spheroid formation, several supplements (e.g., Matrigel) have suggested.²¹⁵ Therefore, matrigel was added in different concentrations (0%, 2.5%, 5%, 7.5%, 10%, and 20%) to the expansion medium during spheroid formation. Afterwards, each group have been fixed, stained, and imaged by confocal microscopy. The volume and cell number of each group are analyzed, respectively. Since matrigel is solvable in cold medium, two controls (pre-warmed and cold medium without matrigel) have been performed.

Figure 18 shows a single spheroid being formed in various matrigel concentrations, most of them are characterized by spherical morphology (almost 95%) and regular borders. The volume and cell number of a single spheroid varies between those generated in the presence of matrigel and the ones obtained in its absence. Their volume and cell number per spheroid changes in matrigel concentration independently. The volume and cell number start to increase from 0% to 2.5% matrigel, by continuing the increment, less cell aggregation is observed during spheroid formation accordingly, the spheroids cultured in the presence of

matrigel are smaller compared to those generated without matrigel. More surprisingly, hPOs form the biggest spheroids in the concentration of 2.5% (~480 nuclei per spheroid and > 0.13 mm³ volume), however after analyzing further with FIJI, a small cloudy-like and fuzzy structure generates around each spheroid that are in the presence of matrigel (in all concentrations) interfering strongly with IF staining.

In the absence of matrigel (two controls), the generated spheroids represent uniform morphology with a well-defined and round-shaped border to the last day of the experiment. Based on results, spheroids in 0% matrigel are bigger (~ > 0.07 mm³ volume) than spheroids cultured in pre-warmed medium (~ > 0.05 mm³ volume), and cellular debris cloud surrounding the compact spheroid is observed. Pre-warmed medium without matrigel is chosen. Also, the use of matrigel does not improve the formation of individualized spheroids within 7 days.

Another parameter, which affects hPOs aggregation, is passage number. After applying LOT in different passage numbers, results show that hPOs with a passage number large than 8 are incapable of aggregation and do not form any spheroid. Thus, the ability of hPOs to generate mature and complete spheroid depends on the number of the times that they had been passaged *in vitro*.

For generating spheroids based on LOT, hPOs were first trypsinized. Trypsin and accutase were tested on hPOs based on published papers, however both were established as harmful for hPOs which caused them death in the next day of formation. TripLE have been performed under cellular cultivation conditions (37 C°, 5% CO₂, 21% O₂, and 95% humidity) for 15 min that is capable of turning the hPOs into the mixture of single cells and small fragments and keeping them alive, however the existence of fragments prevents single spheroid formation. As final step in optimization of spheroid formation, fragments are dissociated by passing the cell suspension once through cell strainer before LOT. That leads to the formation of single and compact spheroid, respectively (Figure 20).

It is also worth noting that, even though results indicate that trypsinization by TripLE coupled with running through cell strainer leads to successful aggregation, these processes could be still harmful for the hPOs. Applying LDA demonstrates that the single cells, which don't collaborate in aggregation are noted as dead ones, therefore a delicate process for turning hPOs into single cell is required (Supplementary Figure).

Taken all together, several changes in LOT process are needed for the formation of single spheroid and adding supplements doesn't improve the aggregation process. Furthermore, hPOs' passage number also plays a fundamental role in the aggregation process.

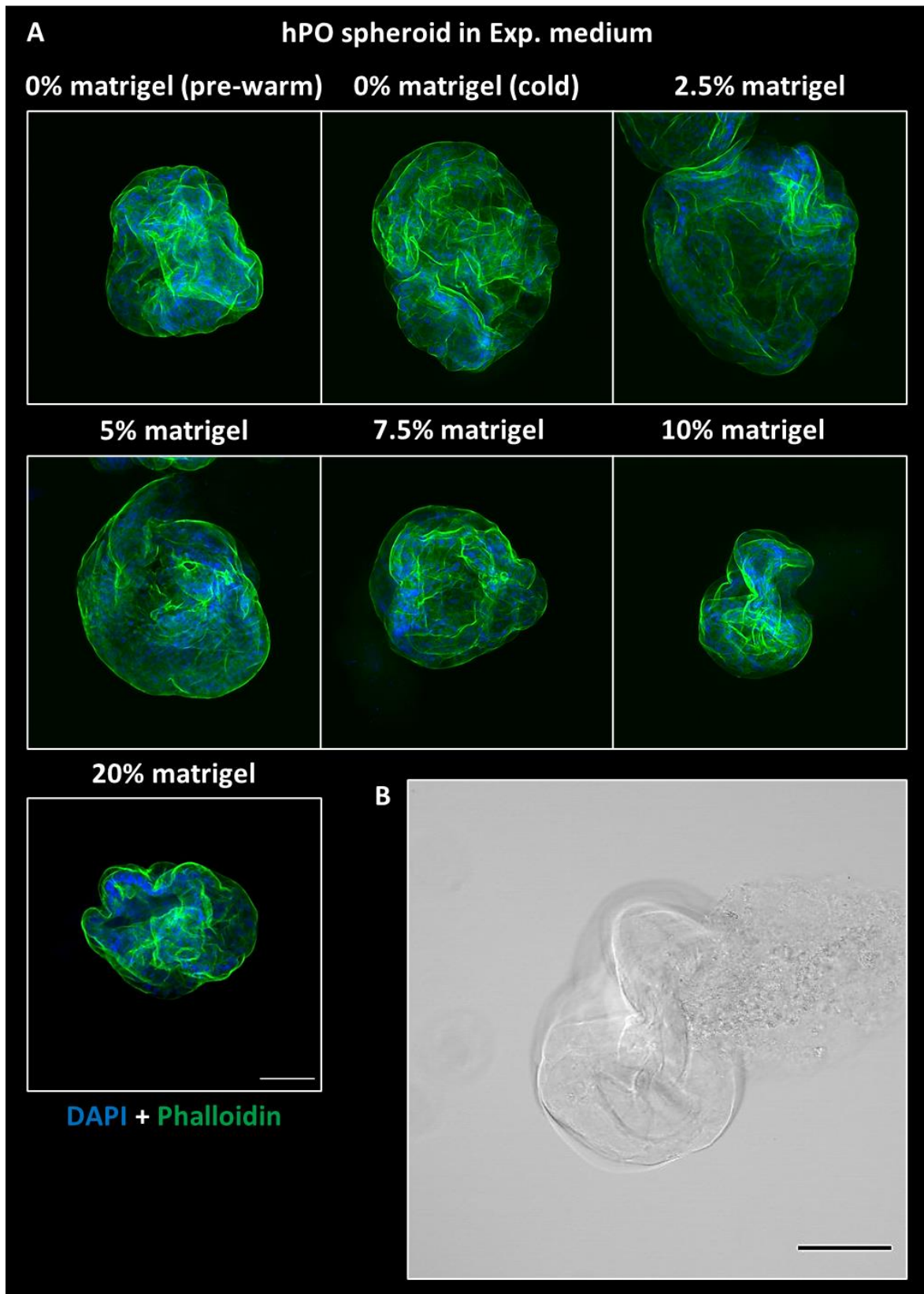


Figure 18: (A) Adding matrigel to the medium negatively affects spheroid size and IF staining. (B) Brightfield image reveals hPO spheroids covered with a cloudy-like structure due to the presence of matrigel in the medium. Spheroids are stained with Phalloidin 488 and presents the cellular cytoskeleton. Representative images are shown. Spheroids are optically cleared, and the images have been processed using Zeiss confocal LSM 780 microscopes with a Plan-Apochromat 20x/0.8 M27 objective lens. Excitation-Emission: 488 nm - 615 nm (Phalloidin 488); Exp.: Expansion; scale bar: 100 μ m.

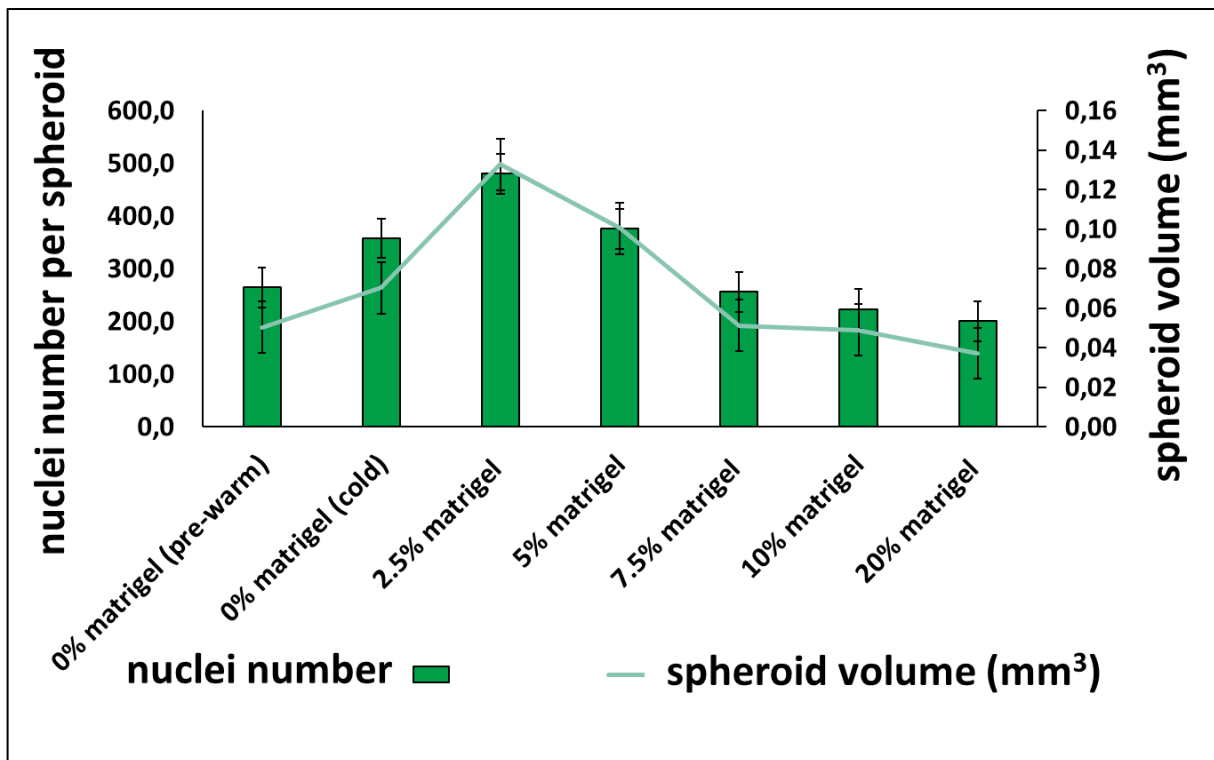


Figure 19: Quantitative analysis of hPOs nuclei number per spheroid after 7 days of cultivation in Expansion and Differentiation medium. For each condition three independent experiments with at least three technical replicates were performed. Data are quantified with ImageJ plugin 3D object counter. The line inside the box denotes the standard error. Excel 365 software is used to illustrate the graphic and perform T-test for statistics analysis. The cultivation in expansion medium significantly increases the nuclei number per spheroid. Exp.: Expansion; Diff.: Differentiation.

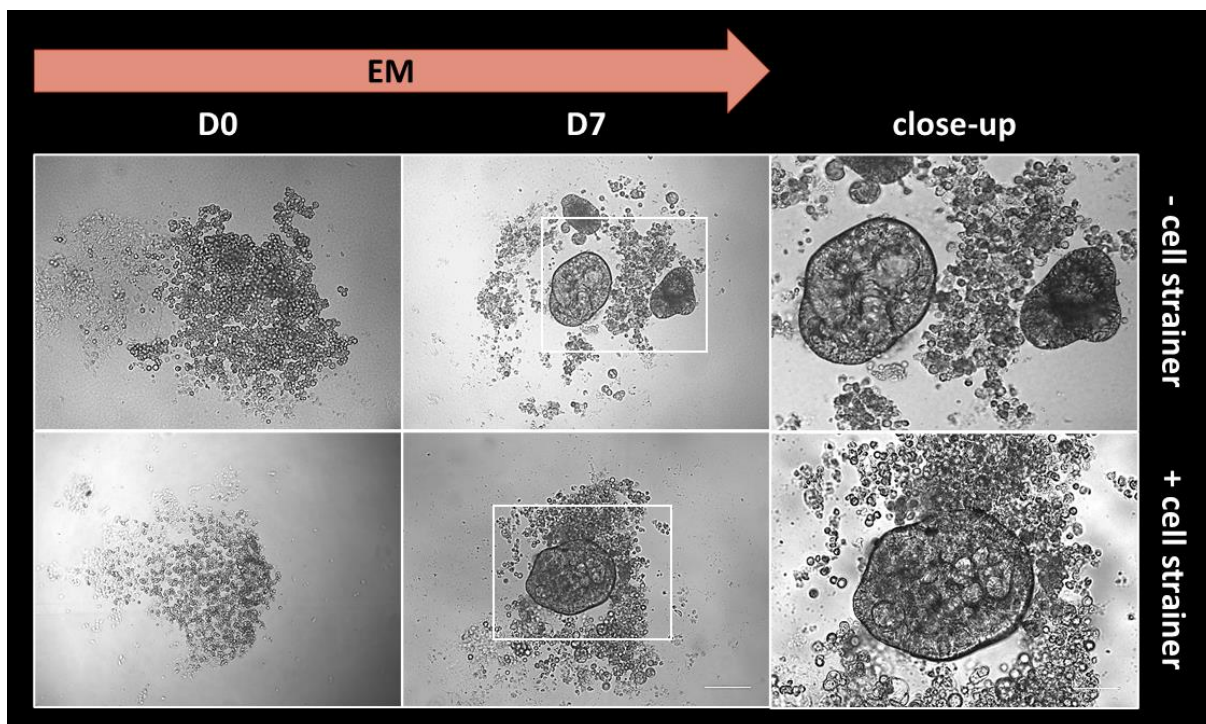


Figure 20: hPOs form a single and compact spheroid by using a cell strainer. By passing the cell suspension through the cell strainer, single and compact spheroid is formed based on the liquid overlay technique (LOT). The images have been processed using Zeiss Axiovert 40 CFL microscope with 5x/0.12 ph0, 10x/0.25 ph1, and 20x/0.35 ph1 objective; D: Day; EM.: Expansion medium; scale bar: 100 μm , close-up: 50 μm .

3.1.3 Aggregation of hPO cells with the liquid-overlay technique (LOT) produces single and compact spheroid in both expansion and differentiation medium

After finding the most efficient method and optimizing it for turning single cell layer and lumen form hPO organoid to a compact and circular spheroid, the capability of hPO cells to aggregate in both media within 7 days was investigated.

Brightfield microscopy demonstrates that hPO cells are capable of aggregation and form spheroid in both expansion and differentiation medium within 7 days. 48 h after hPOs are seeded in 96-well plate coated with 50 μ l low melting agarose, round-shaped spheroids are detected in each well. Having been observed through microscope, spheroids show a multilayer cell assembly (Figure 22). Spheroids continue to aggregate further and form more compact spheroids till harvesting. These data considerably determine rapid generation of spheroids from hPOs based on liquid overlay technique (LOT) in 7 days (Figure 21).

Additionally, to ensure the viability of the hPOs after aggregation, a second image evaluation following the fluorescent labeling of both live and dead cells based on LDA (2.2.6.1 LDA in spheroids) has employed, respectively. Fluorescence images reveal the overall morphology of the spheroids. Differences in cell density and size in both groups are found. The absence of dead cells is evident at all groups, indicative of cell viability in the interior of the spheroids (Figure 23).

Taken all together, human pancreatic organoids aggregate and form well-defined, compact, and alive spheroid in both mediums based on LOT.

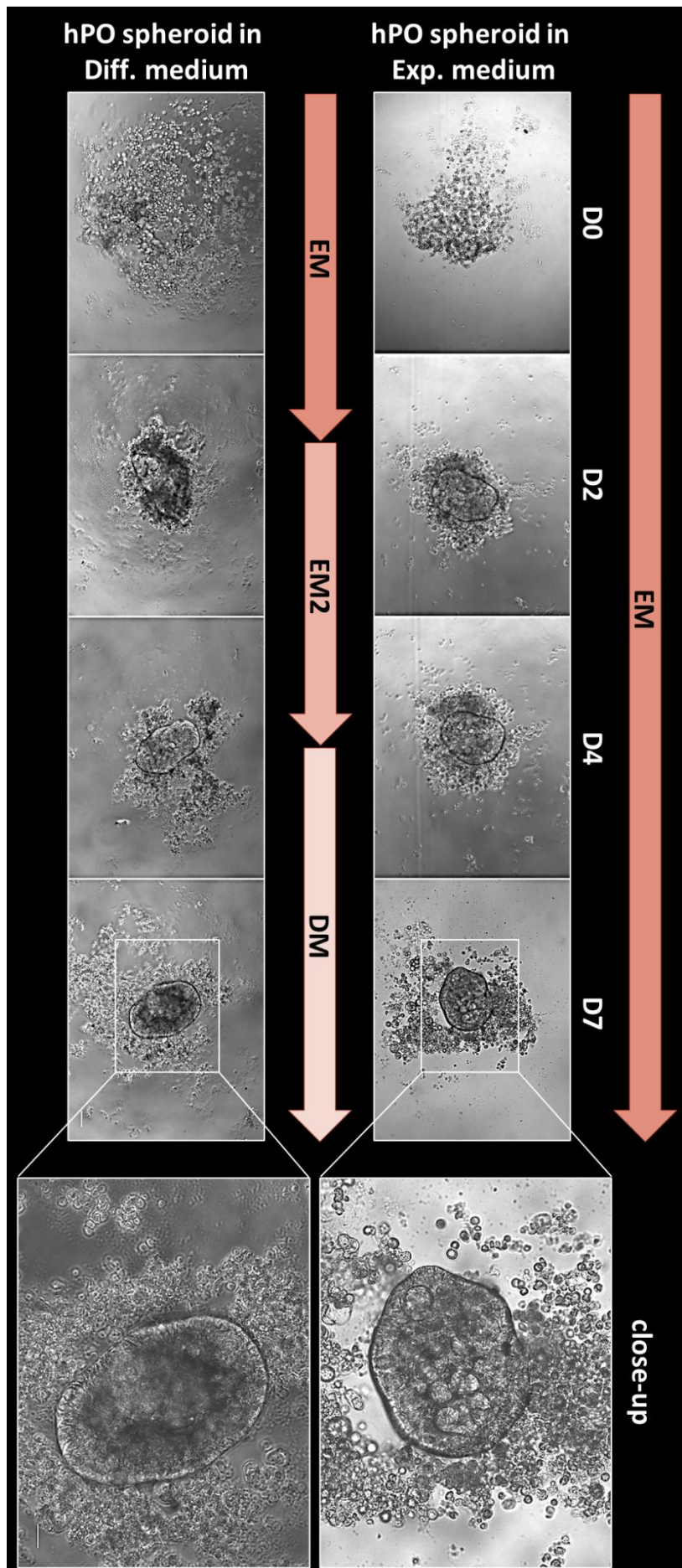


Figure 21: hPOs form single and compact spheroid in both expansion and differentiation medium within 7 days based on the liquid overlay technique (LOT). 3000 single cells were seeded in agarose-coated 96-well plates. After 7 days hPOs aggregate and spheroids form in each well. The medium was replaced every two days. The images have been processed using W Plan-Apochromat microscope with 5x/0.12 ph0, 10x/0.25 ph1, and 20x/0.35 ph1 objective lenses; Exp.: Expansion; Diff.: Differentiation; D: Day; EM: Expansion medium; EM2: Expansion medium 2; DM: Differentiation medium; scale bar: 200µm, close-up: 100 µm.

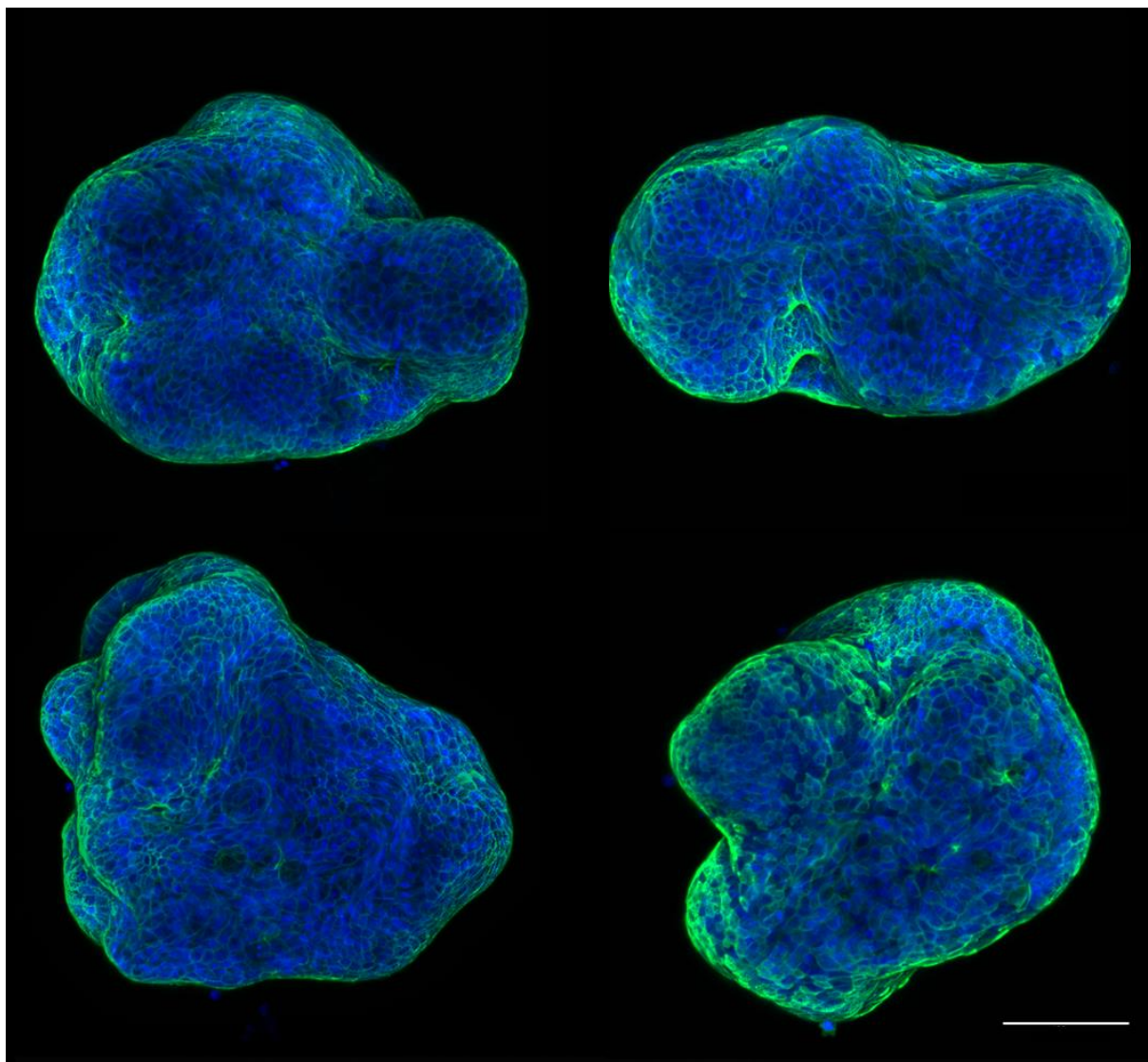


Figure 22: hPO spheroids have spherical morphology and regular borders. Cell nuclei are stained with DAPI (blue) and Phalloidin (green and white) presented in the cell cytoskeleton. Representative Z-project images are shown. Spheroids are optically cleared, and the images have been processed using Zeiss confocal LSM 780 microscopes with a Plan-Apochromat 20x/0.8 M27 objective lens. Excitation-Emission: 405 nm - 450/50 nm (DAPI), 488 nm - 615 nm (Phalloidin 488). DAPI= cell nucleus; scale bar: 100 μ m.

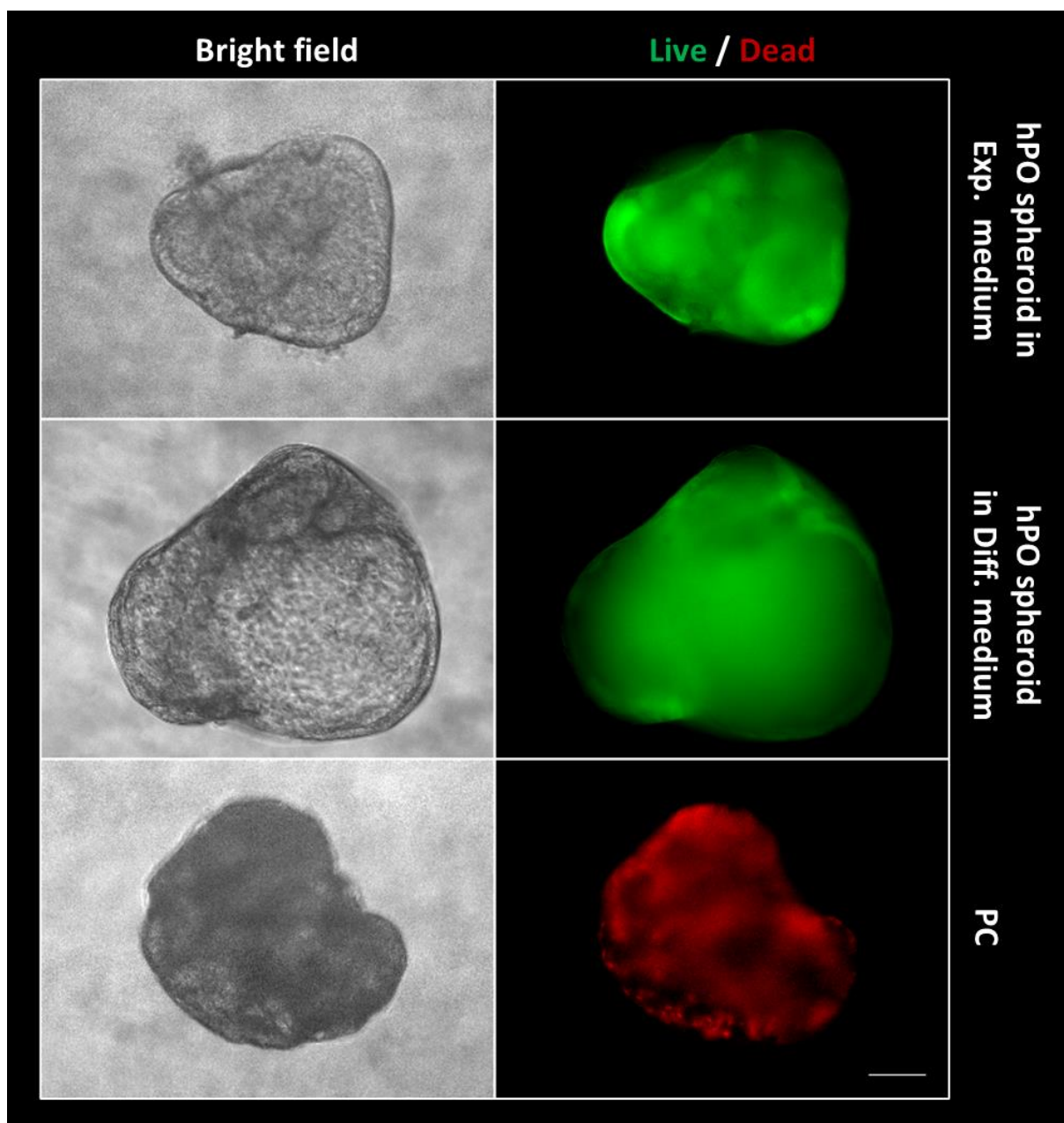


Figure 23: The mortality of hPOs have been analysed after aggregation by live/dead assay. After aggregation, spheroids were stained with FDA (green, alive cells) and PI (red, dead cells) to discriminate between living and dead cells. As a positive control, cells were treated with DMSO for 5 min. No dead cell was detected within spheroids. Representative images for each condition are shown. The images have been processed using Zeiss Axiovert 40 CFL microscope with 10x/0.25 ph1; Excitation-Emission: 561 nm - 670/70 nm (PI), 488 nm - 525/45 nm (FDA); PC: positive control; scale bar: 200 μ m.

3.1.4 The presence of all three cell types (hPO, hMSC, HUVEC) are essential for spheroid formation in differentiation medium

It has been widely reported that the human tissues contain a heterogeneous mixture of different cell types which help reciprocal to promote cell growth and induce differentiation during development.^{132,216} Therefore, the presence of these supporting cells is hypothesized to help the progenitor hPOs to turn into β cells and help to form larger and more mature (compact) spheroid. To investigate the role of supporting cells on the hPOs differentiation and spheroid formation, either primary Human Dermal Microvascular Endothelial (HDMEC) or human Mesenchymal Stem Cells (hMSC) have been co-cultured with hPOs based on LOT, with spheroid formation being monitored. This method is used to analyze the influence of supporting cells (hMSC and HDMEC) on the hPOs phenotype. The characterizations of the hPOs after 3D co-culture were phenotypically and genetically compared by analyzing the expression of defined differentiation markers and IF staining. The functionality of these co-culture and their ability to influence on hPOs was then investigated.

Since the starting cell number has already determined in previous section (3.1.2 Optimization steps leading to the formation of well-defined homotypic hPO spheroids), current experiment with three cell lines has started with the different combinations and cultivation in both mediums.

Given the fact that both hMSC and HDMEC have the ability to aggregate and form spheroid,^{217,218} first, both cell types were cultured based on LOT in each medium separately and simultaneously. As expected, hPOs form compact spheroid in expansion and differentiation medium in 7 days. However, the results clearly demonstrate that hMSC form an aggregation in both media in first 2 days, nonetheless the aggregation doesn't progress and doesn't turn into a tight and mature spheroid till day 7, therefore that was dissociated during collection and no aggregation forms by HDMEC in general.

Next, a couple of co-cultures with different combinations 1:1 (hPOs and hMSC or hPOs and HDMEC) and 1:1:1 (hPOs, hMSC, and HDMEC) ratio have been examined.

The results suggest that after cultivating all groups in both mediums, some aggregation is detected in all conditions till day 4 but they are unstable and only the presence of all three cell lines in differentiation medium leads to the formation of well-defined and circular spheroid.

It was detected that the mixture of hPO, hMSC and HDMEC (1:1:1) in the expansion medium starts to aggregate till day 4, however after replacing the EM2 medium to DM (based on differentiation medium), the cells start leaving the spheroid in the last three days, therefore no spheroid is formed.

Newly formed spheroids are not as compact with clear barriers as single hPOs spheroid, but they are stable enough to be collected, fixed, and stained for further experiments, which is not achievable in other groups. Furthermore, the output of LDA demonstrated that the triple spheroids are alive ergo were used for further experiments (Supplementary Figure).

Taken all together, the presence of supporting cells plays a critical role in the spheroid formation and this formation varies depending on the types of cells and medium respectively.

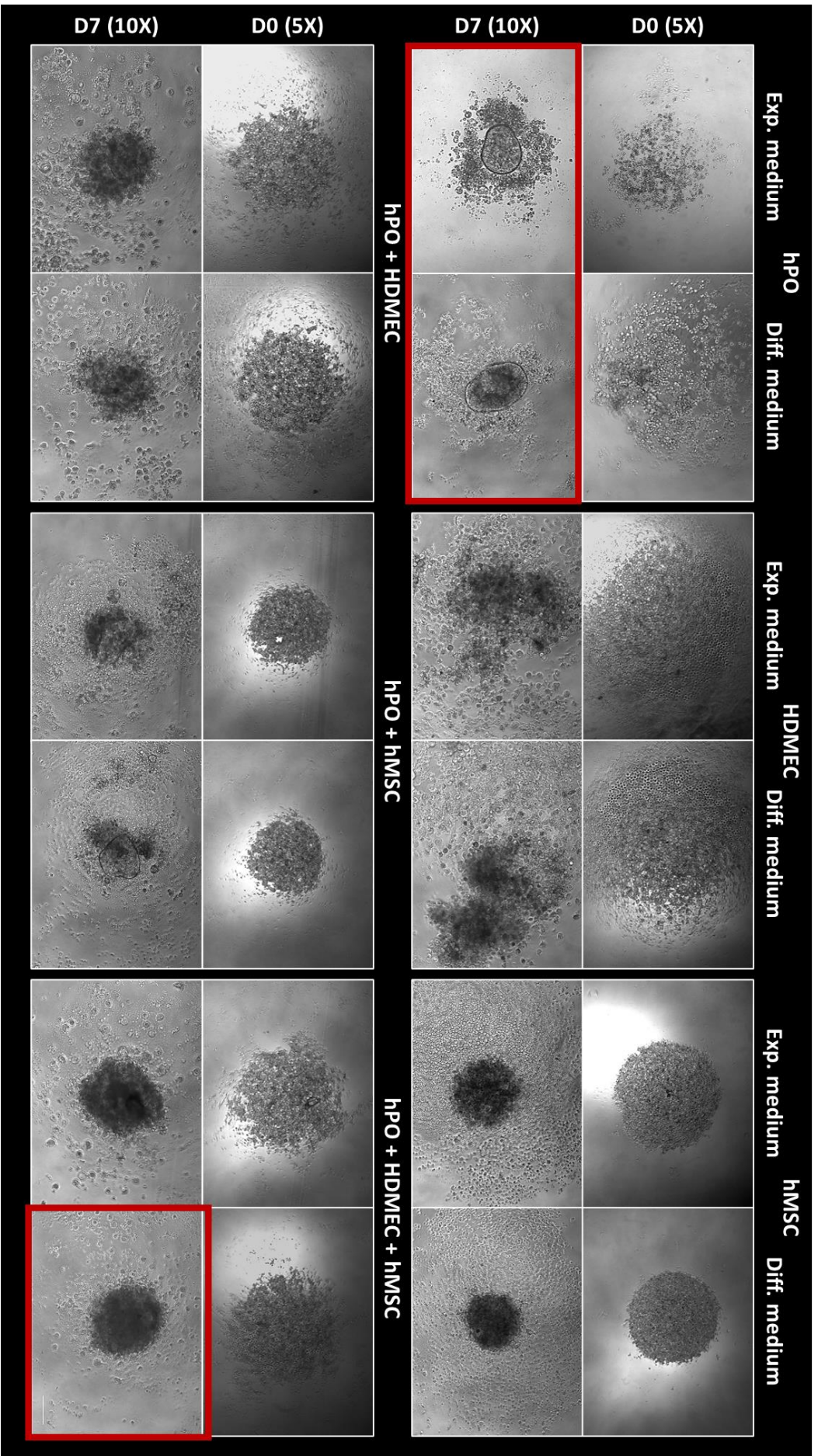


Figure 24: hPOs form single and compact spheroid in both expansion and differentiation medium within 7 days based on the liquid overlay technique (LOT). 3000 single cells were seeded in agarose-coated 96-well plates. After 7 days hPOs aggregate and spheroids are formed in each well. The medium was replaced every two days. Representative images for each condition are shown. The images have been processed using W Plan-Apochromat microscope with 5x/0.12 ph0, 10x/0.25 ph1, and 20x/0.35 ph1 objective lenses; Exp.: Expansion; Diff.: Differentiation; D: Day; scale bar: 200µm.

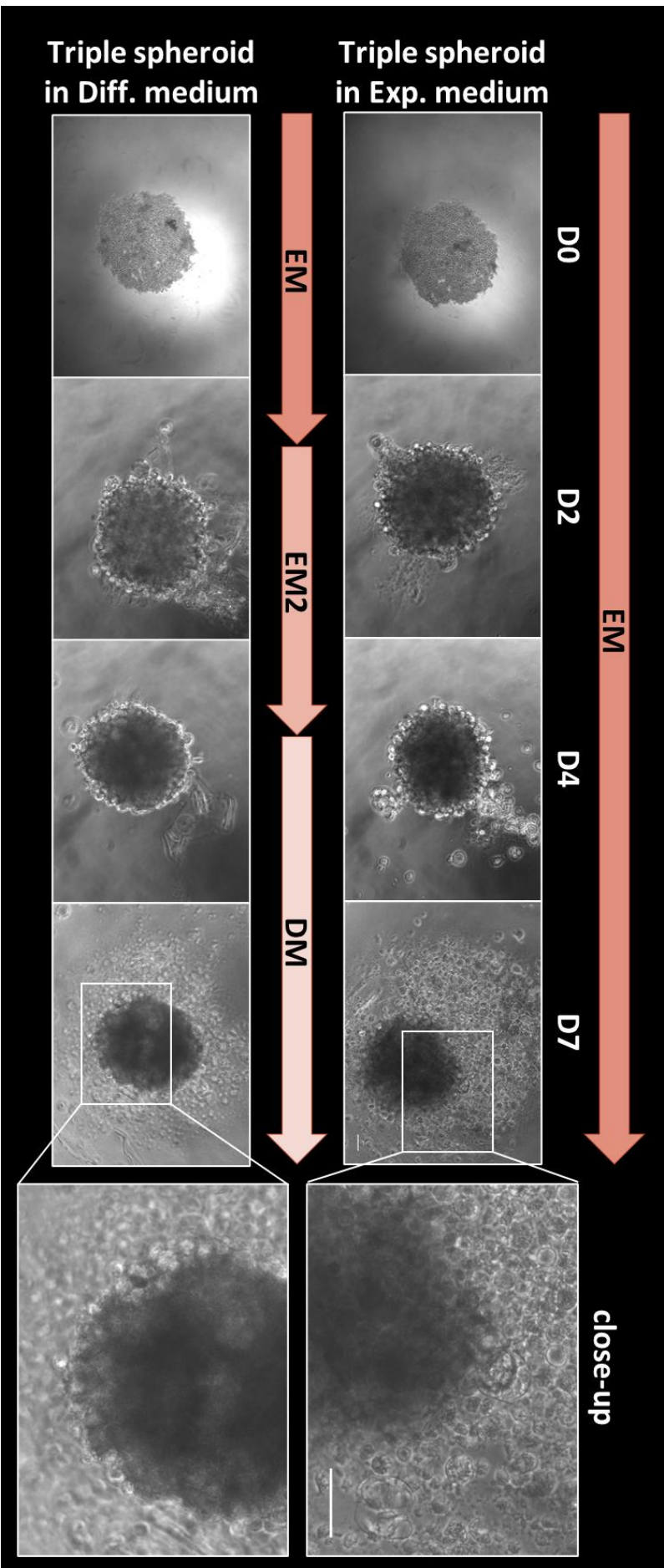


Figure 25: Mixture of hPO, hMSC, and HDMEC (ratio 1:1:1) formed just single and compact spheroid in differentiation medium within 7 days based on the liquid overlay technique (LOT). 3000 single cells for the mixture of cells (ratio of 1:1:1) were seeded in agarose-coated 96-well plates. After 4 days hPOs were aggregate and spheroids were formed in both conditions, however in the last 3 days the spheroids in differentiation medium start to diverge. The medium was replaced every two days. Representative images for each condition are shown. The images have been processed using W Plan-Apochromat microscope with 5x/0.12 ph0, 10x/0.25 ph1, and 20x/0.35 ph1 objective lenses; Exp.: Expansion; Diff.: Differentiation; D.: Day; EM: Expansion medium; EM2: Expansion medium 2; DM: Differentiation medium; scale bar: 200µm, close-up: 100 µm.

3.2 Phenotypical characterization

3.2.1 The morphology of both pancreas organoids and spheroids varies in expansion and differentiation media

Even though organoids and spheroids are both promising 3D cell culture samples, fundamental differences are defined in each one, which may affect their morphology. Organoids are the 3D *in vitro* experimental systems in which cells form a single-layered hollow spherical structure but spheroids are known as cluster of aggregated cells that form multicellular-layered structure, which is clearly observed after IF staining in our samples (Figure 26).

Cells in organoids are uniformly exposed to nutrients and oxygen. In contrast, cell populations within a spheroid are dealing strongly with nutrients- and oxygen-gradient, which conspicuously evolve their proliferation and cell death, consequently the spheroid morphology is affected. As the next step, the effects of each medium on the morphology of organoids and spheroids have been investigated.

After preparing hPO organoids and spheroids in expansion and differentiation medium, IF staining was performed on each group, respectively, and samples have been acquisitioned by confocal laser scanning microscopy. The post-processing has been done by ImageJ software. The 3D object counter plugin for ImageJ has performed on not-optically cleared organoids and optically cleared spheroids.

Quantitatively, a significantly higher number of cells is observed and accordingly, bigger size is detected in spheroids formed in differentiation medium compared to the spheroids formed in expansion medium. The similar result is not observed comparing spheroids formed in expansion medium and triple spheroids. In contrast, organoids in differentiation medium contain of noticeably less cells compared to the organoids generated in expansion medium (Figure 27).

Closer examination reveals that numbers of nuclei per organoids in differentiation medium (~ 200 nuclei per organoid) is by a large amount smaller than the number of nuclei per organoids in expansion medium (~ 440 nuclei per organoid), consistent with the formation of bigger organoids in expansion medium compared to the differentiation medium.

It is worthy to note that, comparing organoids and spheroids in differentiation medium, a noticeable difference is observed in the nuclei number and surprisingly, spheroids contain more cells than organoids under the same cultivation condition (Figure 27).

Taken all together, differentiation medium has significant effect on the phenotype and morphology of organoids and spheroids.

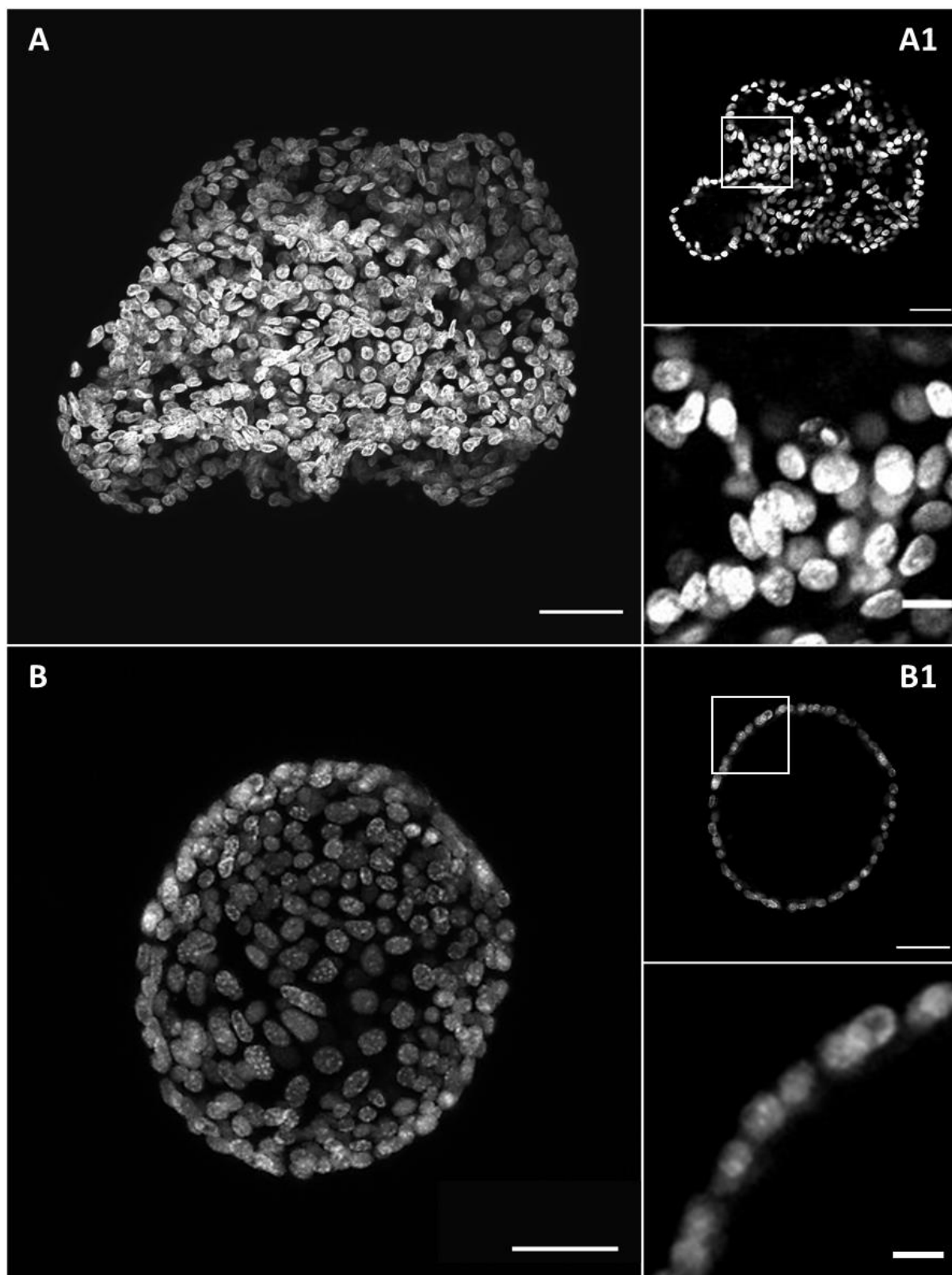


Figure 26: IF staining presents the overall (A, B) and cross section (A1, B1) of hPO spheroid and organoid. Nuclei staining with DAPI reveals the single-layer and bubble-like structure of the organoids as well as spherical and multilayer formation of spheroids. Representative images for each condition are shown. Spheroids are optically cleared, and the images have been processed using Zeiss confocal LSM780 microscope with W Plan-Apochromat 20x/084 M27; Excitation-Emission: 405 nm - 450/50 nm (DAPI); scale bar: 50 μ m, close-up: 25 μ m

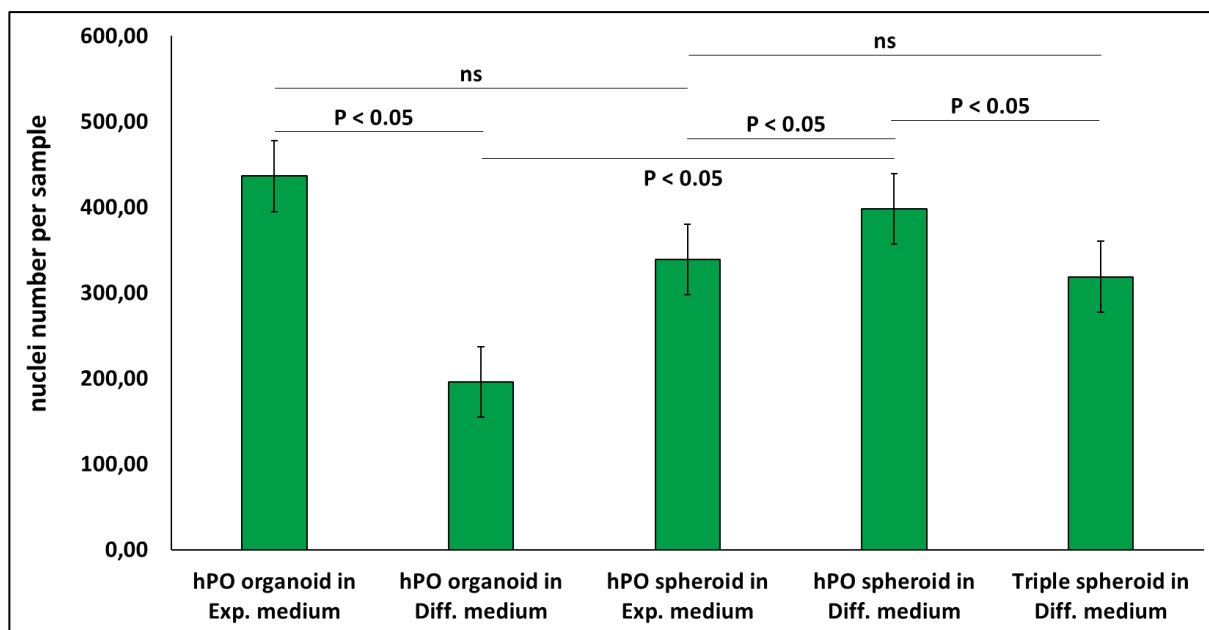


Figure 27: Quantitative analysis of hPO nuclei number per spheroid and organoid after 7 days cultivation in Exp. and Diff. medium. For each condition three independent experiments with at least three technical replicates were performed. Data have been quantified with ImageJ plugin 3D object counter. The lines inside the boxes denote the standard error. Excel 365 software is used to illustrate the graphic and perform T-test for statistics analysis. ns: not significant; Exp.: Expansion; Diff.: Differentiation.

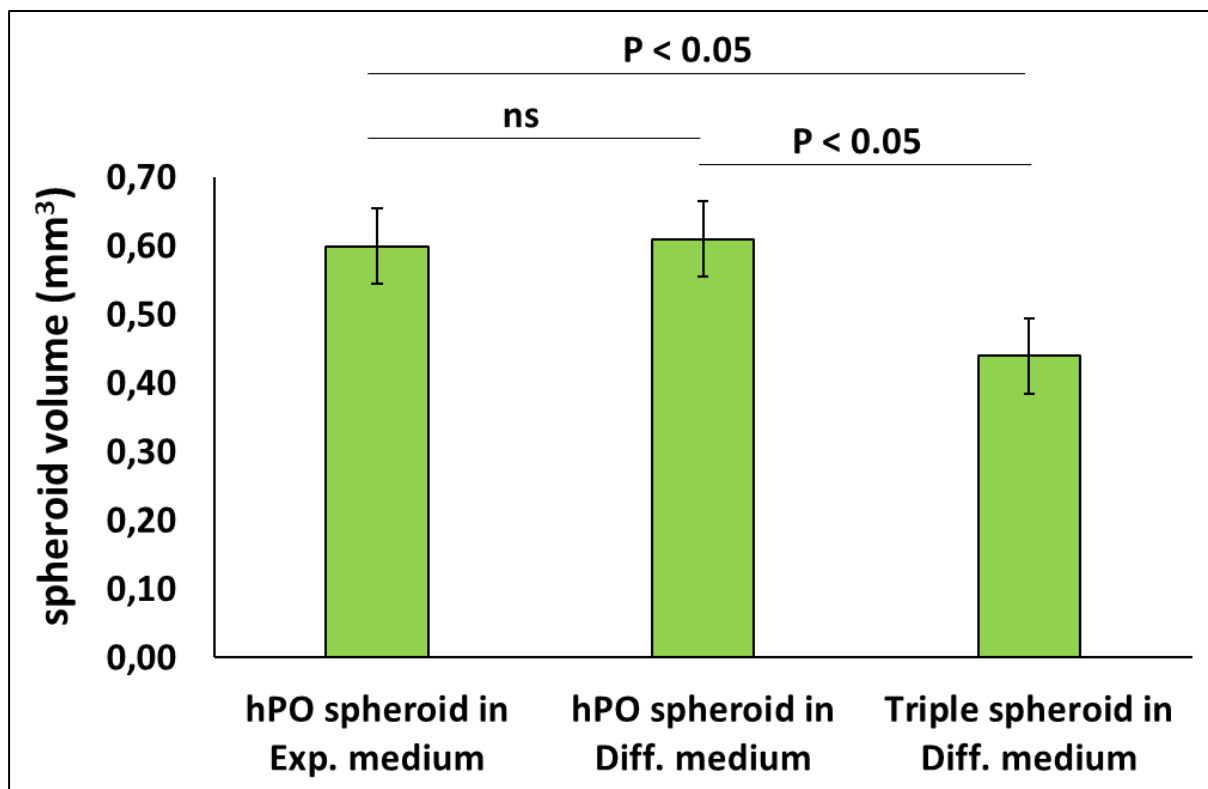


Figure 28: Quantitative analysis of spheroid volume and cells per spheroid after aggregation in Exp. and Diff. medium. For each condition three independent experiments with at least three technical replicates were performed. Data have been quantified with ImageJ plugin 3D object counter. The lines inside the boxes denote the standard error. Excel 365 software is used to illustrate the graphic and perform T-test for statistics analysis. Exp.: Expansion; Diff.: Differentiation.

3.2.2 The differentiation medium induces cell polarization in hPO and hPO spheroids

Alteration in the position of the nucleus in polarized cells is documented in many biological functions such as differentiation or developmental issues. The cytoskeleton is highly stimulated by polarization signals and provides a structural framework for the nuclear and demonstrates changes during different cell statuses. These changes may lead to the differentiation respectively.^{219,220}

After cultivating the organoids and spheroids in both expansion and differentiation medium for 7 days, IF staining was performed on each group to visualize the internal morphology and nuclei arrangement over 7 days. The nuclei were stained and imaged using DAPI or Hoechst 33342 and the actin filaments were stained by Phalloidin 568.

Here the focus is on the almost round and symmetric organoids whose nuclei are centered and localized along to the cell membrane. hPO organoids express strong polarized apical actin filaments facing towards lumen in both expansion and differentiation media. Interestingly, the strong basal nuclear rearrangement is also observed in some of the organoids cultured in differentiation medium (Figure 29).

Based on IF staining, mono-culture and triple co-culture spheroids cultured in differentiation medium show a strong basal rearrangement in their external layer. Furthermore, most of the cells within spheroid contain external actin filaments, which show a polarized distribution with actin filaments at one side of the cell (Figure 30). To determine whether this asymmetry reflects the overall polarity of the cell or not the samples are stained with an antibody as the Golgi marker, GM130. However, the staining was not successful, therefore no image is presented here.

Taken all together, results demonstrate that the differentiation medium leads to the strong nuclear rearrangement within organoids and spheroids. Furthermore, actin filaments reflected the establishment of cell polarity.

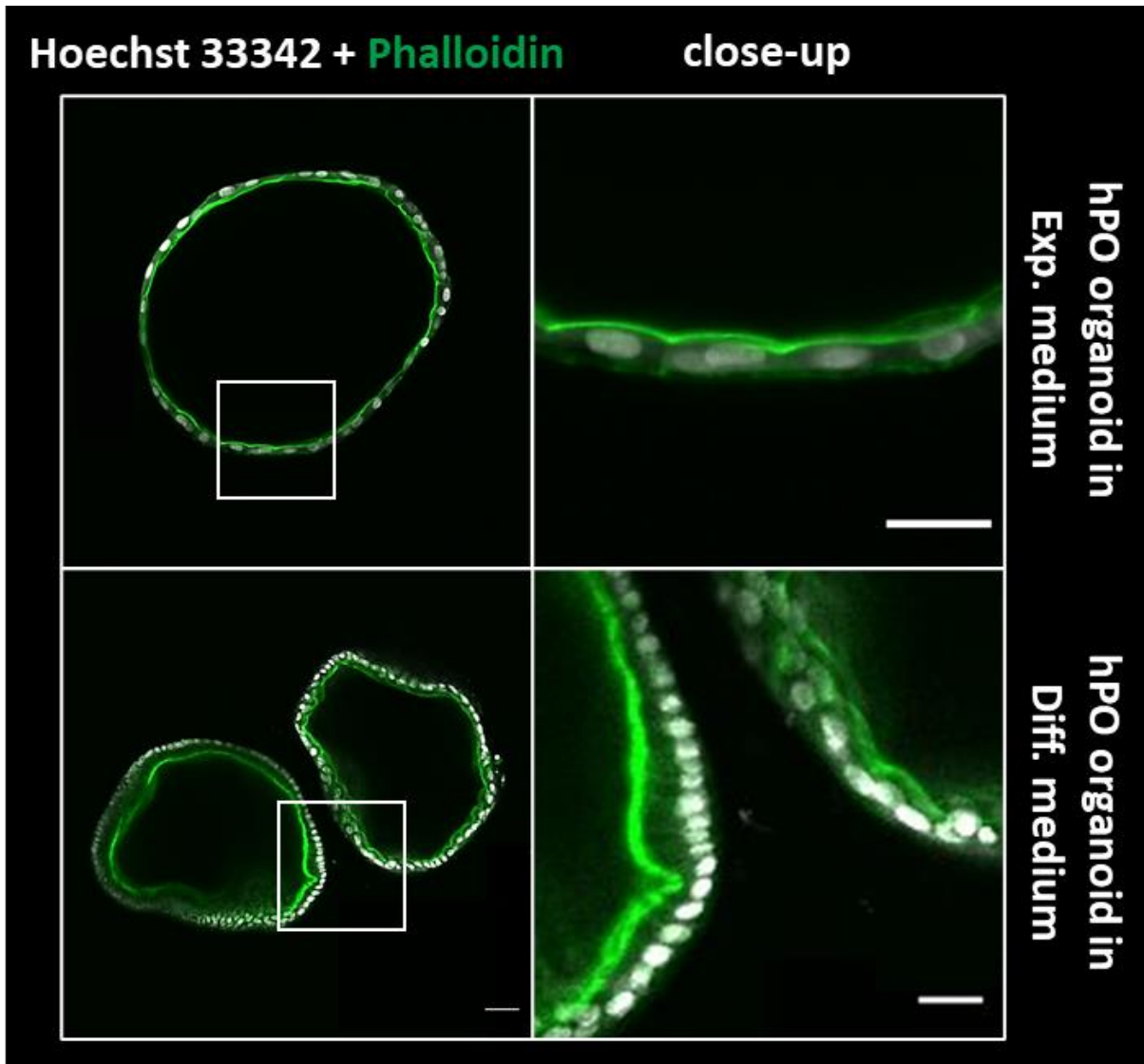


Figure 29: Differentiation medium leads to the basal localization of nucleus in some organoids. IF staining with phalloidin 488 reveals that cell nucleus in some organoids, cultured in differentiation medium, are strongly basal-polarized. Representative images for each condition are shown. The images have been processed using Zeiss confocal LSM780 microscope with W Plan-Apochromat 20x/084 M27; Excitation-Emission: 405 nm - 450/50 nm (Hoechst 33342), 561 nm - 670/70 nm (Phalloidin); scale bar: 50 μ m, close-up: 10 μ m

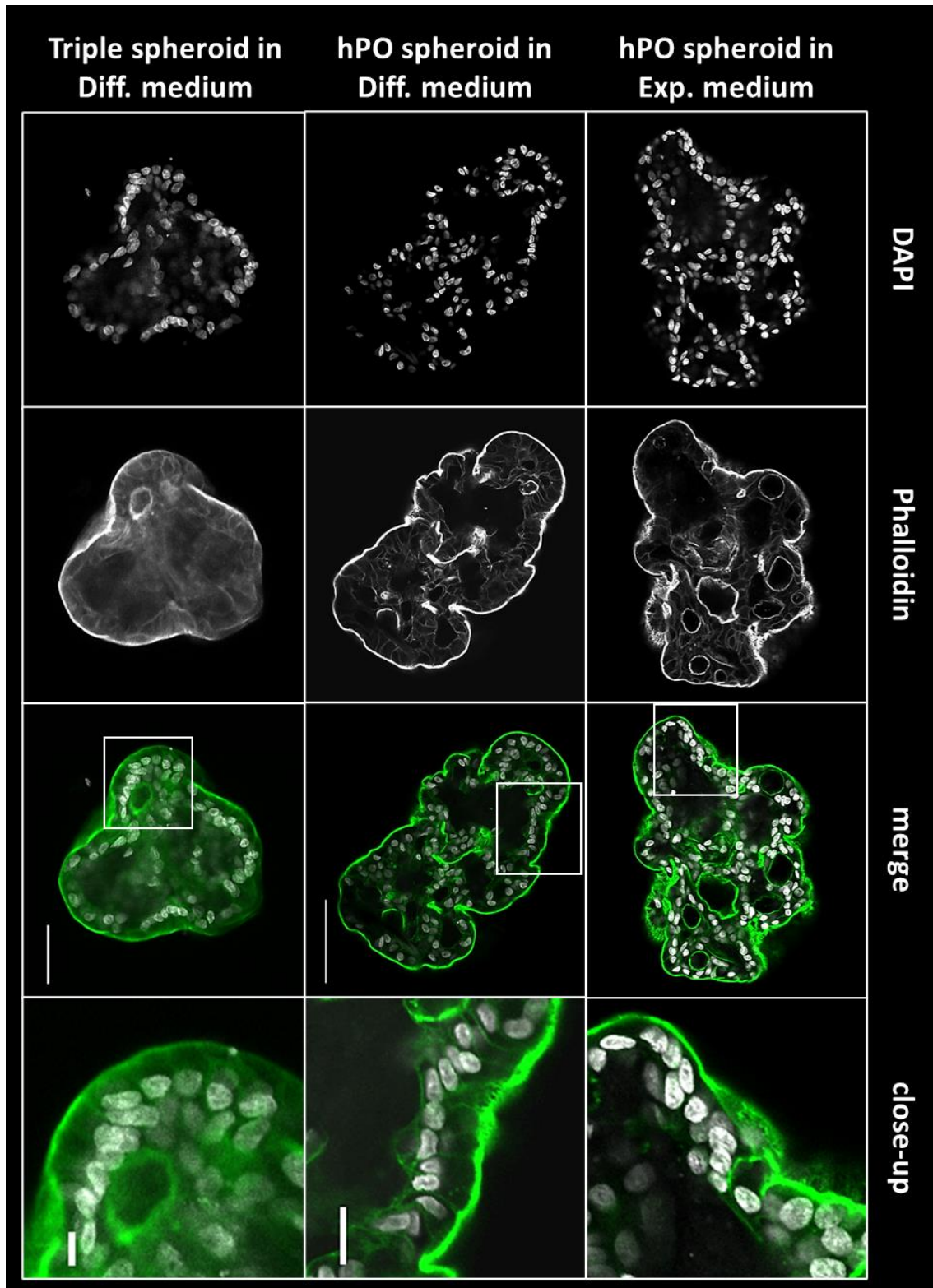


Figure 30: Strong basal polarization in the external layer of the spheroid, cultured in differentiation medium. IF staining with phalloidin 488 reveals that cell nucleus in the outer layer of the spheroids, cultured in differentiation medium, are strongly basal-polarized. Representative images for each condition are shown. Spheroids are optically cleared, and the images have been processed using Zeiss confocal LSM780 microscope with W Plan-Apochromat 20x/084 M27; Excitation-Emission: 405 nm - 450/50 nm (DAPI), 561 nm - 670/70 nm (Phalloidin); scale bar: 50 μ m, close-up: 10 μ m.

3.2.3 hPO spheroids show multiple internal acinar structures

The extracellular matrix (ECM) and particularly the basement membrane (BM) play an important role in orienting the cells during spheroid formation. IF staining against phalloidin to demonstrate the polarization status after aggregation, one of the well-documented properties within spheroids is the formation of internal acini-like structures in different sizes in both mono- and co-cultured spheroids. hPOs form cavities with clear apical-in and basal-out polarization (Figure 31).

Why spheroid aggregation led to the formation of multiple acinar structures remained unclear. To investigate it in more details, the process of aggregation has been monitored in a time-lapse by Z1 microscope. hPOs were trypsinized to single cells followed by staining with 5 μ M CellTracker™ Orange CMTMR. The results clearly demonstrate that hPOs keep their original growth pattern and pump in and out constantly during aggregation which lead to the formation of these cavities with surrounded single cells inside of the spheroids, respectively (Figure 32). Therefore, it is hypothesized that despite all differences between organoids and spheroids, hPOs represent their original morphology and growth pattern of organoids (round, empty, bubble-like and 3D structure) during aggregation inside of spheroid.

Taken all together, phalloidin staining revealed the formation of multiple hollow acinar compartments inside of spheroids and it is observed that hPOs keep their growth pattern even though they are trypsinized to single cells and forced to aggregate and form spheroid.

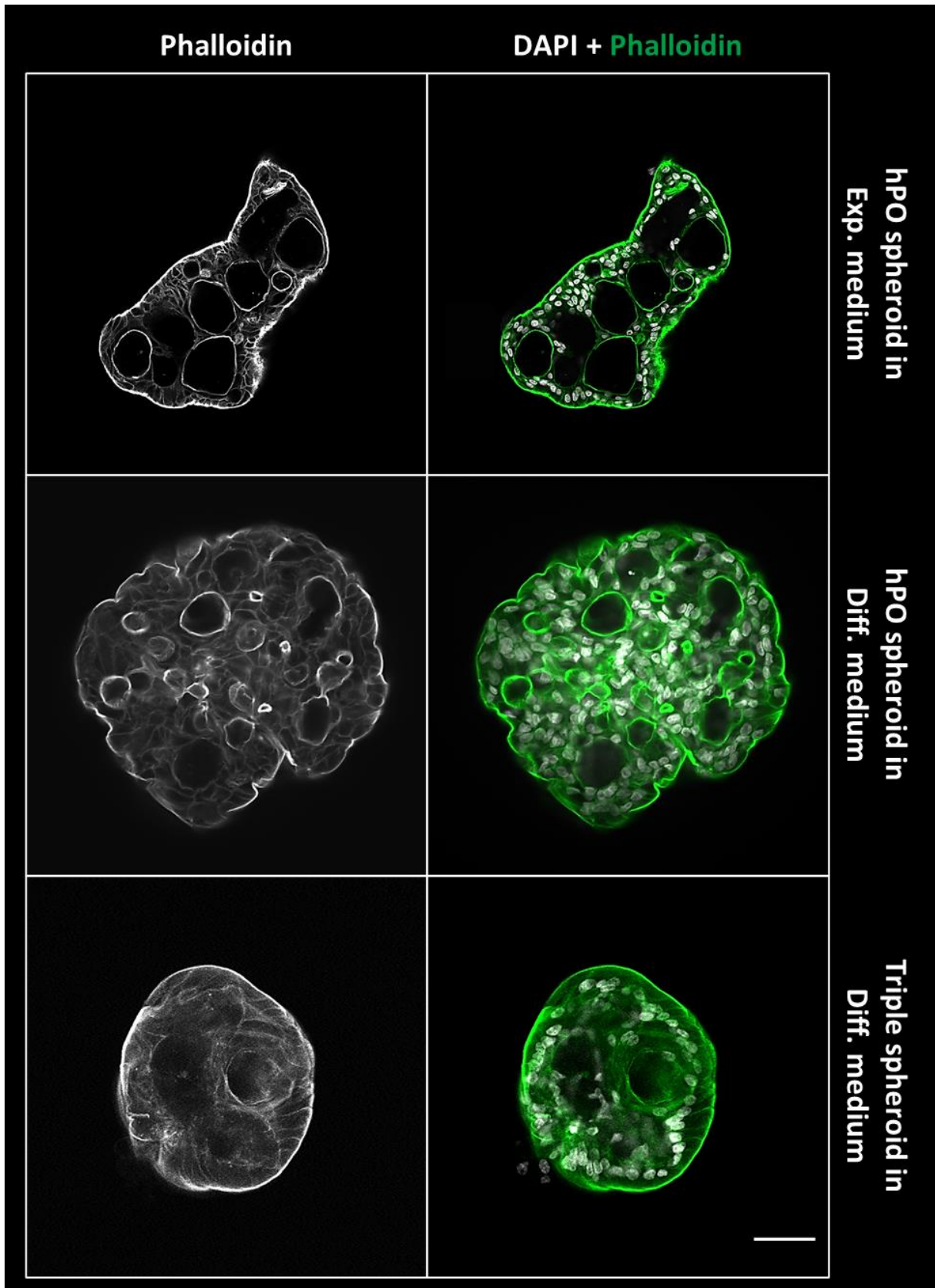


Figure 31: Spheroids consist of small cavity-like structures in all cases. After IF staining the cytoskeleton, circular and bubble-like structures are detected within spheroids in all cases. Representative images for each condition are shown. Spheroids are optically cleared, and the images have been processed using Zeiss confocal LSM780 microscope with W Plan-Apochromat 20x/084 M27; Excitation-Emission: 405 nm - 450/50 nm (DAPI), 561 nm - 670/70 nm (Phalloidin 568); scale bar: 50 μ m.

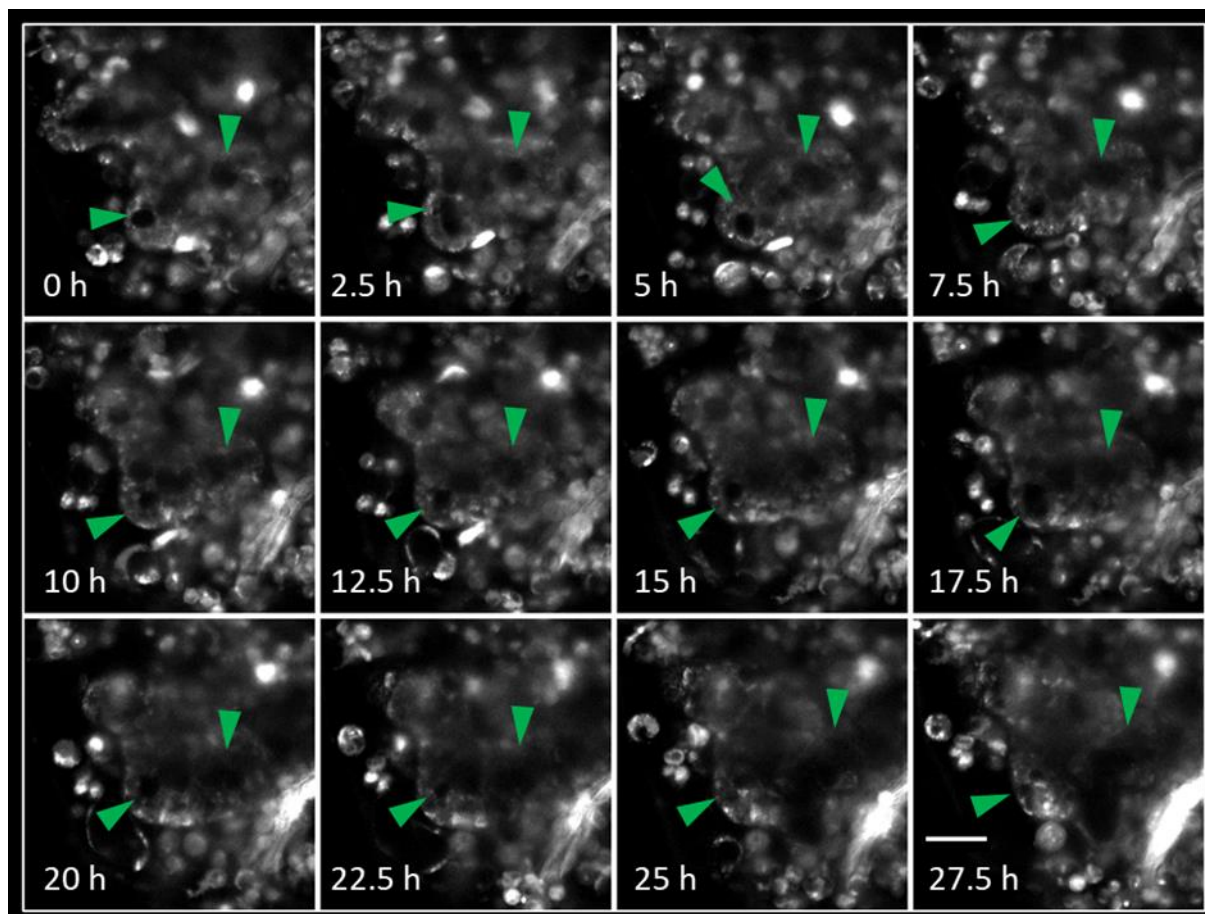


Figure 32: hPOs maintain their original growth pattern and pump in and out constantly during aggregation. hPOs were trypsinized to single cells followed by staining with 5 μ M CellTracker™ Orange CMTMR. The process of aggregation was monitored in a time-lapse by Z1 microscope. The formation of bubble-like structures that were pumping in and out continuously, inside of the spheroids during aggregation has been monitored, respectively. The time-lapse image sequences have acquired at 30 min intervals for 4 days. Arrows are pointing at acinus-like structure within spheroids. Representative images for each condition are shown. The images have been processed using Z1 microscope with Det.: W Plan-Apochromat 20x/1.0 UV-VIS; Illum.: Zeiss LSM 10x/0.2; Laser: 561 nm-571 nm; scale bar: 50 μ m.

3.2.4 Monitoring the aggregation process of pancreas progenitor cell spheroids with time-lapse light sheet microscopy

After optimization of spheroid formation in agarose-coated non-adhesive wells to visualize the process of aggregation in detail time-lapse transmission images were taken using Z1 microscope with one-sided 20x/1.0 detection optics and two-sided 10x/0.2 illumination optics. The image sets were processed using ZEN imaging software. Time-lapse data was further scrutinized to investigate the mechanism of spheroid self-assembly. Tight Z1 holder, which is a special holder established in the Stelzer group, coupled with FEP foil cuvettes were prepared to resemble concave agarose wells. Fluorescent cell trackers in orange, red deep and green were utilized based on manufacturer's instructions to visualize the cells in the reconstruction images and make them easy to track frame-by-frame. A heated stage was assembled in Z1 microscope to maintain the temperature of the cells at 37°C throughout the experiments. To prevent evaporative losses the Z1 holder was sealed with parafilm and completely filled with expansion medium, which regrettably, inhibited us to change medium and run time-lapse imaging for 7 days. Consequently, expansion medium was applied to document aggregation only for 2 days. To minimize harmful effects of laser, the power was kept at minimum and scanning interval was set for 30 min. To demonstrate the results, images were analyzed by Fiji software (Version. 1.49k) and three-dimensional reconstructions were produced by digitally merging the optical sections from each time point.

Initially, the possibility of aggregation as mono- and triple spheroid inside of the Z1 holder was tested in incubator. For 3D time-lapse studies, cultures were prepared as it is explained in material and method coupled with short term cell tracking protocol. By staining the majority of the population with CellTracker, cells can easily be followed over time (Figure 33).

The images clearly demonstrate that hPOs can form round and compact spheroids in different sizes inside of FEP foil (Figure 34, Figure 35). Despite all optimization, there were numbers of barriers against cell accumulation at the bottom of Z1 holder, therefore, to increase the chances of spheroid formation and cell-cell contact, the starting cell number was set higher than 3000. Approximately 9000 single cells were placed per sample which justified the presence of several spheroids inside of each holder. Furthermore, initial results confirm that staining is not hazardous for the cells and does not impair spheroid formation. Albeit the

expression of the dyes decreases constantly during time-lapse, which limits the time of imaging respectively.

hPOs' movement in time-lapse images match with spheroid self-assembly model. Spheroid self-assembly process could be divided into three phases: rearrangement, aggregation, and compaction. Based on time-lapse images of this experiment, initially single cells were attached to the surface but remained dynamic (rearrangement phase, the first 7 hours), followed by moving towards each other to form small aggregates (aggregation phase, the second 7 hours). During the aggregation phase, the cells begin to round up and assemble small multilayer clusters with their neighbors. Finally in the compaction phase, the aggregates approach towards each other and compact into smooth spherical structures that eventually detach from other neighbor cells and form a clear barrier around themselves. In addition, the evaluation of time-lapse images proves the existence of bubbles and relates them to the pumping function of hPOs during growth within spheroids through aggregation process.

Through further experiments, time-lapse images in triple spheroids provided an interesting information from cell localization during spheroid formation. Images demonstrate a strong internal accumulation of hPOs and hMSC (stained with orange) along with external movement of the HUVEC cells (identified with green) during formation, closer evaluation of which revealed cell-cell connection between endothelial cells and formation of a micro prevascular network around the spheroid (Figure 36, Figure 37).

Taken all together, the time-lapse images offer insight into the cell movement mechanism during spheroid formation demonstrating the process of spheroid self-assembly. Furthermore, by combining multiple Cell Tracking protocol and time-lapse experiments an interesting glimpse of cellular rearrangement and localization during spheroid formation was provided.

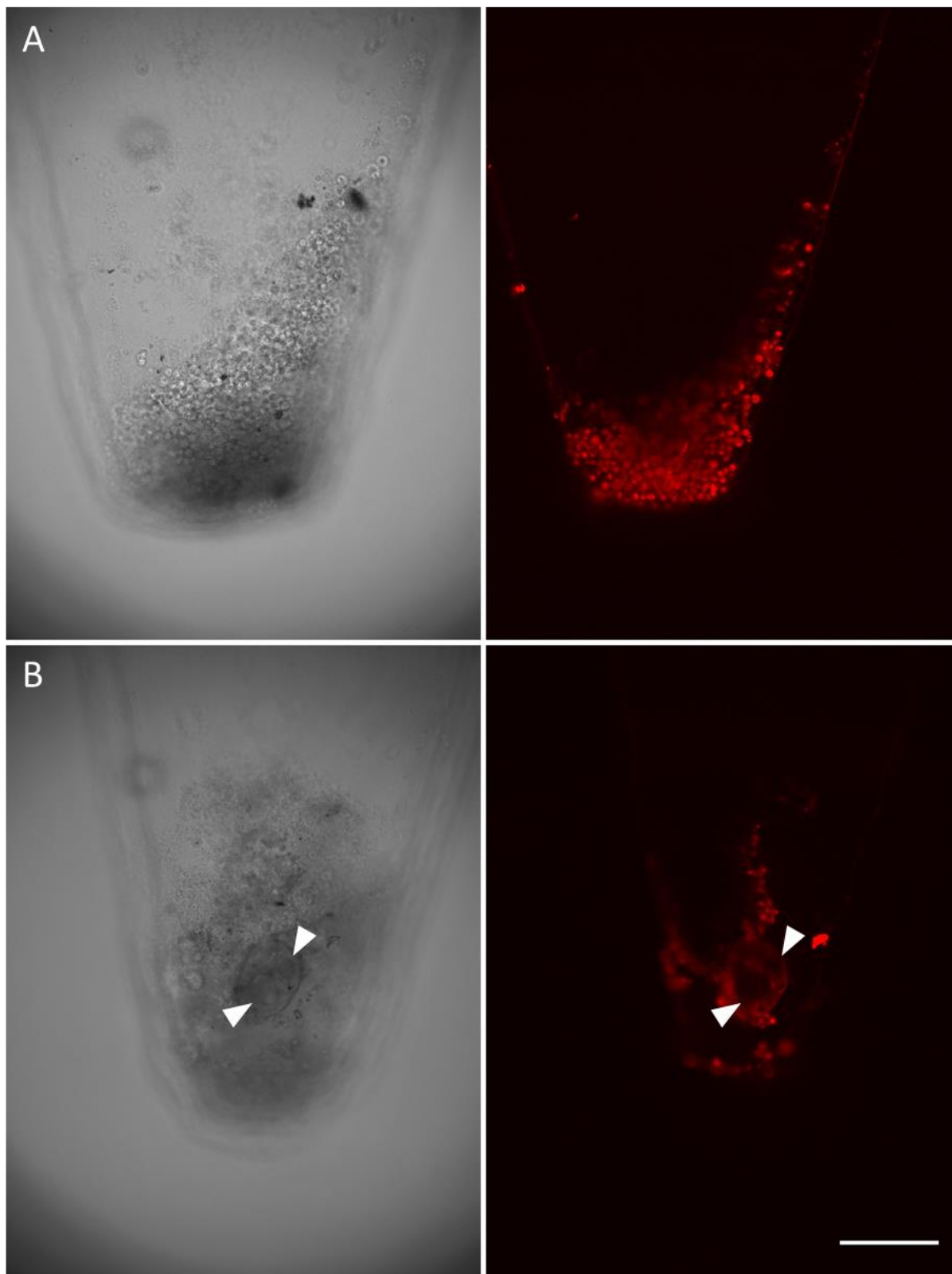


Figure 33: (A) hPOs stained with 5 μ M CellTracker™ Orange and accumulated at the bottom of Z1 holder. After trypsinizing the hPOs, single cells were counted and placed in Z1 holder. By stepwise centrifuging, cells were collected at the end of the Z1 holder. **(B) A compact spheroid detected within Z1 holder after 4 days.** Arrows are pointing at bubble-like structures formation which represents pumping function during hPOs growth, respectively. Representative images for each condition are shown. The images were processed using Z1 microscope with Det.: W Plan-Apochromat 20x/1.0 UV-VIS; Illum.: Zeiss LSM 10x/0.2; Laser: 561 nm - 571 nm. scale bar: 100 μ m.

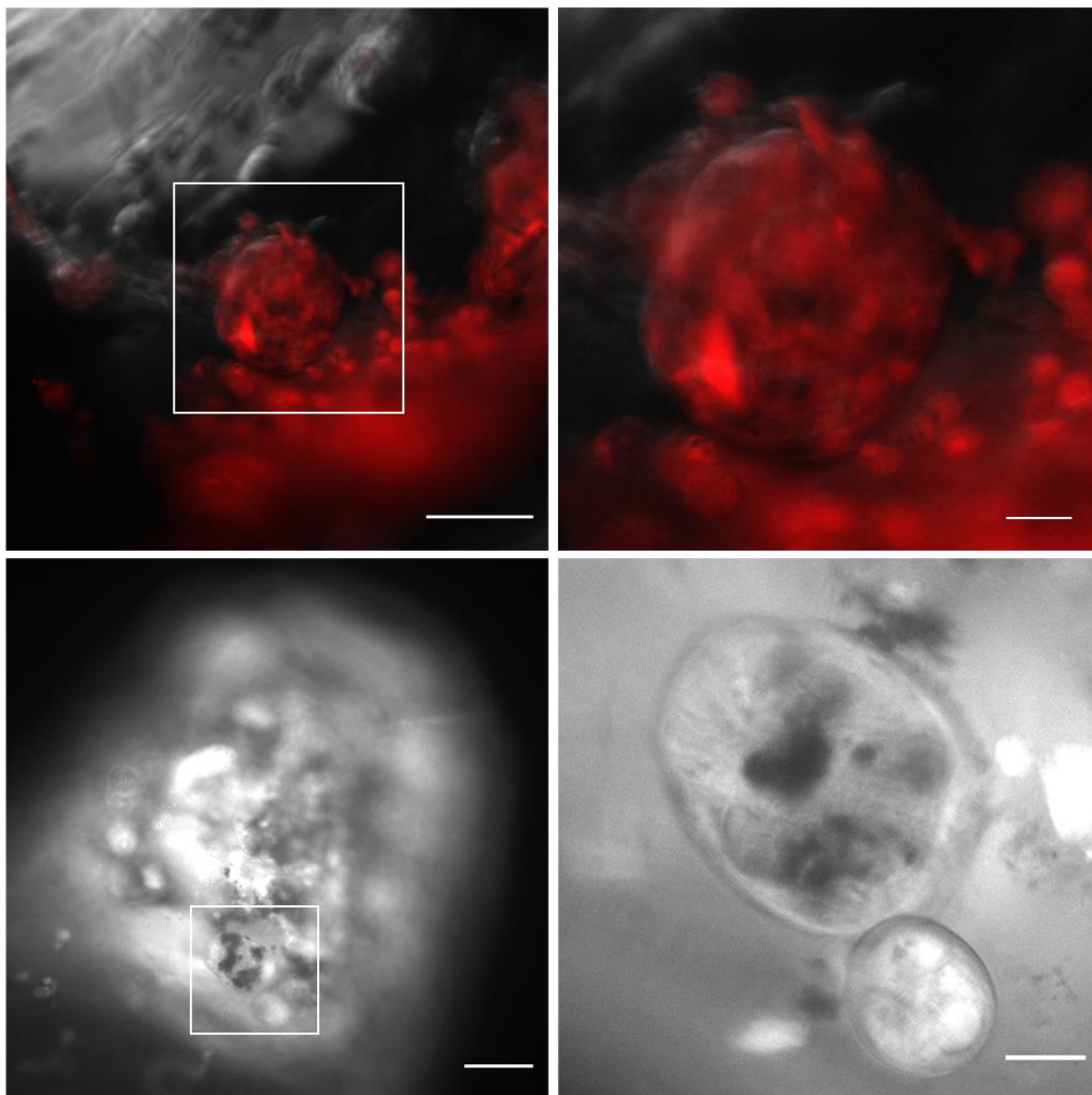


Figure 34: Formation of multiple spheroids in different sizes within FEP foil during/after (?) 4 days incubation. hPOs could be stained harmlessly with 5 μ M CellTracker™ Orange CMTMR and staining did not impair spheroid formation. The progress of aggregation inside of the Z1 holder was checked after 4 days. Rounded and compact spheroids in different sizes were detected inside the Z1 holder. Spheroids form a clear barrier from the neighbor cells. Representative images for each condition are shown. The images were processed using Zeiss Cell Observer microscope with W Plan Achromat 10x/0.25 ph1, 20x/0.35 ph1, 32x/0.40 ph1 objective lens; Excitation-Emission: 561 nm - 670/70 nm; scale bar: 100 μ m; close-up: 25 μ m.

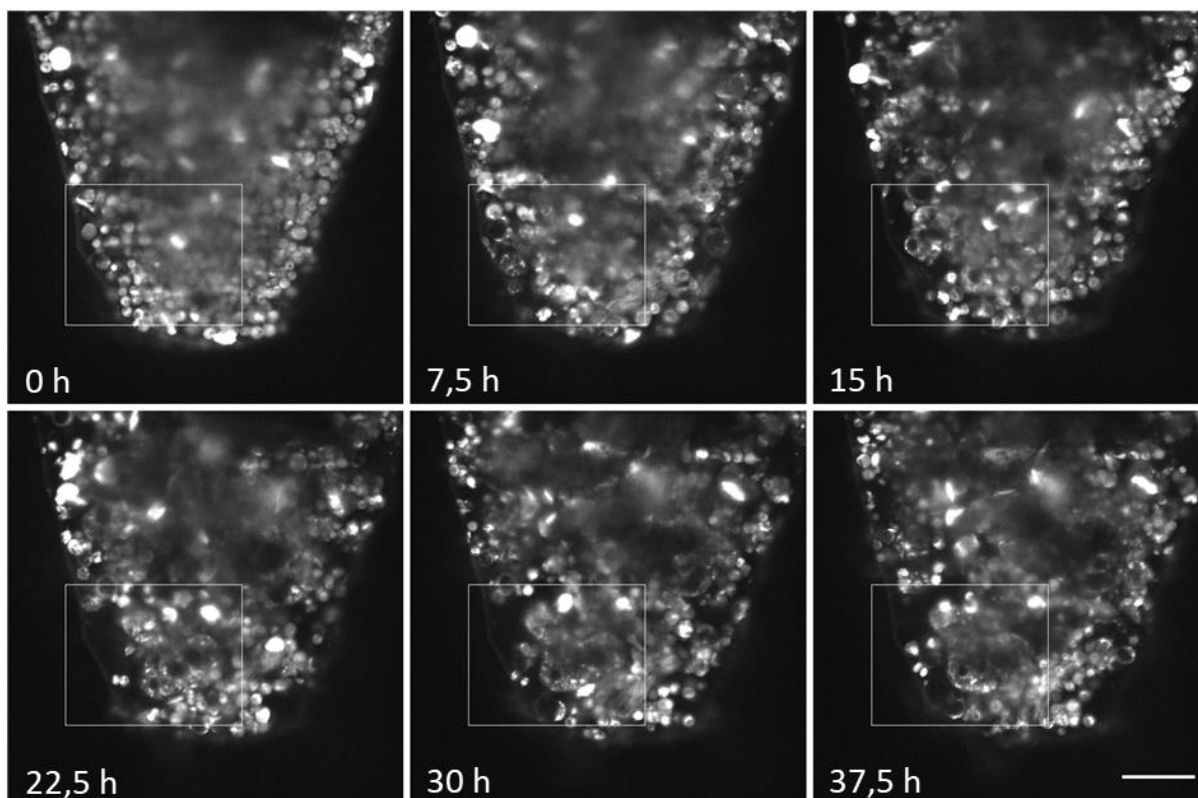


Figure 35: Spheroid formation progress in FEP foil in 2 days inside Z1 microscope. hPOs were trypsinized to single cells followed by staining with 5 μ M CellTracker™ Orange CMTMR, after which they were placed inside Z1 holder. Process of aggregation was monitored with time-lapse method using Z1 microscope. Time-lapse image sequences were acquired at 30 min intervals for 2 days. Initially, the cells were attached to the surface of the FEP foil but remained dynamic. Then the cells started to aggregate and form small aggregates. Finally, the clusters compacted to form spherical aggregates that detached from other neighbor cells. Representative images for each condition are shown. The images were processed using Z1 microscope with Det.: W Plan-Apochromat 20x/1.0 UV-VIS; Illum.: Zeiss LSFM 10x/0.2; Laser: 561 nm - 571 nm; scale bar: 100 μ m.

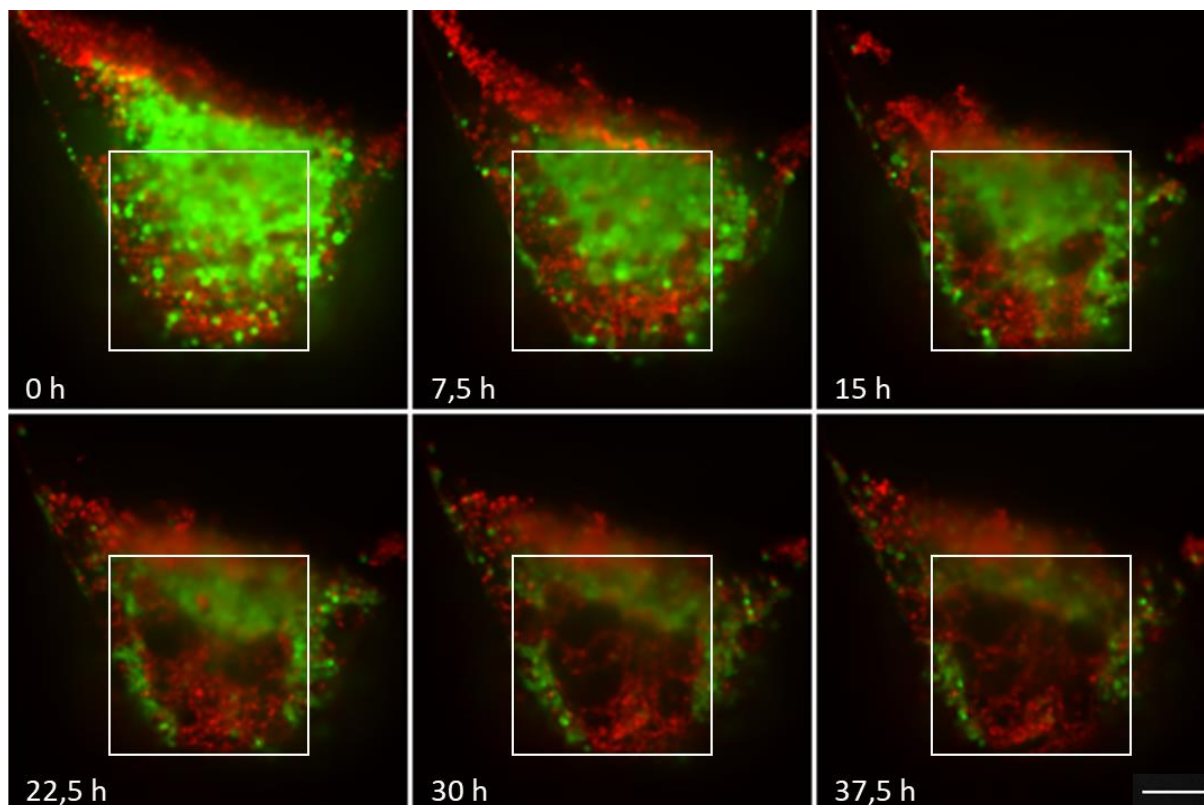


Figure 36: Cell localization assessment during spheroid formation within FEP foil using Z1 microscope. Two populations of hPOs and hMSC were incubated with 5 μM CellTracker™ Orange CMTMR and HUVEC cells were stained with 1 μM CellTracker Green CMFDA, mixed together, they were placed at the bottom of the Z1 holder afterwards for spheroid formation. The aggregation progress was monitored with time-lapse method using Z1 microscope. Time-lapse image sequences were acquired at 30 min intervals for 2 days. Initially the cells were mixed uniformly, over the time hPOs and hMSC were concentrated in the center and begin to round up and compact. Simultaneously, HUVEC cells moved to the external part of the spheroid. Representative images for each condition are shown. Images were processed using Z1 microscope with Det.: W Plan-Apochromat 20x/1.0 UV-VIS; Illum.: Zeiss LSM 10x/0.2; Laser: 488 nm - 615 nm, 561 nm - 571 nm; scale bar: 100 μm

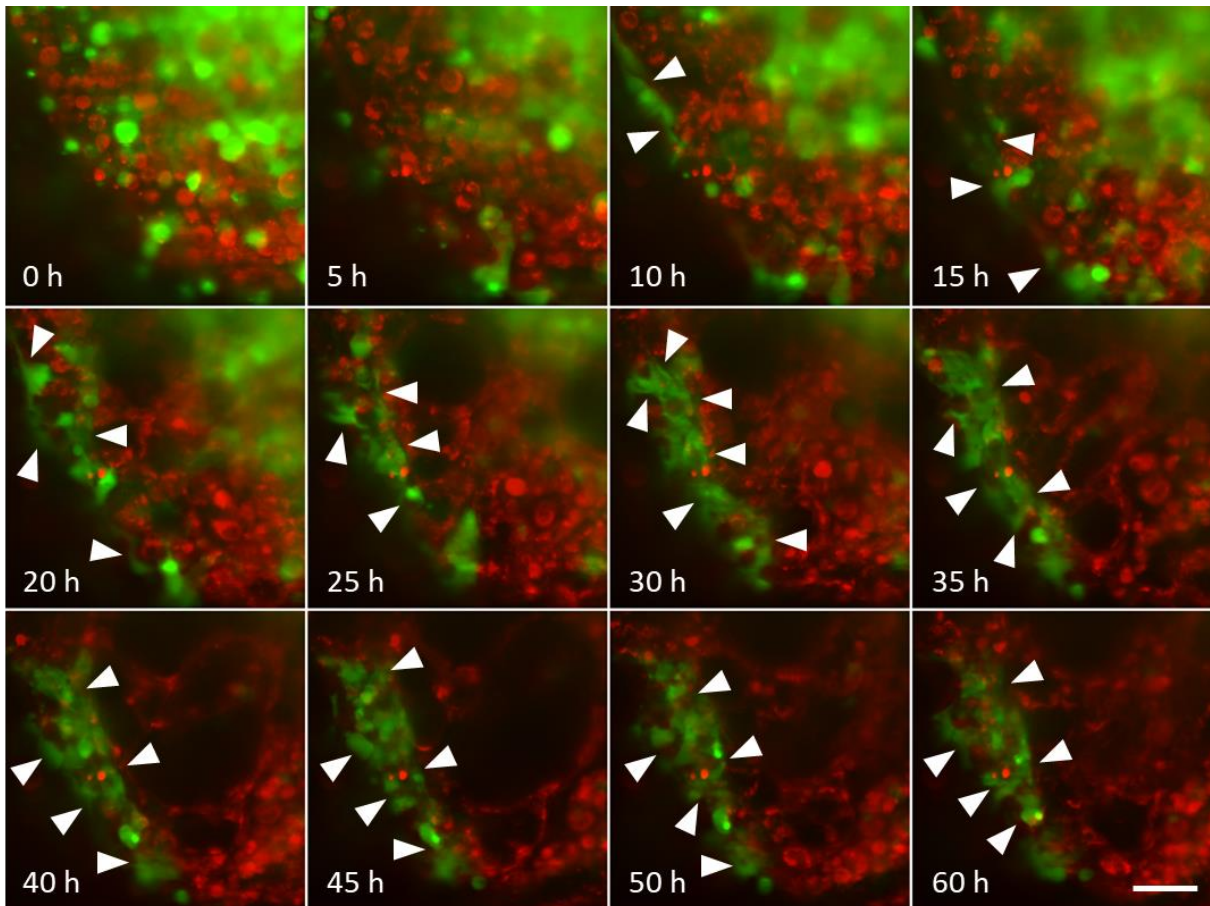


Figure 37: Prevascularized network in the external layer of a triple spheroid. HUVC cells migrate to the external layer of the spheroid during (spheroid?) formation. Arrows indicate cells approaching to one another, forming a micro prevascular network around the spheroid. Representative images for each condition are shown. The images were processed using Z1 microscope with Det.: W Plan-Apochromat 20x/1.0 UV-VIS; Illum.: Zeiss LSM 10x/0.2; Laser: 488 nm - 615 nm, 561 nm - 571 nm; scale bar: 50 μ m

3.2.5 HDMEC segregate in external layers in the co-culture pancreas spheroids

Better understanding about human cellular differentiation requires multicellular structures. The interaction between different cell types and extracellular matrix (ECM) in 3D cell culture play a fundamental role in this process. Co-culture methods allow a variety of cell types to be cultured together to examine the effect of one culture system on another. Not only does the co-culture technique help to investigate the interaction between different cell types, but it also demonstrates the localization of each cell type after mixture and cultivation all together, providing a more representative human *in vivo*-like tissue model.

To determine the cellular localization within the triple spheroid, IF staining against specific marker of HDMEC (CD31) has performed.

IF staining demonstrates HDMEC is in the external layer of the spheroid after the formation of triple spheroid in the differentiation medium (Figure 38). A similar and functional result has reported in Takahashi *et al.*, 2018 paper after co-culturing mouse islets with hMSC and HDMEC (Supplementary Figure). Mouse islets are capable of aggregation after being co-cultured with hMSC and HUVEC and the secretion of insulin after transplantation within mouse has documented in this paper, respectively.

Taken all together, these data determine parallels and similarities between the organization/localization of the hPOs co-culture and islets co-culture with endothelial cells, suggesting that the triple spheroid could also form functional structures.

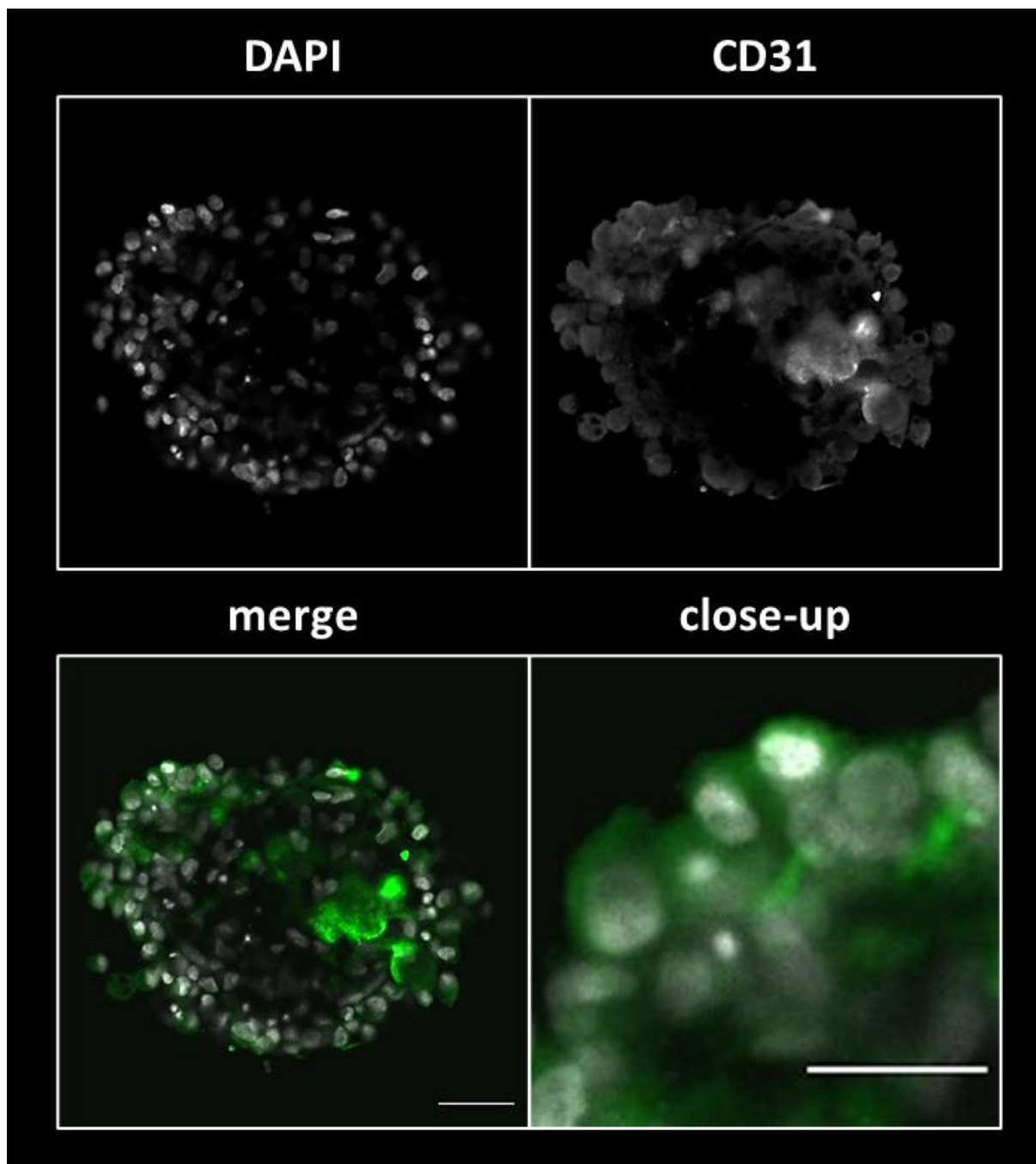


Figure 38: Strong external localization of HDMEC within the spheroid. Co-culturing hPO with hMSC and HDMEC in Differentiation medium show significant accumulation of HDMEC in the outer layer of the spheroid. Representative images for each condition are shown. Spheroids are optically cleared, and the images have been processed using Zeiss confocal LSM 780 microscopes with a Plan-Apochromat 20x/0.8 M27 objective lens. Excitation-Emission: 405 nm - 450/50 nm (DAPI), 488 nm - 615 nm (Alexa Fluor 488). CD31 = HDMEC marker, DAPI= cell nucleus; scale bar: 100 μ m, close-up: 50 μ m

3.3 Genotypical characterization

3.3.1 Significant reduction in the expression of progenitor genes detected in HPO spheroids cultured in differentiation medium

During differentiation, the phenotypical changes strongly associate with downregulation of the expression of progenitor gene products. This effect requires a coordinated network that simultaneously control cell growth and differentiation. Differentially expressed genes are also related to the extracellular matrix, growth factors, cytokines, and Wnt signaling pathway. Expression of the progenitor gene is a highly regulated process in pancreas and progenitor cell markers such as hSOX9 and hLGR5 have essential role in successive pancreas differentiation pathway.

Concerning progenitor gene visualization, all 5 groups were IF stained against hSOX9. Furthermore, RT-qPCR has performed to quantify expression of some known pancreatic progenitor markers such as hSOX9 and hLGR5, respectively. Relative expression of hLGR5, and hSOX9 has normalized to the geometric means of hRPL13 and hTBP (as housekeeping genes) and later to the expression in hPO organoid cultivated in expansion medium.

IF results demonstrate that SOX9 is strongly downregulated by aggregation and cultivation in differentiation medium (Figure 39). At the same time, it is clearly shown that the SOX9 is expressed without any accumulation in all nuclei of hPO organoid, cultured in expansion medium, however the same results are not detected in other groups. The Sox9-positive cells has detected in all layers of the spheroids, in particular a strong signal is observed in the outer layer of spheroids (Figure 39, arrows).

The computational analysis of RT-qPCR reveals that the expression of both genes in all cases are lower than that in hPO organoid, which has cultivated in expansion medium. Along with the mass decline of hSOX9 and hLGR5 genes, interestingly it is observed that hSOX9 is expressed less than hLGR5 in spheroids cultured in both expansion and differentiation medium, on the other hand, hSOX9 is expressed at a higher level than hLGR5 in organoids and triple spheroid cultured in differentiation medium (Figure 40).

In addition, the expression of hSOX9 in hPO organoid, cultured in expansion medium, is distinctly higher than the hPO spheroid in differentiation medium ($P < 0.05$), which is in consistent with the results of the IF staining as well Figure 39 and Figure 40.

Taken all together, spheroid formation and differentiation medium significantly decrease the expression of hPO progenitor genes.

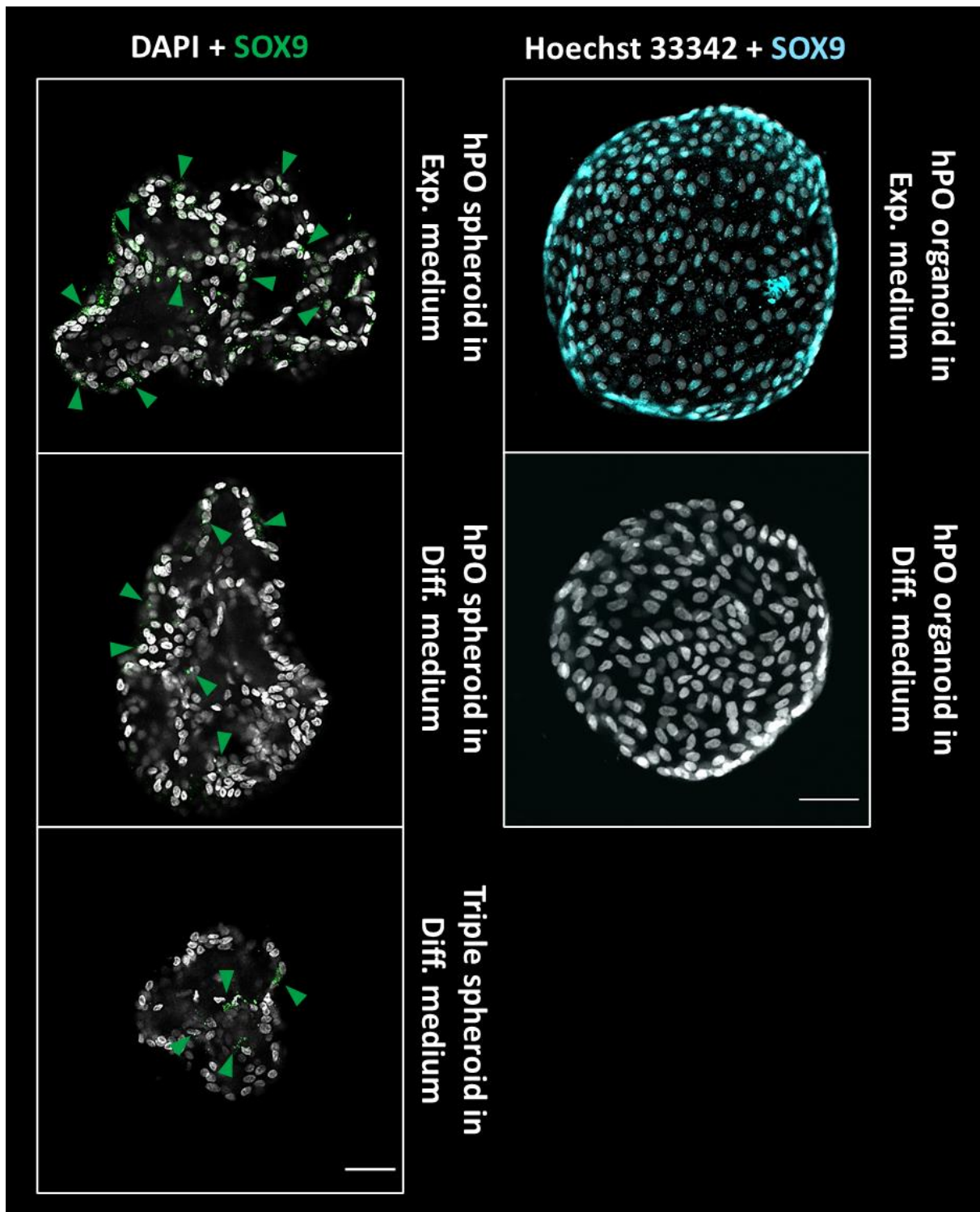


Figure 39: Immunofluorescent staining visualizes the effect of cell aggregation and differentiation medium on progenitor gene expression. hPOs have labeled with progenitor marker (Sox9). Progenitor markers are detected inside and in the periphery of the spheroid. Cell nuclei are stained with DAPI and Hoechst 33342. Representative images for each condition are shown. Spheroids have optically cleared, and the images have been processed using Zeiss confocal LSM780 microscope with W Plan-Apochromat 10x/03 M27 (organoid) and W Plan-Apochromat 20x/084 M27 (spheroid); Excitation-Emission: 405 nm - 450/50 nm (DAPI and Hoechst 33342), 645 nm - 765 nm (SOX9); Exp.: Expansion; Diff.: Differentiation; scale bar: 50 μ m.

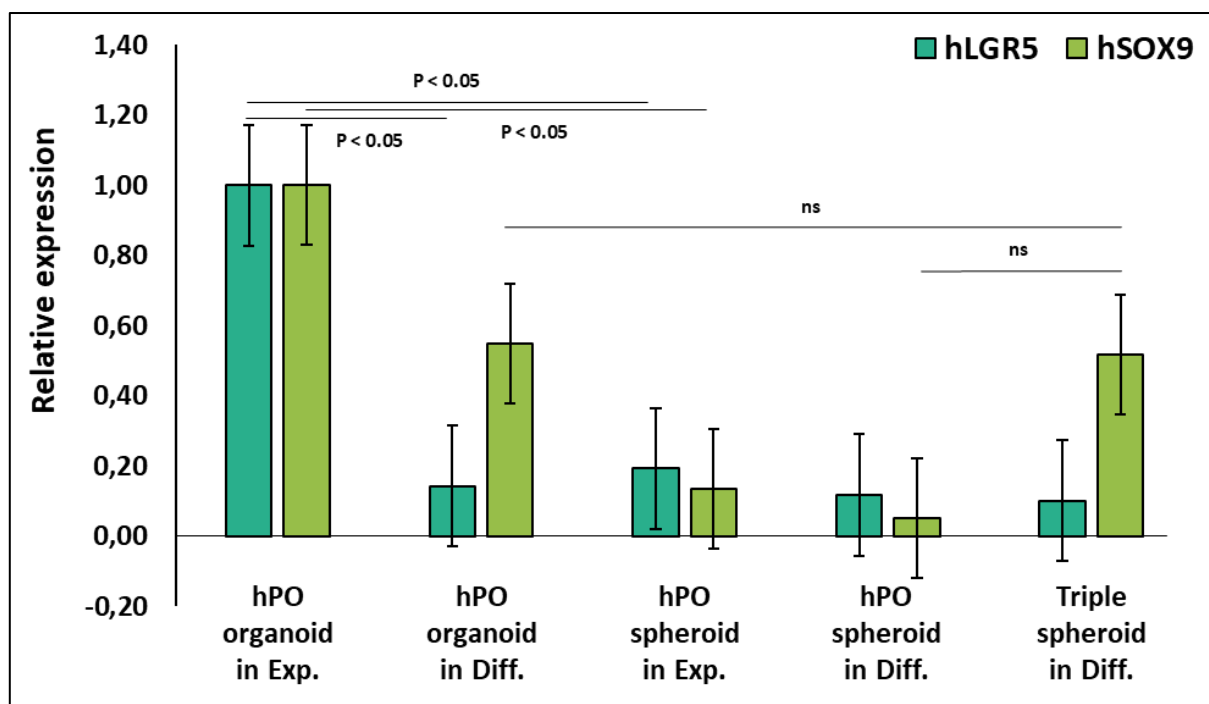


Figure 40: Progenitor gene expression changes are validated by RT-qPCR. A remarkable difference in hLGR5 and hSOX9 expression is detected due to the differentiation medium and aggregation. For each condition three independent experiments with at least three technical replicates have performed. Relative expression of hLGR5 and hSOX9 is normalized to the geometric means of hRPL13 and hTBP (housekeeping genes) and later to the expression in hPO organoids cultivated in expansion medium. The lines inside the boxes denote the standard error. Excel 365 software was used to illustrate the graphic and perform T-test for statistics analysis, and the statistical significance was defined as $p < 0.05$. ns: not significant; Exp.: Expansion; Diff.: Differentiation.

3.3.2 Differentiation medium prevents the proliferation of pancreas progenitor cells in both organoids and spheroids

Cell proliferation and differentiation are highly coordinated by external and internal stimuli that accordingly leads to determine cell fate. Cell proliferation and differentiation have a remarkable inverse relationship with each other²²¹. Progenitor cells keep division before reaching to the fully differentiated state, however terminal differentiation coexists with proliferation arrest and stopping the cell division cycle, permanently.^{40,43,88}

To detect the effect of aggregation and cultivation in two different mediums (expansion vs. differentiation), proliferation of the cells inside the hPO organoids and spheroids was analyzed after 7 days of cultivation in expansion and differentiation medium using EdU incorporation assay in hPO organoids and Ki67 staining in spheroids. During this project, a protocol for EdU incorporation assay in hPO organoids followed by acquisition with confocal laser scanning microscope was established and hPO spheroids were IF stained against proliferation markers (Ki67), respectively.

Based on the results gained by confocal laser scanning microscopy, EdU incorporation assay is shown to work well in hPO organoids, and Ki67 antibody completely penetrates the hPO spheroids. The expression of EdU and Ki67 signal in the nuclei of the samples (nuclei were counterstained with Hoechst in organoids and DAPI in spheroids) is presented in the merged images. Proliferated cells are only detected in the samples that have cultured in expansion medium and no signal is acquired in differentiation medium. It should be noted that, Ki67- positive cells are observed in all layers of the spheroids, indeed.

Taken all together, IF staining against proliferation markers/cells demonstrates that differentiation medium has an anti-proliferation effect on hPO organoids and spheroids.

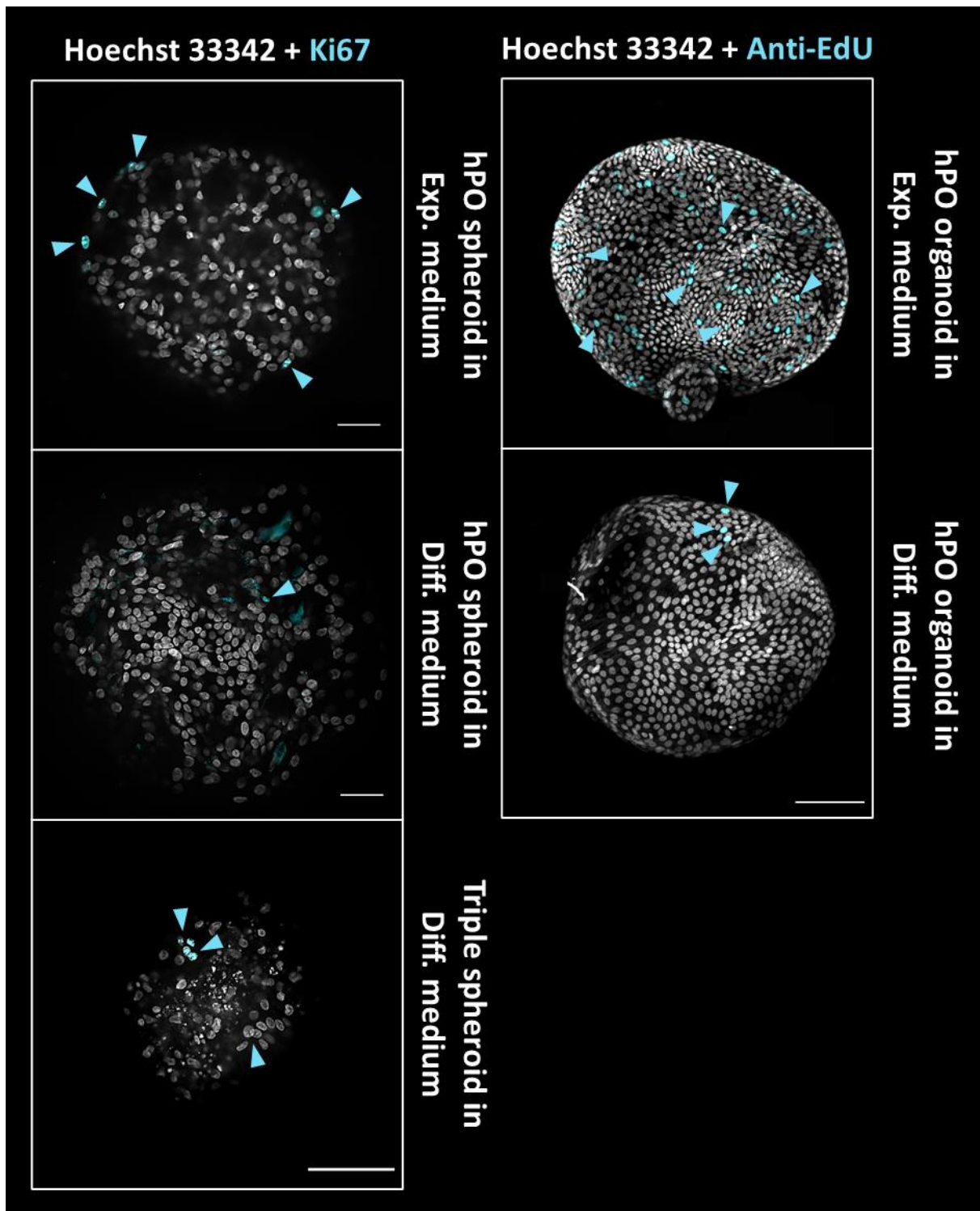


Figure 41: Cell proliferation is inhibited in the differentiation medium. The proliferation signal is only detected in the hPO spheroids cultured in an Expansion medium. hPOs are labeled with proliferation marker (Ki67) and Anti-EdU. Cell nuclei are stained with Hoechst 33342. Representative images for each condition are shown. Spheroids were optically cleared, and the images have been processed using Zeiss confocal LSM780 microscope with W Plan-Apochromat 10x/03 M27 and W Plan-Apochromat 20x/084 M27; Excitation-Emission: 405 nm - 450/50 nm (Hoechst 33342), 488 nm - 525/45 nm (Ki67 and Anti-EdU); Scale bar: 100 μ m.

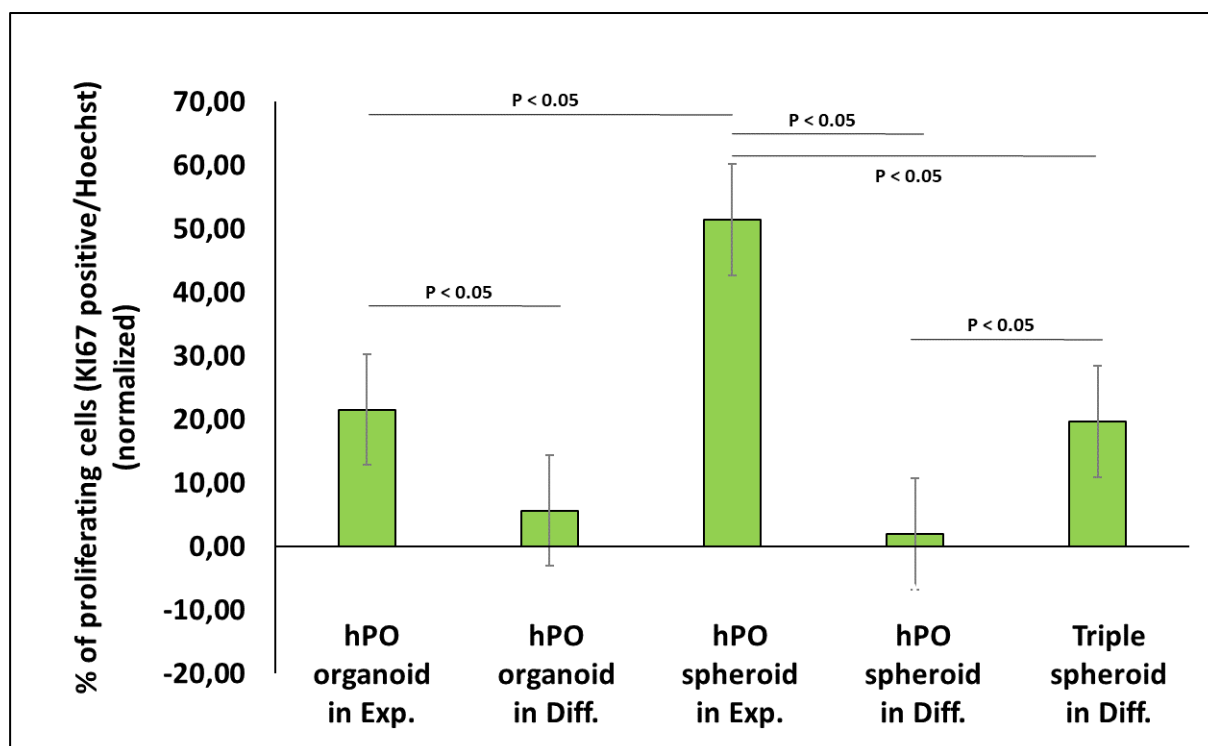


Figure 42: Quantification of proliferation rate within hPO organoids and spheroids after 7 days of cultivation in expansion and differentiation medium. Differentiation medium significantly decreases the ratio of proliferated cells in all conditions compared to the expansion medium. Spheroid formation has inducer effect on proliferation per se. For each condition 3 independent experiments with at least 5 technical replicates were performed. Data are normalized with total nuclei per sample then quantified with ImageJ plugin 3D object counter. Excel 365 software was used to illustrate the graphic and perform T-test for statistics analysis. The lines inside the boxes denote the standard error. Exp.: Expansion; Diff.: Differentiation.

3.3.3 Spheroid formation in differentiation medium drives the gene expression of hPO cells towards endocrine differentiation

Due to the spheroid formation, co-culturing, and cultivation in expansion and differentiation medium the expression of β cell markers (insulin, CHGA and CHGB) and differentiation markers (NGN3, NKX6.1, and PDX1) were evaluated in RNA level using RT-qPCR technique. The results are validated further by IF staining as well.

The quantitative analysis of mRNA expression level of β cell markers have demonstrated a significant (t-test $p < 0.05$) upregulation of insulin and CHGB, two β -cell makers in hPO spheroids, which were cultivated under differentiation medium. Surprisingly, CHGA cultured in differentiation medium is observed to upregulate in all samples (organoids, spheroids, and triple spheroids).

The strong upregulation in mRNA expression level of differentiation markers, NGN3 and NKX6.1 are detected in hPO spheroids cultured in differentiation medium compared to other conditions. Contrary to those markers, PDX1 does not show any changes in any condition.

To determine the effect of cultivation under differentiation medium, IF staining was performed. Based on the IF staining, no significant changes are detected in the morphology of hPO organoids in either condition. hPO organoids are symmetry and circular with a hollow in the middle (Figure 43, Figure 44).

To investigate further, IF staining against insulin, β cell marker, and Pdx1 differentiation marker was done on hPO organoids in expansion and differentiation medium. IF staining results demonstrate remarkable changes in insulin localization. Insulin signals are found in both conditions, however, after cultivation in differentiation medium, insulin is expressed in the basal membrane, but expansion medium leads to the cytoplasmic expression of insulin which is shown in the point-like structures within hPO organoids. Furthermore, IF staining against Pdx1 differentiation marker reveals no significant changes in its expression. IF staining results show the co-expression of Pdx1 in nuclei of hPO organoids in both conditions, respectively. Those data are in line with RT-qPCR results (Figure 45).

Taken all together, cultivation under differentiation medium coupled with spheroid formation significantly upregulates the expression of β cell markers and differentiation markers.

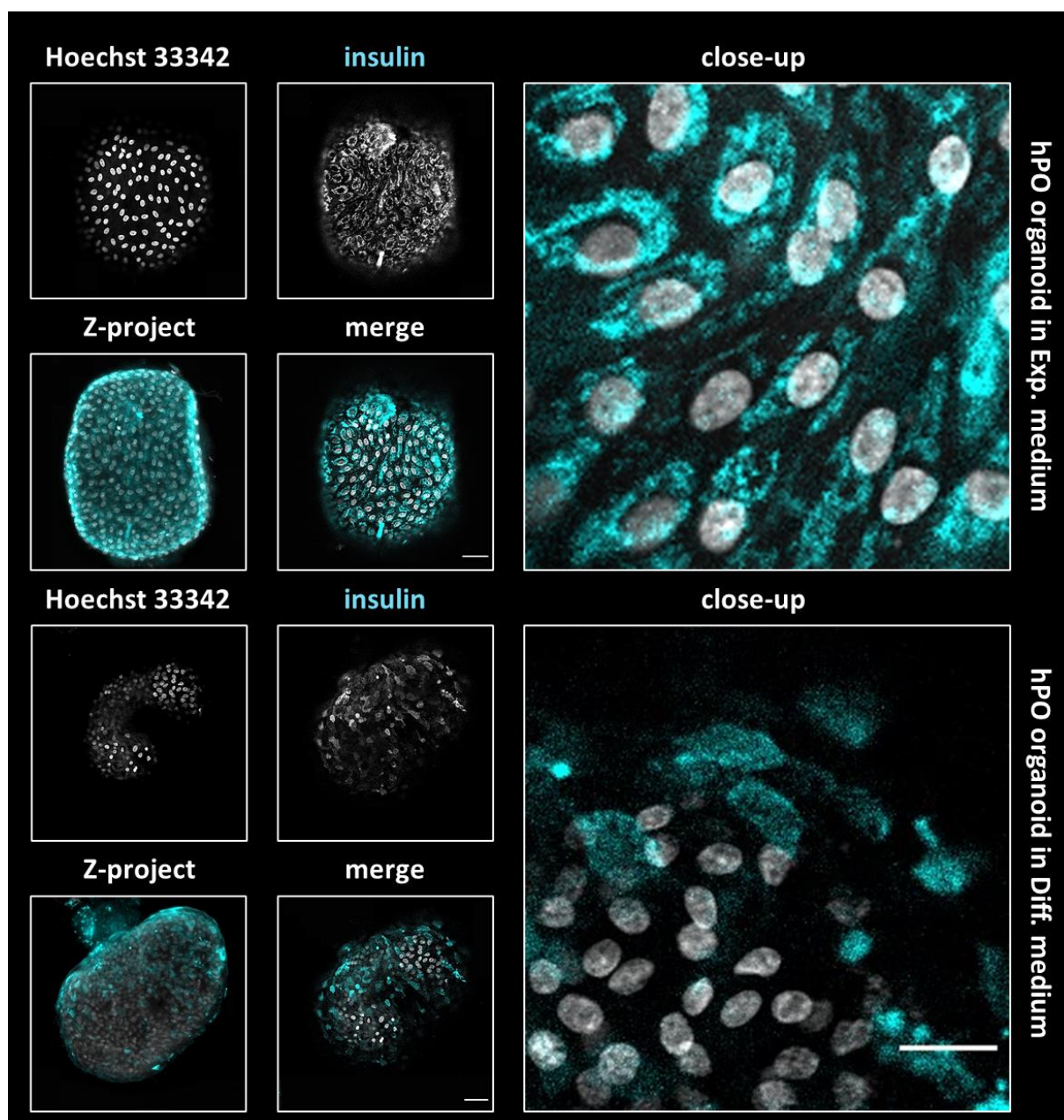


Figure 43: Cultivation under differentiation medium affects the localization of insulin within hPO organoids. Organoids have been cultured under expansion and differentiation mediums for 7 days followed by fixation and immunofluorescent staining against insulin. Insulin expression is detected in the basal membrane under differentiation medium and IF staining visualizes the cytoplasmic and point-like structure for insulin expression in hPO that has been cultured in expansion medium. Z-project represents the expression of insulin in all of the hPOs in both conditions. Cell nuclei are stained with Hoechst 33342. Representative images for each condition are shown. The images have been processed using Zeiss confocal LSM780 microscope with W Plan-Apochromat 10x/03 M27; Excitation-Emission: 405 nm - 450/50 nm (Hoechst 33342), 645 nm - 765 nm (insulin); Exp.: Expansion; Diff.: Differentiation; scale bar: 50 μm ; close-up: 25 μm

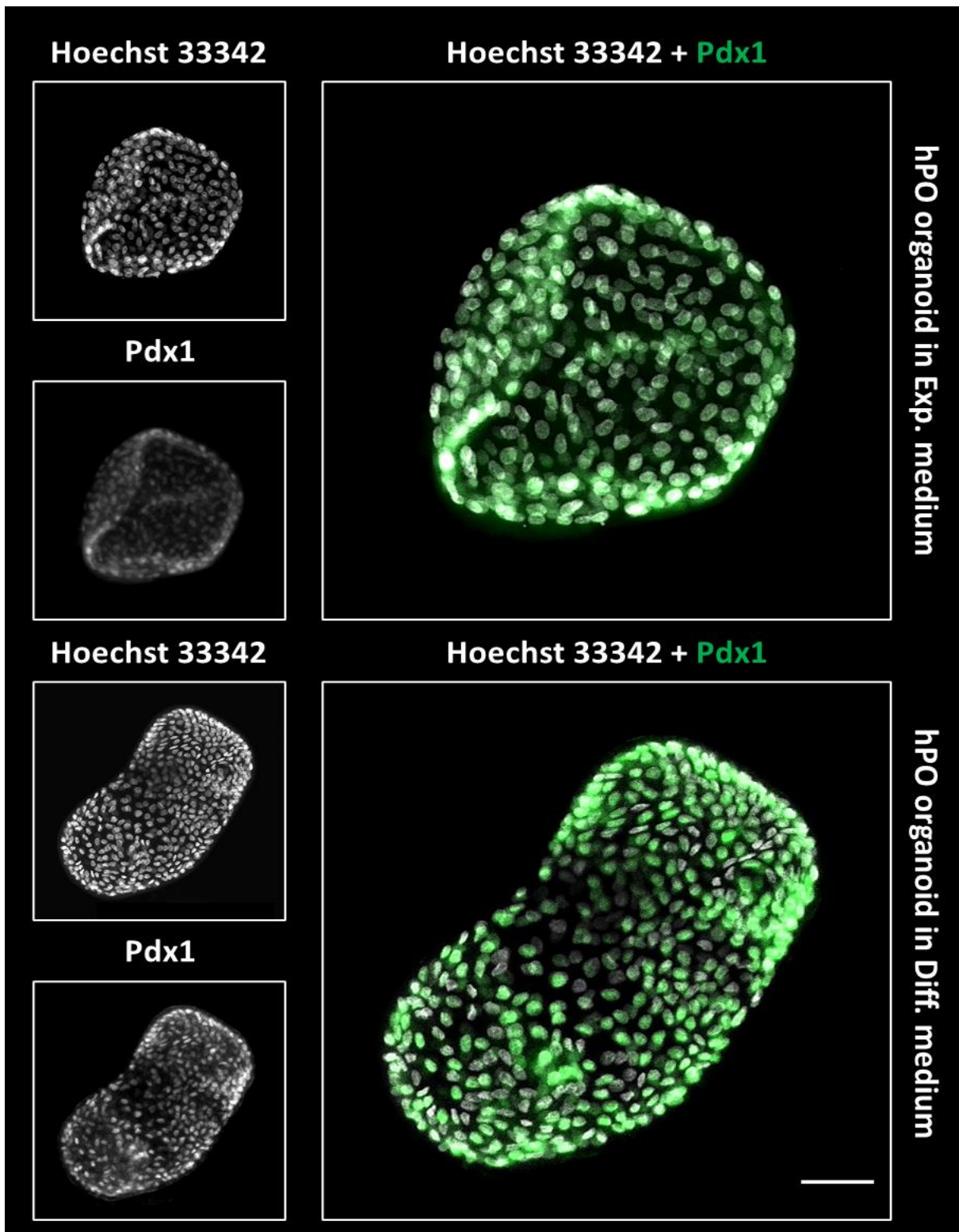


Figure 44: Nuclei-expression of Pdx1 within hPO organoids under expansion and differentiation medium. Organoids have been cultured under expansion and differentiation mediums for 7 days followed by fixation and immunofluorescent staining against Pdx1. IF staining visualizes the expression of Pdx1 in the nucleus of hPO organoids under expansion and differentiation medium. Z-project represented the expression of Pdx1 in the entire of the hPOs in both conditions. Cell nuclei are stained with Hoechst 33342. Representative images for each condition are shown. The images have been processed using Zeiss confocal LSM780 microscope with W Plan-Apochromat 10x/03 M27; Excitation-Emission: 405 nm - 450/50 nm (Hoechst 33342), 561 nm – 607 nm (Pdx1); Exp.: Expansion; Diff.: Differentiation; scale bar: 50 μ m.

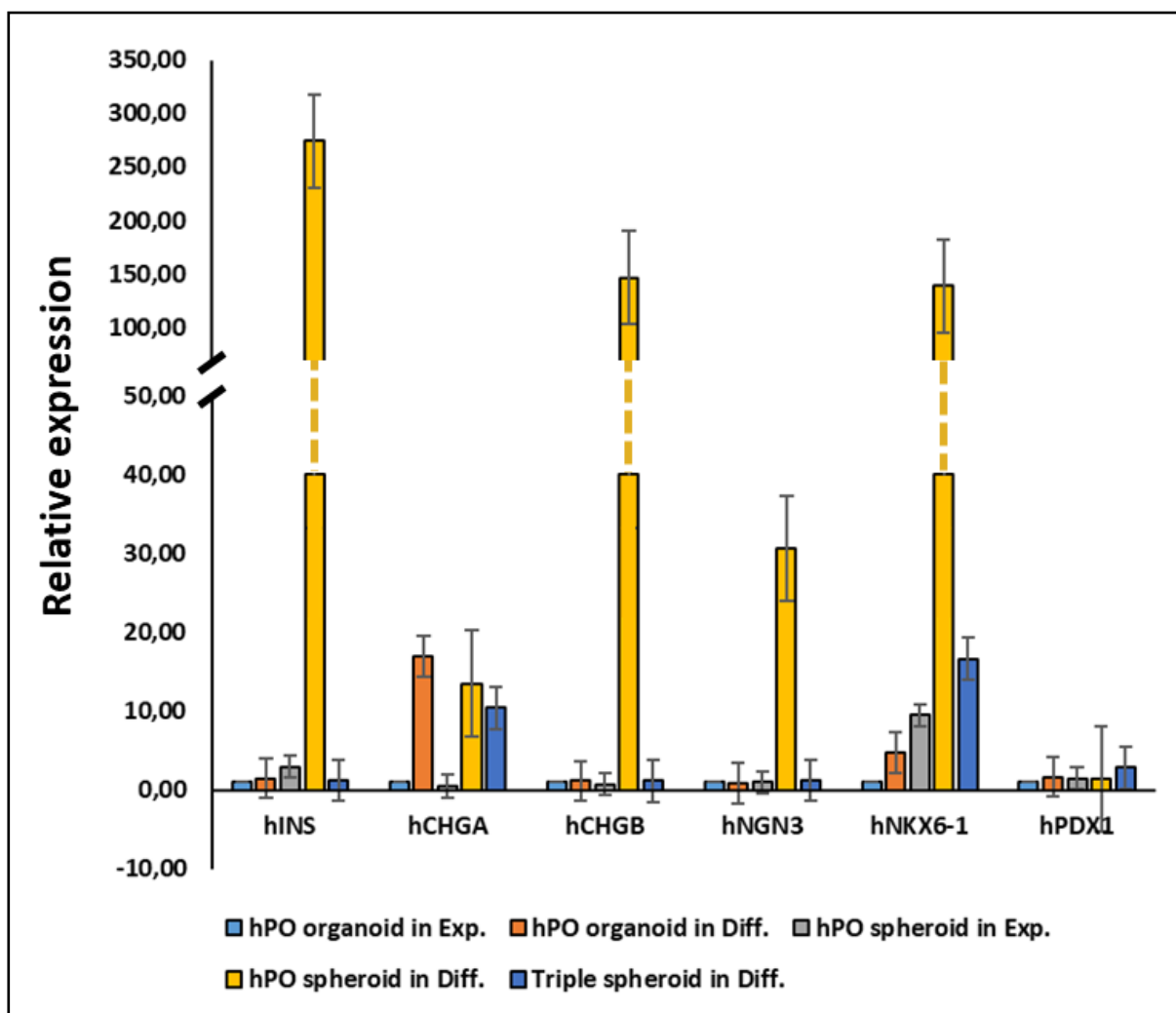


Figure 45: Aggregation coupled with the cultivation in differentiation medium causes the highest expression of β cell and differentiation markers within hPOs. The RT-qPCR results validate the strong difference in β cell and differentiation markers between hPO spheroids cultured in differentiation medium and other groups. For each condition three independent experiments with at least three technical replicates were performed. Relative expression of each gene was normalized to the geometric means of hRPL13 and hTBP (housekeeping genes) and later to the expression in hPO organoids cultivated in expansion medium. The lines inside the boxes denote the standard error. Excel 365 software was used to illustrate the graphic; Exp.: Expansion; Diff.: Differentiation.

3.3.4 Significant decrease in expression of epithelial and progenitor markers in pancreas progenitor cells following the formation of spheroids

hPOs are originally adopted from the pancreas ductal cells and composed of epithelial cells that have the capacity to express progenitor markers, such as SOX9 which make them the best candidate for this project. In order to determine the effect of spheroid formation, cultivation under two mediums (expansion and differentiation) and co-culturing on the original status of hPOs, the expression of progenitor marker and epithelial marker have been investigated based on the RNA expression level. The RT-qPCR results were analyzed using the $\Delta\Delta C_t$ method. Furthermore, IF staining was added to characterize the phenotype of hPOs in more details.

Based on the IF staining, after cultivation under expansion and differentiation medium, no significant difference was detected in either condition. hPO organoids represent a circular structure with a lumen within. The originally status of hPOs is proven by the expression of epithelial marker Krt19, indeed. Krt19 is detected in the whole cytoplasm and surrounds the nucleus in both conditions. These data are in line with the RT-qPCR results and no significant (t-test $p < 0.05$) difference between hPO organoids is detected. Furthermore, as noticed in previous chapter (3.3.1 Significant reduction in the expression of progenitor genes detected in HPO spheroids cultured in differentiation medium) the progenitor capacity of the hPOs (organoids and spheroids) has been validated based on the IF staining against SOX9 expression, respectively (Figure 46).

Additionally, the quantitative analysis of mRNA expression level demonstrates that after spheroid formation the expression of both epithelial and progenitor markers significantly decrease in the same manner. It is interesting to note that in both cases, co-culturing leads to the upregulation of mRNA expression level, which strongly demonstrates the effect of neighbor cells on the cell fate (Figure 47).

Taken all together, epithelial and progenitor markers represent the same pattern of downregulation after spheroid formation. This hypothesizes that aggregation suppress the cells to stay in their progenitor status. Furthermore, the supportive role of co-culturing is observed in both conditions, respectively.

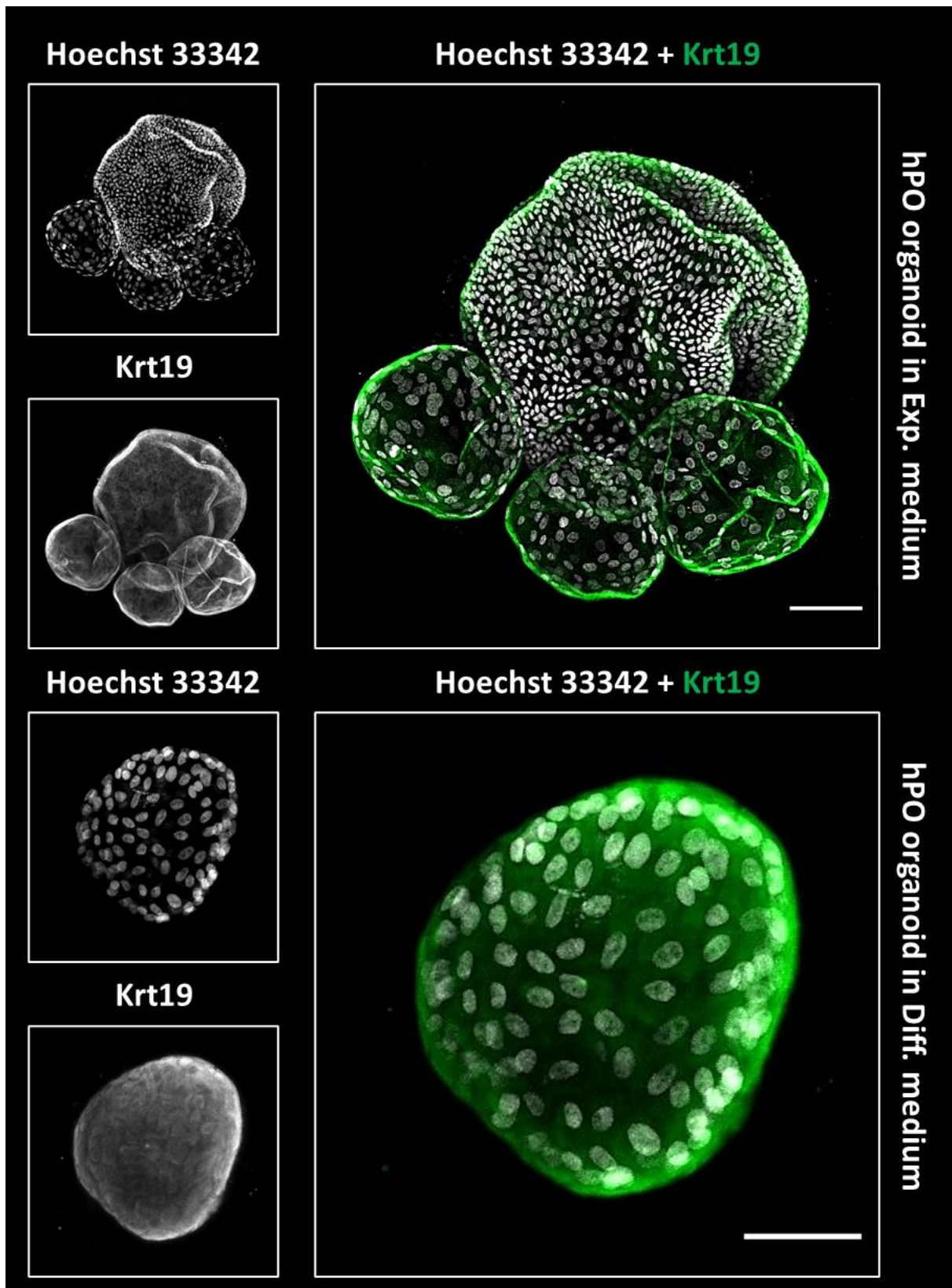


Figure 46: Immunofluorescent staining visualizes the expression of ductal marker after cultivation under expansion and differentiation medium within hPO organoids. Organoids have been cultured under expansion and differentiation mediums for 7 days followed by fixation and immunofluorescent staining against Krt19. Krt19 is detected in all of the hPOs in both conditions. Cell nuclei are stained with Hoechst 33342. Representative images for each condition are shown. The images have been processed using Zeiss confocal LSM780 microscope with W Plan-Apochromat 10x/03 M27; Excitation-Emission: 405 nm - 450/50 nm (Hoechst 33342), 561 nm - 670/70 nm (Krt19); Exp.: Expansion; Diff.: Differentiation; scale bar: 50 μ m.

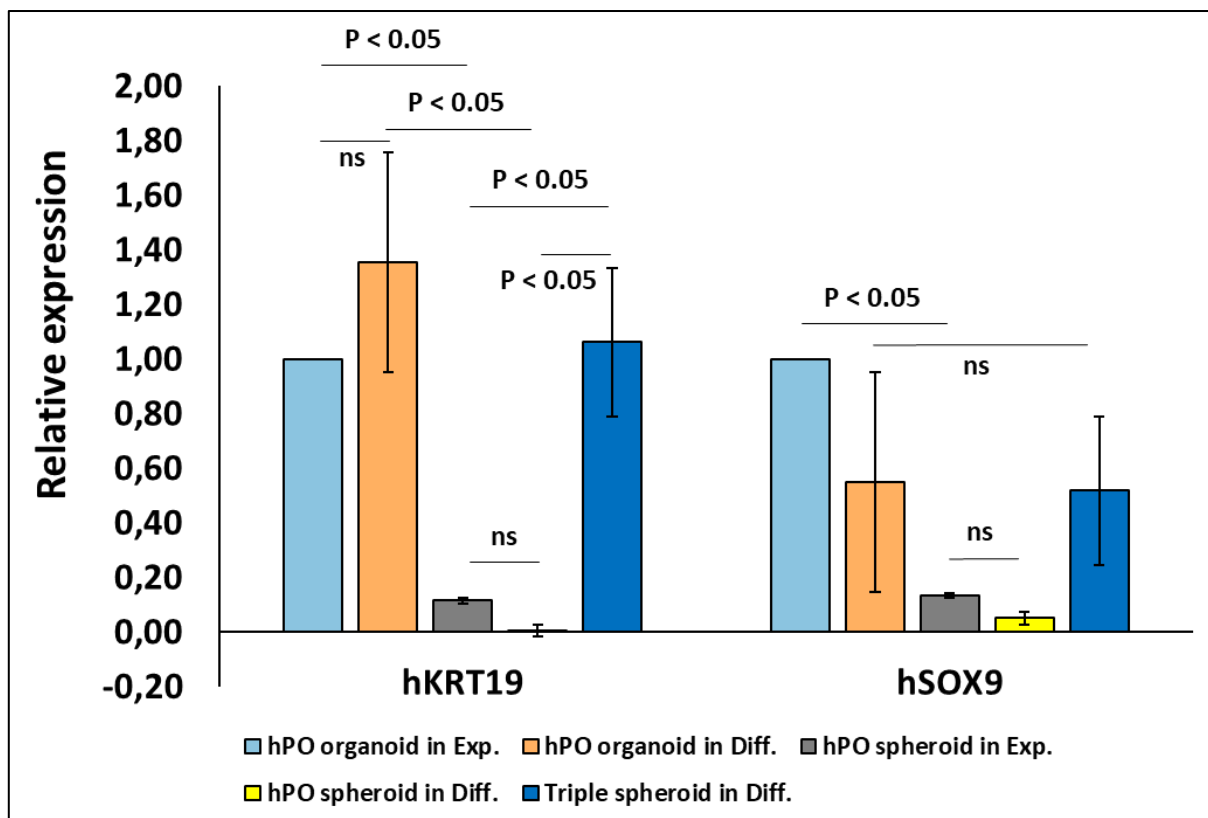


Figure 47: A similar reduction in ductal and progenitor markers are detected due to the spheroid formation. The RT-qPCR results validate strong and similar decreasing in the expression of Krt19, ductal marker, and SOX9, progenitor marker after spheroid formation. For each condition three independent experiments with at least three technical replicates have been performed. Relative expression of each gene is normalized to the geometric means of hRPL13 and hTBP (housekeeping genes) and later to the expression in hPO organoids cultivated in expansion medium. The lines inside the boxes denote the standard error. Excel 365 software was used to illustrate the graphic; Exp.: Expansion; Diff.: Differentiation.

3.3.5 Detection of hallmarks of epithelial-to-mesenchymal transition (EMT) by IF staining after spheroid formation

The epithelial-to-mesenchymal transition (EMT) is defined as a process in which epithelial cells will lose their polarity and transform into mesenchymal cells. This is also known as the first step during differentiation into variety of cell types. Cultivation under two mediums (expansion and differentiation) and co-culturing the expression of epithelial markers and mesenchymal markers were investigated based on the RNA expression level in order to prove EMT occurs in hPOs after aggregation. The RT-qPCR results were analyzed using the $\Delta\Delta C_t$ method. Furthermore, IF staining was added to demonstrate the gene expression within spheroids in more details.

Immunofluorescent staining in spheroids determine that after cultivation under expansion and differentiation medium no remarkable differences are detected in the phenotype of spheroids in both conditions. hPOs formed a circular and compact spheroid. Vimentin, known as a marker for mesenchymal-derived cells or cells undergoing an epithelial-to-mesenchymal transition (EMT) was detected in the whole cytoplasm and surrounded the nucleus in both conditions (Figure 48, Figure 49).

Furthermore, the expression of epithelial markers and mesenchymal markers were investigated by RT-qPCR and significant (t-test $p < 0.05$) differences were detected between all markers. Based on RT-qPCR results, aggregation in both conditions has a significant positive effect on the expression of mesenchymal genes such as hVIM and hCDH2. Similarly, the quantitative analysis of mRNA expression level demonstrates that after spheroid formation, the expression of both epithelial markers (hEPCAM and hKRT19) was considerably decreased. The decrement in hKRT19 is more remarkable compared to hEPCAM. It is interesting to note that based on the mRNA expression level, co-culturing does not improve the EMT which could strongly demonstrate the effect of neighbor cells on the cell fate (Figure 49).

Taken all together, downregulation of epithelial markers strongly couples with upregulation of mesenchymal markers after spheroid formation. This could be defined as one of the main symbols of EMT in hPOs. Furthermore, the supportive role of co-culturing observed in both conditions suggests the necessity to investigate this topic in more details.

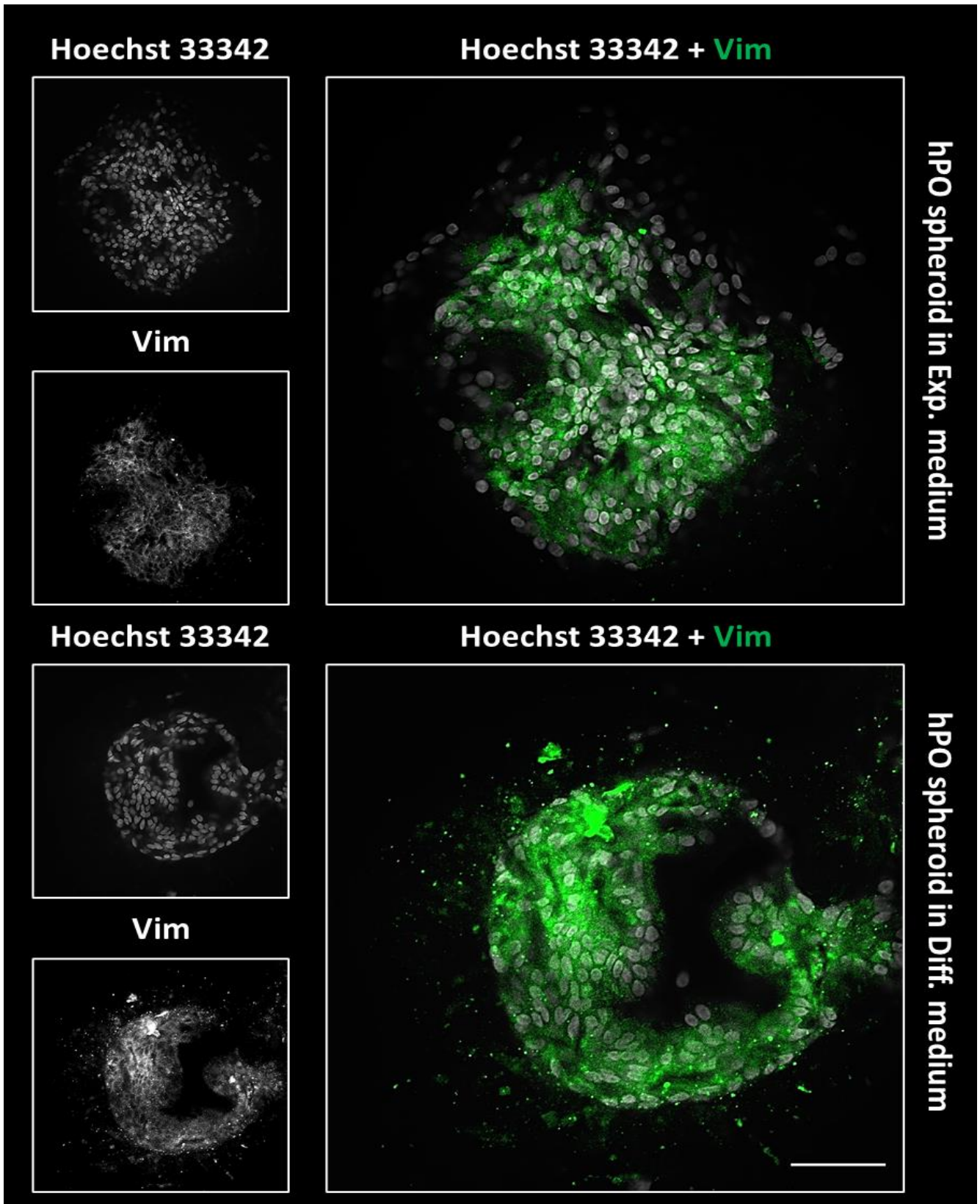


Figure 48: Mesenchymal markers (Vim) detected in the entire of the spheroids in both conditions. IF staining strongly visualized the expression of mesenchymal marker after cultivation under expansion and differentiation medium within hPO spheroids. Spheroids have been cultured under expansion and differentiation mediums for 7 days followed by fixation and IF staining against Vim. Cell nuclei are stained with Hoechst 33342. Representative images for each condition are shown. The images have been processed using Zeiss confocal LSM780 microscope with W Plan-Apochromat 10x/03 M27; Excitation-Emission: 405 nm - 450/50 nm (Hoechst 33342), 561 nm - 670/70 nm (Vim); Exp.: Expansion; Diff.: Differentiation

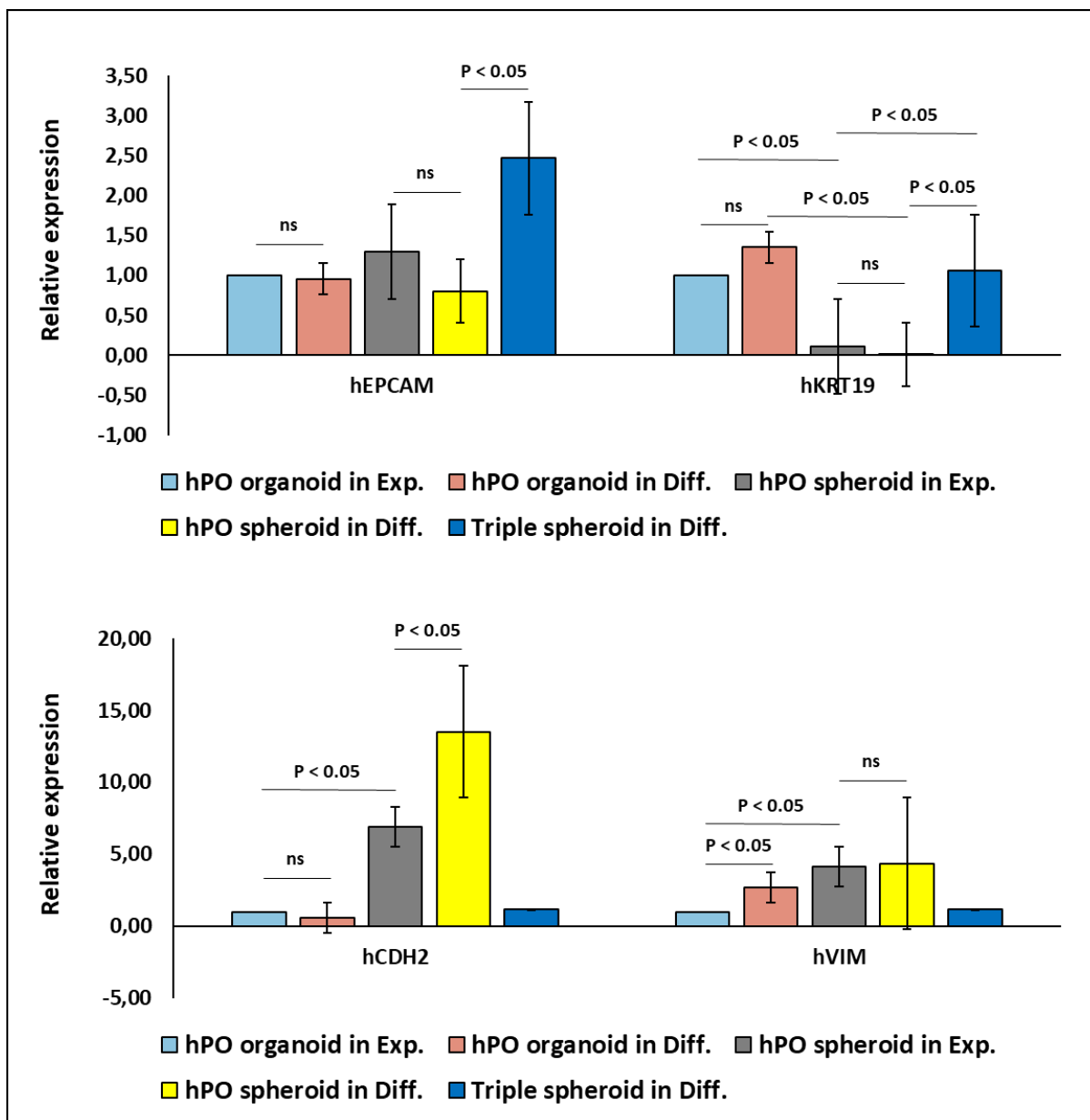


Figure 49: Quantitative analysis of epithelial-to-mesenchymal transition (EMT) markers by RT-qPCR results.
A) Ductal markers (hEPCAM and Krt19) significantly decrease after aggregation and cultivation in differentiation medium. B) Spheroid formation has positive effect on the expression of mesenchymal genes (hCDH2 and hVIM). For each condition three independent experiments with at least three technical replicates were performed. Relative expression of each gene was normalized to the geometric means of hRPL13 and hTBP (housekeeping genes) and later to the expression in hPO organoids cultivated in expansion medium. The lines inside the boxes denote the standard error. Excel 365 software was used to illustrate the graphic; Exp.: Expansion; Diff.: Differentiation.

4. Discussion

Human pancreas consists of exocrine and endocrine cells and is involved in variety of functions within body.^{1,2} There is a remarkable interest in pancreatic endocrine cells due to their importance in regulation of blood glucose levels, subsequently their link to wide-spread diseases such as diabetes mellitus.⁵⁵ Type 1 diabetes (T1D) is correlated with the destruction of β cells within pancreas making patients suffer from lack of insulin in their body for their entire lives.^{60,61} Therefore, regenerative therapies such with *in vitro* β cells is an interesting target to treat T1D.^{34,86,87}

This thesis focuses on characterizing human pancreatic organoids and spheroids after being cultivated in two different mediums (expansion and differentiation medium) and aims to leverage the liquid-overlay technique (LOT) to efficiently generate hPO cell spheroid. We applied brightfield and three-dimensional fluorescence microscopy to investigate which morphological changes occur under differentiation-dependent or -independent culture conditions. By applying RT-qPCR, this study demonstrates the changes in the expression of different genes after aggregation and cultivation in each medium. Furthermore, we examined the effect of different cell types on spheroid formation process and differentiation, by co-culturing human pancreatic organoid (hPO) with primary Human Dermal Microvascular Endothelial Cells (HDMEC) and human mesenchymal stem cells (hMSC).

Mimicking several physiological aspects that are found *in vivo*, spheroids are more advantageous than conventional 2D cell cultures. 3D *in vitro* models are widely being used since they represent both cell-cell and cell-matrix interaction.^{148,206,207} Furthermore, isolated ductal pancreatic progenitor cells can be expanded by forming single cell layer surrounding liquid-filled lumen in an extracted basement membrane hydrogel, so called human pancreatic organoids (hPOs). hPOs express progenitor factors such as SOX9 and LGR5, and have progenitor cell character which makes them the best candidate for this project.^{172,173}

The final goal of this project is develop a straightforward strategy to differentiate progenitor cells towards endocrine pancreas cells with the capacity of producing insulin as a means of cellular replacement therapy for T1D.

4.1 Differentiation medium sustains hPO organoids and spheroids growth and induces phenotypical changes

First, we investigated whether hPOs and hPO cell spheroids are capable of growing and proliferating in expansion and differentiation mediums and whether their overall morphology would change after cultivation in each medium. We successfully achieved the generation of healthy/alive, roundish, and symmetric human pancreatic organoids in both expansion and differentiation media after 7 days of cultivation, which was morphologically and phenotypically checked with time-lapse and IF staining results. Furthermore, spheroids from organoids were successfully propagated. Human pancreatic organoids cultivation were previously reported by others, albeit the formation of spheroid from organoid based on LOT has not documented.^{174,222} We managed to culture organoids for at least 10 passages in expansion medium without any notable changes in morphology or growth rate. However, we observed that only the hPOs below passage 8 can successfully form a spheroid based on LOT and higher passage numbers cannot aggregate and form spheroids. The same limitation was reported by other researchers with other cell lines. Hyo-Jung Kim has noticed the senescence of hMSC with number of passages as one of the problems during 3D spheroid formation that limit their clinical applications significantly.²²³ We also have managed to freeze and thaw frozen organoids using established protocols that originally were performed for human pancreas organoids.^{88,158,224,225} It should be noted that Y-27632 was added to control stress conditions and enhance cell recovery after thawing in the first 4 days.²²⁶

The combination of IF staining, image processing, and quantitative analysis allowed the characterization of the human pancreatic organoids and spheroids. (1) Our observations based on the live-dead assay (LDA) confirmed that human pancreatic organoids and spheroids maintain high viability over 7 days and no dead cells and necrotic part is detected in them. LDA is a simple and efficient cell death assay to identify cell death modality in 3D cultures.¹⁵¹ However, it should be taken into consideration that the protocols requires specific adaptation/optimization to become suitable for 3D cultures.

(2) Quantitative analysis of time-lapse data demonstrates a strong and significant reduction in the number of nuclei of the organoids cultured in differentiation medium compared to the organoids cultured in expansion medium, which is the opposite of what measured on spheroids cultured in expansion and differentiation medium. It should be noted that even

though a great difference in size between spheroids was detected, no visible difference in nuclei number per spheroid was reported based on statistical tests which could be explained by the existence of acinar structures in the spheroids with a broadly heterogeneous internal volume, which surely affects the spheroid's total volume. With IF staining the external localization of HUVECS cells and extracellular matrix production in triple spheroids was clearly observed. Including cells in outer layer (extracellular matrix) the volume of triple spheroids was much smaller than two other groups of spheroids (expansion and differentiation), which is explained by the exclusion of cells in the last 3 days of aggregation process in triple spheroids. These observations are generally consistent with previous reports on the spheroids of other cells and species, including mice.^{227,228} During spheroid formation, a small proportion of cells were observed not to integrate into the spheroid and lost their cell-cell adhesion properties. This was reported in different human colon cancer cell lines such as HCT116, DLD-1, and SW620.²²⁷ The same results have been documented during aggregation of murine mammary carcinoma, the EMT6 cells, as well.^{227,228} The exclusion of one subpopulations of cells from multicellular spheroids could be used as a highly reproducible and robust way to demonstrate loss of cell adhesion in heterogenous cell population, which leads to display a wide range of different spheroid phenotypes.^{227,228} This exclusion affects the number of nuclei leading to significant difference in nuclei number between triple spheroids and spheroids in differentiation medium as well, nonetheless similar difference was not observed for triple spheroids and spheroids in expansion medium. The reason for this discrepancy could not be elucidated.

(3) This project also strongly highlighted the effect of both media (expansion and differentiation) on hPOs proliferation. IF staining against KI67 and Anti-EdU (proliferation markers) demonstrated that the culture in differentiation medium restrain hPOs proliferation.^{48,229,230} The results are confirmed with quantitative segmentation analysis, indeed. In both conditions (organoids and spheroids) by cultivating in differentiation medium, the percentage of proliferated cells were significantly decreased, which highlights the inverse relationship between cell proliferation and differentiation. Moreover, the decrease in proliferation was more pronounced in hPO cell spheroids compared to hPO.⁴⁰

It is known that cell proliferation and cell death occur in different regions of a 3D structure during *in vitro* culture as a cause of relationship with the surrounding environment. Indeed, it

should be noted that a comparison between organoids and spheroids in the expansion medium demonstrated a significant positive effect of aggregation on the proportion of proliferated cells, which proves the role of cell-cell interaction. The observation in this study has been confirmed by various studies and has been shown previously with other cell types such as C2C12, murine myoblast cell line.²³¹ Several researchers have represented different *in vitro* model for cell therapy by taking advantage of this feature, indeed.²³¹ Furthermore, consistent with our findings, other reports have demonstrated that the aggregation of both Human embryonic stem cells (hESCs) and induced pluripotent stem cells (hiPSCs) facilitates the proliferation significantly.²³² Additionally, the similar result was found in the MSC aggregations, which was also in agreement with our proliferation data.

Surprisingly, applying co-culture and cultivation in differentiation medium have a positive effect on proliferation, which shed light to the role of neighbor cells, indeed. It was found that the number of proliferating cells is substantially more in co-cultured samples compared to the mono-culture spheroids cultured in differentiation medium. This observation could be explained as a result of the presence of other cell lines and differences between the content of expansion and differentiation medium. Previous studies have documented that the interaction between cells serve an important role in cell growth and proliferation. It has been reported that co-culturing with hMSC maintained up-regulation of differentiation markers (CD13, CD45 and CD56) in human hematopoietic stem and progenitor cells (HPC) and leads to higher numbers of cell divisions.²³³ This property was tested on mice cells as well and based on the results, it is demonstrated that after co-culturing TM4 cells, mouse BALB/c testis sertoli cell, with MSC the proportion of synthetic phase (S) cells enhance, significantly.²³⁴ In addition, another study with the aim of comparing co-culture and mono-culture on rat synovial stem cells and meniscus cells has shown a promotion in cell proliferation and differentiation, respectively.²³⁵ Furthermore, to imitate the natural microenvironment, recently, researchers have designed a 3D engineered scaffold by bioprinting techniques to improve better interaction between stem cell and feeder cell and check in effects on the cell growth and proliferation. The results suggested that 3D co-culture of hematopoietic progenitor or stem cells (HPSCs) and mesenchymal stem cells (MSCs) inside of engineered scaffold can provide an original and integrated environment for HPSCs growth. Additionally, it was documented that the proliferation ability of both types of cells was promoted in co-culture system, respectively.²³⁶

Regarding to the mediums, the supplements such as B27 that contain retinoic acid and is *in vivo* secreted by the surrounding cells such as mesenchymal cells, plays a key role in the development and proliferation of dorsal buds in human.²³⁷ Furthermore, prostaglandin 2 (PGE-2) is a major regulator of liver versus pancreas cell fate.²³⁸ Several reports have suggested that growth factors such as FGF10, which maintains the notch signaling pathway, plays an important role in conserving the progenitor cells into the undifferentiated state by inducing the repressive effects of Hes1 on the downstream differentiation gene Ngn3, respectively.^{33,239–242} In addition, antioxidants such as N-acetylcysteine promote the endocrine lineage along with other pancreas specific growth factors like gastrin, which keep progenitor cells in a proliferation state.^{21,243–245} Moreover, R-spondin 1 is very important in modulating cell proliferation of β cells and early pancreatic progenitor cells by enhancing the Wnt signaling pathway.^{224,246–248}

However, it should be noted that multicellular spheroids are known to strongly develop gradients of oxygen, carbon dioxide, nutrients, and waste which negatively effects proliferation with increasing size, respectively.²⁴⁹ Therefore, one disadvantage of using spheroids for proliferation testing is that cell death can occur within the spheroid core, that distorting proliferation data. Furthermore, in my project, the challenge remains to elucidate the signal in the 3D environment that regulates the expression of cyclin-dependent kinase (CDK) inhibitors (CKIs) proteins, which play a remarkable role in cell proliferation, indeed.^{40,249}

In summary, there are several noteworthy findings from this study. First, organoids could be frozen, thawed and recultured in expansion medium without any notable changes in morphology or growth rate, plus no dead cells was detected based on LDA staining. Nevertheless, the aggregation capability was dramatically affected by the passaging number. Second, this study provides evidence for significant changes in the nuclei number, spheroid volume, and remarkable morphological changes (presence of acini like structures in spheroids) between all conditions after aggregation and cultivation under different conditions. Third, these findings suggest that the content of medium and neighbor cells contributes to the cell differentiation strongly and are likely to promote proliferation through several interrelated signaling pathways. Furthermore, additional studies are required to determine critical signaling pathways for pancreas differentiation to offer potential new target for an alternative treatment for T2D patients.

4.2 Further optimization of the liquid-overlay technique (LOT) improves pancreas progenitor cell spheroid formation

A 3D cell culture provides a similar physiological and cellular environment *in vivo* by increasing and facilitating cell–cell and cell–matrix interactions to overcome the limitations of traditional 2D cell culture.¹⁸⁸ The LOT is considered as the most efficient, user-friendly, and advantageous technique in comparison to other 3D cell culture techniques such as hanging drops or spinning disk since it combines easy handling process with comfortability in changing medium.^{117,145} In addition, spheroids in this technique were produced under highly controlled conditions with the known initial cell number on the concaved agarose coated wells.^{117,145}

LOT consists of several steps such as cells trypsinization, centrifugation, and cultivation, followed by aggregation on the pre-coated plate.^{117,145} Therefore, it is still necessary to optimize this technique to control the shapes and size of the cellular aggregates. Simultaneous optimization of these parameters promotes the formation of spheroids leading to assemble highly reproducible and individual spheroids with a low cost of production and varieties that can be used for future *in vitro* experiments. The results clearly demonstrate that the single cells of hPO viability is strongly affected by the environmental and handling processes, therefore, several optimizations on the LOT have been performed to produce spheroids.

Spheroid size is one of the critical parameters that is determined by cell type, seeding density, and culture time.^{212,249} The size of spheroid has effect on oxygen and nutrients distribution within the spheroid and subsequently could negatively affect the proliferation and cell viability of spheroids.^{160,186} Optimizing the starting seeding density plays a fundamental role in spheroid formation as well as their lifespan in culture.²⁵⁰ This is also supported by the recent results documented that DU 145 cells, and human prostate cancer cell line can form spheroid after 72h from 40 starting seeding cells till 10,000 starting seeding cells.¹²⁷ However, this number should be checked and optimized for each cell line, specifically. Current results of this project show that hPO spheroids can be generated from limited starting seeding cells (3000 in 100 μ l medium) in high throughput 96 well plates with high viability, therefore, it is hypothesized that restriction in cell number or in other words, in cell-cell and cell-matrix interaction are preventing hPO aggregation. This hypothesis was also proved by strong resistance of hPO single cells to accumulate in the middle of the pre-coated wells and necessity of application a long and step by step centrifugation (twice every 7 min) during LOT.

After demonstrating the hPO single cells resistance against aggregation, following protocol optimization to improve generating compact spheroids with homogenous size, addition of appropriate reconstituted basement membrane in the culture media during spheroid formation was tested. It has been reported that various additives, such as matrigel, Basement membrane extract (BME), Geltrex®, polymer nanofibers, and collagen support spheroid formation and can contribute to forming compact and circular spheroid.^{116,133,137,251,252} Breast cancer cell line (MDA-MB-231), which expresses low levels of E-cadherin (intercellular junction proteins), can successfully generate well-defined 3D spheroids possessing uniform morphology in presence of matrigel.²¹⁵ These data were supported by a study on other breast cancer cell lines (MCF7, BT-474, T47D, and MDA-MB361) as well.²¹⁵ Results demonstrate that additional 2.5% BMs encourage cell-cell interaction causing compact spheroid formation.²¹⁵ In accordance with LOT optimization and improving hPO spheroid formation, matrigel in different concentrations (0%, 2.5%, 5%, 7.5%, 10%, and 20%) was added to the expansion medium during spheroid formation. As described above adding external component was expected to support the spheroid formation, nevertheless, the results of our project determine that hPOs in fact aggregate independently in different additional concentrations of matrigel within medium. This is interpreted as they are independent and as they could reach out each other they would be able to make sufficient cell-cell connection in multi-direction and form a circular and compact spheroid without external matrix support, after making them single cell, hPO organoids growth is strongly interconnected to the presence of external matrix (BME2) and their requirement to this supportive structure to grow.

An essential step for spheroids assembly by LOT is trypsinizing cells by minimally impairing cell viability and reaching the most homogenous single cell suspension, which leads to the highest uniform cell aggregation, and subsequently increasing spheroid formation. Producing a uniform single cell mixture has several challenging issues. As previously mentioned, single cells of hPO are extremely sensitive with respect to handling procedures, therefore they could not be treated for a long time with strong enzymatic detachment solutions such as trypsin or accutase, which are the common solutions for this purpose. Results of this project show that treating hPOs with trypsin or accutase with different concentrations could harm cells by stripping cell surface proteins and subsequently killing them. To eliminate the negative effects of trypsinization and reaching the most uniform single cell solutions together with a single spheroid per well, 15 min incubation with TripLE, the recombinant enzyme used for

dissociating an adherent mammalian cell, combined with passing cell suspension through a cell strainer is required.

Passage number is another major contributor factor for the aggregation process.²²³ The process of moving from organoid (acinar structure) to spheroid (multilayer structure) based on LOT consists of several harsh steps such as long time trypsinization (15 min), passing the cell suspension through cell strainer to gain homogenous single cell mixture, and longtime and prevalent centrifugation (twice every 7 min), therefore higher passaged number hPOs (older cells) could not survive during preparation. Furthermore, external cell-cell connections, cell surface proteins, and receptors, which are the main actors during aggregation could be damaged and unfunctional after preparation.^{86,107,108} Therefore, cells are incapable of approaching each other and form a mature spheroid. With keeping concern to these points, the most successful aggregation would be with fewer number of passages and higher starting number of cells.

In summary, traditional liquid-overlay technique (LOT) is known as one of the most functional and efficient spheroid formation methods for decades, albeit each cell has its own properties, and the main goal of the researchers is to reach the most practically doable, high throughput, and constant protocol, optimizing is unavoidable. This project provides a step ahead of optimizing conditions for spheroid formation from hPOs and improves standardization and reproducibility of this technique.

4.3 Differentiation medium causes remarkable nuclear rearrangement within hPO spheroids and organoids

Phenotypical change is one of the most obvious responses to different environmental conditions and represents the genotypical alteration of cells, respectively. Several genes are involved in the phenotypic alteration.²⁵³ These changes could be monitored during numerous cellular processes such as molecular transport, cell division, differentiation, and directional movement of the cells in a chemotactic gradient or activation towards immune responses.²⁵⁴ The molecular and cellular signals that guide progenitor cells towards specific target cell still remain poorly understood and the phenotypical changes during differentiation are not completely documented. However, one of the well-documented phenotypical alteration within cells, that appears during differentiation is cellular polarization.²⁵⁴ Polarization could

appear in shape, structure, and function of cells or nucleus localization to perform specific tasks such as differentiation, cell growth and division, migration, transmission of stimuli, or immune response.^{221,254,255}

To explore the influence of differentiation medium on the cell polarization within spheroids and organoids, during this project IF staining against cytoskeleton and nuclei was performed. The results demonstrate a strong nuclei polarization within cells in all groups after cultivation in differentiation medium (Figure 30 and Figure 31), indicating the provocative effect of differentiation medium on nuclei localization within cells. Recent studies also indicates the positive effect of differentiation assays on cytokine and its combinations (small, secreted proteins released by cells and affected the interactions and cell communications) in CD4⁺ T cell leading to strong partial polarization.²⁵⁶ Nucleus positioning is working as an integrator of cell fate and representing the cell status, along with cell function.²⁵⁷ It frequently moves to an asymmetric position during different stages of the cell cycle, and differentiation status.^{220,257} Several studies has reported the importance of nuclear properties in driving cell differentiation.²¹⁹ A comprehensive study has reported that during differentiation, embryonic stem cells modify their nuclear structure and position, which is one of the features of polarization as well and is also supported with the results of this project.²⁵⁸ Furthermore, these results are supported by a study done by Tamas Henics on erythroleukemic cells indicating differentiation is dependent on the cytoplasmic distribution and the position of the nucleus can be modified by changes in cytoplasmic organization, resectively.²⁵⁹ some researches have also proved that cytoplasmic mechanical processes maintain the position of the nucleus or move it during specific processes such as nuclear-cytoskeletal coupling, mechano-transduction signaling, tissue regeneration, cell migration, cell proliferation, and cell differentiation.^{257,260}

Nuclei of spheroids and organoids cultured in differentiation medium, were placed asymmetric and moved to the basal part of cells, respectively. Therefore, nucleus rearrangement known as one of the well-documented phenotypical changes during differentiation recorded in this project assumed to move towards β like cells after cultivation in differentiation mediums in both groups of hPOs, spheroids and organoids. Induction of nuclei rearrangement within spheroids and organoids, raise the question of whether cell-cell interaction influences nuclei localization and can improve differentiation process or not. This

hypothesis was strengthened since all spheroids strongly represented nuclei polarization, however, just part of organoids represents nuclei rearrangement. To prove this statement RT-qPCR techniques was added to this study to screen large number of differentiation related genes and analyze their gene expression patterns, simultaneously.²⁶¹

There is a remarkable interplay between cell-cell interaction and cellular differentiation.²⁶² Cellular differentiation depends unavoidably on temporally and locally cellular communication.²⁶³ Based on RT-qPCR results, this thesis strongly supported the idea and demonstrates that spheroid formation coupled with cultivation in differentiation medium increase the expression of differentiation genes such as insulin, NGN3, PDX1, NKX6-1, CHGA and, CHGB and significantly decrease the expression of progenitor genes like SOX9 and LGR5. This is align with other study of Taro Toyoda lab which elucidated aggregation efficiently induced differentiation of pancreatic bud cells in multiple hESC/iPSC lines.²³² They have reported that the combination of the aggregation cultures with the differentiation process on the undifferentiated pancreatic bud cells leads to the efficient induction of PDX1⁺NKX6.1⁺ cells.²³² Their data was improved significantly by applying higher cell density, which also could shed light to the role of starting cell number in the efficiently and productivity of differentiation and aggregation process, which is also considered in our project as well.²³² It is documented clearly in the study that signals elicited by a high cell density and consequently high possibility of cell-cell interaction are potent inducers of the directed differentiation of hESCs/iPSCs into pancreatic lineages.²³² Although the current project does not directly address the role of cell density on differentiation, however based on the previous finding and our current results, which shows the role of cell density on efficiency of aggregation process, it could be concluded that the high cell density acts as a factor to activate the essential signals for differentiation of posterior cells into pancreatic mature cells.²³² one plausible explanation for that, which has been also noted in different research groups' results with different cell types, is cell density-related factors acting at specific time points and explain the variation in the differentiation and aggregation efficiency.²⁶⁴⁻²⁶⁶

In summary, based on above-described examples and our findings in this project, cell polarization is a complex phenomenon in which the interplay among cell cytoskeletal components in which extra- and intra-cellular signals is strongly involved.^{254,267} Furthermore, it could be concluded that since spheroid formation in mono-culture and triple co-culture

significantly increased the cell-cell interactions leads to the strong basal nuclear rearrangement and, significantly increase the expression of differentiation genes compare to progenitor genes based on RT-qPCR results, it could be hypothesized that spheroid formation together with the cultivation in differentiation medium may be the potent inducers of the differentiation of hPO progenitor cells into pancreatic insulin producer cells.

4.4 The combination of spheroid culture and differentiation medium determines the endocrine fate of the pancreas progenitor cells

Establishment of successful protocols for pancreas progenitor cultivation and subsequently differentiation into insulin-producing β cells in *in vitro* is hallmarked in cellular therapy for diabetes.¹³⁹ In this work a 3D spheroid formation protocol from human pancreas progenitor cells is developed. The combination of the 3D cell culture protocol with differentiation medium induces a significant alteration in gene expression in progenitor cells that consequently shift them towards differentiation driving them to a mature-like status which has opened new doors in diabetes research and therapy.

Progenitor cells have shown applicability in various scientific fields such as regenerative medicine as well as personalized therapy researches.^{48,178,189,225,268,269} One of the first approaches in this field was done by Bonner-Weir who had published the development of islet buds from adult human pancreatic tissue. Later several studies were done and researchers have confirmed the capacity of endocrine differentiation from progenitors present in the adult human pancreas, indeed.^{270,271} Their results clearly demonstrate the inhibitor role of serum-contained factors in this process which was also considered in our study.²⁷⁷ By manipulating the expansion medium compositions, done by our collaborator Meritxell Huch, and based on the stepwise protocols samples have been cultivated in a new medium called differentiation medium, which decreases in several serum-contained factors constantly.^{84,225}

Indeed, a strong crosstalk was documented between FGF10 and Notch signaling pathways whose interplay maintain cell fate during pancreas development.^{154,181,272} Notch signaling normally acts to repress *Atoh5/Ngn3* expression during normal endocrine pancreatic development, while FGF10 regulates proliferation and differentiation towards endocrine and exocrine cell types.^{154,273} In pancreatic progenitor cells, expression of *Sox9* promotes production of FGF10-receptors (FGFR) and increases the uptake of FGF10 which subsequently

activated Notch signaling pathway.¹⁶¹ This activation in pancreatic progenitors prevents their differentiation into the endocrine or exocrine cell lineage. In contrast, it has been reported that the blockage of Notch signaling pathway due to FGF10 deficiency in the medium leads to premature differentiation of progenitor cells into endocrine cells.¹⁶¹ That was in line with our observation demonstrating FGF10 absence in the medium causes a strong shift towards endocrine cells in the phenotypical and genotypical level. Future investigations are suggested to reveal further link between downstream of these mechanisms to clarify how FGF10 and Notch signaling interact and effect pancreatic cells differentiation.

The experimental strategy began with the optimization of liquid overlay technique (LOT).^{117,117,145} By applying a spheroid culture system, similar physicochemical environment was provided and the parameters that might be difficult to manipulate in traditional 2D monolayer cell culture, such as effect of cell-cell and cell-matrix interaction can be tested.^{107,109,115,116}

We discovered that increasing the cell-cell contact has a promoter role during differentiation, since this increases and facilitates the communication between the cells and exhibit more *in vivo*-like morphological characteristic between cells.^{211,274–276} It was recently published that aggregated human embryonic stem cells (hESCs) were differentiated efficiently towards hepatic lineage and form high quality and functional hepatocyte-like cells.²⁷⁷ This is consistent with our finding that spheroid generation in combination with the elimination of FGF10 in the differentiation medium, significantly induces the up-regulation in differentiation- and mature-related genes. Progenitor genes expression consistently decreases.

Further RT-qPCR results evaluation have documented varieties of mesenchymal and epithelial genes expression. These changes suggested to evaluate occurrence of epithelial-to-mesenchymal transition (EMT) or unjamming transition (UJT) in the samples.^{278–281} Epithelial cells play a main role during these transitions. These cells are solid-like and sedentary placed on the surface of almost every organ. However, they become fluid-like and gain mesenchymal cell phenotypes and migrate during the morphogenesis. They also remodel and repair during malignant invasion or metastasis. The experiment shed light on over-expression of mesenchymal genes in the samples after aggregation and cultivation in differentiation medium which was coupled with the down-regulation of epithelial markers. That results point to the occurrence of EMT, which may take place in ductal cells during the spheroid formation

and led us to the validation of EMT within our samples. The undergoing of EMT during pancreas organogenesis is totally validated in endocrine progenitor cells.²⁷⁹ Based on our IF staining, progenitor status of hPOs were clarified by SOX9 and LGR5 expression, respectively, and changes in the epithelial and mesenchymal cells were documented. EMT is validated in our samples which could be an element within hPOs for shifting towards mature-like status after aggregation and cultivation in differentiation medium.

This conversion is defined as EMT or the partial EMT (pEMT). Moreover, EMT is a hallmark in pancreatic development and plays important roles in β cell differentiation and islet formation. EMT is mostly documented by up-regulation of mesenchymal-related genes and constantly down-regulation of epithelial-related genes. In some cases, morphological changes were aligned with these changes, indeed.^{278–281} It is reported that this conversion has been attributed to the recently discovered unjamming transition (UJT) in which epithelial cells move collectively and cooperatively during physiological events such as embryonic development.^{278–281} In other words, epithelial cells can transition from a jammed, solid-like, and quiescent phase to an unjammed, fluid-like, and migratory phase which is called UJT. EMT and UJT have quite a similar procedure. It is extremely difficult to distinguish UJT from pEMT since they share certain aspects of cellular migration and gene expression, furthermore, the extent to which these processes remain largely unexplored.^{278–281}

Surprisingly, it should be noted that the results demonstrated the highest level of expression for Pdx1 in triple co-culture spheroids compared to organoids and mono spheroids. Pdx1 plays a remarkable role in pancreas development and is detected during different processes such as pancreatic regeneration and trans differentiation of extra-pancreatic cells into insulin-producing cells.^{84,252,279,282–285} It is documented that Pdx1 is expressed transiently during embryonic development: first it is needed for the outgrowth of pancreatic progenitor cells located in ducts then it is reported during the final differentiation of β and δ cell precursors within pancreas.^{279,282} The potential role of Pdx1 in epithelial-to-mesenchymal transition (EMT) *in vivo* is well studied. Pdx1 actively increases epithelial marker expression.²⁸⁶ One recent study reported that Pdx1 down-regulation is required during EMT.²⁸⁷ In this work, by evaluating the expression of EMT related genes and differentiation related genes the over-expression of hEPCAM and hKRT19 (epithelial markers) coupled with down-expression of hCDH2 and hVIM (mesenchymal markers) were documented, which is aligned with Pdx1 over-

expression supporting that its loss might be necessary for EMT. In addition, Nkx6.1 over-expression suppresses cell invasion by inhibiting EMT which is in agreement with our RNA expression data, indeed.²⁷⁸ The results demonstrated a strong increment in Nkx6.1 expression compared to hPO organoids cultivated in both growth and differentiation mediums. However, expression of the same genes was significantly higher in the mono-culture spheroids cultured in the differentiation medium. Therefore, it could be hypothesized that EMT is not detected in triple spheroid, albeit, this point should be considered that our results required to be interpreted with caution due to spheroid formation in differentiation medium only. Furthermore, the ratio of the cells (1:1:1) should be considered regarding to the expression rate of specific pancreas differentiation-related genes and differentiation processes such as EMT. Moreover, since the triple spheroid consists of different cell types it could be possible that the RNAs level, that were detected during RT-qPCR were produced by neighbor cells instead of hPOs. Triple staining of each cell type can be performed in order to reveal the source of the genes more accurately. Evidence for this hypothesis comes from the prior work done by Shang Zhang and his group.²⁸⁸ He has documented Nkx6.1 expression from the Porcine pancreas-derived mesenchymal stromal cells (PMSCs).²⁸⁸ To validate the source of pancreas related genes within triple spheroids, application of different cellular techniques such as genetical manipulation or labeling desire proteins with red fluorescent proteins (RFPs) is recommended in order to determine the specific source of each product in triple spheroids. In general, even though it could be assumed that triple spheroid is the most similar *in vivo*-like sample and represents the same phenotypical characteristic compared to mono-spheroids, it is not a good candidate for examining EMT process during differentiation.

In summary, our experiments have established 3D cell culture protocols that are valuable to model pancreas development *in vitro*. Spheroid provides a similar physicochemical environment in *in vitro* by increasing cell-cell and cell-matrix interaction in which pancreatic gene expression is altered due to the spheroid formation and differentiation medium. The combination of differentiation medium and spheroid formation has proved EMT induction within hPOs, which is a promising model for endocrine lineage commitment. The results from this thesis provide designed strategy for shifting pancreatic progenitors toward mature-like pancreatic cells.

4.5 Long term imaging of dynamic cell behavior and cell type segregation during spheroid formation with light sheet microscopy

To provide further insight into the aggregation process time-lapse imaging by the light sheet Z1 microscope was performed. Indeed, time-lapse fluorescent microscopy provides information about cell behavior and its localization over time can give detailed view of cellular processes.^{289,290} Understanding the localization of cells during the process is critical to understand the biological processes.²⁹¹ Despite the strengths of time-lapse microscopy there are several challenges and limitations. Fluorescence trackers are limited by their stability and specificity.²⁹² It is critical to choose a tracker that is photo-stable and bright, it is also necessary to consider the procedure of staining and its effects on cells' viability.²⁹³ Specific care in concentration and incubation time must be taken to ensure they are not toxic.^{293,294} In addition, there are many technical challenges in growing and observing cells under a microscope. The major challenge faced during this work was determining the optimum incubation time and the suitable concentration of fluorescent dyes for cell tracking coupled with the trypsinization of hPOs. Unfortunately, Orange Cell Tracker was not compatible with long-term live imaging and extensive cell death was observed after few hours of live imaging, therefore, only two cell tracker dyes (Deep red and Green) have been used.. Furthermore, temperature, humidity, and contamination during the time-lapse influences the performance of the the fluorophores, which several time resulted in the in loss of data or of the entire experiment. In addition to the physical and mechanical interactions between the cells during spheroid formation, a large amount of interplay may occur during sample preparation. It is likely that some events such as applying pre-washing steps with Hellmanex, which decrease the surface- adhesion lead to increase cell aggregation. Another aspect of long-term time-lapse which is often underestimated is data management and file size. Time lapse imaging generates large amounts of image data files, whose storage and retrieval can be a time-consuming process. It should also be noted that high intensity light and long-time exposures are further major concerns when performing long term time-lapse microscopy, since they cause photobleaching and phototoxicity.^{199,295} These can have large effects on cell survival and lead to artifacts in the experiment.^{198,199,296} Light sheet fluorescence microscopy (LSFM), used for these experiments, offers a fluorescence microscopy technique with diffraction-limited

optical resolution, low fluorophore bleaching, low photo toxicity, good optical sectioning capabilities and high recording speed.

In this thesis, time-lapse imaging was used to visualize the process of spheroid self-assembly. Spheroid formation or self-assembly remains as an ideal system to study *in vitro* tissue development and formation.^{223,289,297} There are two main hypotheses about the cell aggregation; The first one, which was suggested by Steinberg in 1963, is based on a minimization of free energy occurrence.²⁹⁸ Steinberg have assumed that: If a cell-substratum has a strong adhesion, it would lead to decreasing the surface free energy by maximizing surface adhesion bonds and as a result, the monolayer conformation/aggregation will be formed.²⁹⁸ Based on this hypothesis, he suggested that maximizing the intercellular adhesions lead to cellular aggregation.²⁹⁸ The second hypothesis was proposed by Tzanakakis in 2001 which gives the cellular cytoskeleton the main role during aggregation.²⁹⁹ In this scenario, during the early aggregation stage of spheroid formation, the contractile forces generated by the internal cellular cytoskeleton compared to the cell-substratum adhesion forces determine the formation of spheroid.²⁹⁹ The knowledge gained by our time-lapse investigation supports both hypotheses. As accumulating single cells at the bottom of the well, the surface free energy is minimized significantly, on the other hand, cell-cell contact and cellular cytoskeleton contractile forces, which drive the spheroid formation process, are increased. Based on our data, we suggest that cell-cell contact come to play later in the compaction stage (during the rapprochement of aggregates and formation of micro prevascular network around the spheroid) to develop compact, vascularized, and free-floating spheroids. Furthermore, the results obtained from the analysis of individual spheroid formation process over the time confirm our theory that hPOs that were trypsinized to single cells, kept their original growth pattern and pumped in and out constantly during aggregation which led to formation of multiple acinar structures inside of both mono- and triple-spheroids. Therefore, it can be hypothesized that despite all differences between organoids and spheroids, hPOs cells maintain some aspects of their original morphology and growth pattern of organoids (round, luminal, acinar 3D structure) during aggregation inside of a spheroid. There are plenty of experiments that have evaluated the crosstalk between pancreatic cells and MSC or EC. Despite all positive feedbacks, there is insufficient document about the combination of all three cell lines together. Therefore, we have set a co-culture with all three cell lines together to rebuild the complexity in *in vivo* and have demonstrated promotion or inhibition effect of

both cell lines simultaneously on pancreas differentiation. The triple spheroids are capable to be formed only in differentiation medium. Also, based on the IF staining, co-culture samples have been representing a similar phenotype and genotype like mono spheroids.

Co-culturing represents significant cellular and molecular properties during differentiation and development. In addition, since 2 main hypotheses remarked the fundamental role of cell-cell contact and cytoskeleton on the cell aggregation process and considering this fact that different kinds of cell are presented inside of the body during the development, co-culture was performed to study the interactions among different cell populations in a way to improve the spheroid formation and investigate the procedure of differentiation in the presence of other cell lines in more details.²⁷⁴ Co-culturing gives chance to a variety of cell types to be cultured together so as to examine the effects of one culture system on the other(s) and provides a more representative human *in vivo*-like tissue model for high-throughput testing and in-depth monitoring of cell–cell interactions.^{132,274} In addition, researchers can determine the natural interactions between two or among more different organisms altogether by activation or inhibition of gene clusters during various cellular processes such as differentiation.^{236,274,300} Nevertheless, it should be noted that, co-culturing challenges regarding the cell culture medium, concerning medium composition, volume, and exchange for individual cell types were important in our experiment requiring numerous troubleshooting. The co-culturing was applied in different forms and fields, and its positive effect on the cellular and molecular processes, which is going to be described later, were a fundamental basement for our co-culture designs. Unfortunately, a 3D co-culture system as a human-like model was mostly performed in cancer research in terms of cell proliferation and invasion investments, albeit, they have been inspired clear insights to the compatibility of different cell types with pancreas-resourced cells. Several co-culturing between pancreatic ductal adenocarcinoma cells (PDAC) and different cell types such as fibroblasts, mesenchymal cells, and endothelial cells demonstrated the undeniable cell-cell contact and crosstalk between different cell types and reported their effect on the cellular and molecular processes.^{301–304} In addition, the complex organization of the cells, composed of several cells, vessels, nervous fibres, and ECM molecules, provides a three-dimensional environment inside of the body that has a special organization and interacts with the others which leads to the transcription of several genes and regulating molecular processes such as homeostasis or differentiation during development. Illustrating the point above, a study done by Takahashi

and his group in 2018 showed that mouse islets are capable of aggregation after being co-cultured with hMSC and HUVEC and the secretion of insulin after transplantation within mouse has documented in their paper, respectively (Supplementary Figure).¹⁵² Another experiment that proved the cross-effect in co-culture in relation to cellular differentiation was the co-culture of nerve cells and pancreatic islets, which regrettably was not applied in this thesis. Researchers have documented the differentiation of nerve endings around the endocrine islet cells after two weeks of co-culturing.³⁰¹ There was another trial with the aim of protecting islets from injury and improve their viability to increase the chance of transplantation afterwards. It was reported that co-culturing of islets with MSCs has the potential to protect islets from injury and their supportive effect on their viability.³⁰⁵ Moreover, Yamada and his group demonstrated the importance of VEGF for islet survival in combination to co-culturing concept. They have co-cultured islets with mesenchymal stem/stromal cells and reported that islet viability was significantly lower in the co-culture group treated with bevacizumab, an inhibition of VEGF, compared to the non-treated co-culture condition.³⁰⁵ Furthermore, they concluded that VEGF might play role in vasculogenesis and angiogenesis as well as anti-apoptotic effects. In other study done by Kono, the expression of VEGF and TIMP-1 was detected in the presence of stressed murine islets in an indirect co-culture system.³⁰⁶ TIMP-1 is a member of matrix metalloproteinase inhibitor family and is involved in regulating several biologic processes, such as cell growth, migration, and apoptosis.³⁰⁶ In this regard, the up-regulation of anti-apoptotic signaling molecules in the murine islets were reported after being co-cultured with human umbilical cord blood-derived mesenchymal stem cells (hUCB-MSCs) as well. At mRNA level, Park has observed increased expressions of angiogenesis-related genes in islets from the co-cultured condition and claimed that AKT pathway activation play a crucial role in survival of β cells.³⁰⁷ Furthermore, other results also indicate an improvement effect of co-culturing in insulin secretion, indeed. That result was proved by the comparison between islet cultured alone and co-cultured with MSCs.³⁰⁵ Moreover, the positive role of endothelial cells in the maturation of human embryonic stem cell into insulin producing islet-like cells was explored, respectively. The maturation is achieved by a co-culture configuration between rat heart microvascular endothelial Cells (RHMVEC) and human embryonic stem cells (hESC).³⁰⁸

Another aspect that could be documented within co-culture samples during the 3D time-lapse images in this thesis, was cell localization. In recent years, fluorescence microscopy techniques

for localization and tracking single cells have become well-established and have been indispensable tools for investigating cellular behavior.^{194,212,290,292} It helps us to understand how cells mediate their behavior in terms of cell-cell connection during biological processes. Based on acquisition images in this thesis, cell trackers continued to fluoresce upon laser excitation even after more than 48 hours of repeated scanning (30 min interval) without disruption of cell motility. In addition, the 3D reconstructions accurately represented behavior of the hPOs, hMSC and HUVEC including shape, localization, and morphology during the process of spheroid formation, respectively. Finally, the ability to examine the interaction of a single cell with its surroundings was visualized by applying multiple staining and tracking cells over time during the mechanism of spheroid formation. The ability to identify individual cells in a population and track them over time in 3D is an asset. In addition to the points mentioned at the beginning of this chapter about the fluorescent cell tracking technique, applying this method is ideally suited to studies of mixed cell populations over time. Use of several fluorescent cell trackers on alive cells in co-culture samples eliminates the need of plasmid transformation or usage of cell-specific markers such as antibodies, in which imaging does not require fixation. In addition, since the staining was applied rapidly and individually to each cell type and not simultaneously to the cell mixture, the risk of dye transfer between cell types was minimal. Despite being a helpful method for investigating mixed-cell interactions, the transferring to daughter cells and fluorescent stability is low, which makes these studies not optimal for proliferating cells.

Since the external localization of HUVECS was documented in previous experiments, they were stained in green, hMSC and hPOs were colored in red deep. Results in this thesis are aligned with the ones in the Takahashi paper. External movement of HUVECS was clearly documented during the spheroid formation.¹⁵² By further analyzing the HUVECS in the peripheral part of spheroids over time, it is easy to identify regions of contraction or lengthening of some endothelial cells during the aggregation process. This behavior was like the formation of micro-vascular-like network around the islets during the pancreas development *in vivo*. During the last decade, several works have shed light on the role of vascular network on the pancreas development and function. They have also pointed out its positive effect on the improvement of islet transplantation.^{27,28,30,309,310} In addition to the severe demand of close contact between islets and blood vessels to determine blood sugar levels and subsequently secreting the appropriated amount of insulin, it is reported that

oxygen is a crucial determinant of pancreas development.^{89,311,312} It is demonstrated that hypoxia leads to fewer β cells differentiation. Samples with genetical ablation of von Hippel-Lindau gene (Vhl) were indicated that hypoxia was mediated by hypoxia-inducible factor 1 α (HIF1 α) and HIF1 α is involved in regulating insulin secretion in adult islets, respectively.^{311,313} Moreover, formation of functional blood vessels within/around islets can increase the success rate of islet transplantation in patients. Insufficient vascularization in islet fragments restricted the successful transplantation in clinical practices.^{45,82,314} It is reported that prevascularized islets are rapidly blood-perfused after transplantation with the help of interconnection between micro-vascular-like networks and surrounding blood vessels. Also, paracrine signaling between β cells and micro vessels exhibit a significantly higher angiogenic activity and increase the islets function, respectively. Consequently, a lower number of islets are required for therapy in the diabetic animals such as mice.^{38,313} Therefore, introducing the novel strategy for co-culturing to the generation of micro-vascular-like networks can help the researchers to overcome this problem and improve the success rate of clinical transplantation. My strategy may be extended/ improved by the application of long-term cultivation with the addition of vascular endothelial growth factor-A (VEGF-A).¹⁶¹⁻¹⁶³

In summary, by citing the mentioned experiments and our obtained results in this project, it could be concluded that due to the non-invasive nature of cell tracking technique and its minimal effects on cell activities, our method is optimal to identify individual cells in a population and track them over time in 3D samples, also, it is suitable for using in many other investigations, indeed. Furthermore, these time-lapse experiments have provided an interesting glimpse of cellular behavior and localization during spheroid self-assembly process. Despite the short imaging time, all steps of the spheroid self-assembly including rearrangement, aggregation, and compaction were documented respectively and the hPOs pumping function was discovered during aggregation, indeed. Moreover, clear external localization and micro-vascular-like networks formation by HUVEC was observed within triple spheroids, which indicates that co-culturing coupled with spheroid formation can be effective techniques to improve transplantation in clinical practices.

5. Conclusion and outlook

5.1 Conclusion

This thesis provides a novel approach for the differentiation of pancreas human organoids to *bona fide* endocrine cells expressing insulin. This work could represent a significant contribution to a personalized cell therapy of diabetes 1 type (T1D). Starting from the original differentiation media developed by Meritxell Huch's group (MPI-CBG, Dresden, Germany) and the hPO cell bank generated by Lorenza Lazzari's group (Policlinico di Milano, Milan, Italy) in the framework of the LSF4Life project, we have studied the role of microenvironments, cell-cell and cell-matrix interactions, cellular structure, neighbor cells and small molecule inducers in transdifferentiating progenitor cell lines to mature-like endocrine cells in human pancreatic organoids (hPOs) in details.

A protocol to form multilayer spheroid from hollow acinar organoids based on liquid overlay technique (LOT) has been successfully established for the first time in this study. For comparison, both organoids and spheroids were cultivated in expansion and differentiation medium followed by examination of the expression of several pro-endocrine genes with immunofluorescent staining (IF) and RT-qPCR. In addition, the influence of a co-culture with stromal and endothelial cells (i.e. HUVEC and hMSC) on the differentiation of hPO cells was investigated.

The culture of both organoids and spheroids in differentiation medium and the application of co-culturing lead to remarkable phenotypic changes both in morphology and gene expression. IF staining has revealed that the combination of co- hMSC and HUVEC culture with with spheroid formation in differentiation medium increases the expression of proteins that regulate cytoskeletal remodeling and causes the formation of baso-apical polarized acinar structures. Moreover, we observed that the same conditions significantly decrease cell proliferation, which is an initial hallmark of the onset of differentiation. The RT-qPCR analysis indicates that after cell aggregation and cultivation in differentiation medium, hPO progenitor cells differentiate, as signaled by the under-regulation of progenitor and ductal genes and the strong over-regulation of endocrine cell-specific genes.

Finally, after evaluating the data, this thesis has achieved to demonstrate that 3D cell culture is more consistent with *in vivo*, and this model is capable of mimicking aspects of natural human development which represents better cell-cell and cell-matrix communications, microenvironments, and differentiation signatures that are not reflected in 2D models.

Nevertheless, current study has presented molecular insights into *in vitro* lineage reprogramming events, showing that successful implementation of 3D models requires exhaustive phenotypic characterization to verify the relevance of implementing these models to treat T1D patients.

We are delighted to present this thesis after working through quarantine and restrictions which affected working in the lab. It is with joy to note that our department has been perfectly provided the grounds for us to work, however with difficulty, to help us make accomplishment in science.

5.2 Outlook

To facilitate differentiation induction within hPOs, it was decided to apply electroporation technique to them. Therefore, the transfection with pmaxGFPTM vector by P3 Primary Cell 4D-Nucleofector™ X Kit S (LONZA) was applied to check its compatibility (supplementary figure 47). Because of the difficulties and complexity in transfecting process and vulnerability of hPOs, the primary results were not successful, meaning the technique still requires further optimizations, which is challenging due to the slow growth rate of hPOs. It is highly recommended that with optimizing electroporation technique and inducing with differentiation-inducing plasmids within the hPOs coupled with increasing cell-cell and cell-matrix communication by spheroid formation, advantages of 3D cell culture formation could be proved, respectively.

A further aspect that was not possible to address in the current study is to perform insulin challenging experiments of the differentiated organoids. Insulin expression was confirmed by using RT-qPCR and IF staining studies. However, C-peptide antibodies are needed to provide further evidence that the precursor of insulin is expressed. Therefore, it is important to investigate C-peptide expression in samples as well to identify the extent of insulin protein expression and secretion.

Moreover, due to the unavailability of some antibodies, the expression of pancreatic transcription factors in hMSC or HDMEC were not explored in a way to determine the specificity and source of transcription factors in co-culture samples. The results were mostly in accordance with the literature but need further strengthening by incorporating important pancreatic transcription factors such as: Ngn3, YAP1, NKX6.1 and quantitative methods e.g. Microarrays or Western blotting.

In addition, it is possible that the differentiated cells represent a mixed population in terms of differentiation status and thus using specific cell surface markers will present the proportion of mixed cells. Several techniques such as fluorescence-activated cell sorting (FACS) could be a useful technique that provides quantification of fluorescent signals from individual cell types in addition to physically separating cells of particular interest.

As the local production of vascular endothelial growth factor-A (VEGF-A) by the β cells is high, endocrine capillaries are approximately 10 times greater than exocrine pancreatic capillaries and receive up to 20% of pancreatic blood flow.^{9,26,27} Super close and compact capillaries network in islets facilitate monitoring glucose levels, consequently, release the related amount of insulin within bloodstream. Within this network, pancreas plays a key role by producing and secreting insulin and its opponent glucagon to control normal blood glucose levels.^{7,12,13} Blood vessel-like vascular system formation in 3D cell cultures is critically important for nutrient delivery and enhancing cell-cell interactions and would be another challenge in 3D cell culture, which due to time constraints was not addressed in this thesis.¹⁶¹⁻¹⁶³ Therefore, adding VEGF-A to the co-culture, so as to enhance capillary networks formation and observing its effect on HDMEC and hPO differentiation, causing insulin production is one of the most interesting topics suggested to further my thesis.

Recently, researchers have demonstrated undeniable effect of temperature on molecular diffusion being in line with vital cellular functions such as perfusion, cellular growth, and proliferation. It is documented that spheroids are less sensitive to heat compared to monolayer cultures and showed different patterns in shrinking and regrowth after exposing to heat, respectively.³¹⁵ Since hPOs are instable, the cultivation process and temperature range was limited in my study. Further analysis of dynamic spheroid response in a temperature dependent manner was encouraged. It shows how temperature-dependent, heat-induced physiological changes, such as enhanced, decreased perfusion or immunogenic effects could affect cell death, proliferation, and differentiation.

Finally, recent findings illustrated the significant role of co-culturing on pancreatic differentiation and maturation of ESCs *in vitro*. Although, contribution of endothelial cells in pancreatic development has been well studied and was tested in this thesis it should be noted that some of the intercellular interactions presented in islets *in vivo*, such as β cells interaction with nerve cells and immune cells, were not represented in our chosen *in vitro* model. Further experiments should be conducted in more complex, co-culture models to recapitulate the islets microenvironment more accurately.

6. Summary – English

The aim of this work is to induce endocrine lineage commitment in organoids derived from human pancreas organoid progenitor cells (hPO cells) by forming compact three-dimensional spheroids and culturing them in differentiation media.

Differentiation of stem cells into functional tissues occurs through a complex and largely unknown orchestration of cell proliferation, polarization, and death. Fundamental morphological, phenotypic, and physiological changes are initiated during differentiation. Numerous studies have highlighted the importance of intracellular communication and the interaction of cell-cell communication with the extracellular matrix in differentiation processes, and cell aggregation in particular has been shown to have a profound function in cell differentiation.

hPO cells are originally derived from pancreatic ductal progenitor cells. Cultivation of primary pancreatic ductal cells in three-dimensional hydrogels that reconstitute the function of the natural extracellular matrix, favors the growth of pancreatic progenitor cells that express specific progenitor markers such as SOX9 and exhibit self-renewal and self-assembly. Such three-dimensional tissue-like structures are referred to as "pancreatic organoids" *in vitro*.

This work tests on the hypothesis that spheroids as a 3D cell culture model can comprehensively reflect the physiological conditions of intercellular communication as well as cell-matrix interactions during the embryonic development of pancreatic islets of Langerhans. According to this working hypothesis, methods for efficient aggregation of hPO cells have been elaborated. For this purpose, the so-called "liquid overlay" technique was adapted for hPO cells to promote physiological cell-cell communication between pancreatic progenitor cells.

In addition, the effects of co-culturing primary human dermal microvascular endothelial cells (HDMEC) and human mesenchymal stem cells (hMSC) on the differentiation of the progenitor cells into the spheroids were observed.

The influence of spheroid formation on morphogenesis and differentiation of cells to the endocrine lineage was systematically investigated by light microscopy, immunostaining and quantitative PCR.

To investigate the phenotypic features of the interior of the spheroids, *in toto* immunofluorescence staining was applied in combination with optical clearing. Three-dimensional images of the specimens were acquired using confocal laser scanning fluorescence microscopy (CLSM) and light-sheet-based fluorescence microscopy (LSFM). To quantify morphological markers, including the number of nuclei and spheroid volume, the image data were analysed using different segmentation pipelines. In addition, the time-resolved spatial self-assembly of hPO cells as the spheroids formed was examined using live imaging with light sheet microscopy over several days.

The development of spheroids from hPO cells was studied in two different culture conditions, expansion medium and differentiation medium to activate the differentiation genes. The samples were cultured in expansion medium for seven days, while the other group was cultured in differentiation medium for comparison. After seven days, both samples were collected for further experiments. Differentiation protocols stimulate the expression of transcription factors in the hPOs. To study the morphogenetic changes, various molecular methods as well as laboratory techniques were performed in combination with appropriate statistics.

Effective protocols for optimal formation of the spheroids in both media were established and the high survivability of the hPO cells (in the organoids and in the spheroids) in expansion and differentiation media was confirmed by live-dead assay. Longitudinal studies with epifluorescence microscopy show that the organoids and spheroids grow unrestricted and develop without problems in both media.

Organoids grown in differentiation medium form smaller acinar structures and show less cell proliferation on average than organoids grown in expansion medium. Interestingly, comparison of organoids and spheroids suggests clear differences in cell proliferation: the cell density of the spheroids grown in differentiation medium is higher than the cell density in the organoids under the same conditions. A closer examination of the spheroids with confocal laser scanning fluorescence microscopy shows, that the number of nuclei and the volume of the triple co-culture spheroids, composed of hPOs, hMSC and HUVEC, is significantly lower compared to the homogeneous hPO spheroids, which could cause the consequence of cell dissociation in the last three days of spheroid formation.

In addition, the volume of the spheroids was measured using image processing and segmentation. Although there was a significant difference between the number of nuclei in the spheroids under both conditions (expansion and differentiation), no significant difference in the volumes was detected. Next, the internal structure of the spheroids was examined in more detail using the further IF staining (immunofluorescence staining). The analysis shows the formation of several hollow acinar-like compartments, suggesting that the hPO cells retain their ductal character even as part of spheroids and that, therefore, enzymatic disassembly into single cells and subsequent re-aggregation does not affect the identity of the progenitor cells. Furthermore, morphological analysis of the spheroids shows that the differentiation medium leads to a more pronounced cell polarization, manifested by basal rearrangement of the nuclei and actin cytoskeleton in both organoids and spheroids.

The results of EdU incorporation assays and IF staining against the proliferation marker KI67 show that differentiation induction results in a reduction of cell proliferation in both spheroids and organoids.

To visualize the process of spheroid formation dynamically and in three dimensions, longitudinal image stacks were acquired using LSM. The time-lapse data were analysed to elicit the process of spheroid formation: the formation of spheroids from hPO cells begins with the approach of individual cells to each other and the formation of small aggregates, followed by the aggregation of these aggregates and the formation of compact and multi-layered cellular structures.

The study performed with the LSM and CLSM heterotypic spheroids from cocultures of hPO cells, endothelial cells and mesenchymal stem cells. These show that the localization of the different cell types represents a similar spatial structure to cocultures of dissociated Langerhans islet cells with endothelial cells known from the literature. This suggests that the self-assembly of cells in the heterotypic spheroids leads to the tissue architecture consistent with that of the established Langerhans' islet model.

Quantitative PCR and IF staining were used to identify the changes in gene expression that occur as a result of cell aggregation and differentiation of spheroids. The results clearly show that spheroid formation in conjunction with differentiation medium significantly affects gene expression. Expression of differentiation markers (NGN3, NKX6.1, and PDX1) and specific β -cell markers (insulin, CHGA, and CHGB) is significantly upregulated, whereas downregulation

of transcripts (hSOX9 and hLGR5) present in progenitor cells was detected. It is concluded that aggregation forces hPO cells to leave their progenitor status and drives them toward differentiation into β cells. Moreover, significant downregulation of epithelial markers (hEPCAM and hKRT19) was found in association with upregulation of mesenchymal markers (hVIM and hCDH2) in hPO cells, a hallmark of epithelial-to-mesenchymal transition (EMT). This is an interesting observation because EMT represents the first step in the formation of islets of Langerhans during pancreas development.

The results of this work consistently demonstrate that the assembly of hPO cells into spheroids and the resulting intercellular interactions, in synergy with culturing in differentiation medium, induces significant upregulation of differentiation markers and β -cell markers and downregulation of genes mainly expressed in progenitor cells. This process would lead to efficient differentiation to β cells. Therefore, it has been another step in the direction of cellular therapy and personal treatment of type 1 diabetes.

7. Zusammenfassung – Deutsch

Ziel dieser Arbeit ist es, die endokrine Abstammung in Organoiden aus Vorläuferzellen der menschlichen Bauchspeicheldrüse (eng. human pancreas organoid progenitor cells, hPO-Zellen) durch Bildung von kompakten dreidimensionalen Sphäroiden und Kultivierung in Differenzierungsmedien einzuleiten.

Die Differenzierung von Stammzellen zu funktionellen Geweben erfolgt durch eine komplexe und zum Großteil noch unbekannte Orchestrierung von Zellproliferation, -polarisierung und -tod. Grundlegende morphologische, phänotypische und physiologische Veränderungen werden im Laufe der Differenzierung eingeleitet. Zahlreiche Studien haben die Bedeutung der intrazellulären Kommunikation und der Wechselwirkung der Zell-Zell-Kommunikation mit der extrazellulären Matrix für die Differenzierungsprozesse deutlich gemacht und es wurde nachgewiesen, dass insbesondere die Zellaggregation eine tiefgreifende Funktion bei der Zelldifferenzierung hat.

hPO-Zellen werden ursprünglich von duktalem Vorläuferzellen der Bauchspeicheldrüse gewonnen. Die Kultivierung der primären duktalem Pankreas-Zellen in dreidimensionalen Hydrogelen, die die Funktion der natürlichen extrazellulären Matrix rekonstruieren, begünstigt das Wachstum von Pankreas-Vorläuferzellen, welche spezifische Progenitor-Marker wie z.B. SOX9 exprimieren und Selbsterneuerungs- sowie Selbstorganisationsfähigkeiten zeigen. Solchen dreidimensionalen, gewebeähnlichen Strukturen werden *in vitro* als „Pankreas-Organoid“ bezeichnet.

Diese Arbeit überprüft auf der Hypothese, dass Sphäroide als 3D-Zellkulturmodell die physiologischen Bedingungen der interzellulären Kommunikation sowie der Zell-Matrix-Interaktionen während der embryonalen Entwicklung der Langerhans'schen Inseln in der Bauchspeicheldrüse umfassend widerspiegeln können. Dieser Arbeitshypothese zufolge wurden Methoden zur effizienten Aggregation von hPO-Zellen erarbeitet, die erforderlicher Weise nur partiell, nachahmen sollen. Zu diesem Zweck wurde die sogenannte „Liquid Overlay“-Technik für hPO-Zellen adaptiert. Dadurch wurde die physiologische Zell-Zell-Kommunikation zwischen den Pankreas-Vorläuferzellen fördern.

Darüber hinaus wurden die Effekte der Ko-Kultivierung von primären humanen dermalen mikrovaskulären Endothelzellen (eng. HDMEC) und humanen mesenchymalen Stammzellen (eng. hMSC) auf die Differenzierung der Vorläuferzellen in die Sphäroide beobachtet.

Der Einfluss der Sphäroidbildung auf die Morphogenese- und die Differenzierung der Zellen zur endokrinen Abstammung wurde mit Lichtmikroskopie, Immunofärbung und quantitativer PCR systematisch untersucht.

Um die phänotypischen Merkmale des Inneren der Sphäroide zu untersuchen, wurde *in toto*-Immunfluoreszenzfärbung in Kombination mit optischer Aufhellung angewendet. Dreidimensionale Bilder der Proben wurden mit konfokaler Laser-Scanning-Fluoreszenzmikroskopie (eng. CLSM) und lichtscheibenbasierter Fluoreszenzmikroskopie (eng. LSFM) aufgenommen. Zur Quantifizierung verschiedener Merkmale, einschließlich der Anzahl der Zellkerne und des Sphäroidvolumens, wurden die Bilddaten mit unterschiedlichen Segmentierung-Pipelines analysiert. Zusätzlich wurde die zeitaufgelöste räumliche Selbstorganisation der hPO-Zellen im Laufe der Formierung der Sphäroide mit Lebendbeobachtung-Lichtscheibenmikroskopie über mehrere Tage untersucht.

Die Entwicklung der Sphäroide aus hPO-Zellen wurde bei zwei unterschiedlichen Kulturbedingungen untersucht, d.h. in Expansions- und Differenzierungsmedium, um die Differenzierungsgene zu aktivieren. Die Proben wurden sieben Tage lang in Expansionsmedium kultiviert, während die andere Gruppe zum Vergleich in Differenzierungsmedium kultiviert wurde. Nach sieben Tagen waren beide Proben für weitere Experimente gesammelt. Differenzierungsprotokolle stimulieren die Expression von Transkriptionsfaktoren in den hPOs. Um die morphogenetischen Veränderungen zu untersuchen, wurden verschiedene molekulare Methoden sowie Labortechniken in Kombination mit geeigneten Statistiken durchgeführt.

Effektive Protokolle zur optimalen Bildung der Sphäroide in beiden Medien wurden etabliert und die hohe Überlebensfähigkeit der hPO-Zellen (in den Organoide und in den Sphäroiden) in Expansions- und Differenzierungsmedium wurde mit live-dead Assay bestätigt. Longitudinale Untersuchungen mit Epifluoreszenzmikroskopie zeigen, dass sich die Organoide und Sphäroide in beiden Medien uneingeschränkt wachsen und ohne Probleme entwickeln. Die im Differenzierungsmedium wachsenden Organoide bilden kleinere azinären Strukturen und zeigen durchschnittlich weniger Zellproliferation als die Organoide, die im

Expansionsmedium gezüchtet werden. Interessanterweise, deutet der Vergleich von Organoiden und Sphäroiden auf klare Unterschiede in der Zellproliferation hin: die Zelldichte der in Differenzierungsmedium gewachsenen Sphäroide ist höher als die Zelldichte in den Organoiden bei denselben Bedingungen, wobei eine genauere Untersuchung der Sphäroide mit der konfokalen Laser-Scanning-Fluoreszenzmikroskopie zeigt, dass die Anzahl der Zellkerne und das Volumen der dreifachen Co-Kultur-Sphäroide, besteht aus hPOs, hMSC und HUVEC, im Vergleich zu den homogenen hPO-Sphäroiden deutlich geringer ausfällt, was die Folge der Zelldissoziation in den letzten drei Tagen der Sphäroidbildung verursachen könnte.

Darüber hinaus wurde das Volumen der Sphäroide mittels Bildverarbeitung und Segmentierung gemessen. Obwohl ein signifikanter Unterschied zwischen der Anzahl der Zellenkerne in den Sphäroiden unter beiden Bedingungen (Expansion und Differenzierung) bestand, konnte kein signifikanter Unterschied bei den Volumina festgestellt werden. Als nächstes wurde die innere Struktur der Sphäroide mit der weiteren IF-Färbung (eng. Immunofluorescence staining) genauer untersucht. Die Analyse zeigt die Bildung mehrerer hohler, azinusähnlicher Kompartimente, was andeutet, dass die hPO-Zellen ihren duktafen Charakter auch als Teil von Sphäroiden beibehalten und dass daher die enzymatische Zerlegung zu Einzelzellen und die dazu folgende Re-Aggregation die Identität der Vorläuferzellen nicht beeinträchtigt. Darüber hinaus zeigt die morphologische Analyse der Sphäroide, dass das Differenzierungsmedium zu einer ausgeprägteren Zellpolarisation führt, die sich durch die basale Umlagerung der Zellkerne und des Aktin Zytoskeletts sowohl in den Organoiden als auch in den Sphäroiden manifestiert.

Die Ergebnisse von EdU-Inkorporationstests und der IF-Färbung gegen den Proliferationsmarker KI67 zeigen, dass die Differenzierungsinduktion eine Verringerung der Zellproliferation sowohl in den Sphäroiden als auch in den Organoiden zur Folge hat.

Um den Prozess der Sphäroidbildung dynamisch und in drei Dimensionen zu visualisieren, wurden longitudinale Bildstapeln mit dem LSM780 aufgenommen. Die time-lapse Daten wurden analysiert, um den Prozess der Sphäroidbildung zu eruieren: die Formierung der Sphäroide aus hPO-Zellen beginnt mit der Annäherung der einzelnen Zellen aneinander und der Bildung kleiner Aggregate, gefolgt von der Zusammenlagerung dieser Aggregate und der Entstehung von kompakten und mehrschichtigen zellulären Strukturen.

Die mit dem LFSM und CLSM erfolgte Untersuchung heterotypischen Sphäroiden aus Kokulturen von hPO-Zellen, Endothelzellen und mesenchymalen Stammzellen. Diese zeigen, dass die Lokalisierung der unterschiedlichen Zelltypen eine ähnliche räumliche Struktur darstellt, wie die aus der Literatur bekannten Kokulturen von dissoziierten Langerhans'schen Insel-Zellen mit Endothelzellen. Das deutet darauf hin, dass die Selbstorganisation der Zellen in den heterotypischen Sphäroiden zu der Gewebearchitektur führt, die mit der des etablierten Langerhans'schen Insel-Modells übereinstimmt.

Zur Identifizierung der Änderungen in der Genexpression, die sich infolge der Zellaggregation und Differenzierung der Sphäroide ereignen, wurde quantitative PCR und IF-Färbung eingesetzt. Die Ergebnisse zeigen eindeutig, dass die Sphäroidbildung in Verbindung mit dem Differenzierungsmedium die Genexpression signifikant beeinträchtigt. Die Expression von Differenzierungsmarkern (NGN3, NKX6.1, und PDX1) und spezifischen β -Zellen-Markern (Insulin, CHGA und CHGB) wird signifikant hochreguliert, wobei eine Herunterregulierung von Transkripten (hSOX9 und hLGR5), die in den Vorläuferzellen vorkommen, festgestellt werden konnte. Die Schlussfolgerung ist, dass die Aggregation die hPO-Zellen dazu zwingt, ihren Vorläuferstatus zu verlassen und sie in Richtung der Differenzierung zu β -Zellen vorantreibt. Darüber hinaus wurde eine signifikante Herunterregulierung von Epithelmarkern (hEPCAM und hKRT19) in Verbindung mit einer Hochregulierung von mesenchymalen Markern (hVIM und hCDH2) in den hPO-Zellen festgestellt, ein Merkmal der epithelial-to-mesenchymal Transition (EMT). Das ist eine interessante Beobachtung, denn die EMT repräsentiert den ersten Schritt zur Formierung der Langerhans'schen Inseln während der Pankreasentwicklung.

Die Ergebnisse dieser Arbeit zeigen in konsistenter Weise, dass die Zusammenlagerung von hPO-Zellen zu Sphäroiden und die daraus resultierende interzellulären Interaktionen in Synergie mit der Kultivierung in Differenzierungsmedium, eine signifikante Hochregulierung von Differenzierungsmarkern und β -Zellmarkern und die Herunterregulierung von Genen, die hauptsächlich in Vorläuferzellen exprimiert sind, induziert. Dieses Verfahren würde zu einer effizienten Differenzierung zur Beta-Zelle führen. Daher wurde ein weiterer Schritt in die Richtung der zellulären Therapie und persönliche Behandlung von Diabetes Typ 1 sein.

8. Supplements

8.1 Supplemental figures

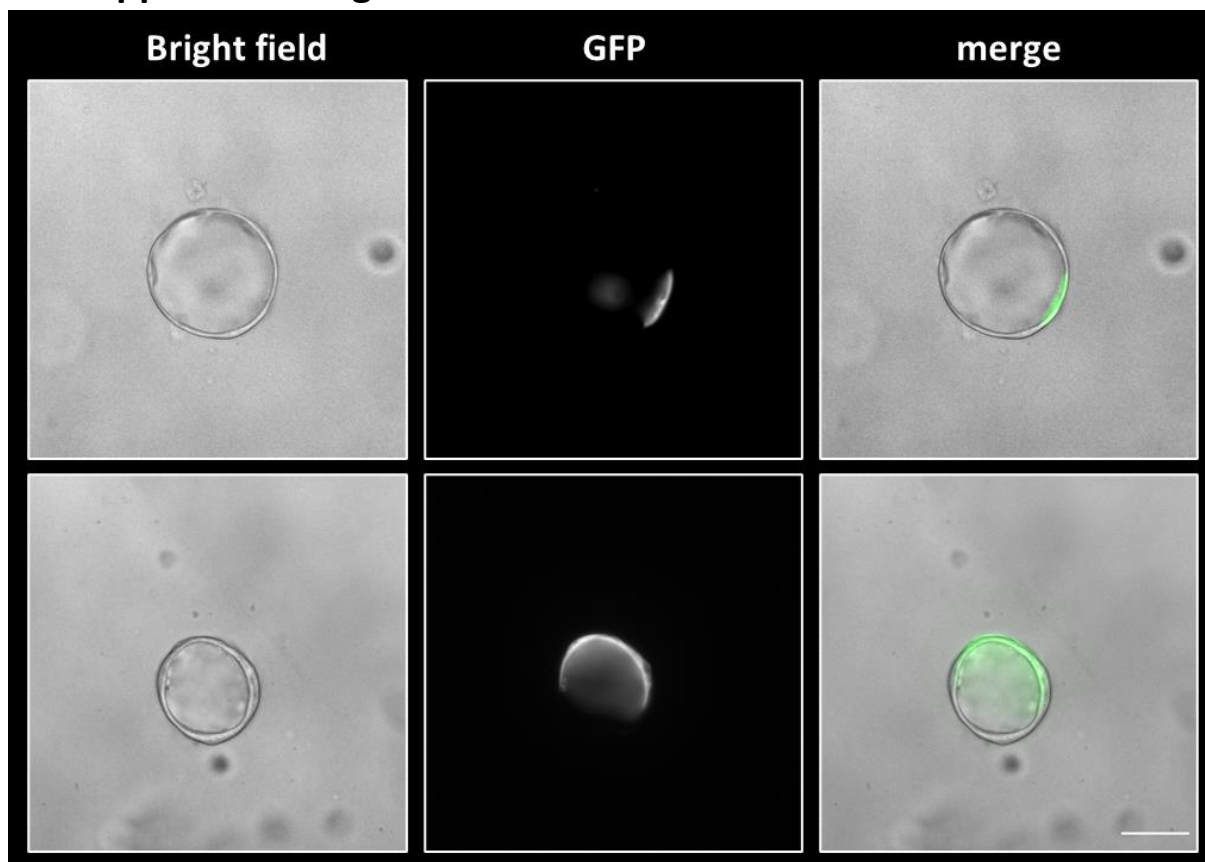


Figure 50: Nucleofection on hPOs under expansion medium after 7 days. Organoids were turned to single cells and after electroporation were cultured under expansion medium for 7 days followed by imaging with brightfield microscope. Transfection was applied with pmaxGFPTM vector by P3 Primary Cell 4D-NucleofectorTM X Kit S (LONZA) on hPO in expansion medium after seven days. Representative images for each condition are shown. The images were processed using Zeiss confocal LSM780 microscope with Zeiss Axiovert 40 CFL microscope with 40x/0.40 ph1 objective lens; Excitation-Emission: 470/40 nm – 525/50 nm (GFP); scale bar:50 μ m.

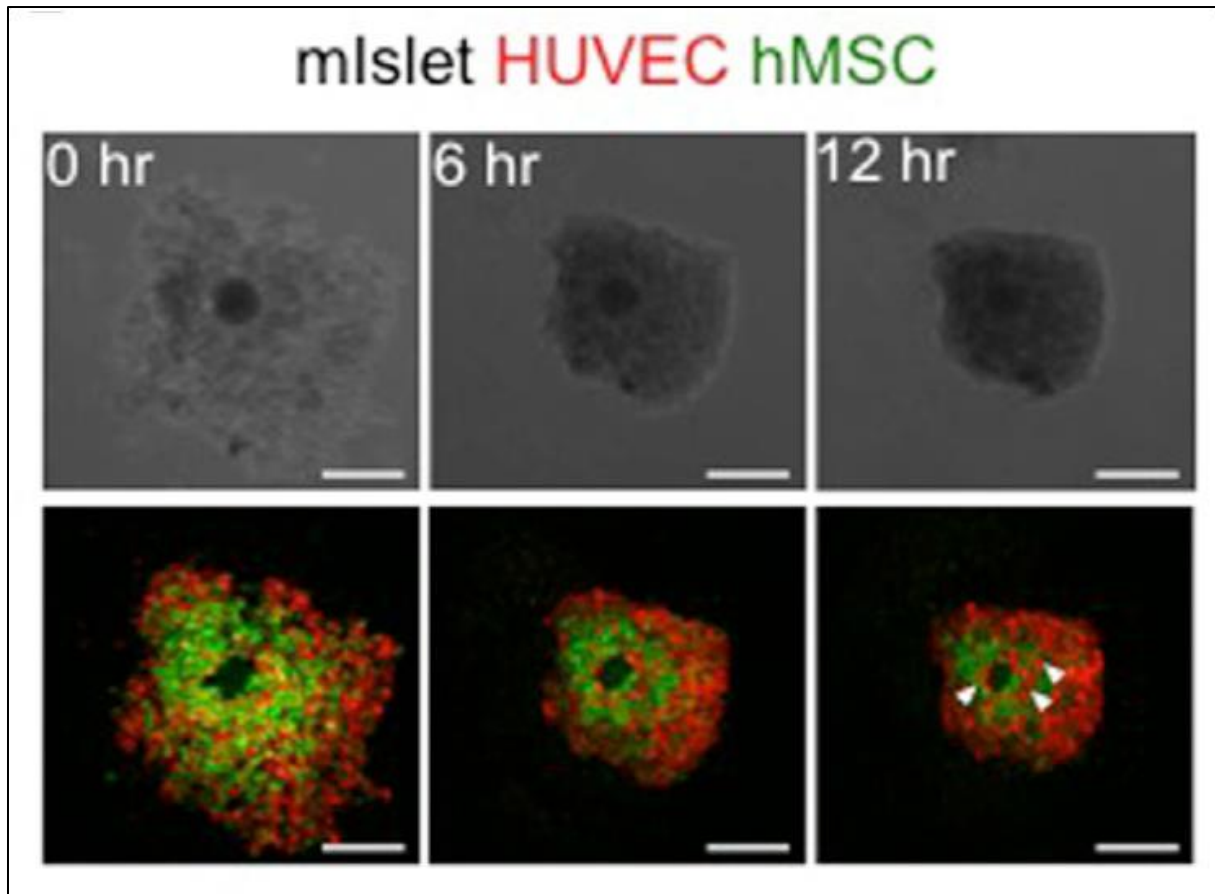


Figure 51: Formation of a three-dimensional mini-sized vascularized mouse islet in co-cultures of islets with HUVECs and human MSCs. The arrowheads indicate the blood vessel-like structures. Scale bars: 250 μ m (Takahashi, Y. et al. (2018))

8.2 Supplemental tables

Table 15: Proportion of counted cells per organoids and spheroids done with 3D object counter plugin for ImageJ.

- hPO organoid in Exp. medium

B1	Total cells	Threshold
1	249	11
2	326	4
3	1397	4
B2	Total cells	Threshold
1	287	30
2	498	26
3	27	50
B3	Total cells	Threshold
1	445	5
2	178	11
3	1647	8
4	651	7
5	1862	6
6	116	80

- hPO organoid in Diff. medium

B1	Total cells	Threshold
1	1098	6
2	97	6
3	164	6

B2	Total cells	Threshold
1	71	31
2	290	25
3	46	30

B3	Total cells	Threshold
1	145	20
2	357	15
3	71	9
4	102	4
5	77	8
6	663	12
7	92	8
8	42	9

- hPO spheroid in Exp. medium

B1	Total cells	Threshold
1	206	70
2	296	50
3	453	50
4	320	60
5	386	60

B2	Total cells	Threshold
1	521	9000
2	349	6000
3	210	12000
4	284	15000

B3	Total cells	Threshold
1	446	12000
2	188	9000
3	399	12000

- hPO spheroid in Diff. medium

B1	Total cells	Threshold
1	387	70
2	409	70
3	542	70
4	439	5
5	456	60
B2	Total cells	Threshold
1	394	13000
2	423	7000
3	400	13000
4	351	15000
B3	Total cells	Threshold
1	380	70
2	355	70
3	335	70
4	351	50

- Triple spheroid in Diff. medium

B1	Total cells	Threshold
1	422	70
2	334	55
3	279	60
4	275	70
5	253	60

B2	Total cells	Threshold
1	503	7000
2	298	8000
3	155	6500
4	347	8000
5	381	13000

B3	Total cells	Threshold
1	370	10000
2	244	9000
3	284	8000
4	329	7500

- Average of all batches

hPO organoid in Exp. medium	Total cells
Average of B1	657,33
Average of B2	270,67
Average of B3	311,83
Total Average	436,13
hPO organoid in Diff. medium	Total cells
Average of B1	453
Average of B2	135,67
Average of B3	51,33
Total Average	195,57
hPO spheroid in Exp. medium	Total cells
Average of B1	332,2
Average of B2	341
Average of B3	344,33
Total Average	339,18
hPO spheroid in Diff. medium	Total cells
Average of B1	446,6
Average of B2	392
Average of B3	355,25
Total Average	397,95
Triple spheroid in Diff. medium	Total cells
Average of B1	312,6
Average of B2	336,8
Average of B3	306,75
Total Average	318,72

- T-test results (p<0.05)

hPO org. vs sph. in Exp. medium	0,06
hPO org. vs sph. in Diff. medium	0,03
hPO org. in Exp. vs Diff. medium	0,02
hPO sph. in Exp. vs Diff. medium	0,04
hPO sph. in Exp. vs Diff. medium	0,04
hPO sph. vs Tripl sph. in Diff. medium	0,00
hPO sph. In Exp. Vs Tripl sph. in Diff. medium	0,12

Table 16: Proportion of spheroid volume in microns³**- hPO spheroid in Exp. medium**

B1	Volume	Threshold
1	4428192,51	3
2	7746200,74	4
3	5984200,06	3
4	6089792,69	3
5	8663918,16	4
B2	Volume	Threshold
1	7021135,86	4
2	6611230,5	6
3	4321353,03	6
4	5452732,97	6
B3	Volume	Threshold
1	4411486,47	5
2	4746118,13	4
3	7473325,86	5

- hPO spheroid in Diff. medium

B1	Volume	Threshold
1	3735080,4	6
2	4219613,0	6
3	6413589,4	3
4	5654486,7	1
5	7518424,4	3
B2	Volume	Threshold
1	6648657,44	6
2	9905022,16	6
3	5780794,93	4
4	5691543,25	4
B3	Volume	Threshold
1	7581303,63	6
2	7595353,28	6
3	3520861,74	5
4	4382537,92	2

- Triple spheroid in Diff. medium

B1	Volume	Threshold
1	6197339,84	3
2	3568746,5	4
3	4979336,11	6
4	4433606,6	6
5	3413482,7	3
B2	Volume	Threshold
1	5062669,21	3
2	3721040,62	4
3	2254519,24	6
4	4478337,96	6
5	5105550,38	3
B3	Volume	Threshold
1	4762916,7	6
2	4488120,82	6
3	4796876,06	5
4	4108879,13	2

- Average of all batches

hPO spheroid in Exp. medium	Volume
Average of B1	6582460,832
Average of B2	5851613,09
Average of B3	5543643,49
Total Average	5992572,47
hPO spheroid in Diff. medium	Volume
Average of B1	5508238,8
Average of B2	7006504,445
Average of B3	5770014,14
Total Average	6094919,13
Triple spheroid in Diff. medium	Volume
Average of B1	4518502,4
Average of B2	4124423,48
Average of B3	4539198,18
Total Average	4394041,34

- T-test results (p<0.05)

hPO sph. in Exp. vs Diff. medium	0,50
hPO sph. vs Tripl sph. in Diff. medium	0,00
hPO sph. In Exp. vs Tripl sph. in Diff. medium	0,00

Table 17: Proportion of proliferated cells per organoids and spheroids.**- hPO organoid in Exp. medium**

B1	# proliferated cells	Total cells	# proliferated cells /total cells*100
1	639	1031	61,98
2	15	125	12
3	38	233	16,31
B2	# proliferated cells	Total cells	# proliferated cells /total cells*100
1	20	534	3,75
2	25	134	18,66
3	60	413	14,53
B3	# proliferated cells	Total cells	# proliferated cells /total cells*100
1	260	1390	18,71
2	648	1666	38,90
3	10	229	4,37
4	42	106	39,62
5	146	1010	14,46
6	75	208	36,06
7	73	373	19,57
8	35	245	14,29
9	162	1199	13,51

- hPO organoid in Diff. medium

B1	# proliferated cells	Total cells	# proliferated cells /total cells*100
1	0	117	0
2	0	245	0
3	34	181	18,78
B2	# proliferated cells	Total cells	# proliferated cells /total cells*100
1	3	342	0,88
2	30	331	9,06
3	20	243	8,23
B3	# proliferated cells	Total cells	# proliferated cells /total cells*100
1	3	350	0,86
2	15	226	6,64
3	10	231	4,33
4	10	153	6,54

- hPO spheroid in Exp. medium

B1	# proliferated cells	Total cells	# proliferated cells /total cells*100
1	134	168	79,76
2	135	158	85,44
3	93	187	49,73
4	78	179	43,58
5	79	136	58,09
B2	# proliferated cells	Total cells	# proliferated cells /total cells*100
1	51	92	55,43
2	77	136	56,62
3	131	370	35,41
4	64	216	29,63
5	112	198	56,57
B3	# proliferated cells	Total cells	# proliferated cells /total cells*100
1	82	152	53,95
2	42	162	25,93
3	98	125	78,4
4	43	135	31,85
5	67	216	31,02

- hPO spheroid in Diff. medium

B1	# proliferated cells	Total cells	# proliferated cells /total cells*100
1	5	168	2,98
2	6	107	5,61
3	3	147	2,04
4	0	148	0,00
5	6	207	2,90
B2	# proliferated cells	Total cells	# proliferated cells /total cells*100
1	3	118	2,54
2	0	149	0,00
3	5	280	1,79
4	4	113	3,54
5	0	142	0,00
B3	# proliferated cells	Total cells	# proliferated cells /total cells*100
1	0	145	0
2	10	286	3,50
3	0	210	0
4	12	292	4,11
5	1	278	0,36

- Triple spheroid in Diff. medium

B1	# proliferated cells	Total cells	# proliferated cells /total cells*100
1	55	422	13,03
2	28	334	8,38
3	22	279	7,89
4	18	275	6,55
5	20	253	7,91
B2	# proliferated cells	Total cells	# proliferated cells /total cells*100
1	8	503	1,59
2	12	298	4,03
3	25	155	16,13
4	54	347	15,56
5	41	381	10,76
B3	# proliferated cells	Total cells	# proliferated cells /total cells*100
1	53	370	14,32
2	37	244	15,16
3	10	284	3,52
4	37	329	11,25

- Average of all batches

hPO organoid in Exp. medium	# proliferated cells /total cells*100
Average of B1	30,10
Average of B2	12,31
Average of B3	22,16
Total Average	21,52
hPO organoid in Diff. medium	# proliferated cells /total cells*100
Average of B1	6,26
Average of B2	6,06
Average of B3	4,59
Total Average	5,64
hPO spheroid in Exp. medium	# proliferated cells /total cells*100
Average of B1	63,32
Average of B2	46,73
Average of B3	44,23
Total Average	51,43
hPO spheroid in Diff. medium	# proliferated cells /total cells*100
Average of B1	2,70
Average of B2	1,57
Average of B3	1,59
Total Average	1,96
Triple spheroid in Diff. medium	# proliferated cells /total cells*100
Average of B1	8,75
Average of B2	9,61
Average of B3	11,06
Total Average	9,81

- T-test results (p<0.05)

hPO org. vs sph. in Exp. medium	0,00
hPO org. vs sph. in Diff. medium	0,02
hPO org. in Exp. vs Diff. medium	0,00
hPO sph. in Exp. vs Diff. medium	0,00
hPO sph. Vs Tripl sph. in Diff. medium	0,00
hPO sph. In Exp. vs Tripl sph. in Diff. medium	0,00
hPO Org. In Diff. vs Tripl sph. in Diff. medium	0,03
hPO org. vs sph. in Exp. medium	0,00
hPO org. vs sph. in Diff. medium	0,02

Table 18: RT-qPCR results of the genes. The Ct values were normalized to the geometric mean of the housekeeping genes (RPL13 and TBP) and hPO organoids in expansion medium based on the $\Delta\Delta C_t$ method.

Gene	Sample	protein of interest			MV (GOI) – MV (Ref. Gene)				
		CT1	CT2	CT3	Geometric mean TBP+RPL13	CT1	CT2	CT3	2 ^{ΔΔCP}
hLGR5	hPO_Org_Exp.	28,27	26,07	29,55	28,36	-0,1	-2,3	1,19	1,00
	hPO_Org_Diff.	29,75	30,67	27,87	27,02	2,73	3,65	0,85	0,14
	hPO_Sph_Exp.	29,56	30,02	29,01	27,56	2,01	2,46	1,46	0,19
	hPO_Sph_Diff.	n/a	35,14	33,17	31,47	n/a	3,67	1,70	0,12
	Triple_Sph_Diff.	32,25	31,02	31,43	28,65	3,59	2,37	2,77	0,10
hSOX9	hPO_Org_Exp.	26,39	26,07	28,15	28,36	-2	-2,3	-0,2	1,00
	hPO_Org_Diff.	27,04	27,04	25,10	27,02	0,02	0,02	-1,9	0,55
	hPO_Sph_Exp.	30,04	29,16	27,67	27,56	2,49	1,61	0,11	0,13
	hPO_Sph_Diff.	37,86	36,53	28,43	31,47	n/a	5,06	-3,0	0,05
	Triple_Sph_Diff.	29,17	27,17	28,01	28,65	0,51	-1,5	-0,7	0,52
hKRT19	hPO_Org_Exp.	22,62	20,94	23,65	28,36	-5,8	-7,4	-4,7	1,00
	hPO_Org_Diff.	20,50	21,66	19,71	27,02	-6,5	-5,4	-7,3	1,35
	hPO_Sph_Exp.	24,69	24,93	24,52	27,56	-2,9	-2,6	-3,0	0,11
	hPO_Sph_Diff.	33,37	35,85	29,06	31,47	n/a	4,38	-2,4	0,01
	Triple_Sph_Diff.	22,79	22,11	22,92	28,65	-5,9	-6,5	-5,7	1,06
hCFTR	hPO_Org_Exp.	27,48	27,21	28,57	28,36	-0,9	-1,2	0,21	1,00
	hPO_Org_Diff.	25,77	26,25	24,74	27,02	-1,3	-0,8	-2,3	1,77
	hPO_Sph_Exp.	25,10	24,53	23,87	27,56	-2,5	-3,0	-3,7	5,43
	hPO_Sph_Diff.	31,70		29,06	31,47	n/a	-31,	-2,4	1,39
	Triple_Sph_Diff.	26,88	26,50	27,36	28,65	-1,8	-2,2	-1,3	2,18
hINS	hPO_Org_Exp.	36,02	36,02	36,66	28,36	7,66	7,65	8,30	1,00
	hPO_Org_Diff.	34,69	34,81	33,44	27,02	7,67	7,79	6,42	1,49
	hPO_Sph_Exp.	33,71	33,72	34,17	27,56	6,15	6,16	6,61	2,94
	hPO_Sph_Diff.	27,24	32,12	34,35	31,47	n/a	0,65	2,89	274,3
	Triple_Sph_Diff.	35,65	35,92	37,20	28,65	6,99	7,26	8,54	1,20
hCHGA	hPO_Org_Exp.	33,78	34,81	35,08	28,36	5,41	6,44	6,72	1,00
	hPO_Org_Diff.	28,65	30,26	28,48	27,02	1,63	3,24	1,46	16,91
	hPO_Sph_Exp.	34,86	35,11	34,19	27,56	7,30	7,55	6,63	0,51
	hPO_Sph_Diff.	36,67	30,64	34,40	31,47	n/a	-0,8	2,93	13,50

	Triple_Sph_Diff.	29,81	32,05	32,54	28,65	1,16	3,39	3,89	10,40
hCHGB	hPO_Org_Exp.	34,89	34,31	34,61	28,36	6,53	5,94	6,24	1,00
	hPO_Org_Diff.	32,76	34,95	31,48	27,02	5,74	7,93	4,46	1,15
	hPO_Sph_Exp.	34,87	34,72	33,01	27,56	7,32	7,17	5,45	0,75
	hPO_Sph_Diff.	34,91	26,67	29,95	31,47	n/a	-4,8	-1,5	146,35
	Triple_Sph_Diff.	33,40	34,32	36,24	28,65	4,74	5,66	7,59	1,18
hCDH2	hPO_Org_Exp.	29,56	28,67	29,43	28,36	1,20	0,31	1,07	1,00
	hPO_Org_Diff.	29,00	29,98	27,19	27,02	1,98	2,96	0,17	0,56
	hPO_Sph_Exp.	26,14	23,01	27,72	27,56	-1,4	-4,5	0,16	6,92
	hPO_Sph_Diff.	29,49	27,57	28,65	31,47	n/a	-3,9	-2,8	13,51
	Triple_Sph_Diff.	29,14	29,59	29,13	28,65	0,48	0,93	0,48	1,17
hVIM	hPO_Org_Exp.	32,42	31,22	31,00	28,36	32,4	31,2	31,00	1,00
	hPO_Org_Diff.	29,16	29,69	27,50	27,02	29,2	29,7	27,50	2,67
	hPO_Sph_Exp.	36,97	32,93	34,98	27,56	21,2	30,0	34,98	4,14
	hPO_Sph_Diff.	33,28	39,55	33,03	31,47	25,0	39,6	33,03	4,36
	Triple_Sph_Diff.	33,10	30,70	31,03	28,65	33,1		31,03	1,17
hNGN3	hPO_Org_Exp.	31,17	31,58	32,26	28,36	2,80	3,21	3,89	1,00
	hPO_Org_Diff.	30,25	31,00	30,42	27,02	3,23	3,98	3,40	0,85
	hPO_Sph_Exp.	31,21	30,83	30,47	27,56	3,66	3,27	2,91	1,02
	hPO_Sph_Diff.	31,83	n/a	27,84	31,47	n/a	-31	-3,63	30,66
	Triple_Sph_Diff.	31,63	31,48	31,74	28,65	2,97	2,82	3,09	1,27
hNKX6.1	hPO_Org_Exp.	33,53	33,91	34,08	28,36	5,16	5,55	5,72	1,00
	hPO_Org_Diff.	32,35	34,21	24,20	27,02	5,33	7,19	-2,82	4,73
	hPO_Sph_Exp.	30,05	30,37	28,92	27,56	2,50	2,82	1,36	9,52
	hPO_Sph_Diff.	31,83	n/a	27,84	31,47	n/a	-31	-3,63	138,27
	Triple_Sph_Diff.	23,47	31,94	34,82	28,65	-5,2	3,29	6,16	16,63
hPDX1	hPO_Org_Exp.	30,50	28,19	32,15	28,36	2,13	-0,2	3,79	1,00
	hPO_Org_Diff.	27,92	29,41	27,24	27,02	0,90	2,39	0,22	1,68
	hPO_Sph_Exp.	29,75	29,09	27,83	27,56	2,19	1,54	0,27	1,49
	hPO_Sph_Diff.	33,58	n/a	32,21	31,47	n/a	-31	0,75	1,40
	Triple_Sph_Diff.	28,73	29,19	29,29	28,65	0,08	0,54	0,64	2,82
hEPCAM	hPO_Org_Exp.	16,94	14,90	14,60	28,36	-11	-13	-13,8	1,00
	hPO_Org_Diff.	11,87	18,26	12,46	27,02	-15	-8,8	-14,6	0,96
	hPO_Sph_Exp.	18,02	12,12	12,74	27,56	-9,5	-15	-14,8	1,30
	hPO_Sph_Diff.	19,13	19,14	18,44	31,47	n/a	-12	-13,0	13,92
	Triple_Sph_Diff.	13,76	14,14	15,50	28,65	-15	-14	-13,2	2,47

- T-test results ($p < 0.05$)

Gene		T-test
hLGR5	hPO org. vs sph. in Exp. medium	0,04
	hPO org. vs sph. in Diff. medium	0,42
	hPO org. in Exp. vs Diff. medium	0,05
	hPO sph. in Exp. vs Diff. medium	0,23
	hPO Triple. vs sph. in Diff. medium	0,41
hSOX9	hPO org. vs sph. in Exp. medium	0,02
	hPO org. vs sph. in Diff. medium	0,32
	hPO org. in Exp. vs Diff. medium	0,20
	hPO sph. in Exp. vs Diff. medium	0,45
	hPO Triple. vs sph. in Diff. medium	0,33
hKRT19	hPO org. vs sph. in Exp. medium	0,01
	hPO org. vs sph. in Diff. medium	0,03
	hPO org. in Exp. vs Diff. medium	0,34
	hPO sph. in Exp. vs Diff. medium	0,11
	hPO Triple. vs sph. in Diff. medium	0,04
hCFTR	hPO org. vs sph. in Exp. medium	0,01
	hPO org. vs sph. in Diff. medium	0,12
	hPO org. in Exp. vs Diff. medium	0,12
	hPO sph. in Exp. vs Diff. medium	0,15
	hPO Triple. vs sph. in Diff. medium	0,13
hINS	hPO org. vs sph. in Exp. medium	0,00
	hPO org. vs sph. in Diff. medium	0,01
	hPO org. in Exp. vs Diff. medium	0,15
	hPO sph. in Exp. vs Diff. medium	0,01
	hPO Triple. vs sph. in Diff. medium	0,01
hCHGA	hPO org. vs sph. in Exp. medium	0,06
	hPO org. vs sph. in Diff. medium	0,02
	hPO org. in Exp. vs Diff. medium	0,00
	hPO sph. in Exp. vs Diff. medium	0,01
	hPO Triple. vs sph. in Diff. medium	0,20
hCHGB	hPO org. vs sph. in Exp. medium	0,27
	hPO org. vs sph. in Diff. medium	0,01
	hPO org. in Exp. vs Diff. medium	0,43
	hPO sph. in Exp. vs Diff. medium	0,00
	hPO Triple. vs sph. in Diff. medium	0,01
hCDH2	hPO org. vs sph. in Exp. medium	0,06
	hPO org. vs sph. in Diff. medium	0,01
	hPO org. in Exp. vs Diff. medium	0,06
	hPO sph. in Exp. vs Diff. medium	0,25
	hPO Triple. vs sph. in Diff. medium	0,00
hVIM	hPO org. vs sph. in Exp. medium	0,01
	hPO org. vs sph. in Diff. medium	0,26
	hPO org. in Exp. vs Diff. medium	0,01

	hPO sph. in Exp. vs Diff. medium	0,27
	hPO Triple. vs sph. in Diff. medium	0,42
hNGN3	hPO org. vs sph. in Exp. medium	0,48
	hPO org. vs sph. in Diff. medium	0,07
	hPO org. in Exp. vs Diff. medium	0,29
	hPO sph. in Exp. vs Diff. medium	0,07
	hPO Triple. vs sph. in Diff. medium	0,07
hNKX6.1	hPO org. vs sph. in Exp. medium	0,00
	hPO org. vs sph. in Diff. medium	0,08
	hPO org. in Exp. vs Diff. medium	0,25
	hPO sph. in Exp. vs Diff. medium	0,08
	hPO Triple. vs sph. in Diff. medium	0,10
hPDX1	hPO org. vs sph. in Exp. medium	0,34
	hPO org. vs sph. in Diff. medium	0,13
	hPO org. in Exp. vs Diff. medium	0,30
	hPO sph. in Exp. vs Diff. medium	0,13
	hPO Triple. vs sph. in Diff. medium	0,14
hEPCAM	hPO org. vs sph. in Exp. medium	0,43
	hPO org. vs sph. in Diff. medium	0,48
	hPO org. in Exp. vs Diff. medium	0,49
	hPO sph. in Exp. vs Diff. medium	0,41
	hPO Triple. vs sph. in Diff. medium	0,07

8.3 Supplemental macro code:

The macro code is shown below to measure the volume of each spheroids: (<https://visikol.com/2018/11/blog-post-loading-and-measurement-of-volumes-in-3d-confocal-image-stacks-with-imagej/>).

```
// ImageJ Macro Code
// Measure Volume of Thresholded Pixels in an Image Stack
//
//

macro "Measure Stack" {
    run("Clear Results"); // First, clear the results table

    // loop through each slice in the stack. Start at n=1 (the
    first slice),
    // keep going while n <= nSlices (nSlices is the total
    number of slices in the stack)
    // and increment n by one after each loop (n++)
    for (n=1; n<=nSlices; n++) {
        setSlice(n); // set the stack's current slice to n
        run("Measure"); // Run the "Measure" function in
ImageJ
    }

    // Create a variable that we will use to store the area
    measured in each slice
    totalArea = 0;
    // Loop through each result from 0 (the first result on
    the table) to nResult (the total number of results on the
    table)
    for (n=0; n < nResults; n++)
    {
        totalArea += getResult("Area",n); // Add the area of
the current result to the total
    }
    // Get the calibration information from ImageJ and store
    into width, height, depth, and unit variables.
    // We will only be using depth and unit
    getVoxelSize(width, height, depth, unit);
    // Calculate the volume by multiplying the sum of area of
    each slice by the depth
    volume = totalArea*depth;
    // Print the result of the volume calculation to the log
    print(volume + " " + unit + "^3");}
```

9. References

I apologize to all researchers whose work could not be cited in this review as a result of space constraints. We apologize to the authors of those primary works that are not cited in this review due to space constraints.

1. H. Hesham A-Kader . Fayez K. Ghishan. The Pancreas_Chapter_198. *Textb Clin Pediatr*. 2012. doi:10.1007/978-3-642-02202-9
2. Shih HP, Wang A, Sander M. Pancreas organogenesis: From lineage determination to morphogenesis. *Annu Rev Cell Dev Biol*. 2013;29:81-105. doi:10.1146/annurev-cellbio-101512-122405
3. Lugea A, Waldron RT, Mareninova OA, et al. Human Pancreatic Acinar Cells: Proteomic Characterization, Physiologic Responses, and Organellar Disorders in ex Vivo Pancreatitis. *Am J Pathol*. 2017;187(12):2726-2743. doi:10.1016/j.ajpath.2017.08.017
4. Geron E, Schejter ED, Shilo BZ. Assessing the secretory capacity of pancreatic acinar cells. *J Vis Exp*. 2014;(90):1-8. doi:10.3791/51799
5. Adam Moser, Kevin Range and DMY. Regulation of Acinar Cell Function in The Pancreas. *Bone*. 2008;23(1):1-7. doi:10.1097/MOG.0b013e32833d11c6.Regulation
6. Grapin-Botton A. Ductal cells of the pancreas. *Int J Biochem Cell Biol*. 2005;37(3):504-510. doi:10.1016/j.biocel.2004.07.010
7. Röder P V., Wu B, Liu Y, Han W. Pancreatic regulation of glucose homeostasis. *Exp Mol Med*. 2016;48(November 2015):e219. doi:10.1038/emm.2016.6
8. Bastidas-Ponce A, Scheibner K, Lickert H, Bakhti M. Cellular and molecular mechanisms coordinating pancreas development. *Dev*. 2017;144(16):2873-2888. doi:10.1242/dev.140756
9. Pénicaud L. Autonomic nervous system and pancreatic islet blood flow. *Biochimie*. 2017;143:29-32. doi:10.1016/j.biochi.2017.10.001
10. El-Gohary Y, Sims-Lucas S, Lath N, et al. Three-Dimensional Analysis of the Islet Vasculature. *Anat Rec*. 2012;295(9):1473-1481. doi:10.1002/ar.22530
11. Jennings RE, Berry AA, Strutt JP, Gerrard DT, Hanley NA. Human pancreas development.

- Dev.* 2015;142(18):3126-3137. doi:10.1242/dev.120063
12. Melenovsky V, Benes J, Franekova J, et al. Glucose homeostasis, pancreatic endocrine function, and outcomes in advanced heart failure. *J Am Heart Assoc.* 2017;6(8):1-11. doi:10.1161/JAHA.116.005290
 13. Thorens B. Contrôle central de l'homéostasie glucidique l'axe cerveau-pancréas endocrine. *Diabetes Metab.* 2010;36(SUPPL. 3):S45-S49. doi:10.1016/S1262-3636(10)70466-3
 14. Paul Langerhans (1847--1888). *South African Med J.* 1970;44(16):461-462.
 15. Da Silva Xavier G. The Cells of the Islets of Langerhans. *J Clin Med.* 2018;7(3):54. doi:10.3390/jcm7030054
 16. Li XY, Zhai WJ, Teng CB. Notch signaling in pancreatic development. *Int J Mol Sci.* 2015;17(1):1-19. doi:10.3390/ijms17010048
 17. Marchetti P, Bugliani M, De Tata VD, Suleiman M, Marselli L. Pancreatic beta cell identity in humans and the role of type 2 diabetes. *Front Cell Dev Biol.* 2017;5(MAY):1-8. doi:10.3389/fcell.2017.00055
 18. Steiner DJ, Kim A, Miller K, Hara M. Pancreatic islet plasticity: Interspecies comparison of islet architecture and composition. 2011;2(3):135-145.
 19. Ionescu-Tirgoviste C, Gagniuc PA, Gubceac E, et al. A 3D map of the islet routes throughout the healthy human pancreas. *Sci Rep.* 2015;5:1-14. doi:10.1038/srep14634
 20. Noguchi GM, Huising MO. Integrating the inputs that shape pancreatic islet hormone release. *Nat Metab.* 2019;1(12):1189-1201. doi:10.1038/s42255-019-0148-2
 21. Ahrén B, Wierup N, Sundler F. Neuropeptides and the regulation of islet function. *Diabetes.* 2006;55(SUPPL. 2). doi:10.2337/db06-S013
 22. Li R, Yu L, Zhang X, Zhou X, Wang M, Zhao H. Distribution of islet hormones in human adult pancreatic ducts. *Digestion.* 2015;91(2):174-179. doi:10.1159/000371796
 23. Jansson L, Barbu A, Bodin B, et al. Pancreatic islet blood flow and its measurement. *Ups J Med Sci.* 2016;121(2):81-95. doi:10.3109/03009734.2016.1164769

24. Huising MO. Tuning to the right signal. *Diabetologia*. 2015;58(6):1146-1148. doi:10.1007/s00125-015-3567-y
25. Narayanan S, Loganathan G, Dhanasekaran M, et al. Intra-islet endothelial cell and β -cell crosstalk: Implication for islet cell transplantation. *World J Transplant*. 2017;7(2):117-128. doi:10.5500/wjt.v7.i2.117
26. Olsson R, Carlsson PO. The pancreatic islet endothelial cell: Emerging roles in islet function and disease. *Int J Biochem Cell Biol*. 2006;38(5-6):710-714. doi:10.1016/j.biocel.2006.02.004
27. Muratore M, Santos C, Rorsman P. The vascular architecture of the pancreatic islets: A homage to August Krogh. *Comp Biochem Physiol -Part A Mol Integr Physiol*. 2021;252(October 2020):110846. doi:10.1016/j.cbpa.2020.110846
28. Cleaver O, Dor Y. Vascular instruction of pancreas development. *Dev*. 2012;139(16):2833-2843. doi:10.1242/dev.065953
29. Ranjan AK, Joglekar M V., Hardikar AA. Endothelial cells in pancreatic islet development and function. *Islets*. 2009;1(1):2-9. doi:10.4161/isl.1.1.9054
30. Nair G, Hebrok M. Islet formation in mice and men: Lessons for the generation of functional insulin-producing β -cells from human pluripotent stem cells. *Curr Opin Genet Dev*. 2015;32:171-180. doi:10.1016/j.gde.2015.03.004
31. Pictet RL, Clark WR, Williams RH, Rutter WJ. An ultrastructural analysis of the developing embryonic pancreas. *Dev Biol*. 1972;29(4):436-467. doi:10.1016/0012-1606(72)90083-8
32. Merino PLH. Developmental biology of the pancreas. *Cell Biochem Biophys*. 2004;40(3 Suppl):127-142. doi:10.1385/cbb:40:3s:127
33. Jeon J, Correa-Medina M, Ricordi C, Edlund H, Diez JA. Endocrine cell clustering during human pancreas development. *J Histochem Cytochem*. 2009;57(9):811-824. doi:10.1369/jhc.2009.953307
34. Bonner-Weir S, Guo L, Li WC, et al. Islet neogenesis: A possible pathway for beta-cell replenishment. *Rev Diabet Stud*. 2012;9(4):407-416. doi:10.1900/RDS.2012.9.407

35. Meredith DM, Borromeo MD, Deering TG, et al. Program Specificity for Ptf1a in Pancreas versus Neural Tube Development Correlates with Distinct Collaborating Cofactors and Chromatin Accessibility. *Mol Cell Biol*. 2013;33(16):3166-3179. doi:10.1128/mcb.00364-13
36. Chen YJ, Finkbeiner SR, Weinblatt D, et al. De Novo Formation of Insulin-Producing “Neo- β Cell Islets” from Intestinal Crypts. *Cell Rep*. 2014;6(6):1046-1058. doi:10.1016/j.celrep.2014.02.013
37. Zhu Y, Liu Q, Zhou Z, Ikeda Y. PDX1, Neurogenin-3, and MAFA: Critical transcription regulators for beta cell development and regeneration. *Stem Cell Res Ther*. 2017;8(1):1-7. doi:10.1186/s13287-017-0694-z
38. Russ HA, Parent A V, Ringler JJ, et al. Controlled induction of human pancreatic progenitors produces functional beta-like cells in vitro . *EMBO J*. 2015;34(13):1759-1772. doi:10.15252/embj.201591058
39. Fowden AL, Gardner DS, Ousey JC, Giussani DA, Forhead AJ. Maturation of pancreatic β -cell function in the fetal horse during late gestation. *J Endocrinol*. 2005;186(3):467-473. doi:10.1677/joe.1.06176
40. Ruijtenberg S, van den Heuvel S. Coordinating cell proliferation and differentiation: Antagonism between cell cycle regulators and cell type-specific gene expression. *Cell Cycle*. 2016;15(2):196-212. doi:10.1080/15384101.2015.1120925
41. Klieser E, Swierczynski S, Mayr C, et al. Differential role of Hedgehog signaling in human pancreatic (patho-) physiology: An up to date review. *World J Gastrointest Pathophysiol*. 2016;7(2):199. doi:10.4291/wjgp.v7.i2.199
42. Murtaugh LC. Pancreas and beta-cell development: From the actual to the possible. *Development*. 2007;134(3):427-438. doi:10.1242/dev.02770
43. Meier JJ, Köhler CU, Alkhatib B, et al. B-Cell Development and Turnover During Prenatal Life in Humans. *Eur J Endocrinol*. 2010;162(3):559-568. doi:10.1530/EJE-09-1053
44. German MS. Anonymous sources: Where do adult β cells come from? *J Clin Invest*. 2013;123(5):1936-1938. doi:10.1172/JCI69297

45. Prasad K, Shiota C, Xiangwei X, Ricks D, Fusco J, Gittes G. A synopsis of factors regulating beta cell development and beta cell mass. *Cell Mol Life Sci.* 2016;73(19):3623-3637. doi:10.1007/s00018-016-2231-0
46. Jennings RE, Berry AA, Kirkwood-Wilson R, et al. Development of the human pancreas from foregut to endocrine commitment. *Diabetes.* 2013;62(10):3514-3522. doi:10.2337/db12-1479
47. L. Charles Murtaugh. development of β cells.pdf.
48. Basile G, Kulkarni RN, Morgan NG. How, When, and Where Do Human β -Cells Regenerate? *Curr Diab Rep.* 2019;19(8). doi:10.1007/s11892-019-1176-8
49. Villasenor A, Cleaver O. Crosstalk between the developing pancreas and its blood vessels: An evolving dialog. *Semin Cell Dev Biol.* 2012;23(6):685-692. doi:10.1016/j.semcd.2012.06.003
50. Schaer M. Pancreatic disorders. *Clin Med Dog Cat Third Ed.* 2016;64(3):361-385. doi:10.5005/jp/books/12977_21
51. Neblett WW, O'Neill JA. Surgical management of recurrent pancreatitis in children with pancreas divisum. *Ann Surg.* 2000;231(6):899-908. doi:10.1097/0000658-200006000-00015
52. Cox KL, Cannon RA, Ament ME, Phillips HE, Schaffer CB. Biochemical and ultrasonic abnormalities of the pancreas in anorexia nervosa. *Dig Dis Sci.* 1983;28(3):225-229. doi:10.1007/BF01295117
53. Forsmark C, Pham A. Chronic pancreatitis: Review and update of etiology, risk factors, and management [version 1; referees: 2 approved]. *F1000Research.* 2018;7(May):1-11. doi:10.12688/f1000research.12852.1
54. Uc A, Andersen DK, Bellin MD, et al. Chronic Pancreatitis in the 21st Century - Research Challenges and Opportunities. *Pancreas.* 2016;45(10):1365-1375. doi:10.1097/MPA.0000000000000713
55. Lauri Burroughs, M.D.1,2, Ann Woolfrey, M.D.1,2, and Akiko Shimamura, M.D. PD. Shwachman Diamond Syndrome. *Bone.* 2008;23(1):1-7.

- doi:10.1016/j.hoc.2009.01.007.Shwachman
56. Hurst JA, Baraitser M. Johanson-Blizzard syndrome. 1989;(June 1988):45-48.
 57. Kharroubi AT. Diabetes mellitus: The epidemic of the century. *World J Diabetes*. 2015;6(6):850. doi:10.4239/wjd.v6.i6.850
 58. Varni JW, Delamater AM, Hood KK, et al. Diabetes management mediating effects between diabetes symptoms and health-related quality of life in adolescents and young adults with type 1 diabetes. *Pediatr Diabetes*. 2018;19(7):1322-1330. doi:10.1111/pedi.12713
 59. Diabetes DOF. Diagnosis and classification of diabetes mellitus. *Diabetes Care*. 2010;33(SUPPL. 1). doi:10.2337/dc10-S062
 60. Chiarelli F, Giannini C, Primavera M. Prediction and prevention of type 1 diabetes in children. *Clin Pediatr Endocrinol*. 2019;28(3):43-57. doi:10.1297/cpe.28.43
 61. Dreyer M. Type 1 diabetes. *Diabetologe*. 2019;15(5):400-407. doi:10.1007/s11428-019-0482-8
 62. Wong MS, Hawthorne WJ, Manolios N. Gene therapy in diabetes. *Self/Nonself - Immune Recognit Signal*. 2010;1(3):165-175. doi:10.4161/self.1.3.12643
 63. Kawasaki E. Type 1 diabetes and autoimmunity. *Clin Pediatr Endocrinol*. 2014;23(4):99-105. doi:10.1297/cpe.23.99
 64. Chiang JL, Maahs DM, Garvey KC, et al. Type 1 diabetes in children and adolescents: A position statement by the American Diabetes Association. *Diabetes Care*. 2018;41(9):2026-2044. doi:10.2337/dci18-0023
 65. Adrian Vella. What is type 2 diabetes? *Bone*. 2008;23(1):1-7. doi:10.1016/j.mpm.2010.08.008.What
 66. Pfeiffer AFH, Klein HH. Therapie des diabetes mellitus typ 2. *Dtsch Arztebl Int*. 2014;111(5):69-82. doi:10.3238/arztebl.2014.0069
 67. Sowers JR, Frohlich ED. Insulin and insulin resistance: *Med Clin North Am*. 2004;88(1):63-82. doi:10.1016/s0025-7125(03)00128-7

68. Alfadhli EM. Gestational diabetes mellitus. *Saudi Med J*. 2015;36(4):399-406. doi:10.15537/smj.2015.4.10307
69. Yessoufou A, Moutairou K. Maternal diabetes in pregnancy: Early and long-term outcomes on the offspring and the concept of “metabolic memory.” *Exp Diabetes Res*. 2011;2011. doi:10.1155/2011/218598
70. Thomas A. Buchanan, Anny H. Xiang and KAP. Gestational Diabetes Mellitus: Risks and Management during and after Pregnancy. 1985;8(11):353-357. doi:10.1038/nrendo.2012.96.Gestational
71. Jiang F-X, Morahan G. Multipotent pancreas progenitors: Inconclusive but pivotal topic. *World J Stem Cells*. 2015;7(11):1251-12561. doi:10.4252/wjsc.v7.i11.1251
72. Soiza RL, Donaldson AIC, Myint PK. Diabetes: the place of new therapies. *Ther Adv Vaccines*. 2018;9(6):259-261. doi:10.1177/https
73. Otto-Buczowska E, Jainta N. Pharmacological treatment in diabetes mellitus type 1 - insulin and what else? *Int J Endocrinol Metab*. 2018;16(1):1-7. doi:10.5812/ijem.13008
74. Colberg SR, Sigal RJ, Fernhall B, et al. Exercise and type 2 diabetes: The American College of Sports Medicine and the American Diabetes Association: Joint position statement. *Diabetes Care*. 2010;33(12). doi:10.2337/dc10-9990
75. Piciocchi M, Capurso G, Archibugi L, Delle Fave MM, Capasso M, Delle Fave G. Exocrine pancreatic insufficiency in diabetic patients: Prevalence, mechanisms, and treatment. *Int J Endocrinol*. 2015;2015. doi:10.1155/2015/595649
76. Ziegler AG, Danne T, Dunger DB, et al. Primary prevention of beta-cell autoimmunity and type 1 diabetes - The Global Platform for the Prevention of Autoimmune Diabetes (GPPAD) perspectives. *Mol Metab*. 2016;5(4):255-262. doi:10.1016/j.molmet.2016.02.003
77. Kroger CJ, Clark M, Ke Q, Tisch RM. Therapies to suppress β cell autoimmunity in type 1 diabetes. *Front Immunol*. 2018;9(AUG). doi:10.3389/fimmu.2018.01891
78. Philippe A. Halban,¹ Steven E. Kahn,² Åke Lernmark³ and Christopher J. Rhodes⁴. Gene and Cell-Replacement Therapy in the Treatment of Type 1 Diabetes. *J Natl Med Assoc*.

- 1962;54:476-478.
79. Meloche RM. Transplantation for the treatment of type 1 diabetes. *World J Gastroenterol*. 2007;13(47):6347-6355. doi:10.3748/wjg.v13.i47.6347
 80. Nair GG, Liu JS, Russ HA, et al. Recapitulating endocrine cell clustering in culture promotes maturation of human stem-cell-derived β cells. *Nat Cell Biol*. 2019;21(2):263-274. doi:10.1038/s41556-018-0271-4
 81. Mittal S, Gough SCL. Pancreas transplantation: A treatment option for people with diabetes. *Diabet Med*. 2014;31(5):512-521. doi:10.1111/dme.12373
 82. Wang HS, Shyu JF, Shen WS, et al. Transplantation of insulin-producing cells derived from umbilical cord stromal mesenchymal stem cells to treat NOD mice. *Cell Transplant*. 2011;20(3):455-466. doi:10.3727/096368910X522270
 83. Robertson RP, Davis C, Larsen J, Stratta R, Sutherland DER. Pancreas transplantation for patients with type 1 diabetes. *Diabetes Care*. 2003;26(SUPPL. 1):2003. doi:10.2337/diacare.26.2007.s120
 84. Loomans CJM, Williams Giuliani N, Balak J, et al. Expansion of Adult Human Pancreatic Tissue Yields Organoids Harboring Progenitor Cells with Endocrine Differentiation Potential. *Stem Cell Reports*. 2018;10(3):1088-1101. doi:10.1016/j.stemcr.2018.02.005
 85. Wu J, Yan LJ. Streptozotocin-induced type 1 diabetes in rodents as a model for studying mitochondrial mechanisms of diabetic β cell glucotoxicity. *Diabetes, Metab Syndr Obes Targets Ther*. 2015;8:181-188. doi:10.2147/DMSO.S82272
 86. Sackett SD, Tremmel DM, Ma F, et al. Extracellular matrix scaffold and hydrogel derived from decellularized and delipidized human pancreas. *Sci Rep*. 2018;8(1):1-16. doi:10.1038/s41598-018-28857-1
 87. Pagliuca FW, Melton DA. How to make a functional β -cell. *Dev*. 2013;140(12):2472-2483. doi:10.1242/dev.093187
 88. Loomans CJM, Williams Giuliani N, Balak J, et al. Expansion of Adult Human Pancreatic Tissue Yields Organoids Harboring Progenitor Cells with Endocrine Differentiation Potential. *Stem Cell Reports*. 2018;10(3):712-724. doi:10.1016/j.stemcr.2018.02.005

89. Vlahos AE, Kinney SM, Kingston BR, et al. Endothelialized collagen based pseudo-islets enables tuneable subcutaneous diabetes therapy. *Biomaterials*. 2020;232(December 2019):119710. doi:10.1016/j.biomaterials.2019.119710
90. Akinci E, Banga A, Tungatt K, et al. Reprogramming of various cell types to a beta-like state by Pdx1, Ngn3 and MafA. *PLoS One*. 2013;8(11):1-11. doi:10.1371/journal.pone.0082424
91. Teo AKK, Tsuneyoshi N, Hoon S, et al. PDX1 binds and represses hepatic genes to ensure robust pancreatic commitment in differentiating human embryonic stem cells. *Stem Cell Reports*. 2015;4(4):578-590. doi:10.1016/j.stemcr.2015.02.015
92. Xu H, Tsang KS, Chan JCN, et al. The combined expression of Pdx1 and MafA with either Ngn3 or NeuroD improves the differentiation efficiency of mouse embryonic stem cells into insulin-producing cells. *Cell Transplant*. 2013;22(1):147-158. doi:10.3727/096368912X653057
93. Talchai C, Xuan S, Kitamura T, DePinho RA, Accili D. Generation of functional insulin-producing cells in the gut by Foxo1 ablation. *Nat Genet*. 2012;44(4):406-412. doi:10.1038/ng.2215
94. Christoph Otto. Antidiabetic Effects of a Tripeptide That Decreases Abundance of Na⁺-D-glucose Cotransporter SGLT1 in the Brush-Border Membrane of the Small Intestine. 2020.
95. Akinci E, Banga A, Greder L V., Dutton JR, Slack JMW. Reprogramming of pancreatic exocrine cells towards a beta (β) cell character using Pdx1, Ngn3 and MafA. *Biochem J*. 2012;442(3):539-550. doi:10.1042/BJ20111678
96. Klein D, Álvarez-Cubela S, Lanzoni G, et al. BMP-7 induces adult human pancreatic exocrine-to-endocrine conversion. *Diabetes*. 2015;64(12):4123-4134. doi:10.2337/db15-0688
97. Chang R, Qin H, Liang Z, et al. An improved method for the isolation and culture of rat pancreatic ductal epithelial cells. *Ann Transl Med*. 2020;8(6):320-320. doi:10.21037/atm.2020.03.75
98. Valdez IA, Dirice E, Gupta MK, Shirakawa J, Teo AKK, Kulkarni RN. Proinflammatory

- Cytokines Induce Endocrine Differentiation in Pancreatic Ductal Cells via STAT3-Dependent NGN3 Activation. *Cell Rep.* 2016;15(3):460-470. doi:10.1016/j.celrep.2016.03.036
99. Anastasi E, Santangelo C, Bulotta A, et al. The acquisition of an insulin-secreting phenotype by HGF-treated rat pancreatic ductal cells (ARIP) is associated with the development of susceptibility to cytokine-induced apoptosis. *J Mol Endocrinol.* 2005;34(2):367-376. doi:10.1677/jme.1.01595
 100. Collombat P, Xu X, Ravassard P, et al. The Ectopic Expression of Pax4 in the Mouse Pancreas Converts Progenitor Cells into α and Subsequently β Cells. *Cell.* 2009;138(3):449-462. doi:10.1016/j.cell.2009.05.035
 101. Gage BK, Baker RK, Kieffer TJ. Overexpression of PAX4 reduces glucagon expression in differentiating hESCs. *Islets.* 2014;6(2):e29236-1-e29236-9. doi:10.4161/isl.29236
 102. Jin Li TC. Artemisinin Target GABA A Receptor Signaling and Impair α Cell Identity.pdf.
 103. Jiang YY, Shui JC, Zhang BX, Chin JW, Yue RS. The Potential Roles of Artemisinin and Its Derivatives in the Treatment of Type 2 Diabetes Mellitus. *Front Pharmacol.* 2020;11(November). doi:10.3389/fphar.2020.585487
 104. Nasteska D, Fine NHF, Ashford FB, et al. PDX1LOW MAFALOW β -cells contribute to islet function and insulin release. *Nat Commun.* 2021;12(1). doi:10.1038/s41467-020-20632-z
 105. Matsuoka TA, Kawashima S, Miyatsuka T, et al. Mafa enables Pdx1 to effectively convert pancreatic islet progenitors and committed islet α -cells into β -cells in vivo. *Diabetes.* 2017;66(5):1293-1300. doi:10.2337/db16-0887
 106. Xiao X, Guo P, Shiota C, et al. Endogenous Reprogramming of Alpha Cells into Beta Cells, Induced by Viral Gene Therapy, Reverses Autoimmune Diabetes. *Cell Stem Cell.* 2018;22(1):78-90.e4. doi:10.1016/j.stem.2017.11.020
 107. Jensen C, Teng Y. Is It Time to Start Transitioning From 2D to 3D Cell Culture? *Front Mol Biosci.* 2020;7(March):1-15. doi:10.3389/fmolb.2020.00033
 108. Edmondson R, Broglie JJ, Adcock AF, Yang L. Three-dimensional cell culture systems and

- their applications in drug discovery and cell-based biosensors. *Assay Drug Dev Technol.* 2014;12(4):207-218. doi:10.1089/adt.2014.573
109. Pampaloni F, Reynaud EG, Stelzer EHK. The third dimension bridges the gap between cell culture and live tissue. *Nat Rev Mol Cell Biol.* 2007;8(10):839-845. doi:10.1038/nrm2236
110. Hsiao AY, Tung YC, Qu X, Patel LR, Pienta KJ, Takayama S. 384 hanging drop arrays give excellent Z-factors and allow versatile formation of co-culture spheroids. *Biotechnol Bioeng.* 2012;109(5):1293-1304. doi:10.1002/bit.24399
111. Aihara E, Mahe MM, Schumacher MA, et al. Characterization of stem/progenitor cell cycle using murine circumvallate papilla taste bud organoid. *Sci Rep.* 2015;5(April):1-15. doi:10.1038/srep17185
112. Chaicharoenaudomrung N, Kunhorm P, Noisa P. Three-dimensional cell culture systems as an in vitro platform for cancer and stem cell modeling. *World J Stem Cells.* 2019;11(12):1065-1083. doi:10.4252/wjsc.v11.i12.1065
113. Chen CS. 3D Biomimetic Cultures: The Next Platform for Cell Biology. *Trends Cell Biol.* 2016;26(11):798-800. doi:10.1016/j.tcb.2016.08.008
114. Kapałczyńska M, Kolenda T, Przybyła W, et al. 2D and 3D cell cultures – a comparison of different types of cancer cell cultures. *Arch Med Sci.* 2018;14(4):910-919. doi:10.5114/aoms.2016.63743
115. Langhans SA. Three-dimensional in vitro cell culture models in drug discovery and drug repositioning. *Front Pharmacol.* 2018;9(JAN):1-14. doi:10.3389/fphar.2018.00006
116. Białkowska K, Komorowski P, Bryszewska M, Miłowska K. Spheroids as a type of three-dimensional cell cultures—examples of methods of preparation and the most important application. *Int J Mol Sci.* 2020;21(17):1-17. doi:10.3390/ijms21176225
117. Costa EC, de Melo-Diogo D, Moreira AF, Carvalho MP, Correia IJ. Spheroids Formation on Non-Adhesive Surfaces by Liquid Overlay Technique: Considerations and Practical Approaches. *Biotechnol J.* 2018;13(1):1-12. doi:10.1002/biot.201700417
118. Knight E, Przyborski S. Advances in 3D cell culture technologies enabling tissue-like

- structures to be created in vitro. *J Anat.* 2015;227(6):746-756. doi:10.1111/joa.12257
119. Baker BM, Chen CS. Deconstructing the third dimension-how 3D culture microenvironments alter cellular cues. *J Cell Sci.* 2012;125(13):3015-3024. doi:10.1242/jcs.079509
120. Fennema E, Rivron N, Rouwkema J, van Blitterswijk C, De Boer J. Spheroid culture as a tool for creating 3D complex tissues. *Trends Biotechnol.* 2013;31(2):108-115. doi:10.1016/j.tibtech.2012.12.003
121. Grapin-Botton A. Three-dimensional pancreas organogenesis models. *Diabetes, Obes Metab.* 2016;18(Suppl 1):33-40. doi:10.1111/dom.12720
122. Huch M, Koo BK. Modeling mouse and human development using organoid cultures. *Dev.* 2015;142(18):3113-3125. doi:10.1242/dev.118570
123. Anton D, Burckel H, Josset E, Noel G. Three-dimensional cell culture: A breakthrough in vivo. *Int J Mol Sci.* 2015;16(3):5517-5527. doi:10.3390/ijms16035517
124. Richards et al. Comprehensive analysis of signal transduction in three-dimensional ECM-based tumor cell cultures. *Physiol Behav.* 2018;176(5):139-148. doi:10.14440/jbm.2015.96.Comprehensive
125. Vinci M, Gowan S, Boxall F, et al. Advances in establishment and analysis of three-dimensional tumor spheroid-based functional assays for target validation and drug evaluation Advances in establishment and analysis of three-dimensional tumor spheroid-based functional assays for target va. 2012;29(March).
126. Cuddihy M. 3D spheroid models enter screening toolbox: Evaluating anticancer drugs and building tissue and tumor co-culture models among uses. *Genet Eng Biotechnol News.* 2012;32(16):24-25. doi:10.1089/gen.32.16.09
127. Cui X, Hartanto Y, Zhang H. Advances in multicellular spheroids formation. *J R Soc Interface.* 2017;14(127). doi:10.1098/rsif.2016.0877
128. Zanoni M, Piccinini F, Arienti C, et al. 3D tumor spheroid models for in vitro therapeutic screening: A systematic approach to enhance the biological relevance of data obtained. *Sci Rep.* 2016;6(November 2015):1-11. doi:10.1038/srep19103

129. Picollet-D'hahan N, Dolega ME, Freida D, Martin DK, Gidrol X. Deciphering Cell Intrinsic Properties: A Key Issue for Robust Organoid Production. *Trends Biotechnol.* 2017;35(11):1035-1048. doi:10.1016/j.tibtech.2017.08.003
130. Fang Y, Eglen RM. Three-Dimensional Cell Cultures in Drug Discovery and Development. *SLAS Discov.* 2017;22(5):456-472. doi:10.1177/1087057117696795
131. Zanoni M, Cortesi M, Zamagni A, Arienti C, Pignatta S, Tesi A. Modeling neoplastic disease with spheroids and organoids. *J Hematol Oncol.* 2020;13(1):1-15. doi:10.1186/s13045-020-00931-0
132. Pastuła A, Middelhoff M, Brandtner A, et al. Three-Dimensional Gastrointestinal Organoid Culture in Combination with Nerves or Fibroblasts: A Method to Characterize the Gastrointestinal Stem Cell Niche. *Stem Cells Int.* 2016;2016. doi:10.1155/2016/3710836
133. Lelièvre SA, Kwok T, Chittiboyina S. Architecture in 3D cell culture: An essential feature for in vitro toxicology. *Toxicol Vitro.* 2017;45(Pt 3):287-295. doi:10.1016/j.tiv.2017.03.012
134. Jaganathan H, Gage J, Leonard F, et al. Three-dimensional in vitro co-culture model of breast tumor using magnetic levitation. *Sci Rep.* 2014;4:1-9. doi:10.1038/srep06468
135. Kim MJ, Chi BH, Yoo JJ, Ju YM, Whang YM, Chang IH. Structure establishment of three-dimensional (3D) cell culture printing model for bladder cancer. *PLoS One.* 2019;14(10):1-15. doi:10.1371/journal.pone.0223689
136. Torres AL, Bidarra SJ, Pinto MT, Aguiar PC, Silva EA, Barrias CC. Guiding morphogenesis in cell-instructive microgels for therapeutic angiogenesis. *Biomaterials.* 2018;154:34-47. doi:10.1016/j.biomaterials.2017.10.051
137. Richbourg NR, Peppas NA, Sikavitsas VI. Tuning the biomimetic behavior of scaffolds for regenerative medicine through surface modifications. *J Tissue Eng Regen Med.* 2019;13(8):1275-1293. doi:10.1002/term.2859
138. Kang YB, Rawat S, Cirillo J, Bouchard M, Noh H. Layered long-term co-culture of hepatocytes and endothelial cells on a transwell membrane: Toward engineering the liver sinusoid. *Biofabrication.* 2013;5(4). doi:10.1088/1758-5082/5/4/045008

139. Greggio C, De Franceschi F, Figueiredo-Larsen M, et al. Artificial three-dimensional niches deconstruct pancreas development in vitro. *Dev.* 2013;140(21):4452-4462. doi:10.1242/dev.096628
140. Genee Y Lee, Paraic A Kenny, Eva H Lee and MJB. Three-dimensional culture models of normal and malignant breast epithelial cells. *Bone.* 2008;23(1):1-7. doi:10.1038/nmeth1015.Three-dimensional
141. Sara I. Montanez-Sauri^{1, 3, 4}, David J. Beebe^{2, 3, 4}, and Kyung Eun Sung^{2, 3, 4}. Responsiveness to basement membrane extract as a possible trait for tumorigenicity characterization. *Vaccine X.* 2019;1:1-8. doi:10.1016/j.jvacx.2019.100004
142. Ware MJ, Colbert K, Keshishian V, et al. Generation of Homogenous Three-Dimensional Pancreatic Cancer Cell Spheroids Using an Improved Hanging Drop Technique. *Tissue Eng Part C Methods.* 2016;22(4):312-321. doi:10.1089/ten.tec.2015.0280
143. Carlsson J, Yuhas JM. Liquid-overlay culture of cellular spheroids. *Recent Results Cancer Res.* 1984;95(Foa 4):1-23. doi:10.1007/978-3-642-82340-4_1
144. Metzger W, Sossong D, Bächle A, et al. The liquid overlay technique is the key to formation of co-culture spheroids consisting of primary osteoblasts, fibroblasts and endothelial cells. *Cytotherapy.* 2011;13(8):1000-1012. doi:10.3109/14653249.2011.583233
145. Costa EC, Gaspar VM, Coutinho P, Correia IJ. Optimization of liquid overlay technique to formulate heterogenic 3D co-cultures models. *Biotechnol Bioeng.* 2014;111(8):1672-1685. doi:10.1002/bit.25210
146. Jaganathan H, Gage J, Leonard F, et al. Three-dimensional in vitro co-culture model of breast tumor using magnetic levitation. *Sci Rep.* 2014;4:1-9. doi:10.1038/srep06468
147. Schwank G, Andersson-Rolf A, Koo BK, Sasaki N, Clevers H. Generation of BAC Transgenic Epithelial Organoids. *PLoS One.* 2013;8(10):6-11. doi:10.1371/journal.pone.0076871
148. Dekkers JF, Alieva M, Wellens LM, et al. High-resolution 3D imaging of fixed and cleared organoids. *Nat Protoc.* 2019;14(6):1756-1771. doi:10.1038/s41596-019-0160-8

149. Mikhail AS, Eetezadi S, Allen C. Multicellular Tumor Spheroids for Evaluation of Cytotoxicity and Tumor Growth Inhibitory Effects of Nanomedicines In Vitro: A Comparison of Docetaxel-Loaded Block Copolymer Micelles and Taxotere®. *PLoS One*. 2013;8(4). doi:10.1371/journal.pone.0062630
150. Nath S, Devi GR. Three-dimensional culture systems in cancer research: Focus on tumor spheroid model. *Pharmacol Ther*. 2016;163:94-108. doi:10.1016/j.pharmthera.2016.03.013
151. Ong LJY, Zhu L, Tan GJS, Toh YC. Quantitative image-based cell viability (QuantICV) assay for microfluidic 3D tissue culture applications. *Micromachines*. 2020;11(7). doi:10.3390/mi11070669
152. Takahashi Y, Sekine K, Kin T, Takebe T, Taniguchi H. Self-Condensation Culture Enables Vascularization of Tissue Fragments for Efficient Therapeutic Transplantation. *Cell Rep*. 2018;23(6):1620-1629. doi:10.1016/j.celrep.2018.03.123
153. Kevin Range and DMYAM. *Microfluidic Techniques for Development of 3D Vascularized Tissue*. Vol 23.; 2012. doi:10.1038/jid.2014.371
154. Li XY, Zhai WJ, Teng CB. Notch signaling in pancreatic development. *Int J Mol Sci*. 2015;17(1):1-19. doi:10.3390/ijms17010048
155. Bordanaba-Florit G, Madarieta I, Olalde B, Falcón-Pérez JM, Royo F. 3D cell cultures as prospective models to study extracellular vesicles in cancer. *Cancers (Basel)*. 2021;13(2):1-17. doi:10.3390/cancers13020307
156. Booi TH, Price LS, Danen EHJ. 3D Cell-Based Assays for Drug Screens: Challenges in Imaging, Image Analysis, and High-Content Analysis. *SLAS Discov*. 2019;24(6):615-627. doi:10.1177/2472555219830087
157. Breiding MJ. Microscale screening systems for 3D cellular microenvironments: platforms, advances, and challenges. *Physiol Behav*. 2014;63(8):1-18. doi:10.1007/s00018-014-1738-5.Microscale
158. Baker LA, Tiriack H, Clevers H, Tuveson DA. Modeling Pancreatic Cancer with Organoids. *Trends in Cancer*. 2016;2(4):176-190. doi:10.1016/j.trecan.2016.03.004

159. Mark W. Tibbitt¹ and Kristi S. Anseth^{1, 2}. Hydrogels as Extracellular Matrix Mimics for 3D Cell Culture. *Bone*. 2008;23(1):1-7. doi:10.1002/bit.22361.Hydrogels
160. Duval K, Grover H, Han LH, et al. Modeling physiological events in 2D vs. 3D cell culture. *Physiology*. 2017;32(4):266-277. doi:10.1152/physiol.00036.2016
161. Wörsdörfer P, Dalda N, Kern A, et al. Generation of complex human organoid models including vascular networks by incorporation of mesodermal progenitor cells. *Sci Rep*. 2019;9(1):1-13. doi:10.1038/s41598-019-52204-7
162. Sano E, Mori C, Nashimoto Y, Yokokawa R, Kotera H, Torisawa YS. Engineering of vascularized 3D cell constructs to model cellular interactions through a vascular network. *Biomicrofluidics*. 2018;12(4):1-9. doi:10.1063/1.5027183
163. Tomasina C, Bodet T, Mota C, Moroni L, Camarero-espinoza S. Bioprinting Vasculature: Materials, Cells and Emergent Techniques. 2019.
164. Jessie S. Jeona,¹ Simone Bersinib,^{c,1}, Jordan A. Whislera, Michelle B. Chena, Gabriele Dubinid, Joseph L. Charest, Matteo Morettic,², and Roger D. Kamma,^{f 2}. Generation of 3D functional microvascular networks with mural cell-differentiated human mesenchymal stem cells in microfluidic vasculogenesis systems. *Bone*. 2008;23(1):1-7. doi:10.1039/b000000x/Jeon
165. Dongeun Huh¹, Geraldine A. Hamilton¹ and DEI. From Three-Dimensional Cell Culture to Organs-on-Chips. *Physiol Behav*. 2018;176(5):139-148. doi:10.1016/j.tcb.2011.09.005.From
166. Grapin-Botton A. Three-dimensional pancreas organogenesis models. *Diabetes, Obes Metab*. 2016;18(Suppl 1):33-40. doi:10.1111/dom.12720
167. Sant S, Johnston PA. The production of 3D tumor spheroids for cancer drug discovery. *Drug Discov Today Technol*. 2017;23:27-36. doi:10.1016/j.ddtec.2017.03.002
168. Metzger W, Sossong D, Bächle A, et al. The liquid overlay technique is the key to formation of co-culture spheroids consisting of primary osteoblasts, fibroblasts and endothelial cells. *Cytotherapy*. 2011;13(8):1000-1012. doi:10.3109/14653249.2011.583233

169. Nie J, Hashino E. Organoid technologies meet genome engineering. *EMBO Rep.* 2017;18(3):367-376. doi:10.15252/embr.201643732
170. Lehmann R, Lee CM, Shugart EC, et al. Human organoids: A new dimension in cell biology. *Mol Biol Cell.* 2019;30(10):1129-1137. doi:10.1091/mbc.E19-03-0135
171. Simian M, Bissell MJ. Organoids: A historical perspective of thinking in three dimensions. *J Cell Biol.* 2017;216(1):31-40. doi:10.1083/jcb.201610056
172. Arora N, Alsous JI, Guggenheim JW, et al. A process engineering approach to increase organoid yield. *Dev.* 2017;144(6):1128-1136. doi:10.1242/dev.142919
173. Yin X, Mead BE, Safaee H, Langer R, Karp JM, Levy O. Engineering Stem Cell Organoids. *Cell Stem Cell.* 2016;18(1):25-38. doi:10.1016/j.stem.2015.12.005
174. Georgakopoulos N, Prior N, Angres B, et al. Long-term expansion, genomic stability and in vivo safety of adult human pancreas organoids. *BMC Dev Biol.* 2020;20(1):1-20. doi:10.1186/s12861-020-0209-5
175. Fleischer A, Vallejo-Díez S, Martín-Fernández JM, et al. iPSC-Derived Intestinal Organoids from Cystic Fibrosis Patients Acquire CFTR Activity upon TALEN-Mediated Repair of the p.F508del Mutation. *Mol Ther - Methods Clin Dev.* 2020;17(June):858-870. doi:10.1016/j.omtm.2020.04.005
176. Kaserman JE, Hurley K, Dodge M, et al. A Highly Phenotyped Open Access Repository of Alpha-1 Antitrypsin Deficiency Pluripotent Stem Cells. *Stem Cell Reports.* 2020;15(1):242-255. doi:10.1016/j.stemcr.2020.06.006
177. Guan Y, Xu D, Garfin PM, et al. Human hepatic organoids for the analysis of human genetic diseases. *JCI insight.* 2017;2(17):1-17. doi:10.1172/jci.insight.94954
178. Gunti S, Hoke ATK, Vu KP, London NR. Organoid and spheroid tumor models: Techniques and applications. *Cancers (Basel).* 2021;13(4):1-18. doi:10.3390/cancers13040874
179. Baker LA, Tiriack H, Clevers H, Tuveson DA. Modeling pancreatic cancer with organoids The Need for Accurate Model Systems of Pancreatic Cancer. 2017;2(4):176-190. doi:10.1016/j.trecan.2016.03.004

180. Brooks MJ, Chen HY, Kelley RA, et al. Improved Retinal Organoid Differentiation by Modulating Signaling Pathways Revealed by Comparative Transcriptome Analyses with Development In Vivo. *Stem Cell Reports*. 2019;13(5):891-905. doi:10.1016/j.stemcr.2019.09.009
181. Takahashi T, Shiraishi A. Stem cell signaling pathways in the small intestine. *Int J Mol Sci*. 2020;21(6):1-18. doi:10.3390/ijms21062032
182. Okamoto R, Shimizu H, Suzuki K, et al. Organoid-based regenerative medicine for inflammatory bowel disease. *Regen Ther*. 2020;13:1-6. doi:10.1016/j.reth.2019.11.004
183. Laschke MW, Menger MD. Spheroids as vascularization units: From angiogenesis research to tissue engineering applications. *Biotechnol Adv*. 2017;35(6):782-791. doi:10.1016/j.biotechadv.2017.07.002
184. Holub AR, Huo A, Patel K, Thakore V, Chhibber P, Erogbogbo F. Assessing advantages and drawbacks of rapidly generated ultra-large 3d breast cancer spheroids: Studies with chemotherapeutics and nanoparticles. *Int J Mol Sci*. 2020;21(12):1-16. doi:10.3390/ijms21124413
185. Wasungu L, Escoffre JM, Valette A, Teissie J, Rols MP. A 3D in vitro spheroid model as a way to study the mechanisms of electroporation. *Int J Pharm*. 2009;379(2):278-284. doi:10.1016/j.ijpharm.2009.03.035
186. Lamichhane SP, Arya N, Kohler E, Xiang S, Christensen J, Shastri VP. Recapitulating epithelial tumor microenvironment in vitro using three dimensional tri-culture of human epithelial, endothelial, and mesenchymal cells. *BMC Cancer*. 2016;16(1):1-12. doi:10.1186/s12885-016-2634-1
187. Shen H, Cai S, Wu C, Yang W, Yu H, Liu L. Recent Advances in Three-Dimensional Multicellular Spheroid Culture and Future Development vivo and in vitro biology research . So far , a series of cells have be duction of MCSs , including cancer cells [4 , 12], induced pluripote fibroblasts [15 , 16. 2021.
188. Ryu NE, Lee SH, Park H. Spheroid Culture System Methods and Applications for Mesenchymal Stem Cells. *Cells*. 2019;8(12):1-13. doi:10.3390/cells8121620
189. Boj SF, Hwang C II, Baker LA, Engle DD, Tuveson DA, Clevers H. Model organoids provide

- new research opportunities for ductal pancreatic cancer. *Mol Cell Oncol*. 2016;3(1):2015-2017. doi:10.1080/23723556.2015.1014757
190. George McNamara. *Microscopy and Image Analysis*. Vol 176.; 2018. doi:10.1002/0471142905.hg0404s46.Microscopy
191. Michael J. Sanderson^{1,4}, Ian Smith², Ian Parker² and MDB. Fluorescence Microscopy. *Physiol Behav*. 2014;63(8):1-18. doi:10.1101/pdb.top071795.Fluorescence
192. Thorn K. A quick guide to light microscopy in cell biology. *Mol Biol Cell*. 2016;27(2):219-222. doi:10.1091/mbc.E15-02-0088
193. n, Eunsung Mouradian MM. High-resolution wide-field microscopy with adaptive optics for spherical aberration correction and motionless focusing. *Bone*. 2008;23(1):1-7. doi:10.1111/j.1365-2818.2009.03315.x.High-resolution
194. Bayguinov PO, Oakley DM, Shih CC, Geanon DJ, Joens MS, Fitzpatrick JAJ. Modern Laser Scanning Confocal Microscopy. *Curr Protoc Cytom*. 2018;85(1). doi:10.1002/cpcy.39
195. Grzywacz A, Góral T, Szpila K, Hall MJR. Confocal laser scanning microscopy as a valuable tool in Diptera larval morphology studies. *Parasitol Res*. 2014;113(11):4297-4302. doi:10.1007/s00436-014-4125-0
196. HAGINOYA M, Matsumoto S. Confocal laser scanning microscopic photoconversion: a new method to stabilize fluorescently labeled cellular elements for electron microscopic analysis. *J Japan Soc Colour Mater*. 1991;64(1):34-41. doi:10.4011/shikizai1937.64.34
197. Keller PJ, Schmidt AD, Wittbrodt J, Stelzer EHK. Reconstruction of zebrafish early embryonic development by scanned light sheet microscopy. *Science (80-)*. 2008;322(5904):1065-1069. doi:10.1126/science.1162493
198. Stelzer EHK. Light-sheet fluorescence microscopy for quantitative biology. *Nat Methods*. 2014;12(1):23-26. doi:10.1038/nmeth.3219
199. Santi PA. Light sheet fluorescence microscopy: A review. *J Histochem Cytochem*. 2011;59(2):129-138. doi:10.1369/0022155410394857
200. n, Eunsung Mouradian MM. Light Sheet Fluorescence Microscopy (LSFM). *Bone*.

- 2008;23(1):1-7. doi:10.1002/0471142956.cy1237s71.Light
201. Manton JD, Ströhl F, Fiolka R, Kaminski CF, Rees EJ. Concepts for structured illumination microscopy with extended axial resolution through mirrored illumination. *bioRxiv*. 2019;11(4):2098-2108. doi:10.1101/828632
202. Xu J, Ma H, Liu Y. Stochastic optical reconstruction microscopy (STORM). *Curr Protoc Cytom*. 2017;2017:12.46.1-12.46.27. doi:10.1002/cpcy.23
203. Mitch Leslie. Two microscopes are better than one. *Shipp World Shipbuild*. 2001;202(4179):32. doi:10.1083/jcb.201009037.bryos
204. McIntosh JR. Electron microscopy of cells: A new beginning for a new century. *J Cell Biol*. 2001;153(6):25-32. doi:10.1083/jcb.153.6.F25
205. Franken LE, Boekema EJ, Stuart MCA. Transmission Electron Microscopy as a Tool for the Characterization of Soft Materials: Application and Interpretation. *Adv Sci*. 2017;4(5):1-9. doi:10.1002/adv.201600476
206. Lidke DS, Lidke KA. Advances in high-resolution imaging - techniques for three-dimensional imaging of cellular structures. *J Cell Sci*. 2012;125(11):2571-2580. doi:10.1242/jcs.090027
207. Colin S, Coelho LP, Sunagawa S, et al. Quantitative 3D-imaging for cell biology and ecology of environmental microbial eukaryotes. *Elife*. 2017;6:1-15. doi:10.7554/eLife.26066
208. Huisken J, Swoger J, Del Bene F, Wittbrodt J, Stelzer EHK. Optical sectioning deep inside live embryos by selective plane illumination microscopy. *Science (80-)*. 2004;305(5686):1007-1009. doi:10.1126/science.1100035
209. Chang JB, Chen F, Yoon YG, et al. Iterative expansion microscopy. *Nat Methods*. 2017;14(6):593-599. doi:10.1038/nmeth.4261
210. Smyrek I, Stelzer EHK. Quantitative three-dimensional evaluation of immunofluorescence staining for large whole mount spheroids with light sheet microscopy. *Biomed Opt Express*. 2017;8(2):484. doi:10.1364/BOE.8.000484
211. Pampaloni F, Ansari N, Stelzer EHK. High-resolution deep imaging of live cellular

- spheroids with light-sheet-based fluorescence microscopy. *Cell Tissue Res.* 2013;352(1):161-177. doi:10.1007/s00441-013-1589-7
212. Schmitz A, Fischer SC, Mattheyer C, Pampaloni F, Stelzer EHK. Multiscale image analysis reveals structural heterogeneity of the cell microenvironment in homotypic spheroids. *Sci Rep.* 2017;7(March):1-13. doi:10.1038/srep43693
213. Hiroyuki Miyoshi TSS. In vitro expansion and genetic modification of gastrointestinal stem cells as organoids. *Bone.* 2008;23(1):1-7. doi:10.1038/nprot.2013.153.In
214. Vinc Boyd¹, Olivia Maria Cholewa^{2,§} and KKP. Limitations in the Use of Fluorescein Diacetate/Propidium Iodide (FDA/PI) and Cell Permeable Nucleic Acid Stains for Viability Measurements of Isolated Islets of Langerhans. *Trends Biotechnol.* 2010;2(2):66-84.
215. Gavin RH. Diversity of cell-mediated adhesions in breast cancer spheroids. *Methods Mol Biol.* 2016;1365:v-vi. doi:10.1007/978-1-4939-3124-8
216. Kao DI, Lacko LA, Ding B Sen, et al. Endothelial cells control pancreatic cell fate at defined stages through EGF17 signaling. *Stem Cell Reports.* 2015;4(2):181-189. doi:10.1016/j.stemcr.2014.12.008
217. Tietze S, Kräter M, Jacobi A, et al. Spheroid Culture of Mesenchymal Stromal Cells Results in Morphorheological Properties Appropriate for Improved Microcirculation. *Adv Sci.* 2019;6(8). doi:10.1002/advs.201802104
218. Heiss M, Hellström M, Kalén M, et al. Endothelial cell spheroids as a versatile tool to study angiogenesis in vitro. *FASEB J.* 2015;29(7):3076-3084. doi:10.1096/fj.14-267633
219. McColloch A, Rabiei M, Rabbani P, Bowling A, Cho M. Correlation between Nuclear Morphology and Adipogenic Differentiation: Application of a Combined Experimental and Computational Modeling Approach. *Sci Rep.* 2019;9(1):1-13. doi:10.1038/s41598-019-52926-8
220. Almonacid M, Terret ME, Verlhac MH. Nuclear positioning as an integrator of cell fate. *Curr Opin Cell Biol.* 2019;56:122-129. doi:10.1016/j.ceb.2018.12.002
221. Ruijtenberg S, van den Heuvel S. Coordinating cell proliferation and differentiation:

- Antagonism between cell cycle regulators and cell type-specific gene expression. *Cell Cycle*. 2016;15(2):196-212. doi:10.1080/15384101.2015.1120925
222. Huch M, Bonfanti P, Boj SF, et al. Unlimited in vitro expansion of adult bi-potent pancreas progenitors through the Lgr5/R-spondin axis. *EMBO J*. 2013;32(20):2708-2721. doi:10.1038/emboj.2013.204
223. Kim HJ, Sung IY, Cho YC, et al. Three-Dimensional Spheroid Formation of Cryopreserved Human Dental Follicle-Derived Stem Cells Enhances Pluripotency and Osteogenic Induction Properties. *Tissue Eng Regen Med*. 2019;16(5):513-523. doi:10.1007/s13770-019-00203-0
224. Huch M, Bonfanti P, Boj SF, et al. Unlimited in vitro expansion of adult bi-potent pancreas progenitors through the Lgr5/R-spondin axis. *EMBO J*. 2013;32(20):2708-2721. doi:10.1038/emboj.2013.204
225. Broutier L, Andersson-Rolf A, Hindley CJ, et al. Culture and establishment of self-renewing human and mouse adult liver and pancreas 3D organoids and their genetic manipulation. *Nat Protoc*. 2016;11(9):1724-1743. doi:10.1038/nprot.2016.097
226. Driehuis E, Gracanin A, Vries RGJ, Clevers H, Boj SF. Establishment of Pancreatic Organoids from Normal Tissue and Tumors. *STAR Protoc*. 2020;1(3):100192. doi:10.1016/j.xpro.2020.100192
227. Stadler M, Scherzer M, Walter S, et al. Exclusion from spheroid formation identifies loss of essential cell-cell adhesion molecules in colon cancer cells. *Sci Rep*. 2018;8(1):1-16. doi:10.1038/s41598-018-19384-0
228. Twentyman PR. Exclusion of host cells during spheroid formation from disaggregated solid tumours. *Br J Cancer*. 1983;47(4):541-543. doi:10.1038/bjc.1983.85
229. Ciulla MM, Acquistapace G, Toffetti L, et al. Ki67 cytoplasmic expression: Observations in normal tissue from heart atrial appendages of healthy rats. *Cell Cycle*. 2009;8(13):2125. doi:10.4161/cc.8.13.8785
230. Minami K, Seino S. Pancreatic acinar-to-beta cell transdifferentiation in vitro. *Front Biosci*. 2008;13(February 2008):5824-5837. doi:10.2741/3119

231. Bayoussef Z, Dixon JE, Stolnik S, Shakesheff KM. Aggregation promotes cell viability, proliferation, and differentiation in an in vitro model of injection cell therapy. *J Tissue Eng Regen Med.* 2012;6(10). doi:10.1002/term.482
232. Toyoda T, Mae SI, Tanaka H, et al. Cell aggregation optimizes the differentiation of human ESCs and iPSCs into pancreatic bud-like progenitor cells. *Stem Cell Res.* 2015;14(2):185-197. doi:10.1016/j.scr.2015.01.007
233. Walenda T, Bork S, Horn P, et al. Co-culture with mesenchymal stromal cells increases proliferation and maintenance of haematopoietic progenitor cells. *J Cell Mol Med.* 2010;14(1-2):337-350. doi:10.1111/j.1582-4934.2009.00776.x
234. Luo Y, Mohsin A, Xu C, et al. Co-culture with TM4 cells enhances the proliferation and migration of rat adipose-derived mesenchymal stem cells with high stemness. *Cytotechnology.* 2018;70(5):1409-1422s. doi:10.1007/s10616-018-0235-3
235. Xie X, Zhu J, Hu X, et al. A co-culture system of rat synovial stem cells and meniscus cells promotes cell proliferation and differentiation as compared to mono-culture. *Sci Rep.* 2018;8(1):1-11. doi:10.1038/s41598-018-25709-w
236. Zhou D, Chen L, Ding J, et al. A 3D engineered scaffold for hematopoietic progenitor/stem cell co-culture in vitro. *Sci Rep.* 2020;10(1):1-11. doi:10.1038/s41598-020-68250-5
237. Martín M, Gallego-Llamas J, Ribes V, et al. Dorsal pancreas agenesis in retinoic acid-deficient Raldh2 mutant mice. *Dev Biol.* 2005;284(2):399-411. doi:10.1016/j.ydbio.2005.05.035
238. Nissim S, Sherwood RI, Wucherpfennig J, et al. Prostaglandin E2 regulates liver versus pancreas cell-fate decisions and endodermal outgrowth. *Dev Cell.* 2014;28(4):423-437. doi:10.1016/j.devcel.2014.01.006
239. Bonfanti P, Nobecourt E, Oshima M, et al. Ex Vivo Expansion and Differentiation of Human and Mouse Fetal Pancreatic Progenitors Are Modulated by Epidermal Growth Factor. *Stem Cells Dev.* 2015;24(15):1766-1778. doi:10.1089/scd.2014.0550
240. Gradwohl G, Dierich A, LeMeur M, Guillemot F. Neurogenin3 Is Required for the Development of the Four Endocrine Cell Lineages of the Pancreas. *Proc Natl Acad Sci U*

- S A. 2000;97(4):1607-1611. doi:10.1073/pnas.97.4.1607
241. Watson J, Francavilla C. Regulation of FGF10 Signaling in Development and Disease. *Front Genet.* 2018;9(October):1-10. doi:10.3389/fgene.2018.00500
242. Lemper M, Leuckx G, Heremans Y, et al. Reprogramming of human pancreatic exocrine cells to β -like cells. *Cell Death Differ.* 2014;22(7):1117-1130. doi:10.1038/cdd.2014.193
243. Zafarullah M, Li WQ, Sylvester J, Ahmad M. Molecular mechanisms of N -acetylcysteine actions. *Cell Mol Life Sci.* 2003;60(1):6-20. doi:10.1007/s000180300001
244. Li W, Li W, Leng Y, et al. Mechanism of N-acetylcysteine in alleviating diabetic myocardial ischemia reperfusion injury by regulating PTEN/Akt pathway through promoting DJ-1. *Biosci Rep.* 2020;40(6):1-17. doi:10.1042/BSR20192118
245. Wierup N, Sundler F, Scott Heller R. The islet ghrelin cell. *J Mol Endocrinol.* 2013;52(1). doi:10.1530/JME-13-0122
246. Wang S, Yan J, Anderson DA, et al. Neurog3 gene dosage regulates allocation of endocrine and exocrine cell fates in the developing mouse pancreas. *Dev Biol.* 2010;339(1):26-37. doi:10.1016/j.ydbio.2009.12.009
247. Rulifson IC, Karnik SK, Heiser PW, et al. Wnt signaling regulates pancreatic beta cell proliferation. *Proc Natl Acad Sci.* 2007;104(15):6247-6252. doi:10.1073/pnas.0701509104
248. Afelik S, Pool B, Schmerr M, Penton C, Jensen J. Wnt7b is required for epithelial progenitor growth and operates during epithelial-to-mesenchymal signaling in pancreatic development. *Dev Biol.* 2015;399(2):204-217. doi:10.1016/j.ydbio.2014.12.031
249. LaRue KEA, Khalil M, Freyer JP. Microenvironmental Regulation of Proliferation in Multicellular Spheroids Is Mediated through Differential Expression of Cyclin-Dependent Kinase Inhibitors. *Cancer Res.* 2004;64(5):1621-1631. doi:10.1158/0008-5472.CAN-2902-2
250. Li L, Lu Y. Optimizing a 3D culture system to study the interaction between epithelial breast cancer and its surrounding fibroblasts. *J Cancer.* 2011;2(1):458-466.

- doi:10.7150/jca.2.458
251. Blanke M, Carl HD, Klinger P, Swoboda B, Hennig F, Gelse K. Transplanted chondrocytes inhibit endochondral ossification within cartilage repair tissue. *Calcif Tissue Int.* 2009;85(5):421-433. doi:10.1007/s00223-009-9288-9
 252. Song L, Yuan X, Jones Z, et al. Assembly of Human Stem Cell-Derived Cortical Spheroids and Vascular Spheroids to Model 3-D Brain-like Tissues. *Sci Rep.* 2019;9(1):1-16. doi:10.1038/s41598-019-42439-9
 253. Park KS, Jang YS, Lee H, Kim JS. Phenotypic alteration and target gene identification using combinatorial libraries of zinc finger proteins in prokaryotic cells. *J Bacteriol.* 2005;187(15):5496-5499. doi:10.1128/JB.187.15.5496-5499.2005
 254. Vicente-Manzanares M, Sanchez-Madrid F. Cell polarization: A comparative cell biology and immunological view. *Dev Immunol.* 2000;7(2-4):51-65. doi:10.1155/2000/70801
 255. Piroli ME, Blanchette JO, Jabbarzadeh E. Polarity as a physiological modulator of cell function. *Front Biosci - Landmark.* 2019;24(3):451-462. doi:10.2741/4728
 256. Martinez-Sanchez ME, Huerta L, Alvarez-Buylla ER, Luján CV. Role of cytokine combinations on CD4+ T cell differentiation, partial polarization, and plasticity: Continuous network modeling approach. *Front Physiol.* 2018;9(AUG):1-14. doi:10.3389/fphys.2018.00877
 257. Gregg G. Gundersen¹ * and Howard J. Worman. Nuclear Positioning. *Bone.* 2008;23(1):1-7. doi:10.1016/j.cell.2013.02.031.Nuclear
 258. Lammerding J. Mechanics of the nucleus. *Compr Physiol.* 2011;1(2):783-807. doi:10.1002/cphy.c100038
 259. Henics T. Differentiation-dependent cytoplasmic distribution and in vivo RNA association of proteins recognized by the 3'-UTR stability element of α -globin mRNA in erythroleukemic cells. *Biochem Biophys Res Commun.* 2000;279(1):40-46. doi:10.1006/bbrc.2000.3900
 260. Stewart RM, Zubek AE, Rosowski KA, Schreiner SM, Horsley V, King MC. Nuclear-cytoskeletal linkages facilitate cross talk between the nucleus and intercellular

- adhesions. *J Cell Biol.* 2015;209(3):403-418. doi:10.1083/jcb.201502024
261. S.A. Deepak, K.R. Kottapalli, R. Rakwal, et al. Real-Time PCR: Revolutionizing Detection and Expression Analysis of Genes. *Curr Genomics.* 2007;8(4):234-251. doi:10.2174/138920207781386960
262. Wang INE, Bogdanowicz DR, Mitroo S, Shan J, Kala S, Lu HH. Cellular interactions regulate stem cell differentiation in tri-culture. *Connect Tissue Res.* 2016;57(6):476-487. doi:10.1080/03008207.2016.1230106
263. Motose H, Fukuda H, Sugiyama M. Involvement of local intercellular communication in the differentiation of zinnia mesophyll cells into tracheary elements. *Planta.* 2001;213(1):121-131. doi:10.1007/s004250000482
264. Toivonen S, Ojala M, Hyysalo A, et al. Comparative Analysis of Targeted Differentiation of Human Induced Pluripotent Stem Cells (hiPSCs) and Human Embryonic Stem Cells Reveals Variability Associated With Incomplete Transgene Silencing in Retrovirally Derived hiPSC Lines. *Stem Cells Transl Med.* 2013;2(2):83-93. doi:10.5966/sctm.2012-0047
265. Najafabadi MM, Bayati V, Orazizadeh M, Hashemitabar M, Absalan F. Impact of cell density on differentiation efficiency of rat adipose-derived stem cells into schwann-like cells. *Int J Stem Cells.* 2016;9(2):213-220. doi:10.15283/ijsc16031
266. Xue R, Li JYS, Yeh Y, Yang L, Chien S. Effects of matrix elasticity and cell density on human mesenchymal stem cells differentiation. *J Orthop Res.* 2013;31(9):1360-1365. doi:10.1002/jor.22374
267. Kozlov MM, Mogilner A. Model of polarization and bistability of cell fragments. *Biophys J.* 2007;93(11):3811-3819. doi:10.1529/biophysj.107.110411
268. Iriguchi S, Yasui Y, Kawai Y, et al. A clinically applicable and scalable method to regenerate T-cells from iPSCs for off-the-shelf T-cell immunotherapy. *Nat Commun.* 2021;12(1):1-15. doi:10.1038/s41467-020-20658-3
269. Aguirre A, Planell JA, Engel E. Dynamics of bone marrow-derived endothelial progenitor cell/mesenchymal stem cell interaction in co-culture and its implications in angiogenesis. *Biochem Biophys Res Commun.* 2010;400(2):284-291.

- doi:10.1016/j.bbrc.2010.08.073
270. Gao R, Ustinov J, Pulkkinen MA, Lundin K, Korsgren O, Otonkoski T. Characterization of endocrine progenitor cells and critical factors for their differentiation in human adult pancreatic cell culture. *Diabetes*. 2003;52(8):2007-2015. doi:10.2337/diabetes.52.8.2007
 271. Bonner-Weir S, Taneja M, Weir GC, et al. In vitro cultivation of human islets from expanded ductal tissue. *Proc Natl Acad Sci U S A*. 2000;97(14):7999-8004. doi:10.1073/pnas.97.14.7999
 272. Seymour PA. Sox9: A master regulator of the pancreatic program. *Rev Diabet Stud*. 2014;11(1):51-83. doi:10.1900/RDS.2014.11.51
 273. Murtaugh LC, Stanger BZ, Kwan KM, Melton DA. Notch signaling controls multiple steps of pancreatic differentiation. *Proc Natl Acad Sci U S A*. 2003;100(25):14920-14925. doi:10.1073/pnas.2436557100
 274. Goers L, Freemont P, Polizzi KM. Co-culture systems and technologies: Taking synthetic biology to the next level. *J R Soc Interface*. 2014;11(96). doi:10.1098/rsif.2014.0065
 275. Geron E, Boura-Halfon S, Schejter ED, Shilo BZ. The Edges of Pancreatic Islet β Cells Constitute Adhesive and Signaling Microdomains. *Cell Rep*. 2015;10(3):317-325. doi:10.1016/j.celrep.2014.12.031
 276. Fischer MS, Wu VW, Lee JE, O'Malley RC, Glass NL. Regulation of Cell-to-Cell Communication and Cell and Transcription Factors in *Neurospora crassa*. 2018;209(June):489-506.
 277. Subramanian K, Owens DJ, Raju R, et al. Spheroid culture for enhanced differentiation of human embryonic stem cells to hepatocyte-like cells. *Stem Cells Dev*. 2014;23(2):124-131. doi:10.1089/scd.2013.0097
 278. Li HJ, Yu PN, Huang KY, et al. NKX6.1 functions as a metastatic suppressor through epigenetic regulation of the epithelial-mesenchymal transition. *Oncogene*. 2016;35(17):2266-2278. doi:10.1038/onc.2015.289
 279. Fanjul M, Gmyr V, Sengenès C, et al. Evidence for epithelial-mesenchymal transition in

- adult human pancreatic exocrine cells. *J Histochem Cytochem.* 2010;58(9):807-823. doi:10.1369/jhc.2010.955807
280. Mitchel JA, Das A, O’Sullivan MJ, et al. In primary airway epithelial cells, the unjamming transition is distinct from the epithelial-to-mesenchymal transition. *Nat Commun.* 2020;11(1):1-14. doi:10.1038/s41467-020-18841-7
281. De Marzio M, Kiliç A, Maiorino E, et al. Genomic signatures of the unjamming transition in compressed human bronchial epithelial cells. *Sci Adv.* 2021;7(30):1-15. doi:10.1126/sciadv.abf1088
282. Habener JF, Kemp DM, Thomas MK. Minireview: Transcriptional regulation in pancreatic development. *Endocrinology.* 2005;146(3):1025-1034. doi:10.1210/en.2004-1576
283. Sharma A, Zangen DH, Reitz P, et al. R e g e n e r a t i o n . :507-513.
284. Lipsett MA, Castellarin ML, Rosenberg L. Acinar plasticity: Development of a novel in vitro model to study human acinar-to-duct-to-islet differentiation. *Pancreas.* 2007;34(4):452-457. doi:10.1097/MPA.0b013e3180335c80
285. Baeyens L, De Breuck S, Lardon J, Mfopou JK, Rooman I, Bouwens L. In vitro generation of insulin-producing beta cells from adult exocrine pancreatic cells. *Diabetologia.* 2005;48(1):49-57. doi:10.1007/s00125-004-1606-1
286. Roy N, Takeuchi KK, Ruggeri JM, et al. PDX1 dynamically regulates pancreatic ductal adenocarcinoma initiation and maintenance. *Genes Dev.* 2016;30(24):2669-2683. doi:10.1101/gad.291021.116
287. Liya Kondratyeva 1,* , Igor Chernov 1, Eugene Kopantzev 1, Dmitry Didych 1, Alexey Kuzmich 1 2. Pancreatic Lineage Specifier PDX1 Increases Adhesion and Decreases Motility of Cancer Cells.
288. Zhang S, Wang Q, Ji H, et al. Porcine pancreas mesenchymal cell characterization and functional differentiation into insulin-producing cells in vitro. *Mol Med Rep.* 2021;24(4). doi:10.3892/mmr.2021.12377
289. Piltti KM, Cummings BJ, Carta K, et al. Live-cell time-lapse imaging and single-cell

- tracking of in vitro cultured neural stem cells – Tools for analyzing dynamics of cell cycle, migration, and lineage selection. *Methods*. 2018;133:81-90. doi:10.1016/j.ymeth.2017.10.003
290. Hattab G, Wiesmann V, Becker A, Munzner T, Nattkemper TW. A Novel Methodology for Characterizing Cell Subpopulations in Automated Time-lapse Microscopy. *Front Bioeng Biotechnol*. 2018;6(February):1-16. doi:10.3389/fbioe.2018.00017
291. Dragonfly TA. Molecular Mechanisms in Action - High-resolution Time Lapse Imaging in Live Cells " The Andor Dragonfly provides us solutions to the challenges of sensitivity , phototoxicity Research projects at the Department of Cell and Chemical Biology (LUMC). 2021.
292. W. J. Godinez; M. Lampe; S. Worz; B. Muller; R. Eils; K. Rohr. TRACKING OF VIRUS PARTICLES IN TIME-LAPSE FLUORESCENCE MICROSCOPY IMAGE SEQUENCES.
293. Chao X, Qi Y, Zhang Y. Highly Photostable Fluorescent Tracker with pH-Insensitivity for Long-Term Imaging of Lysosomal Dynamics in Live Cells. *ACS Sensors*. 2021;6(3):786-796. doi:10.1021/acssensors.0c01588
294. Miller YI, Chang MK, Funk CD, Feramisco JR, Witztum JL. 12/15-Lipoxygenase Translocation Enhances Site-specific Actin Polymerization in Macrophages Phagocytosing Apoptotic Cells. *J Biol Chem*. 2001;276(22):19431-19439. doi:10.1074/jbc.M011276200
295. Khodjakov VM and A. Circumventing photodamage in live-cell microscopy. *Bone*. 2008;23(1):1-7. doi:10.1016/B978-0-12-407761-4.00023-3.Circumventing
296. Lu Z, Joseph D, Bugnard E, Zaal KJM, Ralston E. Golgi complex reorganization during muscle differentiation: Visualization in living cells and mechanism. *Mol Biol Cell*. 2001;12(4):795-808. doi:10.1091/mbc.12.4.795
297. Pampaloni F, Reynaud EG, Stelzer EHK. The third dimension bridges the gap between cell culture and live tissue. *Nat Rev Mol Cell Biol*. 2007;8(10):839-845. doi:10.1038/nrm2236
298. Steinberg MS. Reconstruction of tissues by dissociated cells. *Sci Sci*. 1963;141(3579):401-408. doi:10.1126/science.141.3579.401

299. Tzanakakis ES, Hansen LK, Hu WS. The role of actin filaments and microtubules in hepatocyte spheroid self-assembly. *Cell Motil Cytoskeleton*. 2001;48(3):175-189. doi:10.1002/1097-0169(200103)48:3<175::AID-CM1007>3.0.CO;2-2
300. Vinale F, Nicoletti R, Borrelli F, et al. Co-Culture of Plant Beneficial Microbes as Source of Bioactive Metabolites. *Sci Rep*. 2017;7(1):1-12. doi:10.1038/s41598-017-14569-5
301. Hooghe-peters EL, Meda P, Orci L. Co-culture of nerve cells and pancreatic islets. 1981;1:287-292.
302. Banerjee I, Sharma N, Yarmush M. Impact of co-culture on pancreatic differentiation of embryonic stem cells. *J Tissue Eng Regen Med*. 2011;5(4):313-323. doi:10.1002/term.317
303. Kuttler B, Wanka H, Hahn HJ. Co-culture of pancreatic islets and allogeneic lymphocytes: Alterations of responder and stimulator cells. *Transplantation*. 1997;64(3):480-489. doi:10.1097/00007890-199708150-00018
304. Kuen J, Darowski D, Kluge T, Majety M. Pancreatic cancer cell/fibroblast co-culture induces M2 like macrophages that influence therapeutic response in a 3D model. *PLoS One*. 2017;12(7):1-19. doi:10.1371/journal.pone.0182039
305. de Souza BM, Bouças AP, Oliveira F dos S de, et al. Effect of co-culture of mesenchymal stem/stromal cells with pancreatic islets on viability and function outcomes: a systematic review and meta-analysis. *Islets*. 2017;9(2):30-42. doi:10.1080/19382014.2017.1286434
306. Kono TM, Ph D, Sims EK, et al. Human adipose derived stromal/stem cells (hASCs) protect against STZ-induced hyperglycemia; analysis of hASC-derived paracrine effectors. 2015;32(7):1831-1842. doi:10.1002/stem.1676.Human
307. Park, Ki-Soo^{1,2}; Kim, Young-Seok^{1,3}; Kim, Jae-Hyeon³; Choi, Bongkum^{1,2}; Kim, Sa-Hyun²; Tan, Alice Hyun-Kyung³; Lee, Myung-Shik³; Lee, Moon-Kyu³; Kwon, Choon-Hyuck⁴; Joh, Jae-Won⁴; Kim, Sung-Joo^{2,4,5}; Kim K-W. Trophic molecules derived from human mesenchymal stem cells enhance survival, function, and angiogenesis of isolated islets after transplantation. *Transplantation*. 2010;89(6):694-701. doi:10.1097/TP.0b013e3181c7dc99

308. Jaramillo M, Banerjee I. Endothelial cell co-culture mediates maturation of human embryonic stem cell to pancreatic insulin producing cells in a directed differentiation approach. *J Vis Exp*. 2012;(61):1-7. doi:10.3791/3759
309. El-gohary Y, Gittes G. Structure of Islets and Vascular Relationship to the Exocrine Pancreas. *Pancreapedia*. 2018;1(17):1-8. doi:10.3998/panc.2017.10
310. Lammert E, Cleaver O, Melton D. Induction of pancreatic differentiation by signals from blood vessels. *Science (80-)*. 2001;294(5542):564-567. doi:10.1126/science.1064344
311. Duvillié B. Vascularization of the pancreas: An evolving role from embryogenesis to adulthood. *Diabetes*. 2013;62(12):4004-4005. doi:10.2337/db13-1421
312. Landsman L. Pancreatic Pericytes in Glucose Homeostasis and Diabetes. *Adv Exp Med Biol*. 2019;1122:27-40. doi:10.1007/978-3-030-11093-2_2
313. Nalbach L, Roma LP, Schmitt BM, et al. Improvement of islet transplantation by the fusion of islet cells with functional blood vessels. *EMBO Mol Med*. 2021;13(1):1-21. doi:10.15252/emmm.202012616
314. Nair GG, Liu JS, Russ HA, et al. Recapitulating endocrine cell clustering in culture promotes maturation of human stem-cell-derived β cells. *Nat Cell Biol*. 2019;21(2):263-274. doi:10.1038/s41556-018-0271-4
315. Brüningk SC, Rivens I, Box C, Oelfke U, ter Haar G. 3D tumour spheroids for the prediction of the effects of radiation and hyperthermia treatments. *Sci Rep*. 2020;10(1):1-13. doi:10.1038/s41598-020-58569-4

10. Posters and Publications

10.1 Posters

1. Saeifar S, Stelzer EHK, Pampaloni F. 04/07/2019. Human pancreatic Organoids aggregation and co-culturing. [poster]. Sommer Fest. Johann Wolfgang Goethe-Universität Frankfurt am Main. Frankfurt am Main. Germany.
2. Saeifar S, Stelzer EHK, Pampaloni F. 23-24/09/2019. Effect of 3D co-culturing on Human pancreatic Organoid differentiation. [poster]. EOS. Miland. Italy.
3. Saeifar S, Stelzer EHK, Pampaloni F. 04-06/12/2019. Spheroid culture for enhancing DIFFERENTIATION OF human pancreatic organoids. [poster]. LSFM2019. Johann Wolfgang Goethe-Universität Frankfurt am Main. Frankfurt am Main. Germany.
4. Saeifar S, Stelzer EHK, Pampaloni F. 21-24/10/2020. Investigation of cellular interaction of human pancreas progenitor cells, mesenchymal cells and microvascular endothelial cells by an in vitro co-culture system. [Online poster]. EMBLE. Heidelberg. Germany.

10.2 Publications

1. Saeifar S, Stelzer EHK, Pampaloni F, Ucan D. 2023. A novel spheroid formation induces loss of progenitor state in human pancreas organoids (hPO). Manuscript submitted als preprint to bioRxiv.

Statutory declaration

I hereby certify that this protocol has been written by myself, and describes my own work, otherwise acknowledged in the text. All references and verbatim extracts have been quoted, and all sources of information have been specifically acknowledged. It has not been accepted in any previous application for a degree.

I hereby state furthermore that I have produced my works according to the principles of good scientific practice in compliance with the Goethe University roles.

Frankfurt am Main,

Sanam Saeifar

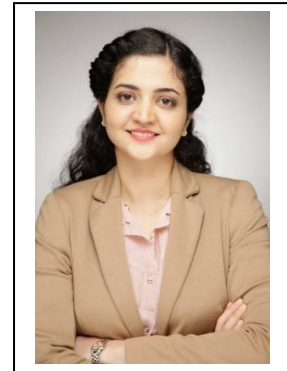
Place, Date

Name, Surname

Signature

Sanam Saeifar

Friedrich Bergius Weg 1,
60438, Frankfurt am Main, Germany
Mobile phone: +49 (0)176-89238638
E-Mail (private): sanamsaeifar@yahoo.com
Birthdate: 27/09/1988, Tehran, Iran



Professional Experience:

06/2022 – Present	Clinical Research Associate I (CRA I) Considerable on-site and remote monitoring of all aspects of clinical trials, in both pharmaceutical and medical device environments across Germany.
03/2022 – 06/2022	Internship of Clinical Research Associate (CRA) IQVIA , Frankfurt am Main, Germany intensive theoretical and practical training for different kind of clinical Monitoring such as (SSV, SMV, SCV) for clinical trials
08/2021 – 10/2021	Scientific consultant YURI GmbH , Meckenbeuren, Germany researching in the field of commercial applications in microgravity
09/2009 – 05/2011	Mouse husbandry Shahid Beheshti University, Tehran, Iran
09/2009 – 05/2010	Research assistant in Genetic Laboratory Shahid Beheshti University, Tehran, Iran
09/2009 – 05/2010	Research assistant in Cellular and Molecular Laboratory Shahid Beheshti University, Tehran, Iran
09/2009 – present	Scientific Editor Sinaps journal (Faculty magazine) Shahid Beheshti University, Tehran, Iran

Education:

07/2018 – 07/2022	Goethe University , Frankfurt am Main, Germany Doctoral candidate at the Buchmann Institute for Molecular Life Science (BMLS) PhD thesis: "Investigating the effect of endothelial cells on the endocrine differentiation of pancreatic progenitor cells, which are in the organoid form, in the direction of the secretion of insulin" Grade average: Not noted
09/2015 – 04/2017	Goethe University , Frankfurt am Main, Germany Master of Science in Cell Biology and Physiology Master's thesis: "The effect of autophagy-related protein 7 (ATG7) on breast cancer spheroids" Grade Point Average: 2
09/2008 – 05/2011	Shahid Beheshti University , Tehran, Iran Bachelor of Science in Cell Biology Grade Point Average: 17.46 out of 20. (1.7)
09/2006 – 05/2007	Khajeh Abdollah Ansari high school , Tehran, Iran High School Diploma Grade Point Average: 19.27 out of 20. (1.0)

Qualifications and Trainings:

Molecular Biology:	RNA and DNA extraction, cDNA synthesis, PCR, qRT-PCR, differentiation of pluripotent mouse stem cells into neuronal cells, reverse transcription, metabolism measurement analysis
Protein Biochemistry:	Protein isolation and extraction, Protein gel electrophoresis, Western Blot (semidry) analysis
Cell Biology:	Culture of 2D cell cultures, formation and culture of 3D cell cultures (liquid overlay, hanging drop), cultivation of organoids
Microscopy:	widefield microscopy, confocal Laser Scanning Microscopy (cLSM), Light sheet-based Fluorescence Microscopy (LSFM and mDSLIM), optical clearing
IT:	MS Office (Excel, Word, Power Point), Fiji, Wave (Seahorse data analyser software), Photoshop, Citavi, Gene runner, Primer 3
Mentoring:	Supervising master and bachelor student and moderating several qPCR and imaging practicums
Other:	ICH-GCP certificate 2022, Oncology certificate 2022, GxP certificate 2021, Certificate of laboratory animal handling (FELASA), taxidermy

Publications:

Sanam Saeifar, Iman Seyhon. "Glance to Nano science", Synaps, Biology magazine, spring 2011, No 12, page 50-58. (Faculty magazine)

Katharina Hötte, Sabine Fischer, Alexander Schmitz, Michael Koch, **Sanam Saeifar**, Ernst Stelzer, and Francesco Pampaloni. "mTOR controls growth and internal architecture of human breast cancer spheroids", in preparation

Sadighpour, T., Mubarak, M., Sabaeifard, P., **Sanam Saeifar** & Kenari, F. "COVID-19 and renal involvement; evolving role of thromboinflammation, vascular and glomerular disease in the pathogenesis". *J. Nephropathol.* 10, e23–e23 (2021).

Language Skills:

Persian	Native
Azeri	Native
German	Test DaF-2013 (C1), DSH2-2014 (C1)
English	University of Cambridge ESOL Examinations, Preliminary English Test (PET)-2005 (B2)

References:

Prof. Dr. Ernst H.K. Stelzer

Professor & group leader of the physical biology group
 Buchmann Institute for Molecular Life Sciences (BMLS),
 Goethe University, Frankfurt am Main, Germany
 Phone: +49 (69) 798-42547 E-Mail:ernst.stelzer@physikalischebiologie.de

Dr. Francesco Pampaloni, PhD

Buchmann Institute for Molecular Life Sciences (BMLS),
 Goethe University, Frankfurt am Main, Germany
 Phone: +49 (69) 798 42544 E-Mail: francesco.pampaloni@physikalischebiologie.de

Sanam Saeifar